Artificial Muscle Morphology

Structure/Property Relationships in Polypyrrole Actuators

by

Rachel Zimet Pytel

B.S. Chemical Engineering
Worcester Polytechnic Institute, 2002

Submitted to the Department of Materials Science and Engineering
in partial fulfillment of the requirements for the degree of

Doctor of Philosophy

at the

MASSACHUSETTS INSTITUTE OF TECHNOLOGY

June 2007

Author .....
Department of Materials Science and Engineering
May 2, 2007

Certified by .....
Edwin L. Thomas
Morris Cohen Professor of Materials Science and Engineering
Thesis Supervisor

Certified by .....
Ian W. Hunter
Hatsopoulos Professor of Mechanical Engineering
Thesis Supervisor

Certified by .....
Timothy M. Swager
John D. MacArthur Professor of Chemistry
Thesis Supervisor

Accepted by .....
Samuel M. Allen
Chairman, Department Committee on Graduate Students

Artificial Muscle Morphology

Structure/Property Relationships in Polypyrrole Actuators

by

Rachel Zimet Pytel

Submitted to the Department of Materials Science and Engineering
on May 2, 2007, in partial fulfillment of the
requirements for the degree of
Doctor of Philosophy

Abstract

We seek to improve polypyrrole and other conducting polymer actuators by discovering and exploiting the connection between nanoscale transport events and macroscale active strain. To this end we have used diffraction and electron microscopy to investigate the microstructure of polypyrrole, and propose a new description consisting of disordered polypyrrole chains held together by small crystalline bundles, around which solvent and counterions are randomly distributed. We utilize different modes of deformation to impart orientational texture to polypyrrole films, and show that by controlling polymer chain conformation and packing at a sub-micron level a conducting polymer actuator can be engineered that shows a significantly larger macroscopic electroactive response. We also alter the synthesis and doping conditions to produce films with widely varying surface morphologies, allowing us to control the rate of electroactive response. Our detailed understanding of polypyrrole morphology at different lengthscales provides valuable insight to the mechanisms of polypyrrole actuation, and has helped us process polypyrrole more intelligently for improved electroactive devices.

Thesis Supervisor: Edwin L. Thomas
Title: Morris Cohen Professor of Materials Science and Engineering

Thesis Supervisor: Ian W. Hunter
Title: Hatsopoulos Professor of Mechanical Engineering

Thesis Supervisor: Timothy M. Swager
Title: John D. MacArthur Professor of Chemistry

Acknowledgments

The most striking thing about my experience at MIT has been the quality of people I have met here. I thought I was going to be able to individually thank everyone who really helped me through this process, but once I started I realized that would be impossible - there are too many. My DMSE colleagues have been an incredible resource for me, somehow being both brilliant and well grounded, driven and fun. My volleyball teammates and coach (in addition to providing an outlet to hit something) have given me both their unconditional support and dose of reality, two things that are not easy to give at the same time. My colleagues in the Hunter and Thomas groups have inspired me to work harder, be more clever, and ask more questions. It sounds a bit clichéd to thank someone for "stimulating discussions," but they really have been stimulating, I've been inspired, and I've learned so much from you. I must specifically thank Ellen Chen and Arjun Naskar for their efforts in producing and processing films used in this work, Nate Vandesteeg and Priam Pillai for building and maintaining the EDMA, Vahik Krikorian for his help with TEM and EELS, and Carl Michal and Jenny Chien-Hsin Tso from the University of British Columbia for measuring the diffusivities of my processed samples.

I decided to come to MIT to work for the "dream team" of conducting polymer advisors, and I have been so lucky to be a part of three world-class research groups in completely different areas. I thank Professor Ian Hunter for providing such an amazing environment in which to work, where I was able to learn from and work with people and equipment often foreign to materials scientists. I thank Professor Tim Swager for sharing his experience and insight, and for the opportunities to interact with and be part of his subgroups even though my research focus was so far outside the rest of the group's. I thank Professor Edwin Thomas for pushing me to be a better scientist, for the hours spent tearing apart my manuscripts and discussing my research, and for showing me just how cool polymer morphology is. My advisors share an enthusiasm for discovery and a healthy skepticism that I hope to carry with me throughout my career.

I have been blessed with such a loving and supportive family. My sisters are so similar and so different, and I thank them for the perspective and worldliness they continue to give me. I count myself lucky to have them as friends. I thank my dad for showing me what can be accomplished through hard work and ambitious goals, but perhaps more importantly how to identify what is really important and always put that first. I thank my mom for teaching me the value of being yourself no matter what, and that by continuously working hard at whatever it is you do you can make a real difference in the lives of those around you. My parents both posses an interest and curiosity about the world and the desire to leave it slightly better than before. I think I inherited my enthusiasm and ability to work from them, as well as the attitude that with those two tools I can excel at whatever I pursue.

Finally, I thank my husband Chad for his unwavering love and support. There were many times when I doubted myself, but he not only knew I could do it, he knew I would. Looks like he was right, as usual. I couldn't have done it without him.

Contents

1 Introduction **17**

1.1 Motivation 17

1.2 Material Platform 19

1.3 Thesis Overview 21

2 Synthesis and Characterization of Polypyrrole Actuators **23**

2.1 Synthesis 23

2.1.1 Electropolymerization 24

2.1.2 Chemical Polymerization 26

2.2 Film Quality 26

2.2.1 Conductivity Measurements 27

2.2.2 Surface Morphology Evaluation 28

2.3 Electroactive Response 31

2.3.1 Warm-up 32

2.3.2 Isotonic Testing 36

2.3.3 Isometric Testing 38

2.3.4 Mobile Species 40

2.3.5 Solvent Transfer 43

2.3.6 Actuation in Liquid Salts 44

2.3.7 Speed of response 47

2.3.8 Dynamic Elastic Modulus 48

2.3.9 Effect of Ageing 56

2.4 Chapter Conclusions 58

3 Review of Previous Work on Polypyrrole Microstructure **61**

3.1 Electrical Conductivity 62

3.1.1 Temperature Dependence of Conductivity 63

3.1.2 Determination of Conductivity Regime 66

3.1.3 The Effect of Deposition Counterion 67

3.2 Morphology 68

3.3 Parameters in Electrochemical Synthesis 73

3.3.1 The Effect of Counterion Choice 74

3.3.2 The Effect of Deposition Potential and Current Density 75

3.3.3 The Effect of Solvent Choice 78

3.3.4 The Effect of Deposition Temperature 82

3.3.5 The Effect of Electrode Material 83

3.3.6 The Extent of Reaction 85

3.4 Chapter Conclusions 87

4 Polypyrrole Microstructure as Probed by Scattering Techniques **91**

4.1 Wide Angle X-ray Scattering 92

4.1.1 Degree of Orientation 98

4.1.2 Unoriented Component 99

4.1.3 Crystal Size 100

4.1.4 Determination of Crystal Structure 101

4.1.5 Percent Crystallinity 106

4.2 Electron Diffraction 108

4.2.1 Prior Work 109

4.2.2 Electron Diffraction of Polypyrrole Samples 112

4.2.3 Beam Sensitivity 115

4.3 Microstructural Response to Electrochemical Actuation 118

4.3.1 Microstructural Change upon Mild Redox 119

4.3.2 Microstructural Change upon Severe Redox 119

4.3.3 Microstructural Change in Very Thin Films 124

4.4 Chapter Conclusions 128

5 Microstructure Manipulation I: Post-Deposition Processing 133

5.1 Procedure 134

5.1.1 Polypyrrole Film Processing 134

5.1.2 Processed Film Testing 134

5.2 Evaluation of Microstructure 136

5.2.1 Wide Angle X-ray Scattering 136

5.2.2 Scanning Electron Microscopy 140

5.3 Electroactive Properties 142

5.3.1 Rate of Actuation 144

5.4 Discussion 145

5.4.1 Polymer Microstructure 145

5.4.2 Anisotropy of Actuation 147

5.4.3 Anisotropic Diffusivity 151

5.5 Chapter Conclusions 153

6 Microstructure Manipulation II: Synthetic Approaches 155

6.1 Procedure 156

6.2 Surface Morphology 157

6.3 Wide Angle X-ray Scattering 160

6.4 Electroactive Characterization 163

6.4.1 Actuation Without Warm-up 164

6.5 Further Manipulation of Microstructure 167

6.6 Chapter Conclusions 171

7 Conclusions and Future Outlook 173

7.1 Description of Polypyrrole Microstructure 173

7.2 Manipulations of Polypyrrole to Improve Properties 177

7.3 Suggestions for Future Work 178

7.4 Concluding Remarks 181

References 183

List of Figures

1-1 Commonly used conducting polymers 20

2-1 Polymerization mechanism for polypyrrole 24
2-2 Schematic of standard deposition cell 25
2-3 Solution and electrode faces of nodular polypyrrole film 29
2-4 Electron beam damage in polypyrrole sample 30
2-5 Electrochemical Dynamic Mechanical Analyzer (EDMA) 32
2-6 Passive modulus measurements for polypyrrole samples 34
2-7 Electrochemical warm-up 35
2-8 Isotonic actuation in 0.1M LiTFSI/PC 37
2-9 Isometric actuation in 0.1M LiTFSI/PC 39
2-10 Relative sizes of species in anion-dominated electrolyte system 41
2-11 Relative sizes of species in cation-dominated electrolyte system 42
2-12 Relative sizes of species in neat BMIMPF6 45
2-13 Isometric testing in BMIMPF6/PC 46
2-14 Electroactive response under constant and oscillatory strain 52
2-15 Modulus response for polypyrrole in neat BMIMPF6 53
2-16 Estimated modulus for polypyrrole in different electrolyte solutions . 57
2-17 Isotonic response for unprocessed films of different ages 59

3-1 Films deposited from solutions of DBS concentrations, from [1] 69
3-2 Polypyrrole deposited on different substrates, from [2] 70
3-3 Polypyrrole films deposited onto different working electrodes, from [3] 72
3-4 SEM micrographs of solution side of polypyrrole films, from [4] 77

3-5 SEM micrographs of polypyrrole film cross-sections, from [5] 80
3-6 Polypyrrole films deposited onto polished and unpolished platinum electrodes, from [6] 84
3-7 AFM images of polypyrrole films deposited onto polished and unpolished copper electrodes, from [7] 85
3-8 STM images of polypyrrole deposition, from [8] 86

4-1 Theoretical unit cell 93
4-2 Schematic of scattering experiment 95
4-3 WAXS patterns for semicrystalline polyethylene [9] 96
4-4 Comparison of WAXS patterns for stretched polyethylene and stretched polypyrrole 97
4-5 Diagram of characteristic reflections in stretched polypyrrole 103
4-6 Schematic illustration of staggered polypyrrole chains 104
4-7 Polypyrrole unit cell, as proposed by Nogami et al [10] 105
4-8 1D diffraction patterns for polypropylene and polypyrrole 107
4-9 Polpyrrole unit cell as proposed by Geiss et al. [11] 110
4-10 Helical polypyrrole structure as proposed by Chu et al. [12] 111
4-11 Procedure to make TEM samples from thin polypyrrole films 113
4-12 Electron diffraction pattern from thin polypyrrole film 114
4-13 Electron diffraction patterns from thin polypyrrole film after electron beam exposure 116
4-14 X-ray diffraction of oxidized and reduced polypyrrole film 120
4-15 X-ray diffraction of severely reduced and re-oxidized polypyrrole film 122
4-16 Separation of curves from Figure 4-15 123
4-17 Electron diffraction of as-deposited and reduced polypyrrole samples . 125
4-18 EELS of as-deposited and reduced polypyrrole samples 127
4-19 Illustration of bundled microstructure in oriented polypyrrole 130

5-1 Wide-angle x-ray scattering of unprocessed polypyrrole 136
5-2 Wide-angle x-ray scattering of stretched polypyrrole 138

5-3 Wide-angle x-ray scattering of rolled polypyrrole 139
5-4 1D WAXS patterns for stretched and rolled films 140
5-5 SEM images of processed film fracture surfaces 141
5-6 Isotonic response for stretched and rolled films 142
5-7 Isometric response for stretched and rolled films 143
5-8 Isotonic testing of stretched samples at different voltage ramps 144
5-9 Microstructure of polypyrrole chains in as-deposited and processed films 146
5-10 Schematic (2-D) diagram of expansion and contraction for oriented films 149
5-11 Stretched and rolled films tested 12 weeks after deposition and processing 150
5-12 Change in interchain spaces upon oriented polypyrrole actuation in liquid salt 152

6-1 Sizes of species varied in polypyrrole depositions 157
6-2 Glassy carbon and nickel foil working electrode surfaces 158
6-3 Solution-facing surfaces of films from Table 6.1 159
6-4 Electrode-facing surfaces of films from Table 6.1 160
6-5 1D x-ray diffraction patterns of solvents and films from Table 6.1 . . 162
6-6 Actuation of films with different surface morphologies 164
6-7 Isotonic actuation of Film G in aqueous solution 165
6-8 Isotonic actuation of Film G in 60/40 water/PC 166
6-9 Tensile testing of films from deposition E 168
6-10 SEM micrographs of films A, E and G 169
6-11 Isotonic actuation of stretched Film G 170
6-12 Dry and wet modulus tests for stretched film G 170

7-1 Illustration of the bundled composite microstructure in as-deposited polypyrrole 174
7-2 Illustration of bundled microstructure under different conditions . . . 176

List of Tables

1.1 Properties of different actuator materials, from [13] 18

2.1 Previous investigations of static modulus in polypyrrole 49

5.1 Electroactive results for stretched and rolled films 143

6.1 Conditions for different polypyrrole electrodeposition recipes 156

6.2 Measured properties of films from Table 6.1 158

Chapter 1

Introduction

1.1 Motivation

As engineers develop devices inspired by nature in their function, mechanics, and style, they create a need for new, muscle-like materials to drive these devices. Engines and motors can be made to be very efficient, but they tend to be bulky, inflexible and not always appropriate for biomedical engineering or personal actuator applications. For example, small machines that emulate fish or insect locomotion must be powered by something that is lightweight and flexible. Soldiers, fire-fighters and other first responders are often hindered by having to carry heavy loads into intense situations. Muscle-like actuators incorporated into their equipment to increase their performance and help keep them safe will not be practical if the actuators require very heavy battery packs, noisy combustion engines or continuous access to a stationary power source. Instead, a new technology must be developed that can convert energy to work quietly and efficiently, without the bulky constraints of traditional motors and engines.

To address this need, a range of novel, "artificial muscle" technologies are being developed, some examples of which are presented in Table 1.1. These materials respond to an electrical, thermal or chemical impulse by changing shape, and can be used to move parts in devices in the same way that human muscles move parts of the body. It should be noted that these artificial muscle materials cannot replace

natural muscle, and may never do so. They are so named because they operate in a muscle-like way, i.e. they operate silently, they are lightweight, flexible, and powerful, and they consume relatively little energy.

Duplicating the properties of natural muscle is a significant challenge for engineers, as natural muscle has evolved over thousands of years and is seamlessly coupled with systems for sensing, energy supply, waste removal, and self-regeneration. However, much can be learned from the highly specialized nature of muscle, in that it is nanostructured to have exactly the right elements for actuation. The overall goal of this thesis is to produce an actuator out of synthetic materials that uses a specialized microstructure to increase its electroactive properties to mimic skeletal muscle.

Actuator	Active strain (%)	Active stress (MPa)	Work density (kJ/m^3)	Peak Strain Rate (%/s)	Efficiency (%)	Advantages	Disadvantages
Mammalian Skeletal Muscle	**20**	**0.35**	**8**	**> 50**	**~ 40**	Has systems for heat and waste removal, energy delivery and regeneration	Requires specialized chemical and thermal environment, not synthetically produced
Dielectric Elastomers	Up to **380**	**~ 1**	Up to **3400**	**4,500**	Typically **30**, up to **90**	Very high strains and strain rates	High voltages (>1 kV) and fields (~150 MV/m) required
Liquid Crystal Elastomers (thermally or electrically activated)	**45** in thermal, **2-4** in electrical materials	**0.01-0.5**	**~ 20**	**30** in thermally activated, **1000** in electrically	**75** in electrical materials	Large strain for thermal materials, fast strains for electrical. Photo-activation has been achieved	Thermal versions are slow unless very thin or photoactivated. Electrical versions require high fields (1- 25 MV/m)
Polypyrrole (conducting polymer)	Up to **39** reported, **5** reliably	Up to **30**	**100**	**12**	**20**	Low voltage (~2 V) High stress and strain	Slow (often run at several Hz to achieve full strain)
Ionic Polymer Metal Composites	**0.5-3**	**3**	up to **5**	**3**	**1.5-3**	Low voltage (<10 V), mechanical amplification gives large displacements	Only useful for bending (not linear) motion
Carbon Nanotube Actuators	**< 1**	up to **30**	**2**	**20**	**0.1**	Large operating temperature range. Low voltage.	Materials are expensive, active strains are very low
Thermally Activated Shape Memory Alloys	**5**	up to **200**	**> 1000**	**300**	**< 5**	Very high power (>100 kW/kg). Low operating voltage	Difficult to control (run between fully contracted and extended but not between)

Table 1.1: Properties of different actuator materials, from [13]. Some materials, such as dielectric elastomers and liquid crystal elastomers, can achieve very high strains and strain rates but require large voltages or electric fields to run them. Other materials, such as ionic polymer metal composites and carbon nanotube actuators, run at much lower voltages but do not show strains that are comparable to muscle. Polypyrrole provides a material that runs at a low operating voltage, but still achieves moderate actuation metrics.

The ideal actuator would not only actuate in a muscle-like way, its metrics would actually exceed mammalian skeletal muscle. It would strain above 20% when actuated, but not require more than a few volts to do so. It would be flexible enough to show a large active strain, but stiff enough to provide a large active stress and to be held in tension without excessive creep. It would work at the range of temperatures in which humans live (-20°C to 40°C) and run off of a portable power source. And finally, it would be able to run for millions of cycles without degradation. As shown in Table 1.1, there are currently no technologies that can meet all of these requirements. For example, dielectric elastomers can have exceptionally high strains and efficiencies, but require huge power supplies to run them at voltages of 1 kV or more. This makes them impractical and dangerous for many biological applications. Carbon nanotubes, on the other hand, are lightweight, require very little voltage and show a reasonably high strain rate. Unfortunately, the total active strain achievable is too low for many applications.

The perfect artificial muscle material does not yet exist, but in this thesis we seek to improve our understanding of and the performance achievable by a certain class of actuators: conducting polymers. By studying the connection between microscale structure and macroscale electroactive response, we improve our understanding of conducting polymer actuation and develop methodologies for harnessing that microstructure to improve electroactive response.

1.2 Material Platform

Of the artificial muscle technologies available, conducting polymers such as polypyrrole provide a particularly attractive platform because they are inexpensive to manufacture ($3/kg). thermally and chemically robust, require very little voltage to operate (1 to 3 V). and have good electroactive properties (Table 1.1). The first conducting polymer. polyacetylene. was first published in 1977 [14] and garnered the Nobel prize in chemistry for Shirakawa, MacDiarmid and Heeger in 2000 [15]. Some other commonly used conducting polymers are shown in Figure 1-1. Conducting polymers have

conjugated backbones that allow electrons or holes introduced into the backbone via doping to easily travel along the chain. Details about the mechanism of conductivity in conducting polymers will be discuss in Section 3.1.

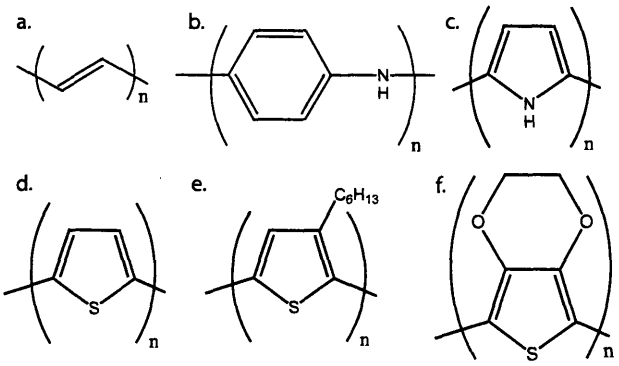

Figure 1-1: Commonly used conducting polymers. a) Polyacetylene (PA). b) Polyaniline (PANI). c) Polypyrrole (PPy). d) Polythiophene (PT). e) Poly(3-hexylthiophene) (P3HT). f) Poly(3,4-ethylenedioxythiophene) (PEDOT).

Actuators made from conducting polymers were first proposed in the early 1990s [15–18], when it was discovered that cycles of oxidation and reduction in an electrochemical cell led to a volume change and force production. It is interesting to note that at the time, conducting polymers were generally being developed for electronic and battery applications in which a volume change upon charging or discharging was a *problem* to be overcome. The accepted actuation mechanism for these materials is based on volume changes that result from the uptake or exclusion of counter ions to maintain electro-neutrality during a redox cycle [19, 20], and will be discussed in detail for polypyrrole in Section 2.3.

Of the electroactive polymers currently available, polypyrrole and polyaniline have shown the largest active stresses and strains, and have spawned the most actuator-related research and development. Polyaniline is an interesting actuator candidate because it is more processable than polypyrrole [21,22], but it is used in acidic environments where the pH is below 4.5 [23,24]. Polypyrrole provides a conducting polymer actuator platform that regularly achieves comparable active strains to polyaniline and can be actuated in a variety of less severe environments [13, 20, 25, 26]. Recently, very large metrics (up to 39% maximum strain, over 10% repeatable strain) have

been reported for polypyrrole synthesized [3, 27–29] and actuated [3, 30, 31] in novel electrolytes. As will be discussed in Chapter 6, we have observed some of these large maximum strains to be transitory and therefore currently impractical for electraoctive devices. However, we have observed large (over 10%) repeatable strains for processed films (Section 5.3), and the promise of larger strains with improved processing remains. The large electroactive metrics, light weight, low operating power and potential for improvement make polypyrrole an attractive candidate for actuator development.

The microstructure of polypyrrole is yet unclear, as will be discussed at length in Chapter 4. Questions typically asked about polymer systems, such as the molecular weight or percent crystallinity, are still unknown for polypyrrole. After it is synthesized, polypyrrole is insoluble and unmeltable, rendering many polymer characterization techniques impossible and making it very difficult to manipulate or change its microstructure. Conducting polymers such as polypyrrole can be substituted, copolymerized or blended with flexible polymers to improve their processability or solubility, but it is difficult to significantly increase their processability via thermal and chemical means without negatively affecting their conductivity [32–39].

Polypyrrole has been extensively studied as an electroactive material, but these studies have provided little elucidation as to the nanoscale mechanisms of actuation and how the morphology accommodates (or hinders) those mechanisms. We believe that it is imperative to discover and to take advantage of the link between morphology and electroactive performance. Moreover, controlling polymer chain configuration and electronic properties at a sub-micron level will enable development of a superior conducting polymer actuator that shows a larger, faster macroscopic electroactive response.

1.3 Thesis Overview

The first step towards understanding how actuation is controlled by structure is to further elucidate the microstructure of polypyrrole. We have used electrochemistry,

microscopy and x-ray and electron diffraction to probe the micro and nanoscale structural elements that contribute polypyrrole's success as an actuator. The results of these studies are presented in Chapter 2 and Chapter 4. In Chapter 4, we propose a new description of polypyrrole microstructure that explains the diffraction patterns we (and others) observe, as well as polypyrrole's mechanical, electrical, and electroactive properties.

We also seek to manipulate the structure of polypyrrole to increase the electroactive properties currently observed. It has been previously shown that every aspect of the polypyrrole polymerization conditions (including solvent, dopant, temperature, electrochemical conditions and electrode material) contributes to the morphology of the final polypyrrole product. In order to understand how the material can be changed and what effect these changes may have on actuation, we have reviewed prior studies on polypyrrole production and structure in Chapter 3. Our work to achieve new morphologies by altering the polymerization conditions is presented in Chapter 6.

While altering the deposition conditions can change the polymer film properties significantly, we also seek to improve the properties of polypyrrole films post-deposition. By mechanically deforming the films to have anisotropic textures (observable by x-ray diffraction) and then measuring the films' electroactive properties, we can observe how different chain arrangements affect the electroactive response. This work has led us to new insights to the nanoscale mechanisms of actuation as well as significant improvements in the magnitude of electroactive response, and is presented and discussed in Chapter 5.

Over the course of this thesis, new insights to polypyrrole structure and the mechanism of actuation are discussed and methodologies to control structure and improve polypyrrole actuation are presented. These findings are summarized with our suggestions for future work in Chapter 7.

Chapter 2

Synthesis and Characterization of Polypyrrole Actuators

In this chapter, our standard methods for producing and testing polypyrrole films are discussed, to give the reader a context for the polypyrrole actuators we develop. Production of polypyrrole is discussed in Section 2.1 and methodologies for testing conductivity and surface morphology are presented in Section 2.2, to set the stage for the experimental results that will be presented in the following chapters. We test the electroactive properties of our films using a custom-built electrochemical dynamic mechanical analyzer that is described in Section 2.3, along with the testing details and factors influencing the electroactive response. The way that polypyrrole's mechanical properties change during actuation is reviewed and further studied in Section 2.3.8, to improve our understanding of the mechanics of actuation. Finally, the effect of the ageing on polypyrrole actuators is discussed Section 2.3.9.

2.1 Synthesis

Polypyrrole is representative of many conducting polymers in that it can be electrically or chemically polymerized to make an insoluble, free-standing film. Electropolymerized polypyrrole typically has a conductivity of to 3 to 5 $\times 10^4$ S/m, an elastic modulus around 0.2 GPa, and an ultimate tensile strength around 30 MPA.

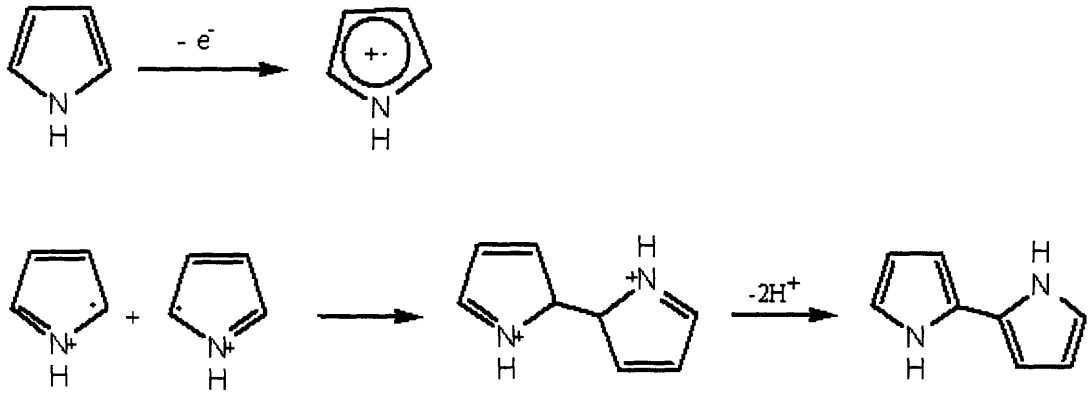

Figure 2-1: Polymerization mechanism for polypyrrole. A typical deposition solution is 0.05 M pyrrole, 0.05 M tetraethylammonium hexafluorophosphate and 1%vol water in propylene carbonate. The polymerization results in a robust, conducting film doped with hexafluorophosphate anions.

2.1.1 Electropolymerization

The most conductive and electroactive pyrrole films are made via electropolymerization. The exact mechanism of the polymerization reaction is the subject of debate [40], but it is generally believed that a pyrrole monomer is oxidized, forming a cation with several resonance forms. Two cations then come together to form a dimer. This reaction is shown in Figure 2-1 [41, 42]. This dimer is then oxidized to form a new cation, and the chain continues to grow. Whether additional pyrrole monomers, dimers or chains are added to the growing chain is not yet well understood. Sadki et al. published a review in 2000 that covered several of the possible mechanisms [40].

Electropolymerization takes place in an electrochemical cell, an example of which is shown in Figure 2-2. Polypyrrole is polymerized from a solution of 0.05 M pyrrole, 0.05 M counterion salt (tetraethylammonium hexafluorophosphate (TEAPF6) or tetrabutylammonium hexafluorophosphate (TBAPF6)), and 1%vol water in propylene carbonate. We deposit from a two-electrode cell, with a glassy carbon working electrode and copper foil counter electrode. Films are deposited at constant current (galvanostatically), at 1 A/m^2 of working electrode. The entire reaction is conducted at -40°C, to minimize cross-linking and branching of the growing polypyrrole chain.

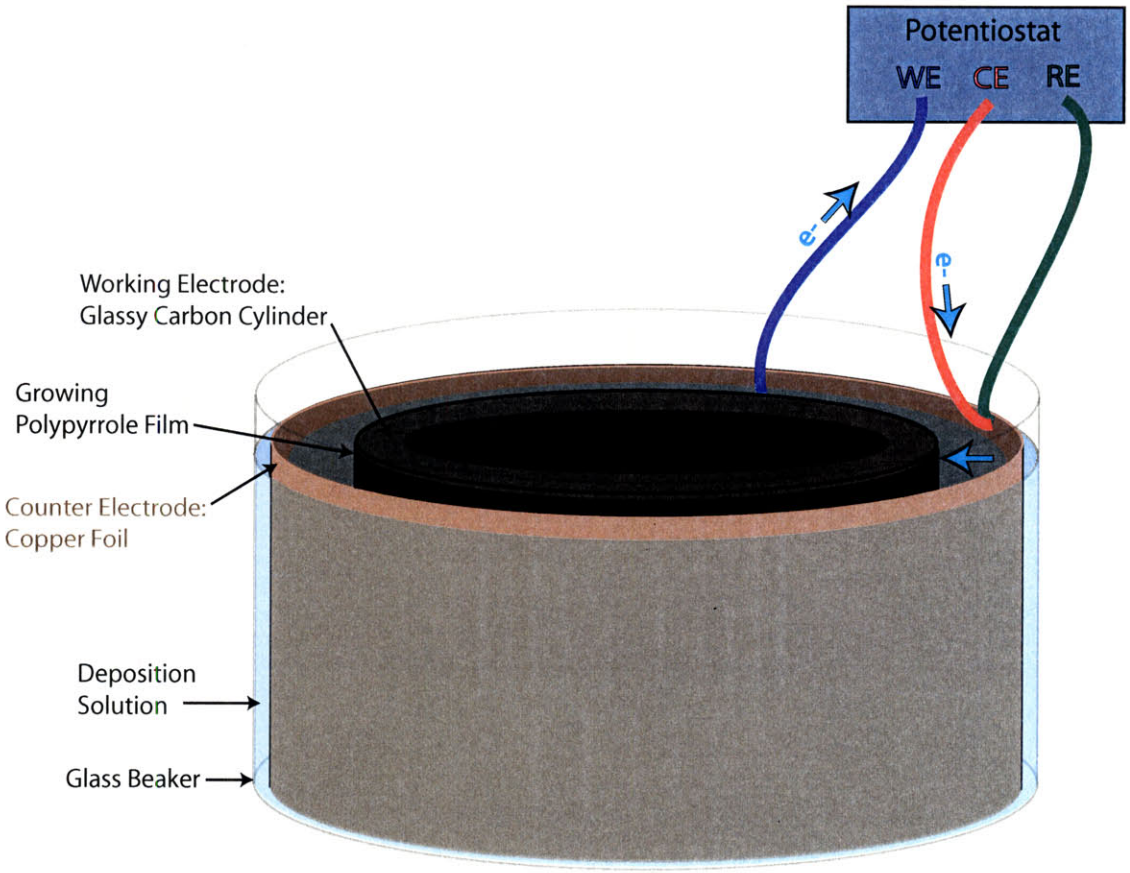

Figure 2-2: Standard large scale deposition cell. A glassy carbon cylinder (diameter = 75 mm, height = 100 mm) is used as the working electrode, and placed in the center of the deposition solution bath. A copper foil is used as the counter electrode and reference electrode. A potential is applied between the working and counter electrodes, such that pyrrole oxidation happens at the working electrode surface. Electron flow is shown with blue arrows.

As the polypyrrole chains grow (and their conjugation increases), their oxidation potential decreases resulting in slightly oxidized polymer chains [40]. Anions from solution are incorporated into the polymer matrix to maintain charge neutrality, resulting in a "doped" conducting polymer film at the end of deposition. When using the deposition conditions described here, the film deposits onto the working electrode at a rate of approximately 2 μm/hour. Films used in free-standing actuator applications are typically 10 to 40 μm thick, as thinner films show a faster active strain response but films that are less than 10 μm thick are usually too fragile to handle.

There are many parameters within the electrochemical synthesis that can affect

the properties of the polypyrrole film, including the choice of solvent, electrolyte salt, and electrode materials, the geometry of the cell, the deposition temperature, and the potential or current density at which the synthesis is conducted. The conditions presented above are our "standard" polypyrrole deposition conditions, and are used for all films in this thesis unless specified otherwise. The effects that changing deposition parameters have previously shown on the morphology and microstructure of polypyrrole films is discussed in Chapter 3, while our work towards better understanding of how the different morphologies affect actuation is discussed in Chapter 6.

2.1.2 Chemical Polymerization

Polypyrrole can also be synthesized via chemical polymerization, using a chemical oxidant such as $FeCl_3$ [43, 44]. During chemical polymerization, pyrrole and a water-soluble counterion salt are added to an aqueous $FeCl_3$ solution. The $FeCl_3$ initiates pyrrole polymerization, and the black polymer falls out of solution. This method can be used to coat fabrics or other non-conducting surfaces with polypyrrole, as the polypyrrole will deposit on any surface exposed to the reaction solution.

Alternatively, anhydrous $FeCl_3$ can be dissolved in an organic solvent. When pyrrole is mixed into this solvent, it will be oxidized, and the resulting polypyrrole will precipitate out of solution. Both methods of chemical polymerization produce powdery products that are not free-standing, and are generally used when one wants to coat a non-conductive surface [43–45] or to make polypyrrole with a very large surface area for capacitor applications [46, 47]. Because free standing films are necessary for actuator applications, this work focuses on polypyrrole produced electrochemically.

2.2 Film Quality

There are several metrics by which one can measure the quality of electropolymerized polypyrrole, but two of our most commonly used checks include the electrical conductivity and surface morphology. Conductivity is measured as an indication of the polymer's electronic properties and robustness, while surface morphology has im-

plications in both the speed and magnitude of the electroactive response. The two are often linked, in that the films with the highest conductivity tend to have the smoothest surfaces. Chapters 3, 5 and 6 discuss the ways in which conductivity and surface morphology have been observed to influence actuation at length, but here we discuss the techniques used to measure and understand these properties on their own.

2.2.1 Conductivity Measurements

When polypyrrole is synthesized electrochemically, the chains are left slightly oxidized. Approximately one out of every three monomers has a positive charge, supported by a counterion [48, 49]. One should note that these counterion dopants are different from substitutional dopants in more traditional semiconductors, as they are separate from the polymer backbone and simply donate or accept charges from the polymer chains [50]. Charges (in the case of polypyrrole, holes) can easily move along the polymer chain, due to the delocalized nature of the electronic orbitals. Because no single polypyrrole chain is long and straight enough to transverse an entire bulk sample, the positive charges must "hop" between chains to move across the sample and give the material a measurable bulk conductivity [51]. It is easier for charges to move along the polymer chain than to hop between chains. The conductivity of the bulk conducting polymer same will increase with increasing conjugation length [52,53] and polydispersity of conjugation lengths [52], as both allow charges to traverse more of the sample along a polymer backbone. The detailed nature of polypyrrole's conductivity will be discussed in Section 3.1.

The conductivities of polypyrrole samples are measured using a standard four-point probe connected to an Agilent 3441A $6\frac{1}{2}$ Digit Multimeter. In a four-point probe measurement, one contacts the sample with four point leads in a straight line. A constant current is applied to the two outer leads and the potential drop is measured by the inner leads. When using the multimeter, the measurement is read as resistivity (measured voltage over applied current). Conductivity is typically calculated via the following equation:

$$\sigma = \frac{ln(2)}{\pi Rt} \tag{2.1}$$

where σ is conductivity in S/m, R is the resistivity as measured with the four point probe, and t is the thickness of the sample. However, Equation 2.1 assumes that the width of the sample is 3 to 4 times the distance between the inner leads. In our case, samples are cut to be 10 - 20 mm long $\times$ 1 - 2.5 mm wide in order to capture any anisotropy that may have been induced into the sample (Chapter 5). The leads on the four point probe are only 2.5 mm apart, so the assumption that the width of the sample is much greater than that between the leads is no longer valid. To account for this, we use the following equation:

$$\sigma = \frac{d}{Rtw} \tag{2.2}$$

where d is the distance between the inner leads, and t and w are the thickness and width of the polymer sample. While it is not the standard equation for four point probe measurements, Equation 2.2 has been shown to be quite accurate as long as w is smaller than d [54]. Unprocessed electropolymerized polypyrrole typically has conductivities of 3 to 5×10^4 S/m, while oriented samples can have conductivities up to 1×10^5 S/m. Work towards achieving high degrees of orientation in polypyrrole and its effect on conductivity are discussed in Chapter 5.

2.2.2 Surface Morphology Evaluation

Depending on the polymerization conditions, the surface morphology of polypyrrole can vary from smooth and featureless to a rough, nodular morphology, as shown in Figure 2-3. In some cases both morphologies will be observed on the same film, as the electrode side is smooth while the solution side is rough and nodular. The effect of polymerization conditions on surface morphology is discussed in Chapter 3, and our work towards manipulating surface morphology to improve electroactive response is discussed in Chapter 6. To some extent, one can infer the surface morphology of polypyrrole simply by visually examining the film. While the surface features are too

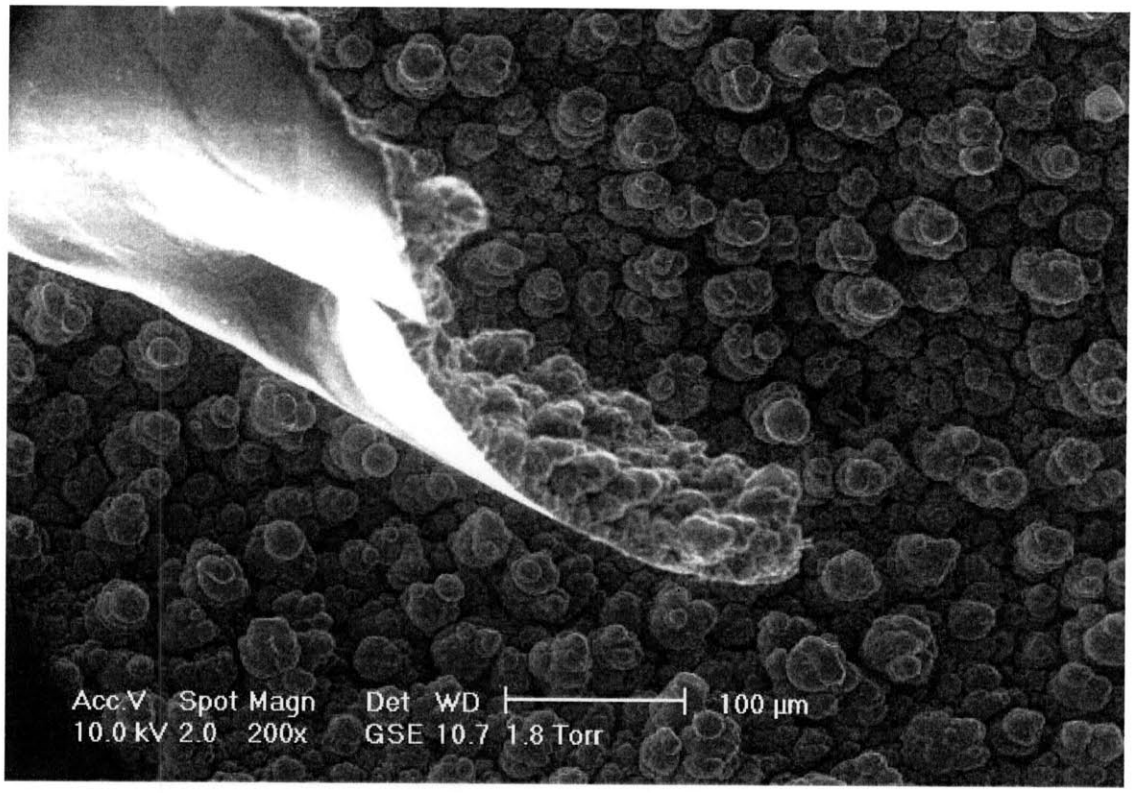

Figure 2-3: Solution and electrode faces of nodular polypyrrole film. A small flap of film has curled back and is observable in the foreground. The bumpy surface observable in the background and on the flap of film is the solution face of the polypyrrole film. The smooth surface observable on the flap of film in the foreground is the electrode face. Microscopy was conducted on an FEI/Philips XL30 FEG ESEM. A voltage of 10 kV and spot side of 2.0 were used. The ESEM was run in environmental mode, and no gold coating of the film was necessary.

small to be discerned by eye, a smooth film will appear shiny under ambient light while a nodular film will appear matte. For more detail on the microscale features that produce this effect, we turn to scanning electron microscopy (SEM).

Electron microscopy of polymeric samples is particularly difficult, as the electron beam can ablate the sample during imaging. Because polymeric materials are generally insulating, there is no mechanism to dissipate the electrons hitting the sample, leading to localized charging and radiation damage. Polypyrrole is more resistant to electron beam damage than non-conductive polymers, as its conjugated structure allows charge to dissipate. However, at slow scan rates, high magnifications, and in

samples of particularly low conductivity, beam damage is often evident (Figure 2-4). Care must be taken to avoid scanning the same area for extended periods of time in order to keep beam damage to a minimum. One alternative is to focus the microscope on one area of the sample, then quickly move the sample and image an adjacent area. As long as the sample height remains constant (so the new area is also in focus) this allows one to avoid imaging areas that have been damaged by focusing. Additionally, a thin (~10 Å) coating of gold can be sputtered onto the sample to help dissipate charge and prevent sample damage during imaging.

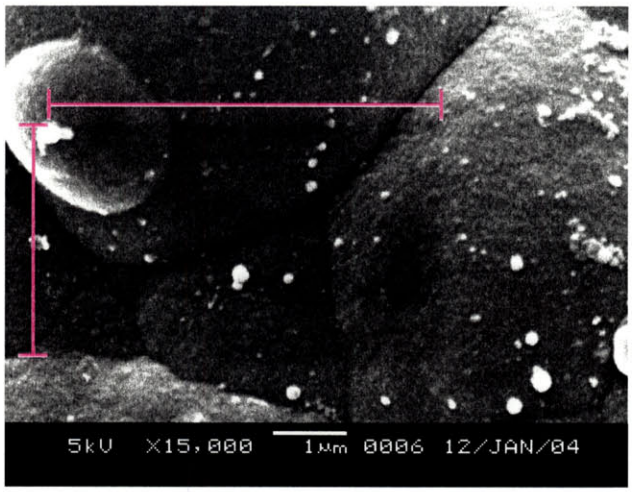

Figure 2-4: Beam damage in polypyrrole sample. Micrograph taken on JEOL JSM-5910 with an accelerating voltage of 5 kV and a spot size of 20. Beam damage is evident in rectangle marked by pink lines. The dark region is due to a lower yield of secondary electrons that may be caused by polymerization of pump oil (deposited onto the sample when the chamber was pumped down) by the electron beam.

For this work, scanning electron micrography was conducted on three instruments: an FEI/Philips XL30 FEG ESEM, a JEOL JSM-5910, and a JEOL JSM-6060. Operating voltages were typically between 10 and 20 kV, and spot size was 2.0 for the XL30 and typically 20 to 40 for the 5910 and 6060. The polypyrrole samples were conductive enough that gold coating of the polypyrrole film was seldom necessary.

2.3 Electroactive Response

Because the goal of this thesis is to increase microstructural understanding and control in order to produce a better actuator, the ultimate measure of polypyrrole film quality is how well it actuates. During actuation, polypyrrole is either oxidized or reduced in the presence of a mobile electrolyte, and ions are incorporated or expelled from the bulk polymer in order to maintain charge neutrality. This incorporation or expulsion results in a net volume change or change in stress state of the polymer. The effect of morphology on actuation is described in Chapter 3, while our work towards improving electroactive response is presented in Chapters 5 and 6. The methods of electroactive testing and typical results for polypyrrole actuators are described here.

We probe polypyrrole's electroactive response either isotonically [55–57], where the polymer is actuated under constant load and its length change is monitored, or isometrically [58,59], where the polymer is held under tension at a constant length and the change in stress upon actuation is monitored. We conduct both testing methods in a custom-built electrochemical dynamic mechanical analyzer (EDMA), a diagram of which is shown in Figure 2-5 [59]. In this apparatus a small ($\sim$ 5 mm $\times$ $\sim$ 2 mm) polypyrrole film is held at constant length (isometric) or constant force (isotonic) while submerged in a liquid electrolyte bath. The film is clamped in two gold-coated clamps, the outsides of which are covered in insulating epoxy to avoid leakage current in the electrochemical cell. One clamp is connected to a Futek 1 N load cell used measure the stress in the polymer, and the other is connected to an Agilent linear stage used to apply tension and measure displacement. Both clamps are used to make an electrical connection between the polypyrrole film and the potentiostat.

The polypyrrole film serves as the working electrode in the electrochemical cell, and is accompanied by a counter electrode (often stainless steel foil) and reference electrode (silver wire). An AMEL 2053 potentiostat is used to apply a user-specified potential waveform between the working and counter electrodes. The applied potential is measured with the reference electrode. A computer is used to control the potentiostat and linear stage, as well as to take current and potential data from the

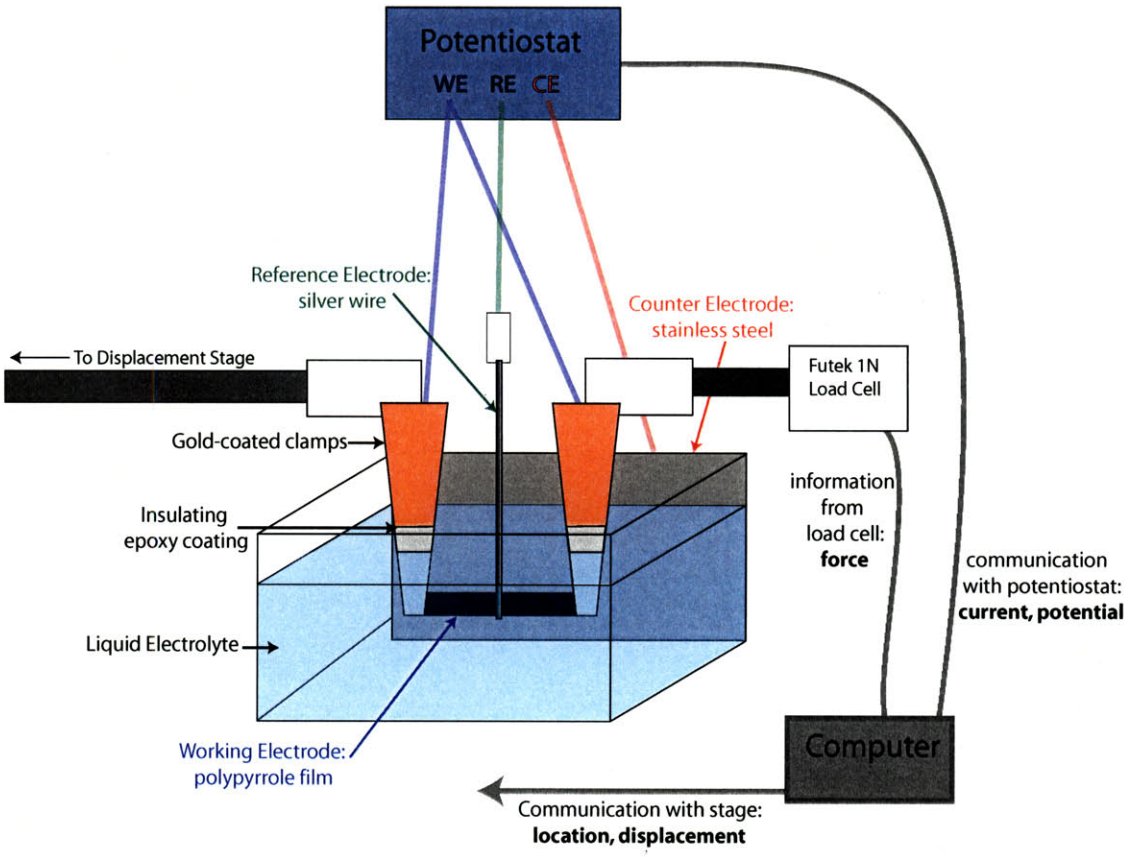

Figure 2-5: Electrochemical Dynamic Mechanical Analyzer (EDMA). The polypyrrole acts as the working electrode in a three-electrode cell, and a potential is applied across the cell by the potentiostat. Linear change in volume or stress state due to ion incorporation or expulsion into the polypyrrole matrix is measured by the load cell and linear stage.

potentiostat, displacement data from the stage, and force data from the load cell. The apparatus is controlled by running custom-built software [59].

2.3.1 Warm-up

Before beginning an isometric or isotonic test, a "warm-up" procedure is conducted to measure the state of the film and ensure that all tests are conducted on comparably swollen films. This procedure also allows one to be sure the active strain measured is not contaminated by the initial uptake of solvent that may occur upon submersion in an electrolyte. This initial uptake can be significantly larger than the repeatable

electroactive response, as will be discussed in Section 6.4.1. Immediately after the film is loaded into the apparatus (before submersion in the electrolyte) its passive elastic modulus is measured by the application of three cycles of 1% strain at a frequency of 1 Hz. The elastic modulus is calculated as the slope of the stress vs. strain curve, and referred to as the "dry" elastic modulus. Figure 2-6i shows the dry modulus for films deposited from propylene carbonate solution. As the black and blue curves in Figure 2-6i show, samples can be stored unsealed for several weeks without an appreciable change in modulus. A significant amount of propylene carbonate (up to 30%wt) remains in the films after deposition, and can remain even after several weeks due to its very low room temperature vapor pressure (40 Pa)[1]. If the film is subjected to vacuum, this residual propylene carbonate is removed and the dry modulus increases (Figure 2-6i, red curve).

A change in deposition recipe may change the dry modulus, as will be discussed in Chapter 6. This change is apparent when comparing the blue curves in parts i and ii of Figure 2-6. The blue curve in Figure 2-6i is from a film deposited from a propylene carbonate solution, and has a modulus of 670 MPa. The blue curve in Figure 2-6ii is from a film deposited from a methyl benzoate solution and has a modulus of 765 MPa. This difference may be due to the higher room temperature vapor pressure of methyl benzoate (130 Pa)[1], which causes more of the residual solvent in the film to evaporate. If a dry film deposited from methyl benzoate solution is soaked in propylene carbonate solution prior to testing, the modulus drops far below that of the standard film (Figure 2-6i, black curve: modulus = 100 MPa).

After the dry passive modulus is measured, the linear stage moves the clamps towards each other until the film is slackened, and the bath is raised to submerge the film into the electrolyte without removal from the clamps. A triangle potential waveform is applied until the current response stabilizes. At this point the film is considered to be in steady state condition for the applied electrochemical conditions. An example of the electrochemistry after warm-up in a solution of 0.1 M Lithium bis(trifluoromethanesulfonly)imide in propylene carbonate (LiTFSI/PC) is shown in

[1]MSDS information from Mallinckrodt Baker, Inc.

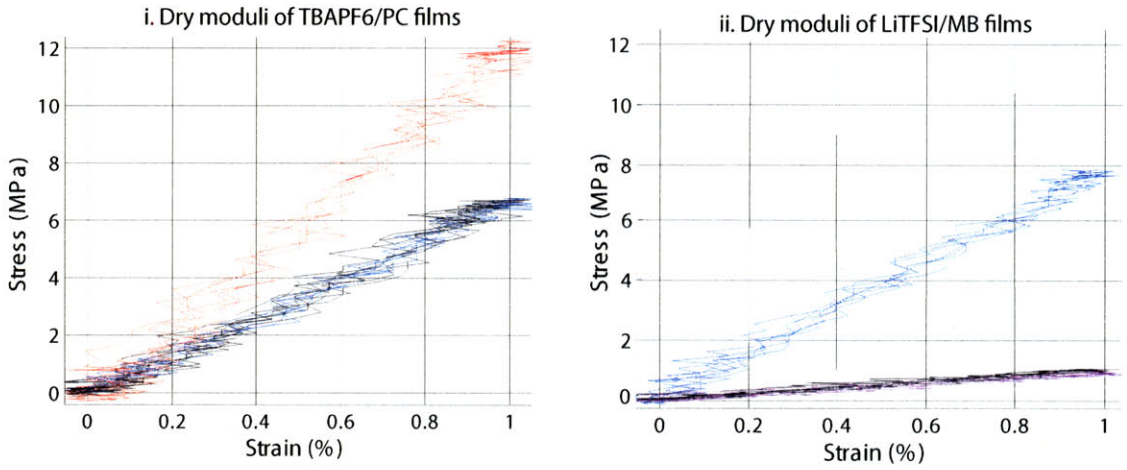

Figure 2-6: Passive modulus measurements for polypyrrole samples. i) Comparison of passive modulus in films synthesized from the standard deposition recipe. Blue curve: film tested one week after deposition. Modulus = 670 MPa. Black curve: film tested five weeks after deposition. Modulus = 670 MPa. Red curve: film tested five weeks after deposition, after exposure to vacuum (94 kPa) for 15 hours. Modulus = 1180 MPa. ii) Comparison of passive modulus in films synthesized from 0.2 M pyrrole, 0.2 M Lithium bis(trifluoromethanesulfonly)imide (LiTFSI) in Methyl Benzoate. Blue curve: film tested four weeks after deposition. Modulus = 765 MPa. Black curve: film tested four weeks after deposition after soaking overnight in 0.1 M LiTFSI/PC Modulus = 100 MPa. Pink curve: soaked film after "warm-up" in 0.01 M LiTFSI/PC/H20. Modulus = 90 MPa.

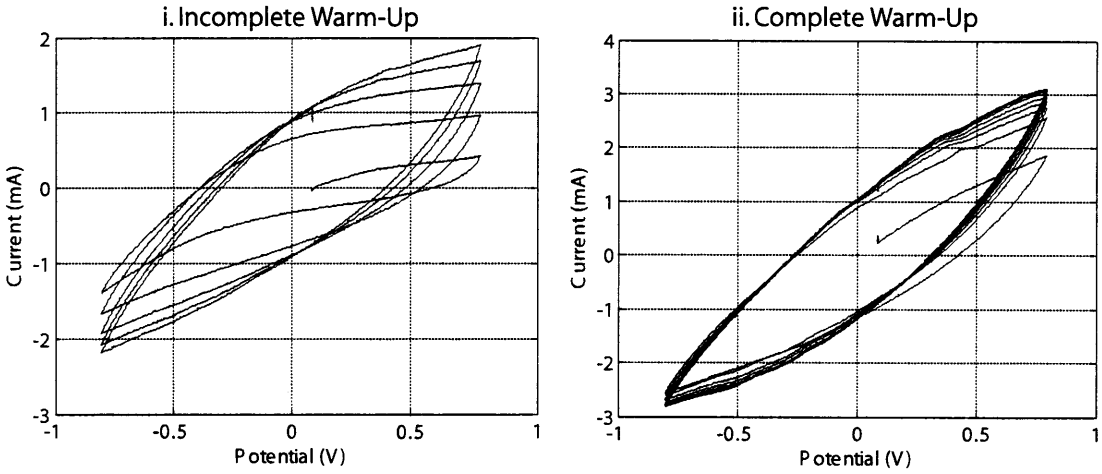

Figure 2-7: Electrochemical warm-up for films actuated in 0.1 M LiTFSI/PC. Films were slackened, and a ± 0.8 V triangle wave was applied at a rate of 0.1 V/s. i) Incomplete warm-up. The current response is changing upon each voltage cycle. ii) Complete warm-up. After initially transient cycles, the current response re-traces the same path upon each additional voltage cycle.

Figure 2-7. The warm-up period usually involves incorporation of solvent and counterions, and when the films are placed back in tension they are usually longer than before warm-up.

After the electrochemical warm-up, the elastic modulus is again measured by the application of three cycles of 1% strain at a frequency of 1 Hz. The electrochemical cycling causes additional solvent and counterions to be incorporated into the film, increasing chain mobility and decreasing elastic modulus (Figure 2-6ii, pink curve). This modulus is referred to as the "wet" elastic modulus.

Elastic modulus can be affected by deposition recipe (Chapter 6) or electrochemical state of the polymer (Section 2.3.8). Post-deposition processing can induce anisotropy to the polymer microstructure, which also significantly affects the passive elastic modulus. This will be discussed in Chapter 5

2.3.2 Isotonic Testing

During isotonic testing, a small load (typically 0.5 to 2 MPa) is applied to the polypyrrole film, and maintained throughout the test. A potential waveform is applied between the film and the counter electrode, causing ions to enter or leave the film, which causes the film to expand or contract. The change in length is measured as the distance the EDMA has to move the stage in order to maintain the constant load. It should be noted that upon ion incorporation the polymer should expand in all three dimensions, but with this apparatus we are only measuring the change in length of the film. The implications of actuation in the other directions will be discussed in Chapter 5.

A diagram of the EDMA cell and an example of typical isotonic data is shown in Figure 2-8. The film in this example is actuated in a solution of 0.1 M Lithium bis(trifluoromethanesulfonly)imide in propylene carbonate (LiTFSI/PC), with the application of a $\pm$0.8 V potential square wave at a frequency of 8.3 mHz (Figure 2-8, line 1). Under these conditions, the $TFSI^-$ anions dominate the electroactive response. As the polymer is held at +0.8 V, it is oxidized (electrons are removed from the film). This causes a buildup of positive charge in the film, so $TFSI^-$ anions are incorporated from solution to balance the charge. The movement of $TFSI^-$ anions causes the observed electrochemical current response (Figure 2-8, line 2), the integral of which is the calculated charge response (Figure 2-8, line 3). The EDMA will allow the polymer film to expand or contract as necessary to maintain the initial load, and this displacement is the measured strain response (Figure 2-8, line 4). In this example, there is a slightly larger expansion (dip to peak) than contraction (peak to dip) as the polymer sample exhibits an overall expansion during testing. The charge also displays a net increase over the course of this test, which may be a result of more ions entering the polymer film than leaving (which would cause this unrecovered film expansion). However, irreversible electrochemistry in the cell (such as degradation of the clamps if they are not perfectly coated, for example) may also lead to a charge imbalance over each cycle.

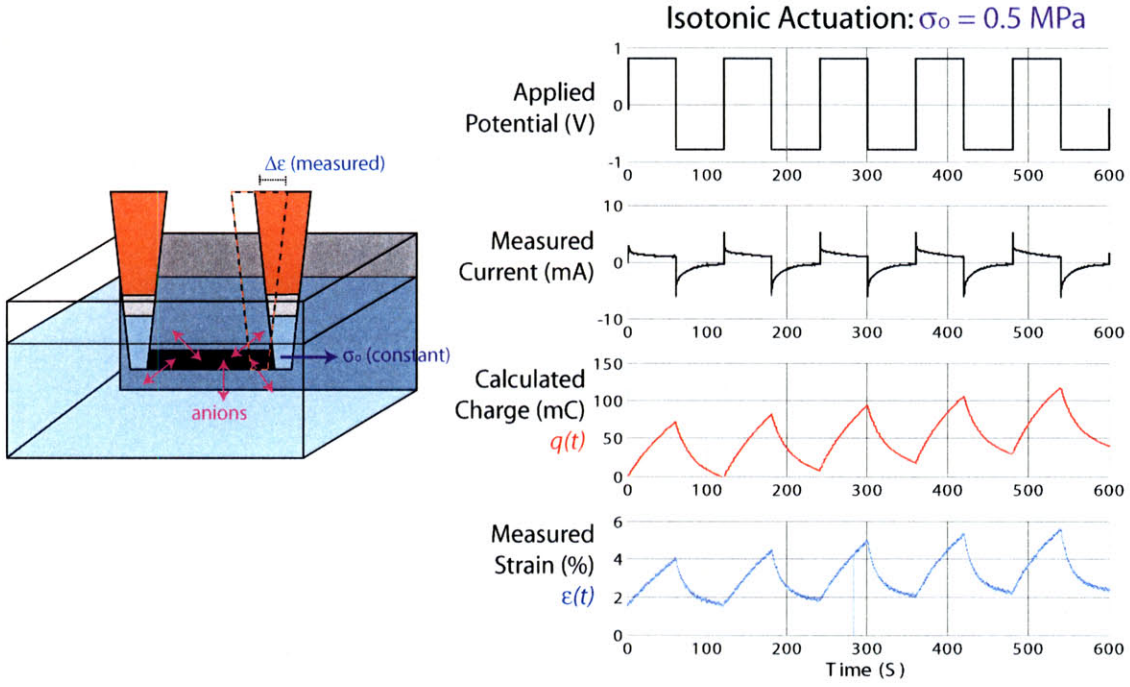

Figure 2-8: Isotonic actuation in 0.1M LiTFSI/PC, with an initial stress of 0.5 MPa. The $TFSI^-$ anions dominate the electroactive response under these conditions. As the polymer is oxidized, $TFSI^-$ anions enter the polymer matrix and the polymer film expands. Upon reduction, $TFSI^-$ anions leave the film and the film contracts.

While it is impossible to exactly quantify the phenomena contributing to charge transfer based on our relatively crude electrochemical tests, one can use the general trend of charge transfer to track ion movement during actuation. When the charge is compared to the isotonically measured strain one can find a constant "strain to charge" ratio for a given sample [41]. This ratio allows one to estimate how much current must be applied (as the current is directly related to the amount of charge inserted into the polymer) to get a certain value of expansion. A good conducting polymer actuator system will have a high strain to charge ratio, so little energy is needed to produce high strains. Polypyrrole has a strain to charge ratio on the order of $\pm 10^{-10}$ m^3/C (assuming isotropic actuation), the sign (positive or negative) of which depends on whether the cations or anions are the mobile species [60]. The exact value of the strain to charge ratio depends on the electrochemical solution used. For example, polypyrrole actuated in 0.1 M tetraethylammonium hexafluorophosphate in propylene carbonate has a strain to charge ratio of approximately 1.3×10^{-10} m^3/C, while polypyrrole actuated in the liquid salt 1-butyl-3-methyl imidazolium tetrafluoroborate has been shown to have a strain to charge ratio up to 8.8×10^{-10} m^3/C [41, 61].

In some cases, the polymer exhibits a net increase in length without a net increase in charge, as the film exhibits irreversible creep. In this work, very small loads are utilized in order to minimize the occurrence of creep, but for some samples it is impossible to avoid. To minimize its impact on our measurements, the "active strain" is measured as the difference between the maximum peak strain and the following minimum strain of each voltage cycle. This corresponds to the contractile strain in the polymer.

2.3.3 Isometric Testing

During isometric testing the polymer film is held at a constant length and subjected to electrochemical cycling. When ions enter the polymer matrix the film would expand, but the length is constrained so instead the stress decreases. As ions leave the film, the film would contract, but the length is constrained so the stress increases. An

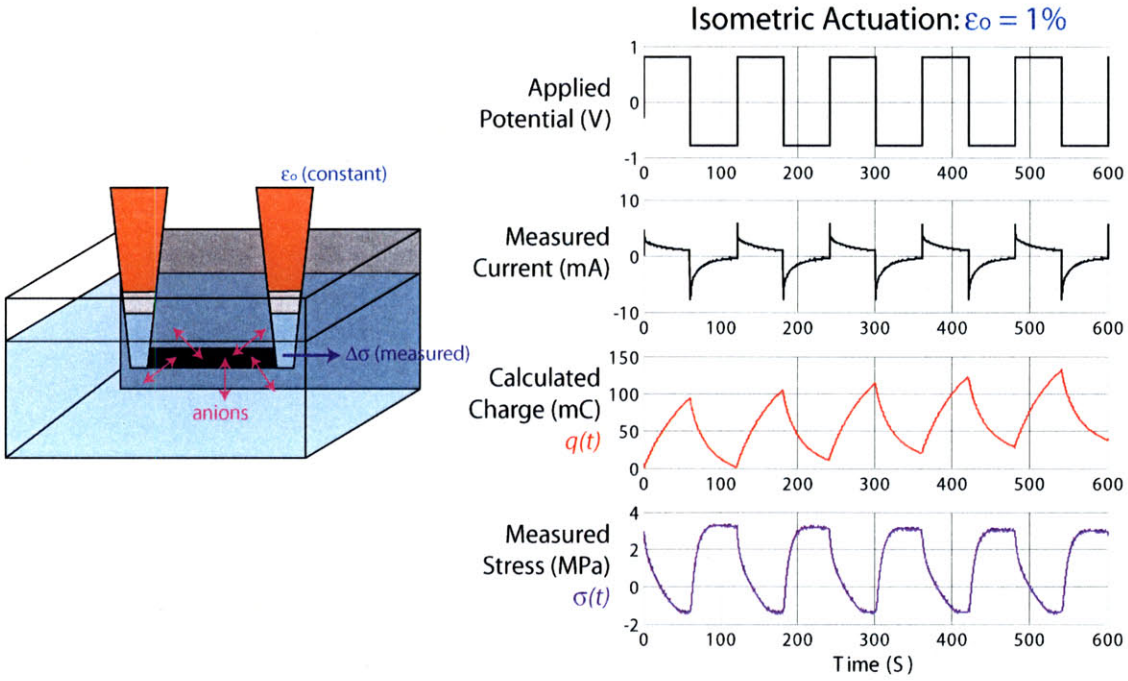

Figure 2-9: Isometric actuation in 0.1M LiTFSI/PC, with an initial stress of 0.5 MPa. The $TFSI^-$ anions dominate the electroactive response under these conditions. As the polymer is oxidized, $TFSI^-$ anions enter the polymer matrix and the polymer film relaxes. Upon reduction, $TFSI^-$ anions leave the film and the stress exerted by the film increases.

example of this is shown in Figure 2-9.

When a film is subjected to the same electrochemical input in isometric and isotonic mode (as was the case for Figures 2-8 and 2-9), the difference in time constants for the two modes is apparent. Upon reduction in this particular electrolyte the $TFSI^-$ anions leave the film and the film either contracts (isotonic mode) or the stress in the film increases (isometric mode). In isotonic mode, the film contracts over the entire 60 second reduction cycle. In isometric mode, the stress increases for the first 10 seconds of the cycle, and then levels off. The geometrical constraint of the isometric test prevents further contraction in the direction being measured. It is likely that after the first 10 seconds the polymer film begins to contract anisotropically - the length is held constant while the unconstrained sides of the film contract.

We have often observed that the rate of ion influx and expulsion are different, and this has previously been reported in the literature for conducting polymer systems

[62]. In Figures 2-8 and 2-9, the shape of the stress and strain responses for ion influx and expulsion are different, and in both cases the ion expulsion happens more quickly than ion incorporation. This may be due to the compressive forces exerted by the polymer matrix. When the polymer film is oxidized, the anions must overcome the resistance of the polymer matrix to expansion, increasing the time needed for swelling. Upon reduction, the retractive forces exerted by the swollen polymer matrix help push the anions out, decreasing the time needed for contraction.

2.3.4 Mobile Species

Both the cations and anions in the electrolyte are theoretically capable of neutralizing the applied charge by entering or exiting the polymer film. However, electropolymerized polypyrrole is a cationic system, i.e. the chains are oxidized [26]. During gentle electrochemical cycling, the chains become slightly more or slightly less oxidized, but remain positively charged. Thermodynamically, this means that the system should be balanced by anion incorporation or expulsion. Whether or not this thermodynamically favored response is observed will depend on the kinetics of the movements of the various species. In some cases the movement of both species is observed, while in other cases one species clearly dominates. The experimental parameters that affect which species are observed in the electroactive response are discussed in the following sections.

While scientifically interesting, systems that exhibit dual ion movement are very inefficient actuators. Expansion or contraction instigated by the movement of one ion is counteracted by the opposite movement of the other ion. When building devices, an electrochemical system should be chosen where one ion dominates the electroactive response.

Effect of Species Size

A significant size differential is the most commonly used method to isolate the movement of one ion. If the anion is small and mobile when compared to the cation, it

will generally dominate the electroactive response. For example, when polypyrrole is placed into a solution of tetrabutylammonium hexafluorophosphate (TBAPF6) in propylene carbonate (the species shown in Figure 2-10), the PF_6^- anions dominate the electroactive response over the majority of potentials. When the polypyrrole is oxidized, the PF_6^- anions enter the polymer film, causing the film to expand. When the polypyrrole is reduced, the PF_6^- anions are expelled from the polymer film, causing the film to contract. If the anion is so large that it is effectively immobile under the electroactive conditions used, the cation will dominate [25, 26, 63]. For example, with sodium dodecylbenzenesulfonate (NaDBS) (the species shown in Figure 2-11), the film expands upon reduction (as cations diffuse into the film) and contract upon oxidation (as cations leave the film).

If a system is chosen to have a cation and anion that are similar in size and mobility, the motion of both species can be observed [20, 26, 63–68]. For example, as the film is reduced, the film may contract while the anions are expelled. As it is reduced further, it will expand while the cations are incorporated. The opposite ion movement will occur upon oxidation [20, 63, 64]. As the discrepancy between the size of the two ions increases, so does the permiselectivity of the actuation mechanism [66].

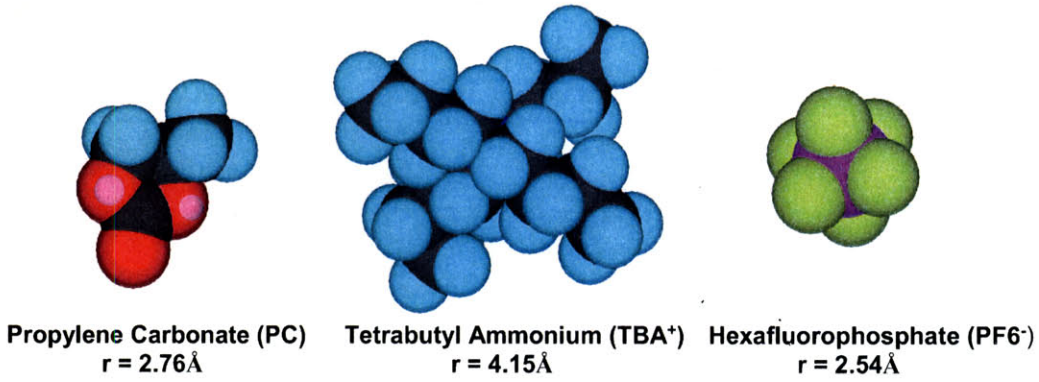

Figure 2-10: Relative sizes [69] of species in an anion-dominated electrolyte system. Tetrabutylammonium hexafluorophosphate is dissolved in propylene carbonate (typical concentrations are 0.05 M to 0.1 M) and used as the electrolyte for electroactive testing.

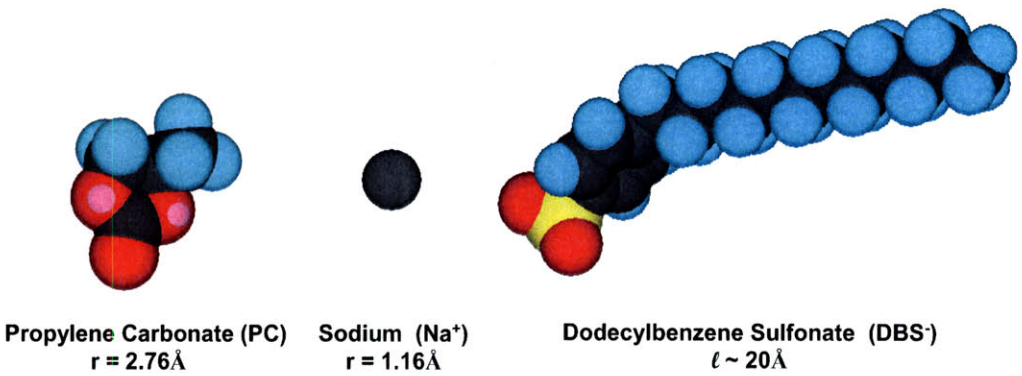

Figure 2-11: Relative sizes [69] of species in a cation-dominated electrolyte system. The dodecylbenzenesulfonate (DBS) anions are too large to effectively enter or leave the polypyrrole matrix, so upon actuation only sodium movement is observed.

Effect of Electrolyte Concentration

The likelyhood of dual ion movement also increases with increasing electrolyte concentration. For polypyrrole doped with DBS and actuated in aqueous NaCl, Bay et al. observed a cation-dominated response at low concentrations, and observed both ions moving at higher concentrations [70]. Bruckenstein et al. also observed a dependence on electrolyte concentration for polypyrrole actuated in aqueous sodium tosylate [62, 65]. At lower concentrations (0.01 or 0.1 M) only anions could be observed moving when the potential was scanned at 2 mV/s. At a higher concentration (0.5 M) this permiselectivity was lost.

Effect of Scan Rate

As an electrochemical stimulus is applied, there will be a competition between the kinetically favored species and the thermodynamically favored species. For example, Bruckenstein et al. used an electrochemical quartz microbalance (EQCM) to measure the mass of a polypyrrole film during electrochemical cycling in 0.5 M NaCl in water, and found that the mobile species could be dictated by the potential scan rate. At high scan rates (100 mV/s) a reduction of the sample led to an increase in mass [62, 65]. This implies that the cations were dominating the electroactive response, as ions entered the film upon reduction. At slow scan rates (2 mV/s) reduction of

the same amount of charge lead to a decrease in mass [62, 65]. This implies that the anions were dominating the electroactive response, as ions left the film upon reduction. It is clear from this data that which species (cations, anions, or solvent) dominates the electroactive response is influenced by the kinetics of the system. At faster scan rates the smaller (and therefore kinetically favored) cations dominated the response, while at slow scan rates the larger (but thermodynamically favored) anions dominated [62, 65].

2.3.5 Solvent Transfer

In addition to ion influx and expulsion, it expected that the electrolyte solvent moves in and out of the material during actuation. Solvated ions will pull solvent molecules into the polymer as they are incorporated [65, 68, 71]. Several authors have also described a contribution from solvent not directly associated with an ion. Bay et al. observed a larger electroactive response for polypyrrole actuated in dilute aqueous NaCl than in more concentrated NaCl, and attributed this to an osmotic effect [68]. The authors theorize that as counterions swell the polymer, solvent also enters the polymer matrix to maintain the osmotic balance with the surrounding electrolyte. This results in a larger net expansion than can be explained by the amount of charge passed. Velmurugu and Skaarup confirmed this result for NaCl and NaBr solutions of different concentrations [71].

During the quartz microbalance experiments discussed earlier, Bruckenstein et al. observed that for all but the slowest scan rate, the sample mass did not return to its original state upon the completion of one cycle, even though the charge did [65, 67]. Other researchers' EQCM experiments have shown similar results [62, 66]. The fact that the change in mass does not correspond to the change in charge implies the transfer of a neutral species at a slower timescale than the species maintaining charge neutrality. Hillman et al. commented that neutral solvent movement would naturally be slower than ion transfer because it is unassisted by migration [62]. Contrary to the conclusions of Bay and Velmurugu, Bruckenstein et al. claim that the neutral species transfer counteracts the ion-induced volume change. They theorize that

solvent enters the polymer matrix as ions leave, helping the film to maintain a constant volume [65, 67]. The assumption that polypyrrole deposited onto an EQCM would maintain constant volume during electrochemical cycling is tenuous, considering polypyrrole's well-documented success an actuator. Bruckenstien et al. did not measure the dimensions of their sample during or after electrochemical cycling, so their assumption of constant volume is unsupported.

One should note that experiments discussed in this section where neutral solvent transfer was observed all took place in aqueous solutions. It is probable that an equivalent phenomenon happens in non-aqueous electrolytes, but this has not yet been explicitly shown.

2.3.6 Actuation in Liquid Salts

The assumption that polypyrrole should thermodynamically be an anion transfer system does not explain the results observed when actuating polypyrrole in 1-butyl-3-methylimidazolium hexafluorophosphate, (BMIMPF6). Neat BMIMPF6 is one of a growing library of ionic compounds that are liquid at room temperature. commonly referred to as "liquid salts." Liquid salts can be used as electrolytes in electrochemical cells without the addition of solvent. In neat BMIMPF6 the cations dominate the electroactive response, which means that film expands upon reduction and contracts upon oxidation [63. 72, 73]. This behavior is surprising, because in this system the $BMIM^+$ cation (ionic radius = 3.30 Å) is larger than the PF_6^- anion (2.54 Å) (Figure 2-12) [74]. It is not entirely understood why in BMIMPF6 the $BMIM^+$ cation dominates the electroactive response. It may be because the diffusivity of the $BMIM^+$ cation is higher than the PF_6^- anion in neat BMIMPF6 [75], or because the cations self-assemble on the polymer film surface, blocking anion movement [59, 76, 77].

Polypyrrole has been shown to give a larger electroactive response in neat liquid salt than in solvated electrolytes [59, 61, 73, 78], but the reason for this improved electroactive performance has not been explicitly proven. It may be because of the extremely high concentration of ionic species in the liquid salts. For neat BMIMPF6 the electrolyte concentration is 4.2 M, which is considerably higher than the 0.05 to

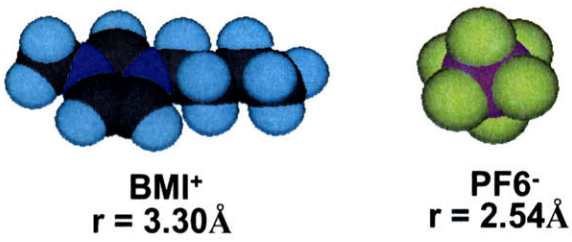

Figure 2-12: Relative sizes of species in neat BMIMPF6 [69, 74].

1 M concentrations typically used in solvated electrolytes. This means that when actuating in neat BMIMPF6 there is an effectively constant reservoir of cations available near the film surface to participate in actuation. Additionally, ionic liquids are more electrochemically stable than most solvated electrolytes [72, 73], so more aggressive potentials can be applied resulting in larger electroactive responses without electrolyte breakdown.

Liquid salts such as BMIMPF6 can also be dissolved in organic solvents, and used as more traditional electrolytes. In dilute (0.05 M) BMIMPF6/PC, the potential waveform can be adjusted such that movement of the $BMIM^+$ cation or the PF_6^- anion can be observed in the electroactive response. Dual ion movement has been observed in many electrolyte systems [20, 63–67], but in this example we specifically chose potentials and timescales at which one ion clearly dominates the response. If the potential is switched between 1 V and 0 V at 0.05 Hz, one observes a stress response dominated by the PF_6^- anions. When the polymer is oxidized, PF_6^- anions enter the polymer bulk and the film relaxes. When the polymer is reduced, the PF_6^- anions leave and the film contracts. This response is shown in the isometric test in Figure 2-13i, where the stress decreases as the charge increases (as PF_6^- enter the film during oxidation), and the stress increases as the charge decreases (as PF_6^- leave the film during reduction). The opposite response is observed when one switches the potential between 0 V and -1 V at 0.05 Hz, as shown in Figure 2-13ii. The stress increases as the charge increases (as $BMIM^+$ cations leave the film during oxidation), and the stress decreases as the charge decreases (as $BMIM^+$ cations enter the film during reduction).

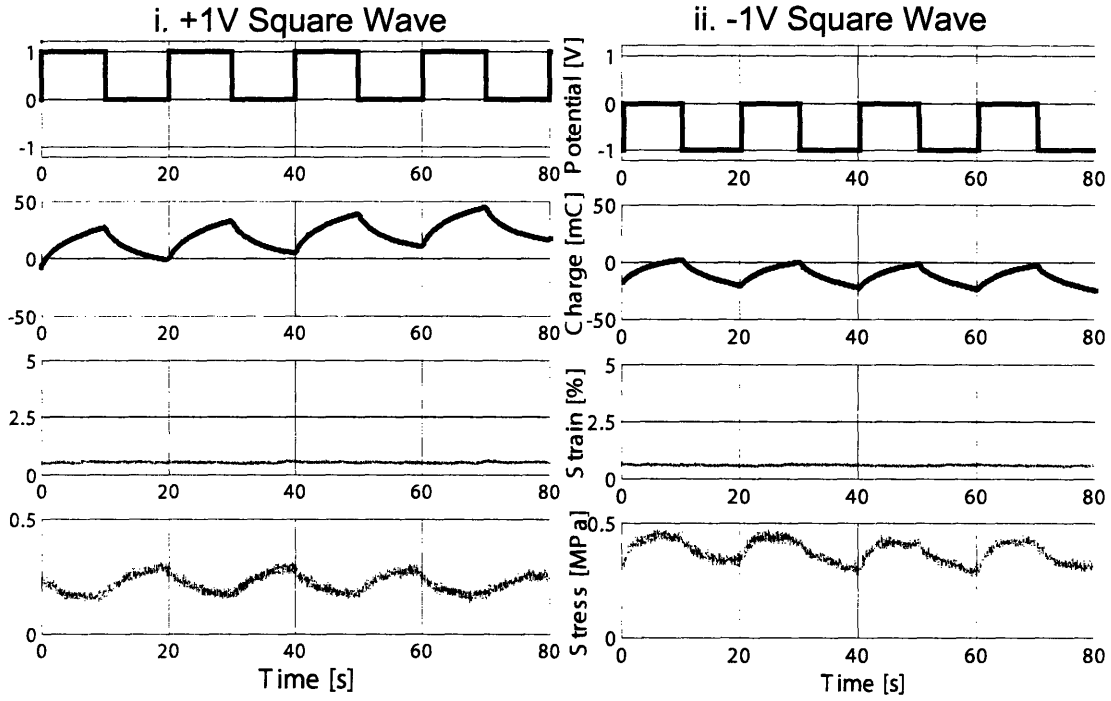

Figure 2-13: Isometric testing in BMIMPF6/PC. i) The film was held in tension at a constant strain of 0.6%, resulting in an initial stress of 0.25 MPa. A +1V potential square wave was applied at a frequency of 0.05 Hz, and the stress response was measured. The active stress decreases upon oxidation and increases upon reduction. ii) The film was held in tension at a constant strain of 0.6%, resulting in an initial stress of 0.32 MPa. A -1V potential square wave was applied at a frequency of 0.05 Hz, and the stress response was measured. The active stress increases upon oxidation and decreases upon reduction

2.3.7 Speed of response

The speed of actuation is limited by the rate at which the counterions can diffuse through the polymer film. When polypyrrole is oxidized in the presence of TEAPF6, the negative PF_6^- anions in the solution are attracted to the polymer surface, while the positive TEA^+ cations are driven away. The high concentration of PF_6^- anions at the polymer surface will drive diffusion of anions into the polymer, causing the increase in volume upon actuation [79]. This diffusion has been described by the equation for Brownian motion (Equation 2.3):

$$x^2 = Dt \tag{2.3}$$

where x is the diffusion length, D is the diffusivity, and t is the time for diffusion. This means that if x is halved t will be quartered, so a small change in the diffusion length will significantly decrease the diffusion time. Polypyrrole film actuators typically have strain rates of approximately 1%/sec [41, 60, 80], and are limited by the small diffusivity of the ions through the polymer film (10^{-10} to 10^{-15} m^2s^{-1}) [41, 81]. The diffusivity of PF_6^- in films produced as part of this work has been measured to be on the order of 10^{-12} m^2s^{-1} [82]. As one would expect, the size of the counterion influences the diffusivity in polypyrrole, with small anions such as Cl^- having diffusivities on the order of 10^{-10} m^2s^{-1}, while a larger ion such as tosylate has a diffusivity on the order of 10^{-13} m^2s^{-1} [81]. Furthermore, polymer chain orientation induced by processing also has implications for the magnitude and anisotropy of diffusion, as is discussed in Chapter 5.

It should be noted that there are factors in this system that complicate diffusion beyond simple Brownian motion. For example, upon severe reduction the polypyrrole film may not be conductive enough to assume all charges are instantaneously transported to the surface, so migration effects may be introduced [83, 84]. The actuation of free-standing films is studied via bulk measurements, so gradients through the film that may occur at short timescales are missed. Furthermore, as was mentioned previously, we have often observed that the rate of ion influx and expulsion are different.

In addition to the resistance of a polymer matrix to expansion, a change in mechanical properties of the polymer film could be occurring during electrochemical cycling. This change may take place on a different timescale from the electrochemically induced swelling and contracting, and is investigated in the next section.

2.3.8 Dynamic Elastic Modulus

In addition to the change in film volume or stress state, it has also been observed that mechanical properties such as the elastic modulus change upon conducting polymer oxidation and reduction. However, previous investigations of this change in modulus in polypyrrole have had quite varied results. For example, several authors have held a polypyrrole film in an electrochemical cell at a constant potential, then slowly stretched the film to measure the elastic modulus. The results of their analyses are shown in Table 2.1.

When comparing these previous works, one is confronted with discrepancies in magnitude of elastic modulus (as will be discussed later) and change in modulus with oxidation state for polypyrrole. As shown in Table 2.1, an increase in modulus and expansion of the film upon oxidation was observed for actuation in tetrabutylammonium hexafluorophosphate in propylene carbonate (TBAPF6/PC) and aqueous $LiClO_4$ [56, 85, 88]. Alternatively, an increase in modulus accompanied contraction of the film during oxidation in aqueous NaCl, aqueous KCl, and the ionic liquid ethylmethyl-imidazolium tetrafluorosulfonic acid (EMITFSA) [70, 85, 87]. In these examples, the modulus was found to be higher in the oxidized state, regardless of whether that state is contracted or expanded. This has also been observed for poly (3-methyl thiophene) actuators [89].

A more complicated response was observed for actuation in aqueous 1 M $NaNO_3$, where polypyrrole exhibits dual ion movement. The modulus increased when the potential was raised from -0.8 V to 0 V (causing film contraction as Na^+ cations were expelled) but then decreased when the potential was further raised from 0 V to 0.4 V (causing film expansion as NO_3^- anions are incorporated) [86, 87]. In this case, a higher modulus was measured in the contracted state than the expanded state,

Author	Electrolyte	Potential (V)	Modulus (MPa)	State	Potential (V)	Modulus (MPa)	State
Spinks[1]	0.25M TBAPF6/PC	-3	40	cont.	3	160	exp.
	liquid salt	-5	70	exp.	5	80	cont.
Murray[2]	1M KCl (aq)	-0.5	1400	exp.	ocp	3400	cont.
	1M $NaNO_3$ (aq)	-0.8	1900	exp.	0	3200	cont.
		0	3200	cont.	0.4	2400	exp.
Bay[3]	0.1 M NaCl (aq)	-0.9	600	exp.	0	900	cont.
Otero[4]	1M $LiClO_4$ (aq)	-0.6	485	cont.	0.8	505	exp.

Table 2.1: Previous static investigations of polypyrrole's Young's modulus under different electrochemical conditions. Films have not been subjected to post-deposition processing. The expanded state is labeled by "exp." and the contracted state by "cont." Not all experimental parameters are given in the published works, but the available details are as follows. 1) Polypyrrole fiber doped with PF_6^-, with embedded Pt wire helix. The desired potential was held for 4 minutes, and the modulus was tested at 0.5 mm/min. One should note that absolute values of the applied potentials in this entry are higher than the potentials at the polymer surface, as the experiments were conducted without a reference electrode [56, 85]. 2) Polypyrrole film doped with tosylate. The desired potential was held, and the modulus was tested at 1 mm/min [86, 87]. "ocp" is the open circuit potential of the electrochemical cell. 3) Polypyrrole film doped with toluene sulfonate. Films were cycled several times, then the modulus was measured at the desired potential. In this work the authors also tested films doped with larger anions, with the same result (increase in modulus and contraction upon oxidation) [70]. 4) Polypyrrole film doped with perchlorate. The desired potential was held for 15 minutes, and the modulus was measured by "gradual stretching" of the polymer film [88].

regardless of which was more oxidized. Other authors have observed the same trend for polyaniline fiber actuators [23, 24, 90].

Work has also been conducted where the modulus of polypyrrole was measured *in-situ* during electrochemical cycling. Koehler et al. conducted electrochemical quartz microbalance (EQCM) experiments to observe the change in shear modulus during actuation of polypyrrole doped with perchlorate or tosylate anions. They observed an increase in shear modulus upon oxidation in both systems, even though the ClO_4-doped polypyrrole expanded during oxidation and the toslyate-doped polypyrrole contracted upon oxidation [91]. Samani et al. observed the modulus of polypyrrole using *in-situ* tensile testing [55], and observed a complex actuation and modulus response when actuating a polypyrrole fiber in 0.1 M TBAPF6/PC. During the oxidataion sweep (-1 V to +1 V) they observed an increase in modulus while the polypyrrole fiber expanded (-1 V to -0.6 V), a further increase in modulus as the fiber contracted (-1 V to 0 V), then a decrease in modulus while the fiber expanded (0 V to 1 V) again. During the reduction sweep (+1 V to -1 V), they observed a further decrease in modulus while the fiber began to contract (+1 V to 0 V), an increase in modulus as the fiber continued to contract (0 V to -0.6 V), and then a much smaller increase in modulus as the fiber expanded again (-0.6 V to -1 V) [55]. Samani et al. also conducted EQCM experiments (similar to those performed by Koehler et al.) in which they observe a response comparably complex to their tensile experiments, with changes in modulus that did not directly correspond to changes in film volume or oxidation state [92].

Clearly, the change in polypyrrole's mechanical properties during actuation is a complicated phenomenon that has not yet been fully characterized. Several mechanisms for the change in elastic modulus have been proposed, including plasticization due to counterion [87, 92] and solvent [55, 68, 92] swelling, stiffening of the polypyrrole chains due to oxidization [87, 92], and ionic crosslinking between charged polymer chains and incorporated anions [87, 91]. It is likely that all of these mechanisms can contribute to the change in mechanical properties upon actuation, and that differences in polypyrrole sample geometries, film qualities, electrolyte chemistry, frequency of

electrochemical stimulation and frequency of mechanical testing cause different mechanisms to dominate in each experiment.

We also observe an electrochemically driven change in polypyrrole stiffness, and by limiting ourselves to moderate potential windows and short timescales we observe that the level of counterion swelling clearly dominates the elastic modulus. By limiting our experiments to these conservative conditions we are not fully investigating every mechanism possibly involved in polypyrrole actuation, but are probing a parameter space in which polypyrrole actuators can be operated in a predictable manner.

To measure dynamic elastic modulus *in-situ*, polypyrrole samples are clamped into the electrochemical dynamic mechanical analyzer described in Section 2.3, and warmed up using the methodology described in Section 2.3.1. After the current response stabilizes, the films are measured in isometric mode. The film is held at a constant ~1% strain, and a potential waveform is applied. The resulting change in stress is measured and considered the "active stress," that is, the stress caused by electrochemical actuation. The applied potential (time dependent) and strain (~1%) and the resulting stress response are shown in Figure 2-14i. The film modulus is then immediately measured under an oscillatory strain input, without removal from the apparatus. The film is held in the electrolyte at ~1% strain, and the same potential square wave is applied. During the electrochemical cycling a small (amplitude = 0.3%) sinusoidal perturbation in strain is applied to the film at a frequency much higher than the frequency of the applied potential (in this case 10 Hz). This results in a high-frequency stress response superimposed on the low frequency active stress. The time dependent applied potential and strain and the resulting stress response for this oscillatory strain input are shown in Figure 2-14ii. The choice of a 10 Hz strain perturbation makes the strain rate in these experiments approximately one order of magnitude higher than the static experiments from Table 2.1, but we have not fully probed the effect of frequency on the elastic modulus of polypyrrole. We do suspect that frequency of testing is the cause of some of the discrepancies between results of previous works, and future work will include *in-situ* observation of the elastic modulus over several orders of frequency.

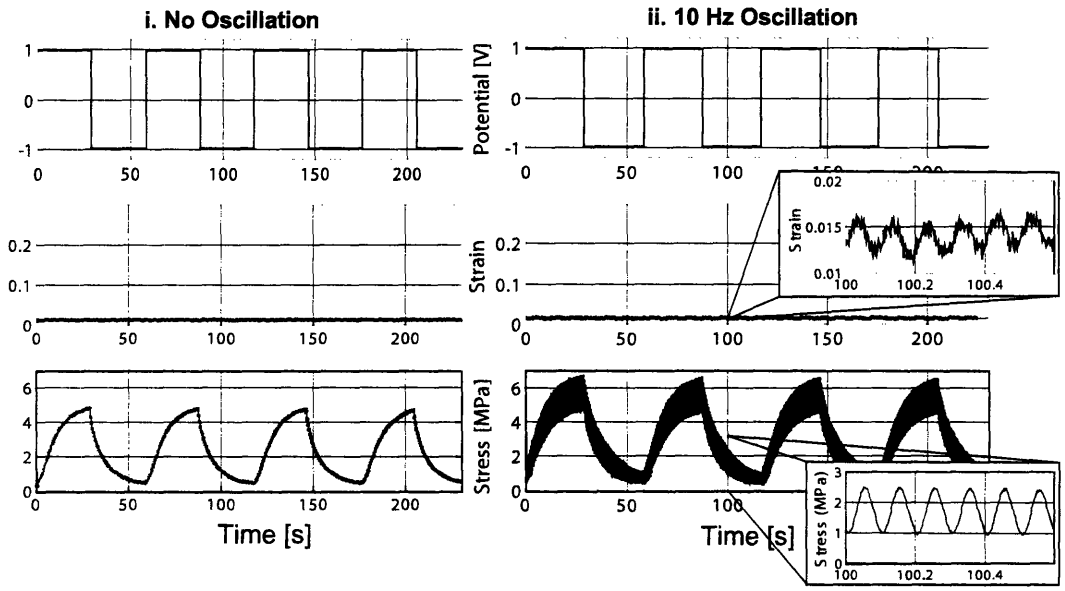

Figure 2-14: Electroactive response under constant and oscillatory strain. i) Testing in BMIMPF6 with constant strain input. The film was held in tension at an initial strain of 1.4%, resulting in an initial stress of 0.5 MPa. A $\pm$1V potential square wave was applied at a frequency of 0.0167 Hz, and the stress response was measured. ii) Testing in BMIMPF6 with oscillatory strain input. The film was held in tension at an initial strain of 1.4%, resulting in an initial stress of 0.5 MPa. A sinusoidal perturbation in strain with an amplitude of 0.003 and frequency of 10 Hz was applied. A $\pm$1V potential square wave was applied at a frequency of 0.0167 Hz, and the stress response was measured.

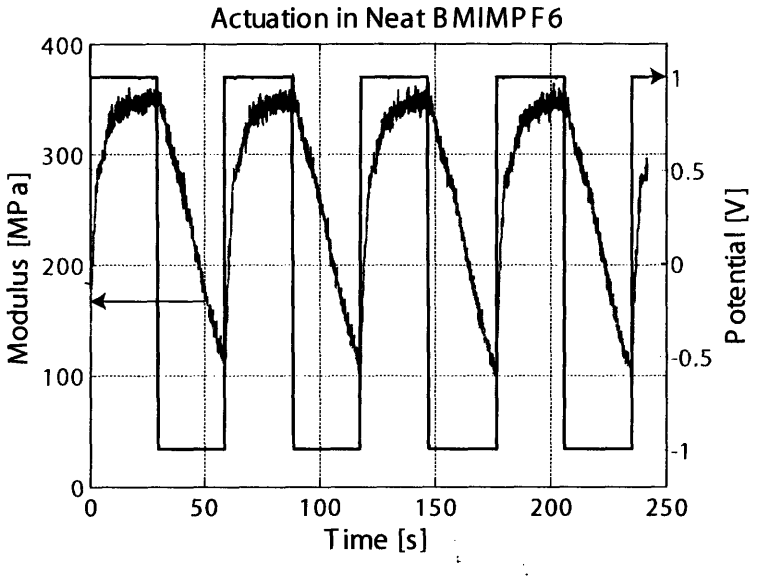

Figure 2-15: Modulus response for tests in neat BMIMPF6. The magnitude of the high frequency response was divided by the magnitude of the applied oscillatory strain to calculate the modulus. Under these conditions, the modulus increases 220% upon oxidation, and decreases to its original value upon reduction.

The high-frequency stress response is isolated by subtracting the isometric active stress (the last curve in Figure 2-14i) from the stress response under oscillatory strain (the last curve in Figure 2-14ii). The modulus (E(t)) is calculated by dividing the high frequency stress response by the high frequency applied strain perturbation, and is shown in Figure 2-15. We do not separate this modulus into real and complex parts, as with a 10 Hz perturbation we do not observe a change in phase lag between the applied oscillatory strain and resulting oscillatory stress even as the oscillatory stress magnitude changes.

As shown in Figure 2-15, we observe an elastic modulus of approximately 100 to 350 MPa for polypyrrole tested at 10 Hz during actuation, while our as-deposited polypyrrole films tested statically (via a stress ramp of 5000 kPa/min) in air have an average modulus of 300 MPa. This is typical for polypyrrole films produced from our standard deposition conditions. As is evident from Table 2.1, there is a large variation in the magnitude of published values for the elastic modulus of polypyrrole (40 - 3400 MPa). Variables in the polypyrrole deposition such as purity of monomer, choice

of solvent, electrolyte, electrode material, deposition current density and deposition temperature will all affect the microstructure and hence the mechanical properties of the polypyrrole samples, while differences in the testing rate and environment will affect the measured modulus [6, 29, 93–96]. These variables make it quite difficult to compare previously published works in this area, and we seek to simplify the experiment by studying one commonly used polypyrrole system (PF_6^- doped polypyrrole films synthesized from propylene carbonate solution) [6, 10, 60, 97] under electrochemical conditions that produce a significant but straightforward electroactive response.

Dynamic Modulus in Different Electrolyte Solutions

To probe the electrochemical dependence of polypyrrole's elastic modulus, we test films in three different electrolyte systems: neat 1-butyl-3-methylimidazolium hexafluorophosphate, (BMIMPF6), an 0.05 M solution of 1-butyl-3-methylimidazolium hexafluorophosphate in propylene carbonate (BMIMPF6/PC) and an 0.05 M solution of tetrabutylammonium hexafluorophosphate in propylene carbonate (TBAPF6/PC).

As was discussed in Section 2.3.6, liquid salts such as neat BMIMPF6 have shown excellent stability and improved performance over solvated electrolytes for conducting polymer actuators [72, 73, 85]. In neat BMIMPF6, the $BMIM^+$ cations dominate the electroactive response over a very wide potential range [63, 72, 73]. This means that as the film is reduced, $BMIM^+$ cations enter the film and the film expands. We use neat BMIMPF6 as an electrolyte containing no neutral solvent, to minimize any modulus change caused by solvent transfer analogous to the osmotic effect described by Bay et al. [68]. We use BMIMPF6/PC as a system where the electroactive response can be easily switched from cation- to anion-dominated, as was discussed in Section 2.3.6. Finally, we use TBAPF6/PC in this study to provide an electrolyte without a liquid salt component. Under the conditions applied in this study, the electroactive response is dominated by the PF_6^- anions for the TBAPF6/PC system. That is, when the polymer is reduced, anions leave the film and the film contracts.

In neat BMIMPF6, we observe a 30% decrease in modulus while the film is held at a negative potential for 10 seconds, as shown in Figure 2-16i. The modulus then

increases as the film is re-oxidized, returning to its original value. Alternatively, when actuating in TBAPF6/PC, the modulus decreases 10% during oxidation and increases during reduction as shown in Figure 2-16ii. In both of these cases, the modulus decreases as ions are brought into the film, and increases as ions are expelled. These results are notably different from static experiments discussed earlier, where the modulus was observed to increase only slightly (1%) when film was oxidized in a liquid salt solution and to increase significantly (300%) upon oxidation in TBAPF6/PC [56, 85]. However, the previous TBAPF6/PC work was performed under static conditions, using a two-electrode configuration. A two electrode cell does not provide sufficient control over the charge state of the polymer, and when the same group probed elastic modulus in a three-electrode cell they observed a softening of polypyrrole over part of the oxidation sweep in TBAPF6/PC [55]. For this study we use a three-electrode cell to control the potential at the polymer film, and by narrowing the potential limits and length of potential holds we avoid the dual ion movement and neutral solvent transfer that has complicated the electroactive response in previous three-electrode studies of polypyrrole in TBAPF6/PC [55, 92].

When a -1V square wave is applied to a film in BMIMPF6/PC, we observe an electroactive response dominated by the $BMIM^+$ cations (Figure 2-13ii). The modulus response for this system is shown in Figure 2-16iii. The direction of modulus change is similar to the neat BMIMPF6 system which is also dominated by the $BMIM^+$ cations, in that there is an increase in modulus upon oxidation and decrease upon reduction. When a +1 V square wave is applied to a polypyrrole film in BMIMPF6/PC, we observe an electroactive response dominated by the PF_6^- anions (Figure 2-16i). The modulus response is similar to that of the TBAPF6/PC system, the other system dominated by the movement of PF_6^- anions, and is shown in Figure 2-16iv. In all cases, regardless of the presence of solvent or liquid salt, the modulus decreases as ions enter the film and increases as ions are expelled. We attribute the decrease in elastic modulus with increasing ion concentration to a plasticization of the polypyrrole film by the small electrolyte molecules. Plasticization resulting from counterion incorporation has been reported during static experiments [23, 87], but has not been

previously shown to dominate the *in-situ* oxidation-reduction modulus response. In our case the polymer is not equilibrated at a particular potential and then tested, instead the change in modulus is observed in real time with the changing counterion swelling of the film.

Under the conditions shown in Figure 2-15, the modulus increases to three times its original value upon expulsion of counterions and contraction of the film. A change of this magnitude will significantly affect the amount of work a polypyrrole actuator will be able to produce under load. The implications that a change in elastic modulus will have on actuation have been discussed at length in the literature [23,56,58,98,99], and it has been shown that a larger work-per-cycle can be achieved by an actuator whose modulus increases upon contraction than by one whose modulus decreases or remains constant [58]. Our results show that all of the conditions applied in this study allow us to operate in this highly productive regime. Awareness of this variation in modulus is critical to developing the mechanics and loading conditions of polypyrrole-driven devices, as well as understanding the theoretical and practical active stress and strain one can achieve in a given electrochemical environment. This will be discussed further in Chapter 7, along with suggestions for additional *in-situ* modulus experiments.

2.3.9 Effect of Ageing

Over the course of this work, we have observed that the achievable active strain is affected by the age of the polypyrrole film. Figure 2-17 shows the isotonic electroactive response for films of different ages, actuated in neat BMIMPF6. A film tested immediately after processing shows an active strain of 4.73%, while a film tested 12 weeks after processing shows an active strain of only 2.27% under the same electrochemical conditions. There are several factors associated with polypyrrole ageing that could contribute to a decrease in electroactive performance, such as an increase in stiffness [100] or a decrease in conductivity with ageing in ambient [100, 101] or heated [102–104] conditions. However, prior studies of ageing in polypyrrole have not addressed the electroactive properties of the material, and have not been conducted

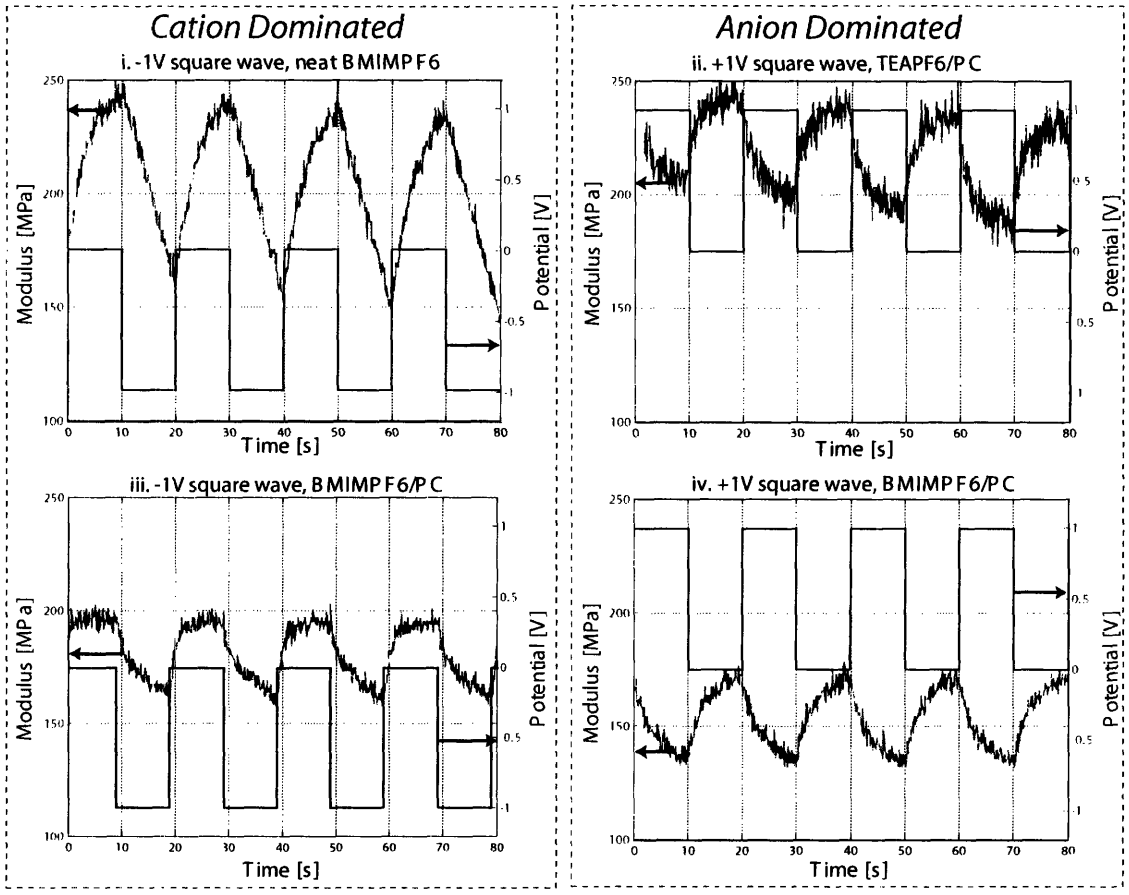

Figure 2-16: Estimated Modulus (E(t)). E(t) was calculated by dividing the high frequency stress response by the high frequency strain input. In i and iii, BMIM+ cations dominate the electroactive response. In ii and iv, PF6- anions dominate the electroactive response. i) -1V square wave in BMIMPF6. E(t) increases 50% during oxidation. ii) +1V square wave in TBAPF6/PC. E(t) increases 20% during reduction. iii) -1V square wave in BMIMPF6/PC. E(t) increases 20% during oxidation. iv) +1V square wave in BMIMPF6. E(t) increases 25% during reduction.

on polypyrrole deposited from our standard recipe.

As was discussed in Section 2.3.1, we do not observe a change in elastic modulus after five weeks of storage in ambient conditions, so we do not believe a stiffening of the films accounts for the decrease in performance shown in Figure 2-17. The conductivities of the films shown in Figure 2-17 were measured immediately after deposition, not immediately before testing, so we do not know whether the conductivity changed over time for these particular samples. In other samples, we have observed a decrease in conductivity with time (up to 30% over two years). Unfortunately, the effects of ageing in our samples were too recently discovered to be a focus in this thesis. These results were surprising to find upon compilation of data from previous years, and are presented here to alert future researchers to the importance of sample age. Additional study is clearly necessary in this area, as is discussed in Section 7.3.

2.4 Chapter Conclusions

It was the intention of this chapter to help the reader understand the testing methodologies we use to study our polypyrrole actuators, and to present typical results for standard polypyrrole films. In the chapters that follow, we will discuss the microstructure of these films, methods to change this microstructure, and the way that microstructure affects the properties we observe. However, throughout the thesis our testing methodologies remain as discussed in this chapter, and any new actuators we produce are compared to the results presented here.

Also in this chapter the importance of different experimental parameters to polypyrrole actuation were stressed. Proper choice of electrolyte can significantly improve the electroactive response, while a change in the applied potential window and switch the system from cation-dominated to anion-dominated. By constraining our electrochemical window we have identified a set of operating conditions in which the movement of one ion clearly dominates the electroactive response, but as was reviewed and discussed extensively, there are many conditions in which a more complicated response is observed. For the remainder of this thesis actuation is conducted under conditions

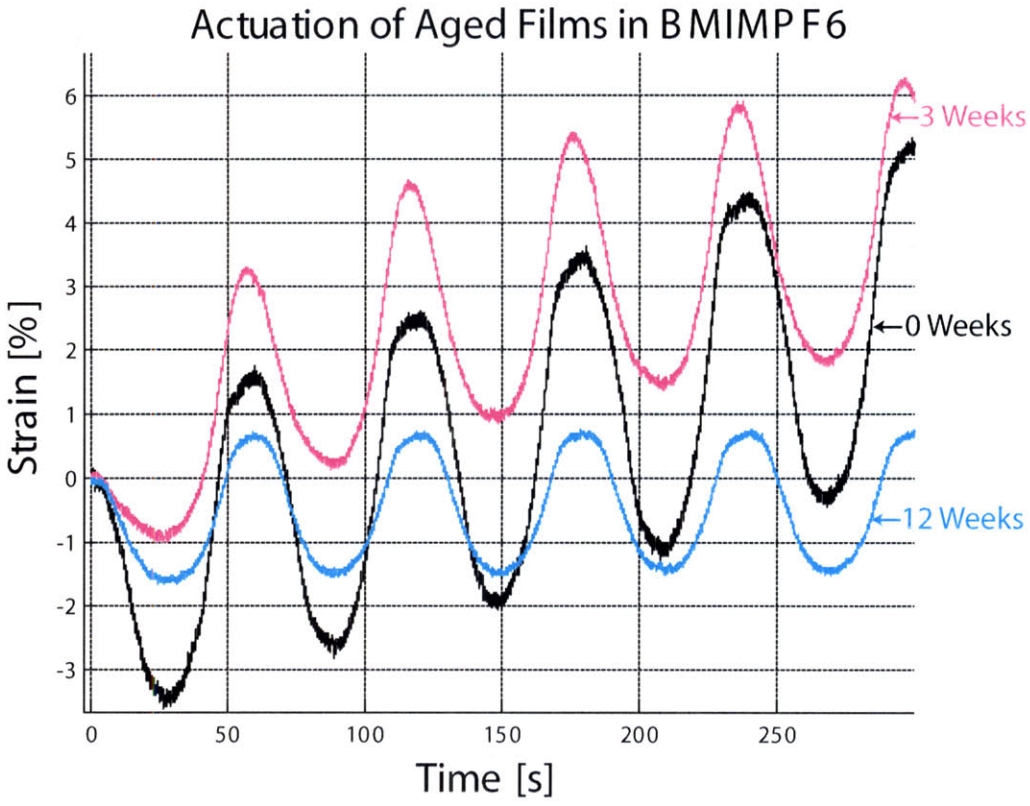

Figure 2-17: Isotonic response for unprocessed films of different ages. Films were held under a static force of 0.5 MPa in neat BMIMPF6, and a ± 1.5 V triangle wave in potential was applied at a rate of 0.1 V/s. The film tested immediately after deposition (black curve) showed an active strain 4.73%, and crept at 0.0143%/s. The film tested 3 weeks after deposition (pink curve) showed an active strain of 3.81% and crept at 0.0156%/s. The film tested 12 weeks after deposition (blue curve) showed an active strain of 2.27 %, and crept at 3.5×10^{-4}%/s.

where one ion dominates the response, but the reader is encouraged to remember that this is not always the case when comparing works in the literature.

Chapter 3

Review of Previous Work on Polypyrrole Microstructure

Polypyrrole is insoluble and unmeltable, so it is quite difficult to change the polymer structure post-synthesis. However, the parameters of the synthesis can be altered, and provide a powerful means to change the morphology and resulting properties of polypyrrole. Conductive polypyrrole is formed by the oxidation of the pyrrole monomer, which can be conducted either chemically or electrochemically. Both methods are covered in Section 2.1, but because the free-standing films needed for actuation have by and large been produced by electrochemical means, electrochemical polymerization will be the focus of this section.

There are many variables that can be altered during the electrodeposition, including solvent, electrolyte, electrode material, cell geometry, temperature, and the current or potential at which the deposition takes place. It is difficult to systematically study the effect of each variable, as one cannot change one without changing others. For example, for galvanostatic (constant current) depositions, when one decreases the deposition temperature the voltage at which deposition takes place increases. Even though the deposition variables are interdependent, a review of the prior work does reveal some overall themes, which will be discussed in this chapter.

The microstructure and morphology as imparted by the deposition conditions have been tied to both the electrical and electrochemical properties. However, in

many cases researchers have altered the deposition conditions and measured the resulting electronic or electrochemical performance without observing or considering the morphological differences that cause the change in performance. Or they have observed the altered microstructure, but not probed its electroactive response. For this reason, while it is widely accepted that the microstructure of polypyrrole actuators affects their performance, the manner in which it does is not entirely understood. In this chapter we seek to organize and compare previous works, where researchers have altered the microstructure of polypyrrole (purposely or not) and observed the resulting changes in properties.

Several authors have studied the electronic conductivity and electrochemical properties of polypyrrole, and observed different behaviors for films produced under different conditions. These works are reviewed first, to provide the reader with an understanding of the effects that changing microstructure can have. There is also a breadth of literature where changes in the deposition conditions have changed the morphology of polypyrrole films, although the impacts of that morphology on actuation or electrochemistry have not always been studied. This work is reviewed next, to give the reader a sense of the wide parameter space that exists in polypyrrole electropolymerization, and the effects that each element of the deposition recipe have on the final product.

3.1 Electrical Conductivity

It is generally accepted that in conducting polymers, a higher degree of order leads to a more conductive material as barriers to charge carrier movement are reduced. Studies of processable polymers such as polyacetylene and polyaniline have shown that samples with larger crystalline domain sizes or a higher percent crystallinity have higher conductivities [105,106]. Because the percent crystallinity and crystalline domain sizes in polypyrrole are not easily determined (as will be discussed in depth in Section 4.1), it is difficult to understand exactly how the structure of polypyrrole affects its electrical conductivity.

Even though the crystal structure of polypyrrole is somewhat ambiguous, it still is generally thought that electrical resistivity is a function of the disorder in the material. In a perfectly crystalline sample, charge carriers would be able to easily travel across the sample by moving along the highly conjugated polymer backbone and hopping between perfectly packed chains. This ease of charge transport would be measured as a very high conductivity. In real samples, the chains have a finite conjugation length and are not packed in a well-organized, crystalline manner. This means the carriers are not only highly localized along the chain due to the finite conjugation, they have a large barrier to hopping between chains due to the less-than-perfect packing [49,107]. The impediments to charge transport induced by disorder in the material cause a lower electronic conductivity to be observed.

3.1.1 Temperature Dependence of Conductivity

Many researchers have studied the temperature dependance of polypyrrole's electronic properties. Two useful parameters for quantifying the conductive behavior of polypyrrole are the resistivity ratio (ρ_r) and the reduced activation energy (W). The resistivity ratio is compares the resistivity (ρ) at liquid helium temperatures[1] to that at room temperature, as is shown in Equation 3.1 [109],

$$\rho_r(1.5\text{ K}) = \frac{\rho(1.5\text{ K})}{\rho(290\text{ K})} \tag{3.1}$$

The reduced activation energy describes how the resistivity changes with temperature, as shown in Equation 3.2 [110],

$$W = -\mathrm{T}\frac{d\ln\rho(\mathrm{T})}{d\mathrm{T}} = -\frac{d\ln\rho}{d\ln\mathrm{T}} \tag{3.2}$$

Polypyrrole's conductivity is strongly dependent on temperature, but the type of dependence (metallic vs. insulating) depends on the conditions under which the sample was made. In general, polypyrrole's conductivity decreases with decreasing

[1]When the temperature at which the low temperature measurement (in the case of Equation 3.1, 1.5 K) is not specified, it can be assumed that it was made below 4 K [108].

temperature until a minimum of T = 10 to 20 K. Below this point, the conductivity increases with decreasing temperature for highly doped (metallic) samples, and continues to decrease for less highly doped (insulating) samples [50, 111, 112]. Whether a particular sample is metallic or insulating is determined by whether the Fermi energy is above or below the mobility edge (the critical energy that differentiates localized and non-localized states) [110].

Metallic Regime

In the metallic regime the Fermi energy is above the mobility edge, in the region of non-localized states. There is a high carrier density, with approximately 1 carrier for every three monomer units [48, 49]. The conductivity is finite even as T approaches zero, and W has a positive temperature coefficient. Polypyrrole doped with PF_6^- is in the metallic regime (so it has a finite conductivity at very low temperatures) when $\rho_r < 10$ [112].

Critical Regime

When the Fermi energy is close to the mobility edge, the sample is said to be in the critical regime. In the critical regime, W is temperature independent, and the conductivity scales with temperature as shown in Equation 3.3 [113],

$$\ln \sigma(\mathrm{T}) \propto \mathrm{T}^{-\beta} \tag{3.3}$$

where $\beta = W$, and varies depending on where the sample is within the critical regime. β can be as small as 0.3 for samples on the metallic side of the critical regime, or as large as 1 for samples on the insulating side [113]. If the power law dependence shown in Equation 3.3 extends even to T = 0, the sample is exactly at the critical point. For polypyrrole doped with PF_6^-, films in the critical regime will have a resistivity ratio of approximately $\rho_r = 4$ to $\rho_r = 10$ [112, 114].

Insulating Regime

For polypyrrole doped with PF_6^-, the insulating regime begins when $\rho_r > 10$ and extends for all larger resistivity ratios [112]. In the insulating regime, W has a negative temperature coefficient and the conductivity approaches zero as T approaches zero. Conductivity in the insulating regime is often modeled using the equations for Mott's variable range hopping (VRH) [48, 50, 110, 112, 113, 115],

$$\sigma(\mathrm{T}) = \sigma_0 \exp[-(\mathrm{T}_0/\mathrm{T})^{\mathrm{x}}] \tag{3.4}$$

$$\mathrm{T}_0 = \frac{18}{k_B \mathbf{L}_c^3 N(\mathbf{E}_f)} \tag{3.5}$$

where k_B is Boltzman's constant, $N(\mathbf{E}_f)$ is the density of states at the Fermi level, and $\mathbf{L}_c$ is the localization length. $\mathrm{x} = \frac{1}{(\mathrm{d}+1)}$, where d is the dimensionality of the system, so $\mathrm{x} = \frac{1}{2}$ for one-dimensional conduction, and $\mathrm{x} = \frac{1}{4}$ for three dimensional conduction [50, 116–118].

Yoon et al. found that samples in the middle of the insulating regime ($\rho_r = 2 \times 10^2$ to $\rho_r = 2 \times 10^3$) show a change in the conductivity behavior at very low temperatures ($\mathrm{T} < 10$ K), as the dominant mechanism of transport changes from Mott's VRH to Efros-Shklovskii (ES) hopping [112]. ES hopping is similar to Mott's VRH with $\mathrm{x} = \frac{1}{2}$, but T_0' is modeled as shown in Equation 3.7.

$$\sigma(\mathrm{T}) = \sigma_0 \exp[-(\mathrm{T}_0'/\mathrm{T})^{\frac{1}{2}}] \tag{3.6}$$

$$\mathrm{T}_0' = \frac{\beta_1 \mathrm{e}^2}{\epsilon \mathrm{k_B} \mathbf{L}_\mathrm{c}} \tag{3.7}$$

where e is the charge of one electron, ϵ is the dielectric constant, and $\beta_1 = 2.8$ [112]. Yoon et al. observe Mott's VRH at low temperatures ($\mathrm{T} < 10$ K) in samples just on the insulating side of the critical regime where ($\rho_r < 10^2$), and ES hopping for samples farther into the insulating regime ($\rho_r = 2 \times 10^2$ to $\rho_r = 2 \times 10^3$) [112]. For very insulating samples ($\rho_r > 10^3$), Yoon et al. observe Mott's VRH in some samples and ES hopping in others. They claim that this is evidence that some samples

are homogenous (those that observe Mott's VRH) while others are granular (those that observe ES hopping) [112]. The authors do not observe granularity or homogeneity by any method other than the type of hopping, but their assumption that granular samples will show ES hopping is supported by experience with other material systems. Reghu et al. blended conductive polyaniline (PANI) with insulating polymethylmethacrylate (PMMA), and changed the fraction of PANI from 0.3% (the minimum fraction necessary to make a conductive material) to 100%. When the fraction of PANI was below the percolation threshold (and a granular texture was confirmed via TEM), the conductivity showed the temperature dependence described in Equation 3.6 [119]. This x = $\frac{1}{2}$ dependence is also typical of granular metals [120].

Mixed Behavior

The conductivity regime in which a sample is placed is usually defined by its behavior at very low temperatures (T < 20 K), but at higher temperatures there are many examples where conducting polymers show mixed metallic and insulating behavior [111]. Metallic polypyrrole, for example, will show a finite conductivity at T = 0 and a positive temperature coefficient of W at low temperatures . However, at more moderate temperatures, the temperature coefficient of W is often negative [111]. The W coefficient may become positive at very low temperatures because interchain hopping and tunneling are suppressed, so intrachain conductivity becomes dominant [111, 115]. At more moderate temperatures, the hopping and tunneling associated with the insulating regime become prevalent, so the overall coefficient of W becomes negative.

3.1.2 Determination of Conductivity Regime

In processable conducting polymers, such as polyaniline, it is possible to cross from the metallic to insulating regime by changing the temperature [121] or decreasing the crystallinity of the system [105]. In polypyrrole, it is possible to move a particular sample from one regime to another by application of high pressures or magnetic

fields, which increase the amount of interchain interaction or move the mobility edge, respectively [110, 113]. Alternatively, one can place the Fermi energy on either side of the mobility edge by synthesizing samples under different conditions.

Yoon et al. synthesized polypyrrole films at -40°C with conductivities of 4×10^5 S/m, that showed metallic behavior at low temperatures. When they changed the polymerization temperature to room temperature, the resulting films had conductivities of 2 - 5×10^5 S/m, and showed insulating behavior at low temperatures [113]. Alternatively, for films deposited at -40°C, samples in the metallic or insulating regimes can be produced by polymerizing at different current densities. When Yoon et al. polymerized samples at a current density of 0.2 A/m^2, the conductivity was at least 2.7×10^5 S/m and the samples showed metallic behavior. When the polymerization current density was raised to 2 A/m^2, the conductivity no longer increased with decreasing temperature below 4 K, showing that the metallic behavior was lost [6].

3.1.3 The Effect of Deposition Counterion

Polypyrrole's conductivity has been shown to depend on the size and type of the counterion used in deposition. In general, increasing the counterion size causes the film to be less conductive [107,115,122,123]. The conductivity behavior of a particular film was found to be dependant on the counterion used during synthesis, but not on the counterions introduced into the film by post-synthesis electrochemical cycling [115], implying that the effect of using a different counterion is manifested in the morphology that counterion brings about during deposition.

Using counterions that introduce a preferential orientation onto the material can be used to change the dominant conduction mechanism from 3D to 2D variable range hopping [118]. Mitchell et al. found that when they deposited polypyrrole doped with aromatic anions such as *p*-toluene sulfonate, the polypyrrole chains preferentially aligned with the pyrrole rings parallel to the film surface [124, 125]. In these highly anisotropic films, the conductivity was found to fit Mott's VRH (Equation 3.4), with $x = \frac{1}{3}$. As was discussed in Section 3.1.1, this is indicative of two-dimensional hopping. Alternatively, when polypyrrole films were deposited with spherical anions such as

perchlorate or sulfate, this preferential orientation was no longer clearly observed [125]. For these isotropic films, the conductivity fit Equation 3.4 with x = $\frac{1}{4}$, indicative of three-dimensional charge transport [118].

3.2 Morphology

The direct effect of morphology on electroactive properties is rarely specifically probed, due to the fact that it is impossible to change the morphology and not other factors (such as the electronic conductivity). However, some authors have attempted to study this by examining both the morphology and the electroactive properties that result from a change in deposition conditions. These works are discussed here.

We have previously observed that as-deposited polypyrrole films are not always morphologically isotropic. It is often observed that the structure on the side of the film in contact with the electrode is very different from the side exposed to the solution, as was shown in Figure 2-3. Naoi et al. showed that for films doped with surfactant molecules such dodecylbenzenesulfonate (DBS), this morphological anisotropy can be quite extreme [1]. For sodium dodecylbenzenesulfonate (NaDBS) in aqueous solution, the critical micelle concentration where the surfractant molecules will self-assemble in solution is 1.5 mM [1]. Naoi et al. compared polypyrrole films synthesized from solutions below and well above this concentration, and found the morphologies shown in Figure 3-1. In both cases the films have a rough, nodular surface, but the film deposited from high NaDBS concentration shows an extremely anisotropic, columnar morphology. Naoi et al. suggest this may be due to an imperfect layer of surfactant that forms on the working electrode, promoting vertical growth of polypyrrole nucleated at defects in the surfactant [1].

Smela et al. conducted *in-situ* AFM experiments to observe the strain perpendicular to the electrode for polypyrrole prepared similarly[2] to that shown in Figure 3-1b. Smela et al. assume they achieve the same columnar morphology as Naoi et al..

[2]Films were potetiostatically deposited from aqueous solutions of 0.1 M pyrrole and 0.1 M NaDBS at 0.55 V vs. Ag/AgCl [26]

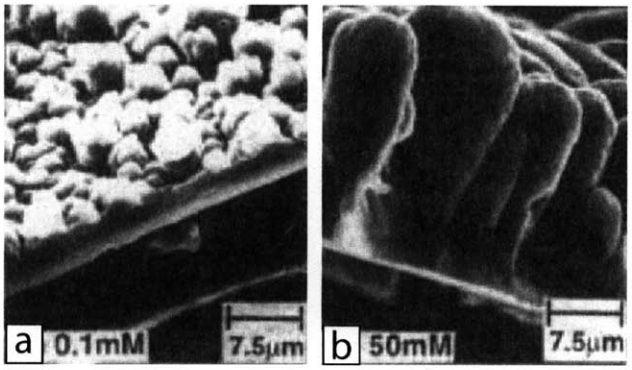

Figure 3-1: Scanning electron micrographs from Naoi et al. [1]. Films were potentiostatically deposited at room temperature from aqueous solution of 0.1 M pyrrole and different concentrations of NaDBS at 0.8 V vs. Ag/Cl onto an ITO working electrode. 2×10^5 C/cm^3 of charge was passed in each case. a) Deposited from 0.1 mM NaDBS (below critical concentration). b) Deposited from 50 mM NaDBS (above critical concentration).

but do not independently verify that they do. For their material, Smela et al. report a repeatable active strain of 35% perpendicular to the working electrode, compared to up to 2% parallel to the film plane [25, 26]. The sample geometry for Smela et al.'s experiments is unusual, and may induce some mechanical amplification of the strain observed perpendicular to the electrode. While this 35% expansion may not be achievable in most film configurations (and has not been reported for flat films), it does highlight the importance of understanding the morphological anisotropy in a given polypyrrole system.

Bay et al. deposited polypyrrole in the presence of 1-pentanol in order to manipulate the film morphology. All films showed a nodular morphology, but films deposited with at least 2.4% pentanol showed large wrinkles ($\sim$ 80 μm $\times$ 20 μm) as the film buckled up from the electrode [126]. The electrical conductivity of the films is not significantly affected by this change in morphology, but the active strain measured isotonically in 0.2 M NaCl is 2.4% for films with no pentanol, and up to 5.6% for films with 2.4% pentanol [126]. Interestingly, EQCM experiments reported in the same paper showed a lower mass transfer in the pentanol-containing films. Assuming the polypyrrole deposited on the EQCM is comparable to that used for linear isotonic testing, this means that the pentanol-containing films exchanged fewer ions, yet ex-

hibited a larger expansion. The authors claim that the buckled morphology of the pentanol-containing films harnesses the high active strains that have been previously reported in the film normal direction (discussed above), resulting in a larger strain even at a lower charge [126].

Pandey et al. deposited polypyrrole doped with β-Napthalene sulphonic acid (β-NSA) onto ITO, stainless steel, and platinum [2,127]. They found that the different electrode materials imparted different surface morphologies, and attributed this to the interaction of the (β-NSA) with the surface. The authors do not characterize the various surfaces prior to deposition, but SEM micrographs of the films produced from this work are shown in Figure 3-2. Pandy et al. observe more dual ion movement in the films deposited onto stainless steel, and attribute this to the fact that this film had a "highly porous, tubular" morphology [2,127]. Unfortunately, the only evidence of this microstructure is the micrograph shown in Figure 3-2a, which does not clearly show porosity or a "tubular" structure.

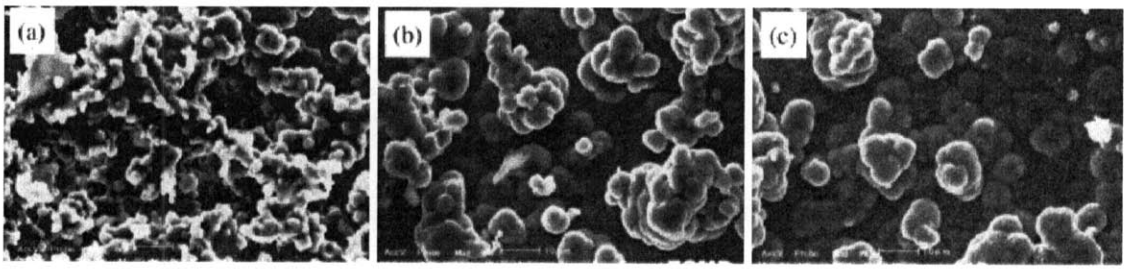

Figure 3-2: Scanning electron micrographs, from Pandy et al. [2]. Polypyrrole was deposited on various substrates, from an aqueous solution of 0.15 M pyrrole and 0.25 M β-NSA. Films were deposited potentiostatically at 1.2 V vs. silver wire for 1 minute, and then galvanostatically deposited at 10 A/m^2. The authors do not explain why the potentiostatic step is necessary, though one could guess it was for adhesion to the substrate. Substrates are as follows: a) stainless steel, b) indium tin oxide (ITO), c) polished platinum

Hara et al. have published several novel deposition recipes, with significant electroactive claims [3,27–30,94,128]. They deposited films in methyl benzoate solutions with very large anions, for example 1,2-dimethyl-3-propylimidazolium tris(trifuoromethylsulfonyl)methide (DMPIMe) [3]. They also actuate using large counterions ($Li(C_nF_{2n+1}SO_2)_2N$ (n = 1-4)), and reported very large electrochemical

strains (they claim up to 39.6% for n = 4)[3] [3,28]. Hara et al. speculate that larger deposition anions cause the polypyrrole chains to be very loosely entangled, allowing the film to swell easily and show large electroactive strains. This may not be ideal for all applications, as they also assert that these loosely packed chains will result in lower measured electrochemical stresses and a lower mechanical strength of the film [28].

These large anion films were polymerized onto a variety of electrodes, and the largest active strains were reported for films deposited onto glassy carbon. Micrographs of the electrode and solution surfaces of comparing films grown on glassy carbon and ITO are shown in Figure 3-3, and a uniquely microporous surface morphology is evident on the electrode side of the glassy carbon films. Films were also deposited onto platinum and gold electrodes, and had surface morphologies similar to the film deposited onto ITO. For films deposited onto a glassy carbon electrode, Hara et al. report 28.0% strain in 100 seconds.[4] For films deposited onto ITO, they report 13.7% for the same actuation conditions [3]. It is clear from Figure 3-3 that the electrode material does change the polymer film morphology, and that the morphologies that Hara et al. achieve are significantly different than that shown in Figure 2-3. However, because Hara et al. do not compare their films directly to films with a smooth surface, it is difficult to know just how much of their reported improvement in strain is due to a difference in morphology.

In order to produce a very fast actuator, Hara et al. electropolymerized polypyrrole films from solutions containing salts of the bis(trifluoromethanesulfunyl)imide anion ($TFSI^-$) and its derivatives [29, 94]. With this system,[5] they report a peak strain of 29% and strain rate of 10.8%/s [29]. Wu et al. also produced films doped with $TFSI^-$, and found that when utilized in a bending beam configuration these films showed a larger and faster electroactive response than those doped with PF_6^- [129]. Unfortunately, Wu et al. did not investigate the morphological differences between

[3]Films deposited from 0.2 M $Li(C_4F_9SO_2)_2N$ in methyl benzoate at 0°C, actuated in 0.5 M $Li(C_4F_9SO_2)_2N$ in propylene carbonate between -0.6 V and +1.5 V at 2 mV/s

[4]Actuating in 1 M $Li(C_4F_9SO_2)_2N$ (LiNFSI) in a 50:50 mix of water and propylene carbonate

[5]Films polymerized using tetrabutylammonium bis(trifluoromethanesulfunyl)imide (TBATFSI), actuated at $\pm$0.7 V in a solution of LiTFSI in 60:40 water:propylene carbonate

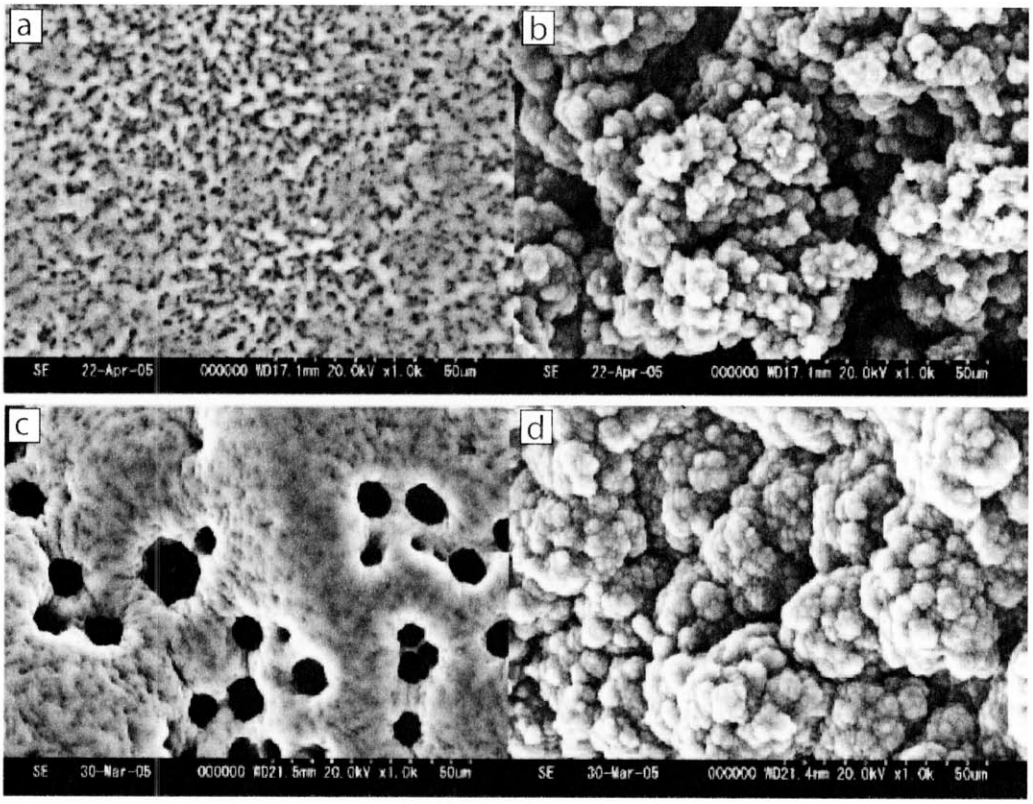

Figure 3-3: SEM micrographs of the electrode and solution sides of polypyrrole films deposited onto different working electrodes, from Hara et al. [3]. Films were polymerized potentiostatically (+1.2 V) at -10°C, from a solution of 0.25 M pyrrole and 0.12 M 1,2-dimethyl-3-propylimidazolium tris(trifuoromethylsulfonyl)methide (DMPIMe) in methyl benzoate. a) Electrode-facing side of film deposited onto glassy carbon. b) Solution-facing side of film deposited onto glassy carbon. c) Electrode-facing side of film deposited onto ITO. d) Solution-facing side of film deposited onto ITO.

films doped with the different anions. They did find that the films doped with $TFSI^-$ showed faster ion transfer, even though they were less electrically conductive. This may be the result of a larger surface area available for transport. We have also attempted to use the $TFSI^-$ anion to increase strain rates in polypyrrole films, and this work will be presented in Section 6.4.

Hara et al. publish strains and strain rates for free standing linear actuators that are far greater than other groups. For example, Hara et al. claim to observe a strain rate of 10.8%/sec for a free standing polypyrrole film [29], while the next highest number in the literature is 3.2%/s [60]. They report linear strains up to 40% [28], while other groups typically report linear strains of 2 to 5% for free-standing films [13, 57]. Many of the numbers Hara et al. report for electrochemical strain are given in tables with no supporting data, and when data is given often only the first and second cycles are shown. The active strain for the second cycle is usually much smaller than the first, even though the first is reported in the tables. For example, the conditions mentioned earlier that showed 39.6% in the first cycle only showed 22.8% for the second cycle [28]. This exceptionally large response is clearly transitory and therefore not useful for practical devices. However, even if the numbers reported are somewhat questionable, it is still evident that there is a structural difference between the material Hara et al. are producing and the polypyrrole used by the rest of the field. Our work to follow their recipes and better understand the material they produce is presented in Chapter 6.

3.3 Parameters in Electrochemical Synthesis

Many groups have altered the parameters associated with polypyrrole electrodeposition, producing polypyrrole films that very widely in conductivity, mechanical properties, and morphology. The deposition recipes are so diverse it is often difficult to draw comparisons between the works of different groups, and in some cases it appears that different groups come to opposite conclusions. Because there are so many variables, each experiment should be thought of as relatively isolated, and we cannot assume

an observed change with one variable will occur again if all other parameters of the deposition are not exactly the same. However, by organizing the previous work in the literature, some overall themes arise that we can use to direct our future study of polypyrrole actuators.

3.3.1 The Effect of Counterion Choice

Mitchell et al. have extensively used x-ray diffraction to investigate the molecular organization in polypyrrole films deposited from aqueous solutions of pyrrole and sodium *p*-toluene sulfonate at 20°C [4, 118, 125]. When polypyrrole is deposited in the presence of an aromatic counterion such as the *p*-toluene sulfonate, the x-ray diffraction pattern shows significant anisotropy. A sharp peak at d $\sim$ 3.4 Å (attributed to the face-to-face stacking between two polypyrrole chains) [10, 11, 57, 123, 130, 131] is observed in the direction of the sample normal, while this peak is notably absent in the sample plane [125]. This implies preferential orientation of the polypyrrole chains with the ring faces flat to the film plane. When polypyrrole was deposited under the same conditions but a spherical anion such as perchlorate was substituted for the *p*-toluene sulfonate, no such anisotropy was measured [118]. This preferential orientation can also be caused by a change in polymerization potential (as will be discussed in Section 3.3.2) or solvent choice (as will be discussed in Section 3.3.3). A change in the locations of the diffraction peaks due to the size of the counterion used during deposition also has been observed [97, 132], and will be discussed in Section 4.1.4 and Section 6.3.

Hara et al. surveyed a range of counterion salts to be used in the deposition, as was discussed in Section 3.2. They recommend that counterions and solvents should be chosen to maximize the interaction between polypyrrole and counterions [30], and report very large strains for films deposited from and actuated in imide-type anions [29, 30, 94, 133]. They report that larger strains are observed when larger counterions are used for deposition and actuation, with an active strain of 39.6% when $Li(C_4F_9SO_2)_2N$ was used, compared to 23.3% for $Li(CF_3SO_2)_2N$.[6] Hara et al.

[6]In both cases films are deposited from 0.2 M solution of counterion in methyl benzoate at 0°C.

also investigated perfluoroalkylsulfonyl containing anions, and again reported strains between 20 and 40% [3]. These films had noduluar, cauliflower-like morphologies, the roughness of which depended on the working electrode material, as will be discussed in Section 3.3.5 [3].

3.3.2 The Effect of Deposition Potential and Current Density

The deposition potential and current density cannot be independently controlled, as they are a function of the cell resistance. For example, if one wants to compare depositions using two different counterions, they will encounter electrolyte solutions with two different resistivities. The researcher must then choose whether to keep the potential or the current constant, and the other will vary depending on the solution resistance. This makes impossible to tell if the resultant films show different properties because of the counterion, deposition current or potential, or both.

Polymerization Potential

The effect of polymerization potential on polypyrrole chain quality is the subject of some debate. Some authors claim that lower polymerization potentials produce shorter chains, because the intermediate species are less reactive [48, 134]. Others claim that that lower potentials may prevent unfavorable side reactions from occurring, allowing neat polypyrrole chains to grow longer [93]. To this end, it has been shown that when the deposition potential is allowed to go too high, the resulting product is less conductive, which suggests shorter polymeric chains with more defects [93, 135]. In fact, it is likely that there is an optimum deposition potential for polypyrrole in each electrolyte system, which will enable the intermediate species to be reactive enough to form long chains, but not so reactive that these chains have lots of defects. For example, Hagiwara et al. found that for films deposited from propylene carbonate solution,[7] a polymerization potential of 1 V to 1.2 V vs. Ag/AgCl

Films are actuated in 0.5 M solution of counterion in propylene carbonate, from -0.6 V to +1.5 V at 2 mV/s

[7]Potentiostatic deposition at -20°C from solution of 0.06 M pyrrole, 0.05 M TEAPF6 and 1 %vol water in propylene carbonate

produced films that were highly processable (able to be drawn up to 2.7 times) and quite conductive ($\sim 4 \times 10^4$ S/m) [93]. Potentials slightly higher or lower than this led to less conductive, less processable films.

Mitchell and Geri. deposited films doped with *p*-toluene sulfonate[8] and varied the deposition potential from 0.5 V to 1.5 V vs. SCE (Saturated Calomel Electrode) [4]. They used x-ray diffraction to evaluate the microstructure of the films, and at higher potentials observed anisotropic scattering that they attribute to a preferential orientation of the polymer chains, with the pyrrole rings lying flat to the film surface plane (similar to that discussed in Section 3.3.1) [4]. Mitchell and Geri also found that the higher potentials resulted in a smoother film as is shown in Figure 3-4, and a significantly higher conductivity (3×10^4 S/m for films polymerized at 1.5 V, compared to 8×10^3 S/m for films polymerized at 0.5 V) [4]. They speculate that higher anodic potentials lead to a higher concentration of polypyrrole intermediates at the electrode surface, so the polymerization occurs more evenly across the entire surface. At lower deposition potentials the deposition may occur in patches, leading to a rough, poorly-organized material as additional polypyrrole is deposited [4].

Galvanostatic Deposition

For films produced galvanostatically, it is generally found that lower current densities lead to smoother, more conductive films. Stankovic et al. compared films deposited with current densities from 10 A/m^2 to 120 A/m^2, and found that those deposited at 10 A/m^2 were the most conductive [135]. They also observed the films' morphologies with SEM, and while many samples showed a cauliflower morphology, the ones deposited at higher current densities (that were less conductive) had larger globules [135]. Li and Ouyang deposited polypyrrole in the presence of a nonionic surfractant, and found that the lowest deposition current density (1 A/m^2) produced the most conductive and strongest film (1.3 S/m, 69.6 MPa), while the highest (3 A/m^2) produced a film with inferior properties (0.96 S/m, 30.1 MPa) [136]. Dyreklev et

[8]Films deposited from aqueous solution of 0.25 M pyrrole and 0.8 M sodium *p*-toluene sulfonate at at 20°C

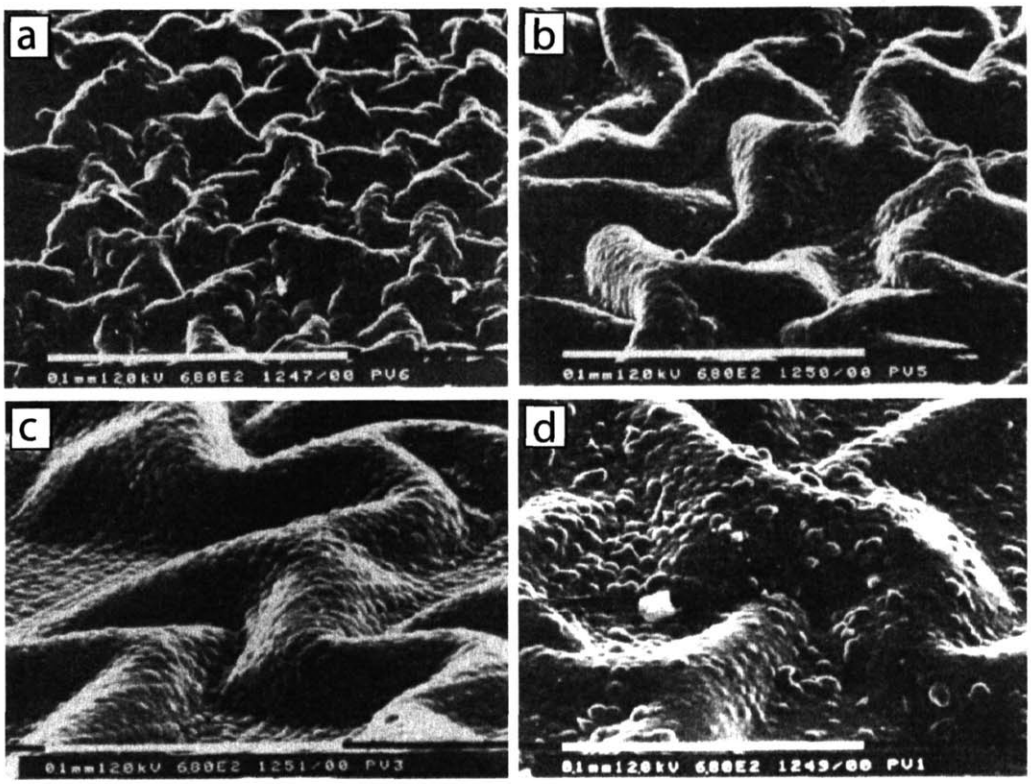

Figure 3-4: SEM micrographs of solution side of polypyrrole films from [4]. Films are polymerized deposited from aqueous solution of 0.25 M pyrrole and 0.8 M sodium *p*-toluene sulfonate at at 20°C, onto glass coated with Baltracon Z10 (to provide conductivity) at the following deposition potentials vs. SCE: a)0.5 V b)0.6 V c)0.8 V d)1.0 V.

al. observed that films deposited at current density of 1.25 A/m^2 (from a solution of 0.1 M Pyrrole and 0.5 M $LiClO_4$ with no water) were shiny and easy to handle while those deposited at 20 A/m^2 were brittle and matte [137]. Unfortunately, the authors do not show any SEM micrographs to explain the micro-scale features that caused this difference, but say that the higher current density films show cauliflowers with 10 μm diameters while the low current density films are smoother with features spreading over 50 μm [137].

Yoon et al. also studied the effect of deposition current density, noting that for films polymerized at -40°C the most conductive films were produced at 0.2 to 0.5 A/m^2. These films also showed the lowest resistivity ratio and the most negative temperature dependence of conductivity, indicating these samples were furthest into

the metallic regime (as discussed in Section 3.1.2) [6].

Maw et al. produced bending beam actuators from polypyrrole synthesized from an aqueous solution of NaDBS [95]. In this system, films synthesized at lower current densities took much longer to warm up, i.e. during cyclic voltammetry the oxidation and reduction peaks did not develop to constant behavior for many cycles. After warm up, however, the films deposited at lower current densities showed significantly higher tip movement upon actuation. For example, the end of a 75 mm long bilayer deposited at 4 A/m^2 curled up to 12 mm, while a bilayer deposited at 400 A/m^2 only curled up to 5 mm when actuated under the same conditions[9] [95]. They found that the deposition current density determined the amount of charge a sample would pass in response to an applied potential condition, but did not change the amount of deformation that results from each mC of charge. The authors do not speculate as to what electrical or morphological features might cause this effect and unfortunately, they do not examine the morphologies of their different samples.

3.3.3 The Effect of Solvent Choice

Polypyrrole films have been grown from a variety of solutions, including supercritical carbon dioxide[10] [138] and neat monomer[11] [139] solutions. Ouyang and Li show a correlation between the conductivity of polypyrrole and the nucleophilic strength of the solvent used for the deposition solution [140]. The authors explain this relationship by noting that the more nucleophilic the solvent, the more likely it is to attack any radical cations produced during electropolymerization, decreasing the molecular weight of the growing chain [140]. While the authors presented SEM micrographs of films deposited from different solvents, the micrographs do not clearly show any morphological changes imparted by the nucleophilicity of the solvent.

Hara et al. have conducted perhaps the most extensive survey of solvents for

[9]Cycled between +0.4 and -1.1 V at 150 mV/s

[10]Films polymerized potentiodynamically from a solution of 0.16 M TBAPF6, 2.4 M acetonitrile, and 0.16 M pyrrole in $scCO_2$.

[11]Films polymerized potentiodynamically from a solution of 0.05 to 0.3 M counterion salt in neat monomer.

polypyrrole electrodeposition [30]. Using $TBABF_4$ as the counterion salt, the authors surveyed a variety of esters, ethers, and higher alcohols. They report the largest electrochemical strains occurred when films were synthesized in methyl benzoate (12.4%) or butyl benzoate (15.1% under same electrochemical conditions[12]), and claim that methyl and butyl benzoate interact relatively weakly with the polypyrrole, allowing more interaction between the polymer and the counterions [30]. However, the authors do not investigate or explain the microstructural difference that these solvents induce.

Aqueous vs. Organic Solutions

A widely used electrodeposition recipe (as was presented in Section 2.1.1) includes pyrrole monomer, counterion salt, and a small amount of water (typically 1%vol) in propylene carbonate [10, 41, 57, 60, 123, 130, 135]. The role of water in solution is not entirely clear, but it may help to accommodate the protons produced during the polymerization reaction. When the water is eliminated from the solution the resulting polypyrrole films tend to be brittle and difficult to handle [135]. When acetonitrile is used instead of propylene carbonate, it has been observed that polypyrrole forms particles in solution instead of a free-standing film if water is omitted [5].

Stanklovich et al. polymerized polypyrrole from propylene carbonate solutions with a small amount of water added [135]. They found that the most conductive films were produced at a concentration of 3%vol water at 0°C. They could not conduct experiments at -40°C because the deposition solution solidified (likely due to the high concentration of water) but still achieved conductivities up to 3.07×10^4 S/m [135]. Stanklovich et al. attribute the decreased conductivity in the films prepared from dry solution to the high acidity at the electrode surface that may occur when there is no water in solution [135]. This high acidity may contribute to formation of less conductive impurities such as 2.5-bis(2-pyrrolyl) [135, 141] which would cause the resulting film to be less conductive.

While a small amount of water may be beneficial to polypyrrole polymerization in organic solutions, too much could hinder polypyrrole film formation. Ko et al.

[12] Actuated in 1 M aqueous $NaPF_6$, scanning between -0.9 V and +0.7 V at 2 mV/s

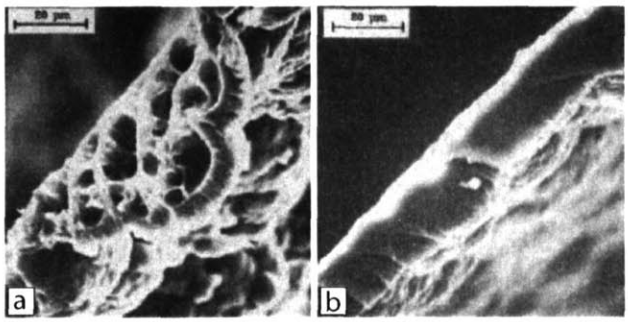

Figure 3-5: SEM micrographs of polypyrrole film cross-sections, from [5]. Polypyrrole films were deposited galvanostatically at 20 A/m^2, from a solution of 0.036 M TEAP and 0.36 M pyrrole in one of the following solvents: a) water b) acetonitrile with 2%vol water.

found polypyrrole polymerized from completely aqueous solutions to be inferior to that polymerized from acetonitrile with 2% water, with the aqueous films showing an electrical conductivity approximately one order of magnitude lower than those produced from acetonitrile solution [5]. This may be due to nucleophilic attack by the water on the radical cation produced during electropolymerization, resulting in chains with a higher concentration of defects [5]. Films produced from aqueous and acetonitrile solutions also show significantly different morphologies, as is shown in Figure 3-5. The films produced from aqueous solution are more rough than those produced from acetonitrile solution, and have large pores on the electrode side of the film. Ko et al. speculate that the parts of the polypyrrole chain attacked by water during the aqueous deposition would be more soluble in water than the rest of the polypyrrole chain, so these sections may aggregate, resulting in the observed highly nodular morhphology [5].

Sutton and Vaughan synthesized *p*-tolune sulfonate (pTOS$^-$) doped polypyrrole onto ITO from solutions of methanol and water, varying the methanol content in order to incrementally change the deposition solution from aqueous to organic [142]. In contrast to the findings of Ko et al., Sutton and Vaughan find that films produced from aqueous solution had electrical conductivities approximately one order of magnitude higher than those produced from organic solution [142]. However, the two studies cannot be directly compared. In addition to the difference in choice of organic solvent,

there also exists a difference in dopant anion (pTOS$^-$ compared to PF_6^- for Ko et al.), electrochemical conditions (potentiostatic at 1.2 V vs. galvanostatic at 20 A/m^2), and working electrode (ITO vs. platinum foil) [5,142], all of which may contribute to the resulting film quality.

Sutton and Vaughan also investigated the microstructure of their films using wide angle x-ray diffraction, and compared diffraction patterns taken with the incident beam parallel to the film normal with the beam parallel to the film plane. They found considerable anisotropy in the aqueous system, where the polypyrrole chains preferentially aligned with the ring face parallel to the film surface plane. This anisotropy decreased as the methanol content was increased [142]. Sutton and Vaughan also observed a decrease in electrical conductivity with increased methanol content, and attributed this to the decreased molecular organization [142]. The authors attribute the lower conductivity and molecular organization in organic solutions to a change in oxidation potential of the pyrrole monomer depending on solution (higher in organic than in aqueous solutions), as well as the inability of the organic solution to properly solvate the protons produced during polymerization.

Mitchell and Geri have observed diffraction patterns very similar to Sutton and Vaughan's for p-toluene sulfonate doped polypyrrole deposited at various anodic potentials, as was discussed in Section 3.3.2 [4]. Sutton and Vaughan comment that by increasing the aqueous content of the deposition solution one is effectively decreasing the oxidation potential of pyrrole, so one might expect the two sets of diffraction patterns to correspond. Furthermore, Sutton and Vaughan show a change in polypyrrole surface morphology (from nodular to wrinkled as the solvent is changed from water to methanol), that looks very similar to the change observed by Mitchell and Geri as they lowered their deposition potential (shown in Figure 3-4). It seems that in Sutton and Vaughan's experiments, they have captured the effects of raising the pyrrole oxidation potential without gaining the benefits of polymerization in organic solution observed by Ko et al. This may be due to their choice of methanol as the organic solvent instead of acetonitrile or propylene carbonate.

3.3.4 The Effect of Deposition Temperature

Several studies have shown that polypyrrole films polymerized at lower temperatures are more conductive, with -40°C being the optimum temperature for polypyrrole deposited from propylene carbonate [6, 93, 143]. Ogasawara et al. compared films polymerized at +20°C and -20°C, and found that the low temperature films were much more conductive (2.87×10^4 S/m as opposed to 0.97×10^4 S/m) and more processable (could be stretched up to 100% as opposed to only 6%), while elemental analysis showed no applicable difference in doping level [143]. Electron Spin Resonance spectroscopy (ESR) showed decreasing linewidth for films polymerized at lower temperatures [93,143]. The ESR linewidth is related to the conjugation length in conducting polymers, and a decreased linewidth is indicative of a higher degree of conjugation [143–145]. In addition, the density of films prepared at lower temperatures has been found to be higher than those prepared at higher temperatures [6, 93].

For films deposited at a constant current density, Yoon et al. showed it is possible to put polypyrrole films in different electronic transport regimes by changing the temperature (as was discussed in Section 3.1.2). For example, films prepared at 0°C were in the critical regime with $\rho_r = 12.5$, while films prepared at -40°C were metallic with $\rho_r = 1.92$ [6].

The electrochemical properties of films synthesized at different temperatures have been also probed by cyclic voltammetry [6]. Films deposited at -40°C show much sharper oxidation and reduction peaks than those deposited at room temperature, which Yoon et al. attribute to the -40°C films having a more homogeneous morphology and lower polydispursity [6]. One would expect a high polydispursity in conjugation lengths to lead to a broadening of the oxidation and reduction peaks, but because polypyrrole is insoluble polydispursity can only be inferred, not directly probed by traditional methods such as size exclusion or gel permeation chromatography. Yoon et al. claim that the films deposited at low temperature are also more stable during repeated electrochemical cycling, but do not show comparable data for room temperature films [6].

3.3.5 The Effect of Electrode Material

There have been several examples where the morphology of polypyrrole films has been affected by the working electrode material. As was presented in Section 3.2, Hara et al. produced films with nodular, cauliflower-like morphologies, the roughness of which depended on the working electrode material [3]. The surface morphologies of these films are shown in Figure 3-3. While it is clear that the electrode material influenced the morphology, the authors do not discuss why the different electrodes produce different films morphologies. Furthermore, they do not describe the surface finish of the electrode, which certainly has an effect that is separate from the chemistry of the electrode material.

Yoon et al. show one example where the effect of the state of the electrode (polished vs. unpolished) is directly investigated. While they do not provide SEM micrographs at comparable magnifications, their images suggest that polishing the electrode reduces the number of pores on the electrode side of the film and the roughness of the solution side of the film (Figure 3-6 [6]).

Cascalheira et al. also investigated the effect of electrode surface roughness on polypyrrole morphology. They compared polypyrrole deposited on mechanically polished (rms-roughness = 4 nm) and electropolished (rms-roughness = 0.3 nm) copper foils, and found that initially, the smoother electrode surface gave rise to a much smoother film. However, after 3000 C/m^2 of charge was passed, the roughness of the each sample was nearly identical [7]. They studied the morphologies of the electrodes and resulting films using tapping mode Atomic Force Microscopy (AFM), and their images are shown in Figure 3-7. Cascalheira et al.'s results are in contrast to the experiment described above in which Yoon et al. passed more charge (up to 3.2×10^5 C/m^2) but still observed an effect of the electrode roughness in the polypyrrole surface morphology. The difference may be that Cascalheira et al. deposited their polypyrrole films from aqueous solution, while Yoon et al. deposited from propylene carbonate solution with only 1%vol water. Depositions conducted from aqueous solutions tend to be very rough and nodular, and in the case of Cascalheira et al. this may

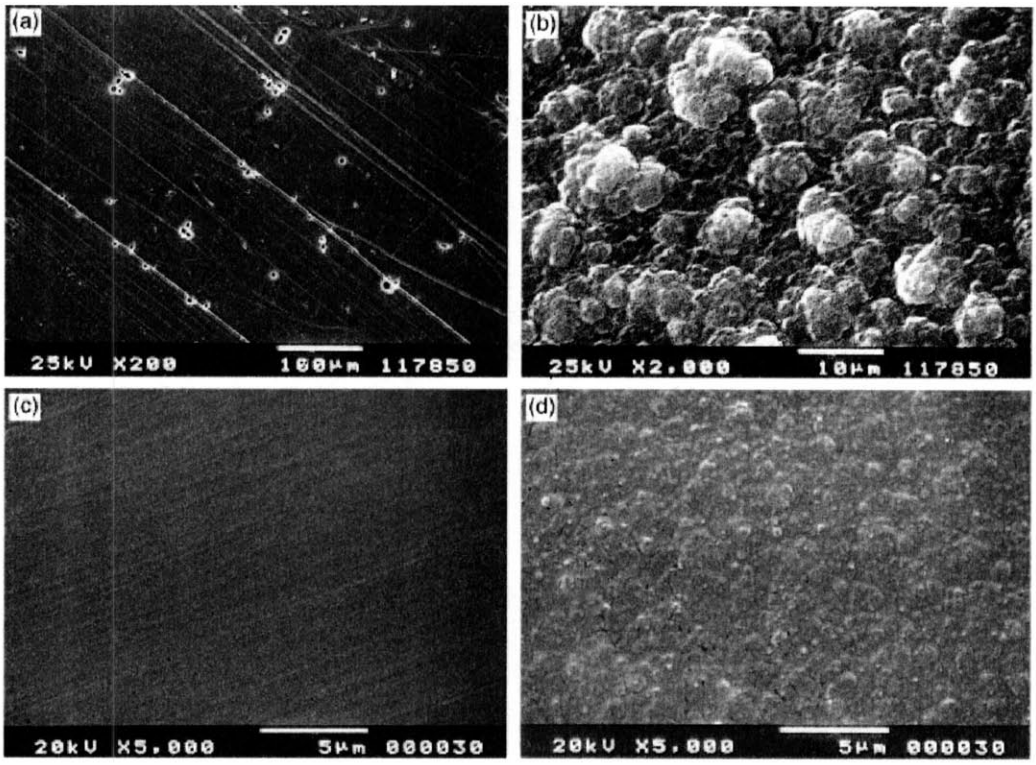

Figure 3-6: SEM micrographs of films polymerized onto platinum electrodes, from [6]. Films were polymerized galvanostatically at 0.2 A/m^2 at -40° C, from a solution of 0.1 M pyrrole and 0.1 M TBAPF6 in propylene carbonate. a) Unpolished electrode, electrode face. b) Unpolished electrode, solution face. c) Polished electrode, electrode face. d) Polished electrode, solution face. Note the different magnifications of each micrograph.

have overshadowed any effect of the electrode roughness. It would be interesting for Cascalheira et al. to repeat their experiment but deposit from propylene carbonate solution, to see if there is a point where the electrode roughness no longer determines the film surface morphology.

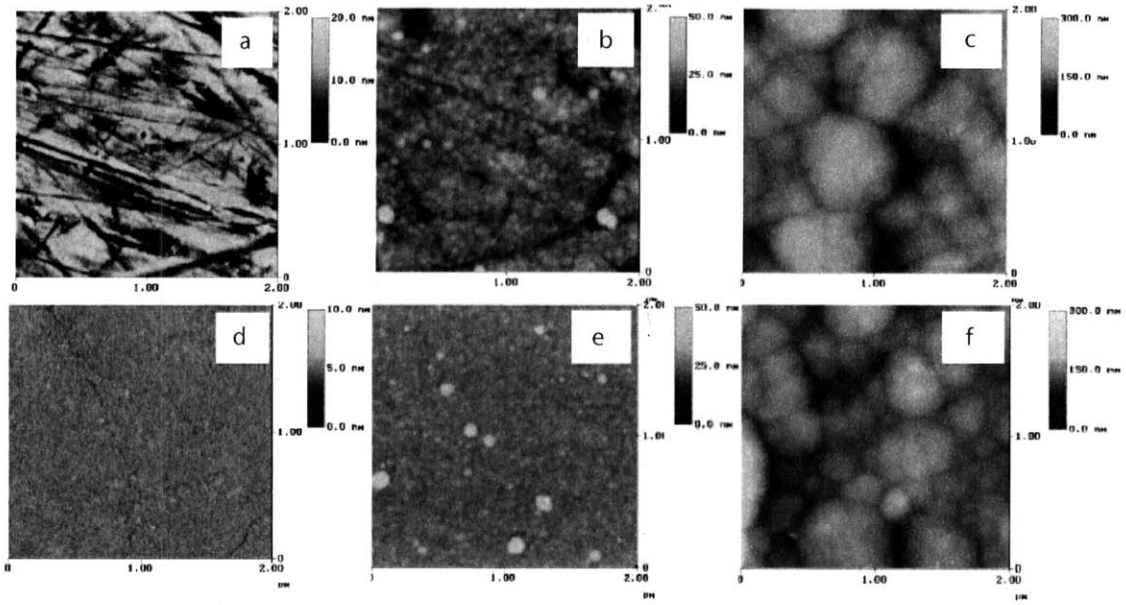

Figure 3-7: Tapping mode AFM images of copper foil electrodes and polypyrrole films, from [7]. Films were deposited galvanostatically at 20 A/m^2 from aqueous solution of 1 M sodium salicylate and 0.5 M pyrrole. The authors do not specify a deposition temperature, so it is assumed to be room temperature. a) Mechanically polished copper electrode. Rms roughness = 4.0 nm. b) Polypyrrole film after 250 C/m^2 was passed on mechanically polished electrode. Rms roughness = 4.7 nm. c) Polypyrrole film after 3000 C/m^2 was passed on mechanically polished electrode. Rms roughness = 17.9 nm. d) Electropolished copper electrode. Rms roughness = 0.3 nm. e) Polypyrrole film after 250 C/m^2 was passed on electropolished electrode. Rms roughness = 1.7 nm. f) Polypyrrole film after 3000 C/m^2 was passed on electropolished electrode. Rms roughness = 17.2 nm.

3.3.6 The Extent of Reaction

The first polymer chains to precipitate from solution onto the electrode have been observed to form a well-ordered structure, then a more nodular morphology develops as the deposition proceeds [8, 146, 147]. Yang et al. used Scanning Tunneling Microscopy (STM) to observe the surface morphology of polypyrrole as it was deposited from acetonitrile solution [8]. Upon initiation of the polymerization reaction, they observed that well-ordered helices formed on the graphite electrode. As the reaction proceeded, the typical "cauliflower" morphology developed on top of this well-ordered film of helices [8]. Possible differences in polypyrrole chain configuration as the film deposition proceeds are discussed at length in Section 4.2.2, while the STM images

that illustrate this transition are shown in Figure 3-8.

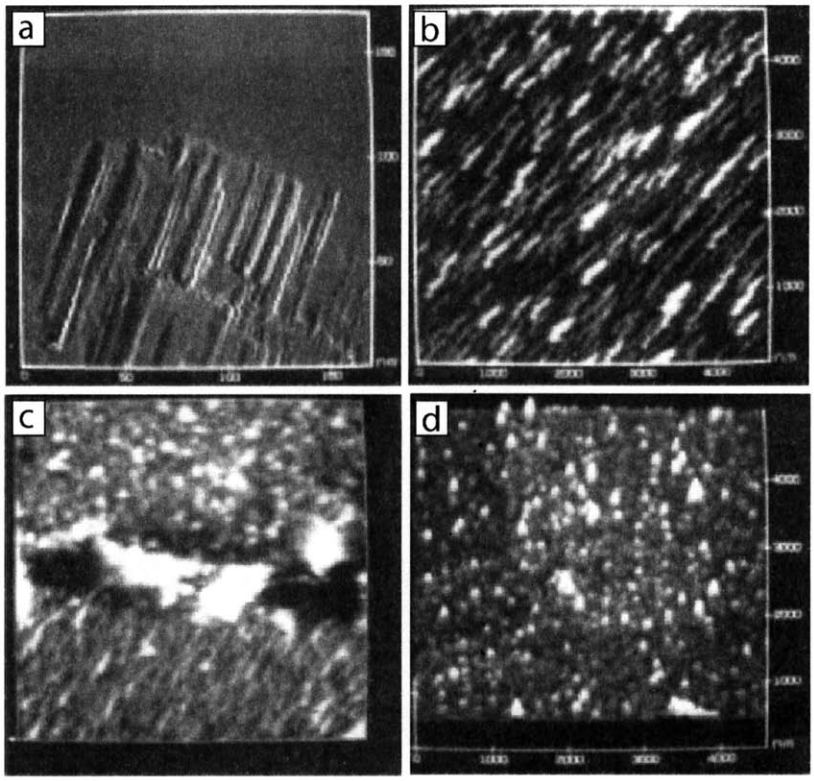

Figure 3-8: STM images of polypyrrole deposition, from [8]. Polypyrrole is deposited galvanostatically at 12 A/m^2 from a solution of 0.1 M pyrrole and 0.1 M tetraethylammonium *p*-toluene sulfonate in acetonitrile. a) Boundary between the graphite substrate (upper half of image) and first layer of polypyrrole (bottom half). b) Ordered polypyrrole film, 50 - 900 nm thick. c) Transition from ordered morphology to nodular morphology. The scale of the image is not given, but the height difference between the ordered and nodular regions is reported to be 110 nm [8]. d) Nodular morphology commonly observed in thick polypyrrole films.

The potential across the electrochemical cell increases over the course of the polymerization, which could cause the material deposited at the end of the deposition to be inferior to that produced in the beginning. Yoon et al. observed that the most highly conductive polypyrrole films (3.3 $\times 10^4$ S/m) were only $\sim$ 17 μm thick. When the reaction was allowed to proceed long enough for the film to grow to over 50 μm thick, the conductivity decreased 2.0 $\times 10^4$ S/m [6].

Stankovic et al. calculated the theoretical thickness that their electropolymerized polypyrrole films should be, based on a density of 1440 kg/m^3 [123] and the measured amount of charged passed [135]. They found that for films less than 30 μm thick,

the measured thickness matched the calculated thickness well, and the conductivity decreased slightly with thickness. For films thicker than 30 μm, the measured thickness was much larger than the theoretical thickness, and the conductivity decreased sharply with increasing thickness [135]. These observations point to a significant decrease in density once the film grew to thicknesses larger than 30 μm, but Stankovic et al. do not measure density directly or show micrographs of thicker or thinner films, so the change of morphology that accompanies this decrease in conductivity is unclear.

3.4 Chapter Conclusions

There is clearly a link between the morphology of conducting polymer actuators and their electroactive performance, although thus far work to this end has been confusing. Researchers have varied electrochemical synthesis parameters that have been shown to affect morphology, but then failed to investigate the resulting morphologies themselves. Or if they have investigated the morphology of their matieral, they have often not studied the materials' electroactive properties. There is such a large diversity of types of polypyrrole films produced that a clear methodology for achieving actuation metrics by controlling the film morphology has not yet been developed. However, there are some general themes, discussed below.

- There is an inverse relationship between deposition temperature and electronic quality. More highly conductive, metallic films are produced at lower temperatures, in almost all recipes. A similar effect is observed with current density in some recipes, i.e. more conductive, metallic films are deposited at lower current densities. In both cases, it may be that reducing the rate of reaction allows production of chains with fewer defects, increasing the metallic character of the product.

- The electrode material significantly changes the morphology of the polypyrrole film, but in a manner that is not necessarily straightforward. The effects of the surface roughness of the electrode and the chemistry of the electrode material have not been clearly separated, and both affect the roughness of the polypyrrole film. The smoothest, most stretchable films have been deposited on polished glassy carbon electrodes.

- The first polypyrrole chains to deposit onto the electrode do so in a well-organized manner, but the material becomes more disordered as the reaction proceeds and the film becomes thicker. This may be because the electrochemistry of the reaction changes due to the increased resistance of the working electrode, or because the surface onto which subsequent polypyrrole chains deposit is changing.

- The dopant counterion used during deposition can significantly change the microstructure of the film by imparting preferential alignment of the polypyrrole chains or changing the average spacing between polypyrrole chains. Large counterions have been reported to produce films that show a large and fast active strain, while smaller counterions provide a more conductive film. It is not entirely clear if the size, shape, or chemistry of the counterion is most important, but the seemingly infinite number of choices of counterions make this an area ripe for exploration.

- Films that have larger surface areas show better electrochemical ion transfer, which may lead to a faster electroactive response. A larger surface area could be produced by altering the counterion, electrolyte solution, and material and surface finish of the working electrode. However, films with higher surface areas also often suffer from lower electronic conductivities.

Polypyrrole can be synthesized under many electrochemical conditions, and the properties of the films deposited from different recipes may vary widely. There is a large body of prior work involving polypyrrole deposition, and therein one will find a library of techniques to achieve different morphologies. However, as of yet, which microstructure is best for actuation remains unclear. Our work to investigate this question will be presented in the remaining chapters of this thesis.

Chapter 4

Polypyrrole Microstructure as Probed by Scattering Techniques

Polypyrrole is a notoriously difficult polymer to study, due to its insolubility. X-ray and electron diffraction techniques are attractive methods by which to investigate polypyrrole's microstructure because they do not require one to dissolve or melt the polymer. X-ray diffraction is a useful tool for polymer microstructure investigation of polymers in general, as the wavelength (usually between 1.3 Å and 1.6 Å) is of the correct order to observe prominent polymer intra and interchain correlations. In addition, x-ray diffraction is a non-destructive technique, allowing one to take many images of the same sample, or image a sample while simultaneously stimulating it with temperature, force, or electricity. For the most easily interpretable data, one desires a highly crystalline and well textured sample that is wider than the diameter of the incoming radiation beam. In x-ray diffraction a typical beam diameter is 0.5 mm, so a highly crystalline sample that is at least 1 mm in diameter would be ideal. Unfortunately, for insoluble and unmeltable conducting polymers like polypyrrole it is impossible to make a such a sample. Electron diffraction allows the analysis of much smaller crystals (nanometers in diameter), as the spot size is significantly smaller. However, electron diffraction requires very thin samples (< 100 nm in thickness), and bombards the sample with a high flux of energetically charged particles, inducing significant changes in local bonding and altering the polymer structure even at low

at low doses. Additionally, electron diffraction requires a high vacuum (10^{-6} torr) sample environment, eliminating the possibility of many types of in-situ experiments. Ideally, a combination of electron and x-ray diffraction would be used to determine the microstructure and crystalline unit cell of a conducting polymer.

In this chapter, the basics behind x-ray diffraction are reviewed for the reader unfamiliar with scattering techniques. Polypyrrole is compared to a more traditional polymer - semicrystalline polyethylene - to help the reader understand the type of information one can gain from x-ray diffraction of polymers and why some commonly used techniques do not work for polypyrrole. Our efforts to probe the microstructure of polypyrrole by x-ray (Section 4.1) and electron (Section 4.2) diffraction are compared to previous works, and a more accurate picture of polypyrrole microstructure is proposed. In the second part of this chapter, we attempt to observe a microstructural change upon polypyrrole oxidation and reduction that could explain polypyrrole's electroactive properties (Section 4.3), and find that our proposed microstructure explains the observed electroactive response quite well.

4.1 Wide Angle X-ray Scattering

Due to its wide availability and relative ease of use, wide angle x-ray scattering (WAXS) is perhaps the most commonly used tool for determination of crystalline structure information in polymers. There is a wealth of information one can gain from diffraction experiments, but the disordered nature of polypyrrole precludes a detailed crystallographic analysis. Instead, diffraction is used to study characteristic spacings in the polypyrrole sample and to probe the microstructure in a qualitative way. The intention of this section is not to give a detailed description of the theory and wide range of applications of x-ray scattering. We seek to give the reader unfamiliar with x-ray diffraction a basic understanding of what kind of information can be gained by diffraction of polymers, and how diffraction can be applied to polypyrrole. For detailed background and experimental methods, the reader should consult the texts of Alexander [148], Kakudo and Kasai [149], and Warren [150].

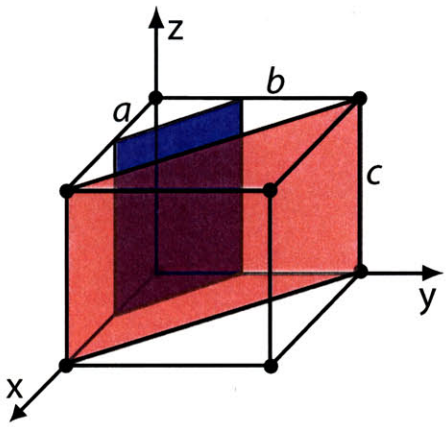

Figure 4-1: Theoretical unit cell, with sides a, b, and c. the (110)(red) and (220)(blue) planes are shown.

The regular, crystalline organization of atoms in a material is typically described in terms of the unit cell. A unit cell is the smallest unit that is repeated throughout a crystal by translation. A nice description of unit cells and crystal symmetry in polymers is presented in Chapter 1 of Alexander [148]. Planes within the unit cell are indexed by their intersections with the three main axes, so if a unit cell has three sides a, b, and c, plane (hkl) will have the intercepts $\frac{a}{h}$, $\frac{b}{k}$,and $\frac{c}{l}$. For example, if the cell shown in Figure 4-1 has the dimensions $a = b = c = 1$, then the (220) plane intercepts the x axis at $\frac{1}{2}$, the y axis at $\frac{1}{2}$, and the z axis at ∞. The distance between planes (hkl) is called the d spacing, can be calculated by the geometry of the unit cell. For example, for the cubic cell shown in Figure 4-1, where $a = b = c$ and the three axes are orthogonal, d can be calculated as follows [148].

$$d_{(hkl)} = \frac{a}{\sqrt{h^2 + k^2 + l^2}} \tag{4.1}$$

In a WAXS experiment (shown in Figure 4-2), a polymer specimen is irradiated with collimated x-ray radiation (typically Cu kα, with a wavelength of $\lambda = 1.54$ Å). The beam is scattered by planes of atoms in the sample, such as the (110) and (220) shown in Figure 4-1.[1] The angles by which these x-rays are diffracted is related to

[1]Both the (110) and (220) are planes of atoms, even though only the (110) intersects atoms within the unit cell. The unit cell is only meaningful in the context of a larger crystal, and the (220) plane will intersect atoms in adjacent unit cells. A good illustration of this is given in Figure 1-9 of Alexander [148].

the d spacings in the sample by Bragg's law (Equation 4.2),

$$\lambda = 2d\sin(\theta) \tag{4.2}$$

where λ is the x-ray wavelength, d is the characteristic spacing, and θ is $\frac{1}{2}$ of the scattering angle. When describing scattering results, it is often more convenient to express spacings in terms of the scattering vector q (shown in Figure 4-2). q is related to d via the following equation.

$$q = \frac{2\pi}{d} = \frac{4\pi}{\lambda}\sin(\theta) \tag{4.3}$$

The distance between the sample and detector should be chosen based on the range of q one is interested in collecting. For this work, the detector was typically 8 to 15 cm from the sample, in order to capture q = 0.1 to 2.5 Å^{-1} (the exact range varies based on the size of the detector). Polymer samples with larger spacings (for example, microphase separated block copolymers with d $\sim$ 50 nm) will require a larger sample-detector distance, in order to record data at a smaller q. The geometry to measure diffraction at $q < 0.1$ Å^{-1} is referred to as Small Angle X-ray Scattering, or SAXS. The only difference between SAXS and WAXS is the range of angles over which intensity is collected, determined by the sample-detector geometry.[2]

We employ a two dimensional area detector, and the places where the scattered beams hit the detector are observable as areas of higher intensity. If the sample is one large crystal (with dimensions comparable to the incident beam, usually $\sim$ 0.5 mm), one will observe a pattern of spots. The intensity and position of these spots can be used to calculate the parameters defining the crystalline unit cell. It should be noted that not all sets of lattice planes may give rise to observable spots, depending on the crystal structure, geometry of incident beam, sample and detector, and wavelength of incident radiation. Because it is only our intention to help the reader understand the presented diffraction data, the reader is directed to references [148–151] for the

[2]Another commonly used term for x-ray scattering is "XRD" (for X-Ray Diffraction). While both WAXS and SAXS are x-ray diffraction techniques, when the term XRD is used it is usually in reference to WAXS only.

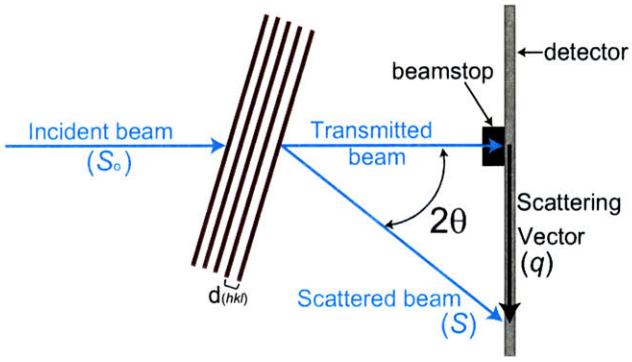

Figure 4-2: Schematic of scattering experiment. The incident beam (S_o) interacts with the planes of atoms in the sample with spacing $d_{(hkl)}$. X-rays that are not diffracted by atoms in the sample are transmitted and absorbed by the beamstop, while those that are diffracted (S) are collected by the detector. The degree of scattering is often quantified by scattering vector $q = 2\pi/\lambda(S - S_o)$

details behind crystalline diffraction and structure determination.

If the sample contains many crystals that are randomly oriented, one will observe a series of rings at the characteristic d spacings, often called a "powder" diffraction pattern. An example of this for semicrystalline polyethylene is shown in Figure 4-3. Detailed analysis of powder diffraction patterns is presented in Chapter 5 of Warren [150] and Section 1-4.5 of Alexander [148].

2D data can be plotted in one dimension by scanning from the center or integrating the intensity around the circular scattering peak as a function of distance from the center. An example of 2D and corresponding 1D WAXS data for semicrystalline polyethylene is shown in Figure 4-3. All diffraction data in this work was collected on a 2D detector, but often x-ray diffraction data is only collected in one dimension. For powder diffraction patterns, 1D data collection is adequate because the sample is the same at all azimuthal angles (ϕ in Figure 4-3). If the sample is not perfectly isotropic, several 1D scans at different azimuthal angles are necessary to capture the texture of the sample. In this case a 2D detector is preferable, as it allows one to collect much more information in a shorter amount of time.

If a polymeric sample is stretched, the polymer chains will orient in the direction of stretch (also called the machine direction or MD). As the chains become more organized, the diffraction pattern will become anisotropic. If the chains were perfectly

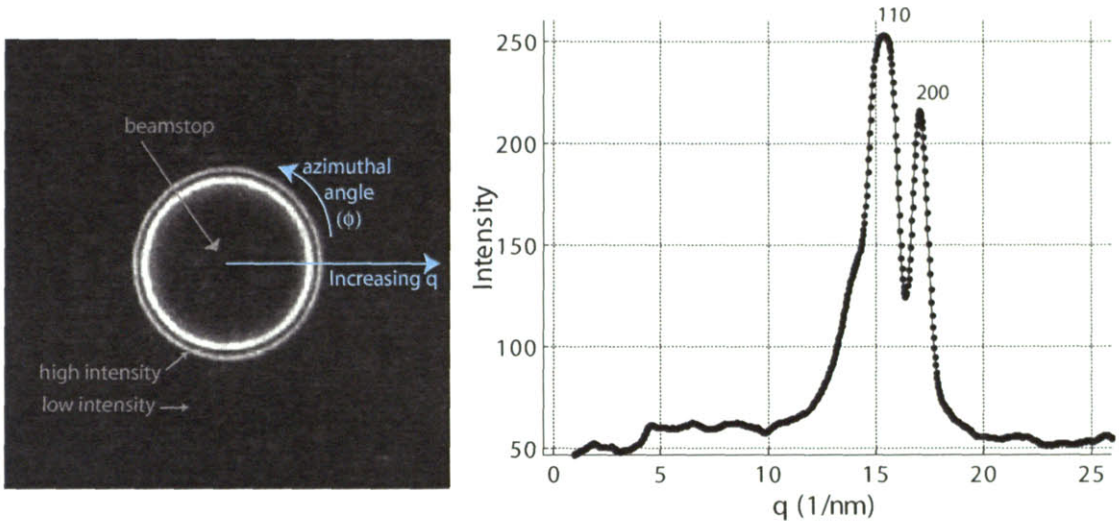

Figure 4-3: WAXS patterns for semicrystalline polyethylene [9]. The characteristic 110 (q = 1.53 $Å^{-1}$, d = 4.10 Å) and 200 (q = 1.70 $Å^{-1}$, d = 3.69 Å) spacings of the polyethylene unit cell are visible as two high intensity rings in the 2D data and two peaks in the 1D data.

organized, one would observe the spots of a single crystal diffraction pattern. However, polymeric single crystals are almost impossible to produce, so some disorder remains in almost every polymeric sample. This means that diffraction pattern of an oriented polymer shows features somewhere between isotropic rings and perfectly crystalline spots. Examples of a 2D WAXS pattern for stretched polyethylene and stretched polypyrrole are shown in Figure 4-4.

The types of microstructural information that can be obtained from a polymer 2D WAXS pattern are highlighted in Figure 4-4i. The distance of each peak from the center of the pattern is related to a characteristic d spacing in the sample via Bragg's law (Equation 4.2). The azimuthal angle (ϕ) and breadth of each peak ($\Delta\phi$) tell us about the orientation in the sample, as will be discussed in Section 4.1.1. The unoriented halos tell us about the amorphous component of the material, as will be discussed in Section 4.1.2. The width ($\Delta 2\theta$) of each peak tells us about the size of the ordered domains in the sample, as will be discussed in Section 4.1.3. Finally, the number of peaks tells us about the degree of long-range order in the sample. As the ordered regions grow larger, the material becomes well-organized enough to observe

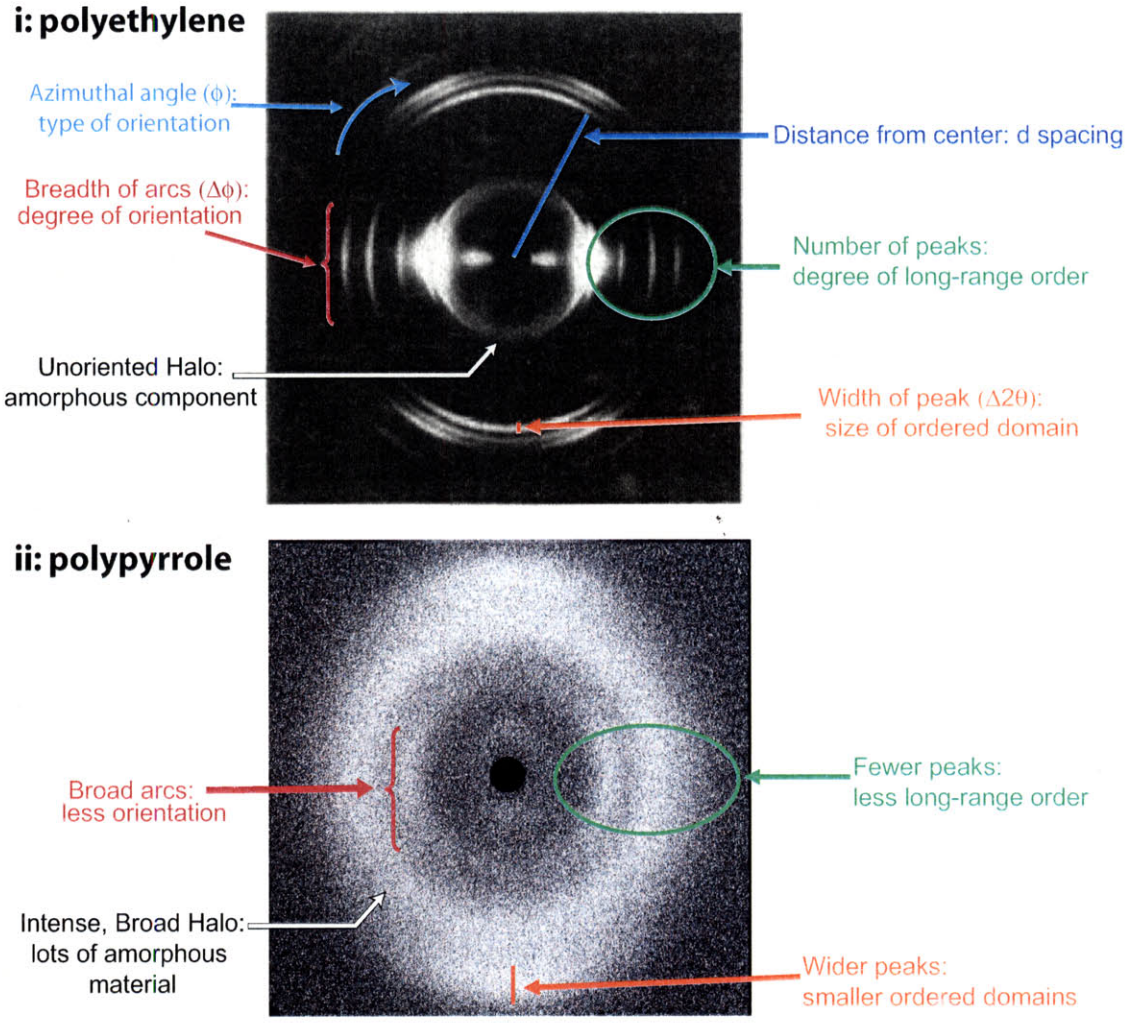

Figure 4-4: 2D WAXS patterns of i) Semicrystalline polyethylene drawn to 1200%, from [9] ii) Electrodeposited polypyrrole stretched to 200% as part of this work

higher-order reflections. For example, instead of just observing a reflection for the 100 plane in the unit cell, one might observe the 200 and 300 reflections as well. Higher order reflections are not observable in part ii of Figure 4-4, and were never observed in polypyrrole samples as part of this work.

4.1.1 Degree of Orientation

The material shown in Figure 4-4i is the same as that shown in Figure 4-3, but the diffraction patterns look very different because the sample in Figure 4-4i has been stretched. This has caused the polymer chain axes to align in the direction of stretch, so the planes of atoms diffracting the x-ray beam have become more organized. The breadth ($\Delta\phi$) of the diffraction peaks (shown in red in Figure 4-4) is inversely related to the degree of orientation via Hermans Orientation Parameter f [152],

$$f = \frac{1}{2}(3\langle cos^2\chi\rangle - 1) \tag{4.4}$$

where $\langle cos^2\chi\rangle$ is the average cosine squared of the azimuthal angle ϕ. For uniaxial orientation (the type that exists in stretched films, as will be discussed in Section 5.4.1), $\langle cos^2\chi\rangle$ is calculated as follows.

$$\langle cos^2\chi\rangle = \frac{\int_0^{\frac{\pi}{2}} I(\phi,\theta) sin\phi cos^2\phi d\phi}{\int_0^{\frac{\pi}{2}} I(\phi,\theta) cos^2\phi d\phi} \tag{4.5}$$

If a sample is randomly oriented (as the sample for Figure 4-3 is) $\langle cos^2\chi\rangle$ will be $\frac{1}{3}$, so the orientation parameter $f = 0$. If a particular reflection is perfectly oriented in direction $\phi = 0$ (the horizontal axis of Figure 4-4), $\langle cos^2\chi\rangle = 1$, so $f = 1$. If a reflection is perfectly oriented perpendicular to that ($\phi = 90°$),$\langle cos^2\chi\rangle = 0$, and $f = -\frac{1}{2}$. The proper calculation of $\langle cos^2\chi\rangle$ will vary depending on the type of orientation observed, and for analysis of more complex orientations the reader is directed to Chapter 10 of Kakudo and Kasai [149].

When comparing parts i and ii of Figure 4-4, it is clear that the polyethylene sample in part i has a much higher degree of orientation than the polypyrrole sample

in part ii. This is not surprising, as the polyethylene sample was drawn to six times the elongation of the polypyrrole sample. As part of this work, extensive effort was put toward orienting polypyrrole samples, as will be presented in Chapter 5.

4.1.2 Unoriented Component

Parts i and ii of Figure 4-4 both show an isotropic halo that consists of scattering from material that does not become oriented when the film is stretched. What material contributes to this halo will be influenced by the glass transition temperature (Tg) of the polymer. Tg is the temperature at which the polymer chains gain enough thermal energy to move around each other. At temperatures below the Tg, a polymer sample is mechanically stiff (the elastic modulus is typically 1 to 100 MPa [153]), and is considered to be "glassy." At temperatures above the Tg, the polymer is considered "rubbery," and sample that had a modulus of 10 MPa below its Tg may only exhibit a modulus of 0.01 - 0.001 MPa above it [153]. The Tg should not be confused with the melting temperature (Tm), which is higher than the Tg and is the temperature at which the sample will begin to flow. The Tg of a particular sample can be influenced by the chemistry and molecular weight of the polymer chain, the presence of small molecules in the sample, cross-linking between chains, and the crystallinity of the sample. Not all polymer samples show a Tg, though most will, even those polymers that do not melt (and therefore do not have a Tm).

The Tg of polyethylene is approximately -120°C, so at room temperature a polyethylene sample is far above its Tg. This means that after the sample used for Figure 4-4i was stretched, the amorphous polymer was able to relax back to its unoriented state. The unoriented halo shown in Figure 4-4i is scattering from this amorphous polymer, and can be separated from the crystalline components in the sample via the methodology discussed in Section 4.1.5.

In contrast to polyethylene, the Tg of polypyrrole has been shown to vary from ~50°C to ~150°C depending on the polymerization conditions [102, 154–156], and may change further depending on the redox state of the polymer. A Tg for polypyrrole films synthesized from our standard deposition recipe has not been published, and we

have not observed a clear Tg between 25°C and 150°C in our polypyrrole films. Based on the published results for other polypyrrole systems and the stiff nature of the films we produce, if there is a Tg for our films we believe that it is above room temperature. When processed at room temperature, our polypyrrole films must be stretched at very slow strain rates so the polymer chains can accommodate the sample deformation even though they have a very low mobility. After stretching, the polypyrrole chains have too little mobility to relax to their unoriented state, resulting in anisotropic scattering in the diffraction pattern. Therefore, the unoriented halo in Figure 4-4ii is not caused by amorphous polymer, and instead must be primarily due to correlations between small molecules that do not assume preferential orientation upon stretching. It has previously been reported to be caused by solvent [157] or counterion [123, 131, 158] scattering. By changing the solvent and counterion used in the deposition, we have shown that it is in fact a result of the counterion scattering. This result will be discussed further in Section 6.3.

4.1.3 Crystal Size

The width ($\Delta 2\theta$) of a given peak (shown in orange in Figure 4-4) is inversely related to the average size of the ordered domain via the Scherrer equation [149, 150],

$$\Delta 2\theta_{hkl} = \frac{0.94\lambda_{hkl}}{Lcos\theta_{hkl}} \tag{4.6}$$

where $\Delta 2\theta_{hkl}$ is the full width at half maximum of peak hkl, λ is the x-ray wavelength, and L_{hkl} is the average size of the ordered region contributing to that diffraction peak along the direction normal to the (hkl) plane.

In samples with highly crystalline peaks that do not overlap, determination of $\Delta 2\theta_{hkl}$ is relatively straightforward. However, in many materials the different peaks are located close enough to each other than their intensities overlap. In this case one must separate the peaks mathematically in order to determine the width at half maximum for each one. There are several commercially available software packages one can use to do this, and we show an example of this separation (conducted in

MATLAB^{tm}) in Figure 4-16. However, any mathematical separation of peaks runs the risk of incorrectly estimating the scattering attributed to each peak, as the peaks may have very different shapes and sizes. For example, scattering from noncrystalline material may produce a very broad hump that overlaps with several crystalline peaks (as is shown in Figure 4-8i), and a given sample may have more than one amorphous hump that overlap with each other. Furthermore, the peak width can be broadened for reasons other than a small crystalline domains, such as a distribution of d_{hkl} within the crystal or straining of the crystal lattice.

The inverse relationship between ordered domain size and peak width highlights an important difference between the two parts of Figure 4-4. The polyethylene sample shows relatively sharp peaks, giving a crystal size of $\sim$ 125 Å for the 200 peak by Equation 4.6. In contrast, the polypyrrole sample has broad peaks that give very small ordered domains ($\sim$ 10 Å for a gaussian fit of the outermost peak. for example). An ordered domain of 10 Å for this reflection would include only 3 chains, which it is significantly smaller that what is typically considered a crystal.

4.1.4 Determination of Crystal Structure

Several authors have conducted x-ray diffraction on stretched polypyrrole films to differentiate between characteristic reflections that occur parallel and perpendicular to the chain axis and assign these reflections physical features [10, 123, 130, 143]. A schematic of these characteristic reflections is shown in Figure 4-5iv. We use the letters "**a**, **b**, **c**" and "**Γ**" to describe the characteristic reflections in polypyrrole, in order to relate their physical origins to a crystalline unit cell. However, diffraction patterns of polypyrrole show that the films do not contain large amounts of crystalline material. Instead, there are very small well-ordered regions ("bundles") within a relatively disordered matrix, as is shown in Figure 4-5. Our description of this bundled microstructure was developed based on the results presented throughout this chapter, and is discussed in detail at the end (Section 4.4). Here we present an illustration of the structure to help the reader understand the characteristic spacings observed in the diffraction patterns. which will be referred to as the evidence for this structure is

discussed.

Reflection **a** occurs at 3.4 Å, and is attributed to the face-to-face distance between polypyrrole rings on adjacent stacked chains [6, 10, 11, 130, 131]. This assignment is shown in Figure 4-5, and is supported by the fact that in oriented films this spacing occurs perpendicular to the chain axis. Reflection **c** orients parallel to the chain axis, and has been attributed to a feature repeated along the polymer chain. Yamaura et al. report the d spacing of reflection **c** to be 7.3 Å, and assign it to the trans-planar dipyrrole repeat [123]. Nogami et al. observed this reflection at a spacing of 6.46 Å, and attributed the difference from the measured size of a dipyrrole unit to the polypyrrole chains having a deviation of 25° to 30° from the machine direction [10]. However, it is expected that the chain axes will align parallel to the MD upon stretching, and we find no logical reason for the chain axes to assume a regular 25° deviation. Furthermore, a regular tilt of the chain axes should also cause reflection **a** to deviate from its expected value, which neither we nor Nogami et al. observe [10]. It is possible that the deviation of reflection **c** from the size of the dipyrrole unit is caused by a staggering of polypyrrole chains that are axially aligned in the MD, as is schematically illustrated in Figure 4-6. Such an offset has been calculated to be energetically favorable in π-stacked quarterthiophene units [159], and we expect it to also be favorable for small sections of polypyrrole. Similarly to what has been previously observed in polyurethanes [160–162], the configuration shown in Figure 4-6 would result in two diffraction maxima approximately $\pm 28°$ from the MD at 6.6 Å instead of one peak along the MD at 7.3 Å. We observe spacing **c** at approximately 6.6 Å, and while we do not observe two separate maxima the peak is so broad that the two maxima could be overlapping. We cannot conclusively determine the reason for the observed deviation from the dipyrrole spacing because the peaks in our diffraction pattern are broad and poorly defined, but we believe it more likely to be caused by a regular offset of the polypyrrole chains than a regular tilting of the chains away from the MD.

Several studies have been conducted to observe how the WAXS reflections change with different counterions [10, 97, 123, 131, 163]. Yamaura conducted a survey of

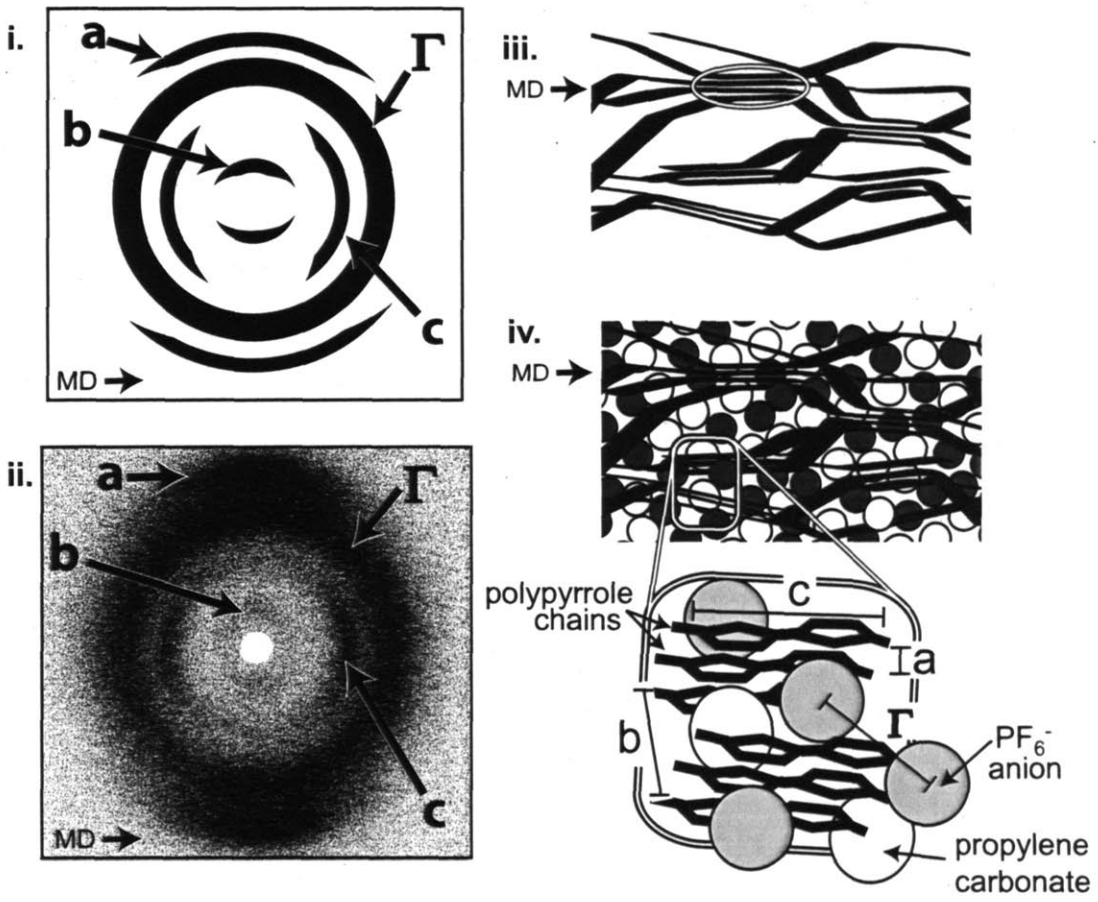

Figure 4-5: Diagram of characteristic reflections in stretched polypyrrole. The direction of stretch (labeled "MD" for machine direction) is horizontal in all parts of this figure. i) Schematic of characteristic reflections observed in wide-angle x-ray diffraction patterns of stretched films. ii) Example of wide angle x-ray diffraction pattern from stretched film. iii) Diagram of polypyrrole chains held together by small well-ordered regions, which we call bundles. The chains and bundles are oriented in the MD, and a single bundle is circled. iv) Diagram of components of stretched polypyrrole film. Two bundles are highlighted, and the physical origins of the characteristic reflections are identified in the enlargement. The chain axes and bundles are preferentially oriented in the MD, while the PF_6^- anions and propylene carbonate are randomly distributed.

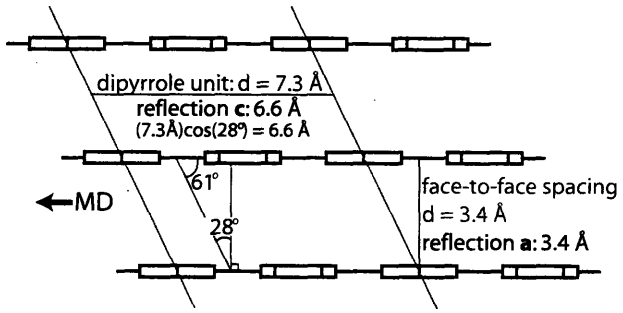

Figure 4-6: Schematic illustration of staggered polypyrrole chains. The polypyrrole chain axes align in the MD (horizontal), but are offset from each other, causing reflection **c** to be observed at 6.6 Å instead of at the dipyrrole spacing (7.3 Å).

polypyrrole films synthesized with different dopant anions subsequently stretched 100%, and found a linear relationship between the d spacing of reflection **b** (Figure 4-5) and the counterion size. They attributed this peak to the side-by-side chain spacing with a counterion in between, and extrapolated to zero counterion size to get a spacing of 7.5 Å for the estimated side-by-side spacing of two pyrrole chains with no counterion in between [97]. Earlier, Wernet et al. produced polypyrrole doped with n-alkylsulfate and n-alkylsulfonate salts of varying length, and observed the x-ray diffraction patterns of the unstretched films [132]. Wernet et al. also observed a linear dependance of the d spacing of the lower angle peak on the number of carbons in the alkyl chain, and assigned this peak (reflection **b** in Figure 4-5) to the spacing between stacks of polypyrrole chains. As larger counterions sit between the stacks, the stacks will move further apart, and the d spacing of reflection **b** will increase. While we believe this assignment for reflection **b** to be plausible, in this thesis we have not observed a straightforward dependance of reflection **b** to the counterion used in deposition. Reflection **b** also seems to be influenced by the choice of solvent and electrode material, as will be discussed further in Section 6.3.

Reflection $\mathbf{\Gamma}$ does not become anisotropic upon stretch, and has often been attributed to scattering of amorphous polymer chains [6,10,158,163–165] as is discussed further in Section 4.1.5. This assignment suggests that there is no contribution from PF_6^- scattering to diffraction pattern, which is highly unlikely given the fact that the PF_6^- anions contain the highest atomic number elements in the system. Further-

more, even non-crystalline polymer chains will assume preferential orientation upon stretching below their glass transition temperature (Tg), as the chain axes align in the direction of stretch. As was discussed in Section 4.1.2, reflection $\mathbf{\Gamma}$ must be caused by small molecules that do not become oriented even as the polymer chains become ordered. We have shown that it is determined by the counterions, as will be discussed further in Section 6.3.

As a result of their x-ray analysis, Nogami et al. proposed the unit cell that is shown in Figure 4-7. PF_6^- anions fit in between the planes of stacked polypyrrole chains (along the b direction), but Nogami et al. do not give a precise distribution for the PF_6^- within this plane, or even the number of anions that fit into the unit cell [10]. It is interesting to note that the unit cell shown in Figure 4-7 does have the staggered chain configuration shown in Figure 4-6, but Nogami et al. do not suggest this may influence the d spacing of reflection **c**.

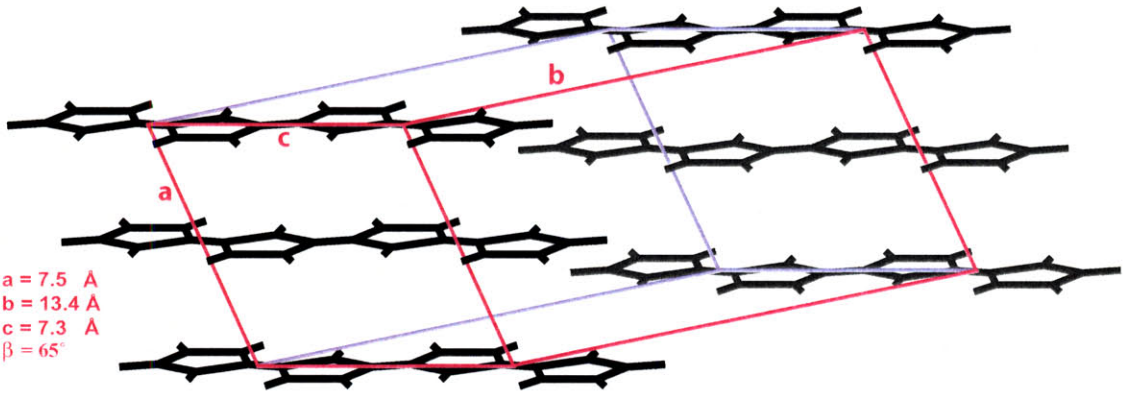

Figure 4-7: Polypyrrole unit cell, as proposed by Nogami et al [10]. Polypyrrole chains are stacked with a 3.4 Å interplanar spacing. The chains are offset with an angle of $\beta = 65°$. PF_6^- anions sit between polypyrrole stacks (along the b axis), but are not ordered in a crystal lattice. The c axis of the unit cell contains one dipyrrole unit, the a axis contains two polypyrrole chains, and the b axis contains one chain and one space for PF_6^- anions.

If one assumes there is one PF_6^- anion for every three pyrrole units [11, 41, 82, 132, 154], the unit cell proposed by Nogami et al. contains 4 pyrrole units and 1.3 PF_6^- anions. The unit cell volume is 6.65×10^{-28} m^3, giving a calculated density of 1130 kg/m^3 for perfectly crystalline polypyrrole/PF_6^-. The calculated crystalline density of a polymeric material is usually higher than the observed density, as the

observed density includes both crystalline and (usually less dense) amorphous material. However, we observe an average density of 1500 kg/m^3 for (unprocessed) films prepared from our standard recipe conditions, a typical value for polypyrrole doped with PF_6^- [6, 41, 93, 123, 166]. Instead of the unit cell proposed by Nogami et al., we propose that the dopant anions are distributed outside of any crystalline bundles as is described in Section 4.4. This would make the observed density higher than the calculated crystalline density, because the non-crystalline material contains heavier elements (namely PF_6^-). Furthermore, we propose that the ordered regions in polypyrrole are so small they should not be considered crystals at all, making the concept of a crystalline unit cell irrelevant.

4.1.5 Percent Crystallinity

In addition to physically unlikely unit cells, the body of polypyrrole literature also contains examples of incorrectly calculated percent crystallinity. The assignment of a gaussian fit of reflection $\mathbf{\Gamma}$ to all of the noncrystalline component leads to a calculation of percent crystallinities of 20% to 50% for polypyrrole doped with PF_6^- [6, 165]. These are extremely high values considering the lack of clear crystalline peaks in the diffraction pattern, and a doping level of one PF_6^- anion for every three pyrrole rings in the as-deposited film [41, 82, 132, 154] so at least 30%vol of the film is non-crystalline PF_6^-. Moreover, elemental analysis shows that films synthesized from propylene carbonate solution contain up to 20 - 30%wt propylene carbonate post-synthesis. A 50% crystallinity for this system would mean that the entire polymer component is crystalline, which is simply not physically realistic.

Determination of percent crystallinity from x-ray diffraction patterns requires the separation of crystalline peaks from the amorphous halo(s). An example of a diffraction pattern where this methodology is appropriate is shown in Figure 4-8i [167]. In this example, there are several peaks caused by scattering from the crystalline part of the material, superimposed upon a broad hump caused by the scattering from the amorphous part. In polypyrrole (Figure 4-8ii) the different peaks cannot be clearly separated, and there is no discernable difference in shape between peaks that

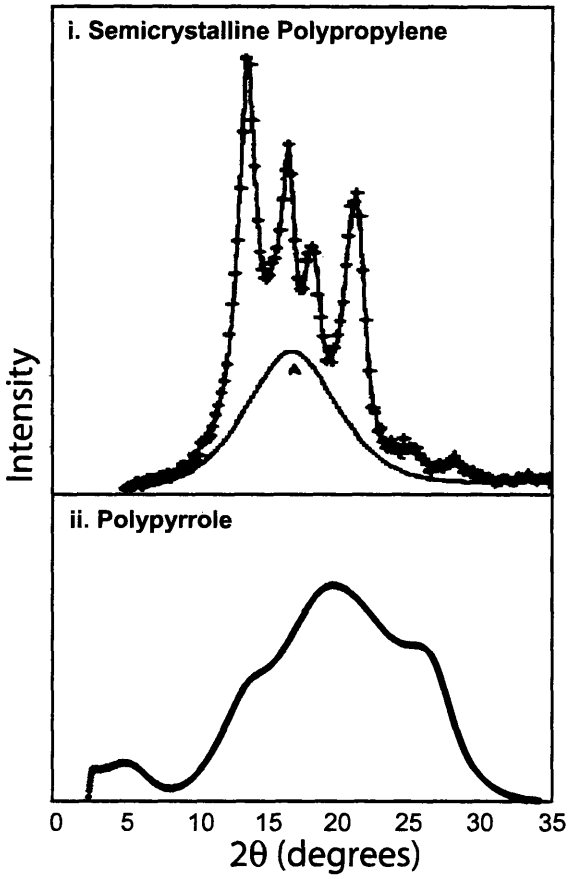

Figure 4-8: 1D diffraction patterns for i) Semicrystalline polypropylene with ~50% crystallinity from [167]. The raw data is plotted with "+", while the contribution from amorphous scattering is labeled "A". ii) Polypyrrole. There are no clear crystalline peaks that can be separated from an amorphous contribution.

have previously been assigned to "crystalline" scattering or "amorphous" scattering. Even if one assigns reflection Γ to non-crystalline PF_6^- anions, the broad. overlapping nature of the other reflections prevents one from unambiguously separating them from an "amorphous" contribution to quantify the percent crystallinity based on the diffraction pattern.

The fact that the different peaks in the diffraction pattern are overlapping also makes it difficult to separate them enough to determine their full width at half maximum. which is necessary to determine crystalline size via the Scherrer equation (Equation 4.6). It is possible to model the diffraction pattern as a series of over-

lapping gaussian peaks (as is done in Figure 4-16), but one should note that this is an estimate of the actual peak shape, at best. It is also possible that there is a non-gaussian contribution from amorphous material (similar to that shown in part Figure 4-8i) that further distorts the peak shape. While the Scherrer equation is a useful tool to demonstrate the inverse relationship between peak breadth and crystallite size, one should note that in a case like polypyrrole, crystallite sizes calculated with the Scherrer equation are very crude approximations.

4.2 Electron Diffraction

The methodology for the calculation of percent crystallinity described in Section 4.1.5 requires crystals that are large enough to be probed by x-ray diffraction. When the average crystal size is small (< 10 nm) and the percent crystallinity is low (< 20%) the peaks observed via x-ray diffraction are generally broad and weak, making them exceedingly difficult to separate from amorphous halos arising from the noncrystalline portions of the sample. In order to search for smaller crystals, we turn to electron diffraction. Electron diffraction is conducted in a Transmission Electron Microscope (TEM), and by controlling the beam settings on the TEM we can vary the electron beam spot size. We do not discuss many details of transmission electron microscopy here, and direct the interested reader to the texts by Williams and Carter [168,169] for more information. Transmission electron microscopy requires very thin films (<100 nm), and by limiting the diameter of the electron beam (~10 nm) we can probe very small sample volumes. When one illuminates only a small volume surrounding (or within) crystalline material, the percent crystallinity of the volume being probed will be high even if the percent crystallinity of the entire sample is very low.

By probing only a small volume surrounding crystalline material, more easily interpretable diffraction patterns can be produced. Unfortunately, it may be very difficult to find the crystalline material if the total percent crystallinity of the sample is low. Even if crystals are discovered, radiation damage from the electron beam will often destroy polymer crystals in a matter of seconds. To avoid this one can

focus the microscope on one area of the sample, block the electron beam, move to an adjacent area of the sample, then unblock the beam to collect the diffraction pattern of this pristine area. However, this method prevents examination of the new area before exposure. If the total percent crystallinity of a sample is low, this method will produce many images of the non-crystalline parts of the sample.

Prior efforts towards electron diffraction of polypyrrole are described in Section 4.2.1, while our efforts towards the same are presented in Section 4.2.2. We do not find significant crystals even with electron diffraction, similarly to others who have worked with PF_6^- doped polypyrrole [170]. We also find that radiation damage from the electron beam changes the structure in the film, as will be discussed in Section 4.2.3.

4.2.1 Prior Work

One of the first structural studies of polypyrrole was conducted by Geiss et al., who studied undoped[3] (non-conductive) polypyrrole by electron diffraction in 1983 [11]. The electron diffraction patterns showed diffuse rings or arcs instead of crystalline peaks, but these diffuse features were located at d spacings that could be assigned to structural features within the polymer. Cross-sectional views implied that the polymer chains were preferentially oriented parallel to the film surface, but no quantification of this orientation was given. Geiss et al. proposed the first published unit cell for polypyrrole (Figure 4-9), which is monoclinic and has $P2_1/a$ symmetry [11]. This unit cell contains 4 monomers, and has a volume of 3.66×10^{-28} m^3 (density = 1180 kg/m^2). The most prevalent spacing observed in electron diffraction is the face-to-face polypyrrole chain spacing, which Geiss et al. call 002 and measure at 3.41 Å. They also observe a second and third order to this spacing (004 at 1.72 Å and 006 at 1.14 Å, respectively), implying a limited amount of long-range order in their structure. Finally, they report observing the third order (2.18 Å) of the 7.35 Å repeat unit along the polymer chain. Geiss et al.'s work was conducted on neutral polypyrrole.

[3]Films were electropolymerized doped with ClO_4, then electrochemically reduced to produce neutral polypyrrole [11].

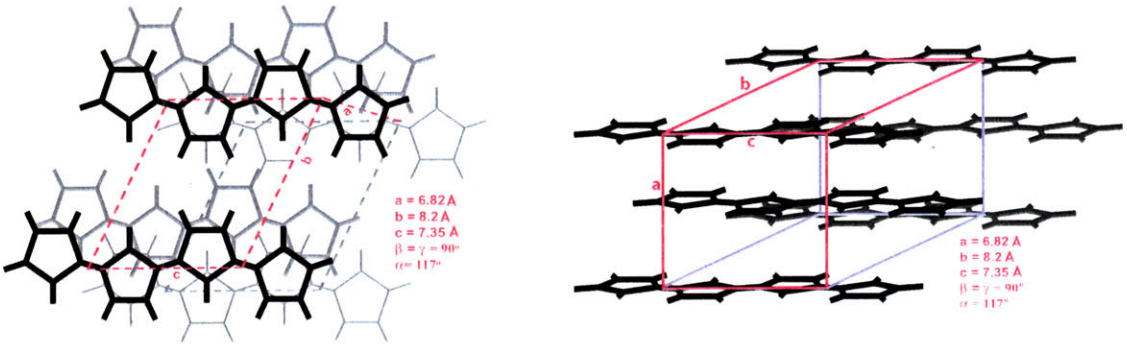

Figure 4-9: Polpyrrole unit cell as proposed by Geiss et al. [11]. Chains of polypyrrole are stacked ABAB in a monoclinic unit cell.

which was electrochemically reduced to be non-conductive. The authors claim (but do not show data) that polypyrrole doped with perchlorate anions produces almost exactly the same characteristic spacings in electron diffraction [11]. However, because the samples were electrochemically reduced, it is likely that all of the perchlorate anions were not removed. As an electrochemical reduction proceeds the polypyrrole film becomes less conductive, effectively stopping the reduction before it is complete.

Fink et al. conducted electron diffraction on polypyrrole produced with a suite of different counterions, and indexed their diffraction maxima to Geiss et al.'s model. They observe reflections at d = 1.12 Å (indexed to 006), d = 1.69 Å (indexed to 004), d = 3.41 (indexed to 002), and 2.18 Å (indexed to 030) for films doped with a variety of counterions [170]. Interestingly, they do not observe the 002 reflection for polypyrrole doped with PF_6^- (which is quite relevant to this work as will be discussed in Section 4.2.2), but they do not discuss why this reflection is missing.

A helical configuration for polypyrrole chains has also been proposed based on electron diffraction studies [12, 171]. If the polypyrrole rings are generally N trans, one should expect planar chains. However, if the polypyrrole rings are N cis, the chains should twist into a helical conformation [172]. Chu et al. observed nanoscopic crystalline fibers via TEM in chemically polymerized polypyrrole, all of which had diameters that were multiples of 20 Å. This led them to propose that each polypyrrole chain coiled into a single helix with a 20 Å diameter, and these helices packed in a hexagonal lattice shown in Figure 4-10 [12]. This is close to the confirmation

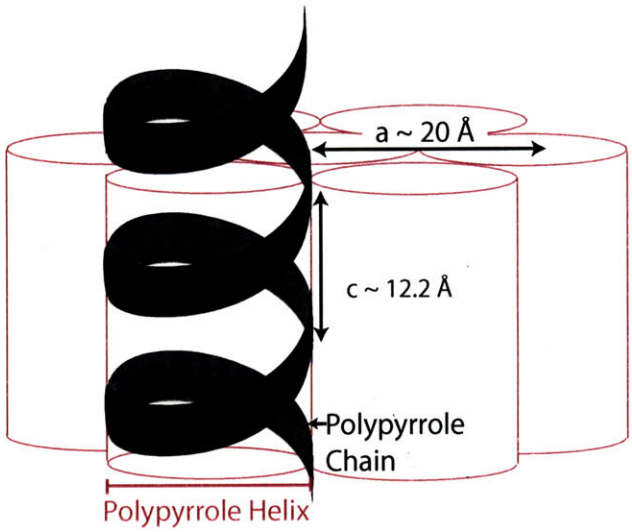

Figure 4-10: Helical polypyrrole structure as proposed by Chu et al. [12] and Davidson et al. [171]. Chains of polypyrrole are coiled into helices approximately 20 Å in diameter, and packed into a helix with dimensions $a \sim 20$ Å and $c \sim 12.2$ Å.

for poly(3-methylthiophene) observed by Garnier et al. [172]. Garnier et al. produced highly crystalline poly(3methylthiophene) samples in which crystalline planes of atoms were visible in TEM micrographs and many crystalline peaks were observed via electron diffraction. They indexed their pattern to hexagonally packed coils, with lattice indices a = 19 Å and c = 12.2 Å [172]. It is interesting to note that on the basis of this hexagonal unit cell, the density of a crystalline polythiophene sample doped with $CF_3SO_3^-$ is calculated to be 1620 kg/m^3, which is slightly higher (as would be expected) than the measured value for that system of 1460 kg/m^3 [172]. Davidson et al. also proposed a helical structure for polypyrrole, based on their electron diffraction of polypyrrole electrochemically synthesized and doped with dodecyl sulfate [171]. Davidson et al.'s model consists of hexagonally packed helical chains, with a = 18 Å and c = 12.4 Å [171]. Yang et al. observed a similar structure using scanning tunneling microscopy (STM) to monitor polypyrrole electrodeposition. They directly observed helical polypyrrole chains with a diameter of 18 Å and a pitch of 8 Å during the initial stages film growth [8, 146].

While a helical structure is certainly possible for polypyrrole, diffraction of stretched films show that this is not the structure found in bulk films. As the polymer film

is stretched, the chain axes (or helical axes) align in the machine direction. X-ray diffraction results have shown that the face-to-face pyrrole spacing ($\sim$ 3.4 Å) aligns transverse to the MD in stretched films [10, 57, 123, 130]. If the polypyrrole chains were helical, this would not be the case. Further analysis of the chain configuration in oriented films will be presented in Section 5.2.

It is possible that polypyrrole assumes a helical configuration only during the first layer of material deposited, when the newest polypyrrole chains are in direct contact with the substrate. Yang et al. observe helices during the very beginning of the deposition, but once the film thickness reaches $\sim$ 500 Å, they observe a disordered, nodular morphology [8]. Davidson et al. only observe crystalline diffraction patterns in the thinnest areas of the film, but do not say how thin the film must be for crystalline peaks to be observed [171]. It is possible that the helical structure proposed by these authors does exist for very thin polypyrrole films, but that this structure is lost as the deposition proceeds far enough to make free-standing films. Geiss et. al. produce their electron diffraction samples by microtoming thin slices from 0.5 - 2 μm films [11]. By the time the films reach this thickness, the helical configuration may have been lost.

4.2.2 Electron Diffraction of Polypyrrole Samples

As part of this work, electron diffraction was used to search for crystals in small areas. Thin polypyrrole films were deposited onto small (9 mm $\times$ 20 mm) gold-coated polyethylene terephthalate or glassy carbon electrodes from a solution of 0.05 M Pyrrole, 0.05 M TEAPF6, and 1%vol water in propylene carbonate. The deposition was conducted at -40°C with a current density of 1 A/m^2 for 60 seconds (passing approximately 5 $\times$ 10^{-11} C/m^2 of charge). The resulting film was reddish in color, and approximately 500 Å thick (as measured by profilometry).

In order to lift off small samples for electron diffraction, the lift-off procedure shown in Figure 4-11 was used. The working electrode (with film) was removed from the electrochemical cell and rinsed in a clean salt solution (0.05 M TEAPF6/PC). Excess solution on the film surface was blotted with a Kimwipe^{tm}. A glass pipette

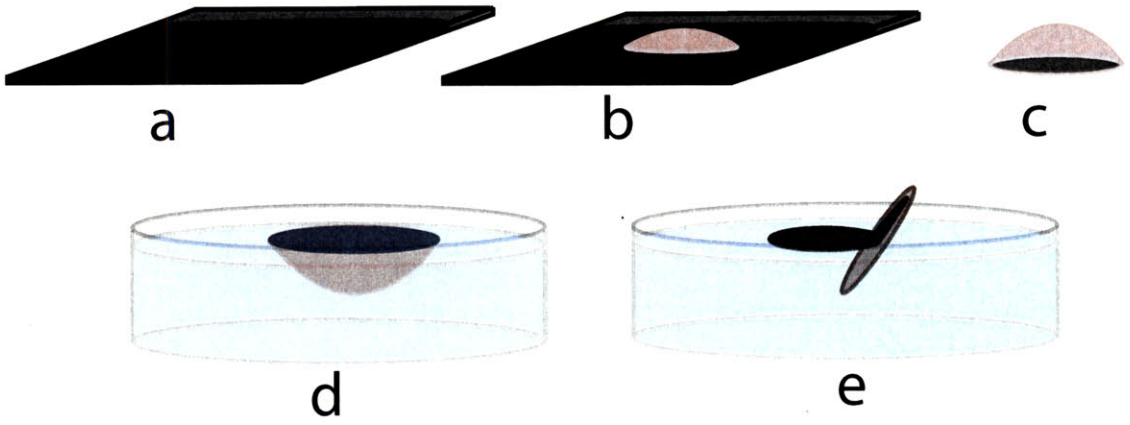

Figure 4-11: Procedure to make TEM samples from thin polypyrrole films. a) Deposit thin polypyrrole film on working electrode. Remove from bath and dry. b) Drop polyacrylic acid solution onto polypyrrole film. Dry in 60°C oven for 1/2 hour. c) Remove hardened polyacrylic acid drop from working electrode. Polypyrrole film will be stuck to bottom of drop. d) Place drop face-up in dish of distilled water. Allow to soak until all polyacrylic acid is dissolved. e) Remove polypyrrole film from water surface using TEM grid. Allow to dry in air.

was used to place a small drop (diameter $\sim$ 2 mm) of polyacrylic acid onto the film surface. The electrode (with film and polyacrylic acid) was placed into an oven at 60°C for 30 minutes to harden the polyacrylic acid drop. Tweezers were used to remove the hardened drop, along with the polypyrrole film underneath. The drop was placed polyacrylic acid side down in a petri dish of water, and allowed to soak overnight. After dissolution of the polyacrylic acid, the polypyrrole film samples remained floating on the surface of the water, and were lifted off with TEM grids. The grids were allowed to dry for several hours before introduction to the high vacuum environment of the microscope.

Electron diffraction was conducted on one of three machines: A JEOL 200CX general purpose (tungsten filament) 200 KV TEM, a JEOL 2011 high contrast digital TEM, and a JEOL 2010F field emission TEM. Unfortunately, crystalline peaks were never observed for polypyrrole samples. Instead, diffuse rings were observed. A typical electron diffraction pattern for polypyrrole is shown in Figure 4-12. The fact that sharp crystalline peaks were never observed, even with very low electron beam doses, means that the polypyrrole films are not crystalline. The features that

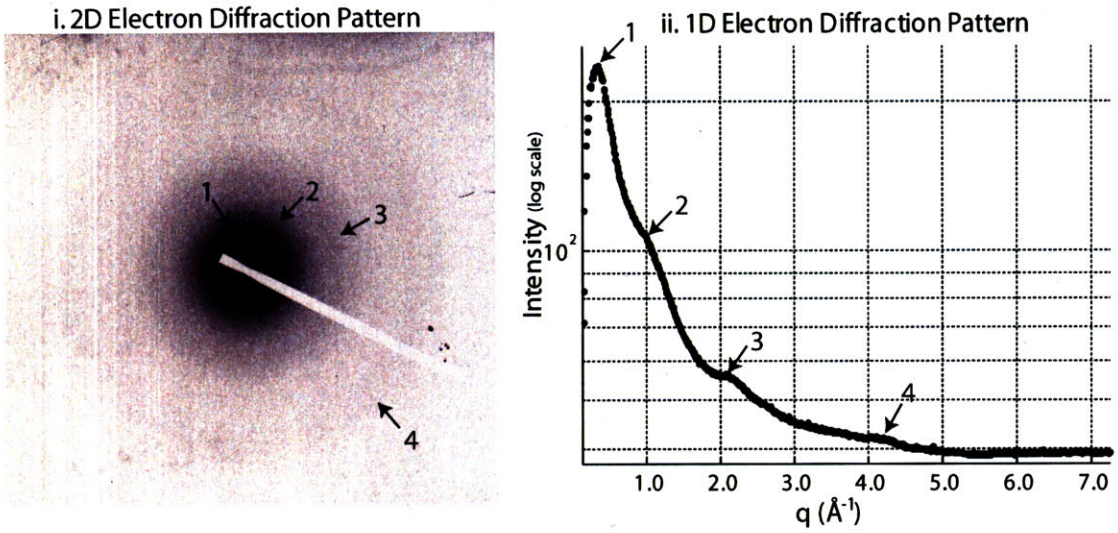

Figure 4-12: Electron diffraction pattern from thin polypyrrole film. Film was deposited from TEAPF6/PC solution at 1 A/m^2 for one minute onto a glassy carbon electrode. Diffraction pattern was taken on a JEOL 2011 TEM with an accelerating voltage of 200 KeV and a working distance of 800 mm. Condenser aperture = 3. Small angle diffraction aperture = 2. Spot size = 4. i) 2D electron diffraction pattern. Three main rings are visible. ii) 1D electron diffraction pattern, with local maxima at the three ring positions of part i.

cause diffraction maxima at characteristic spacings are small enough to be randomly distributed even within the electron diffraction spot size (down to $\sim$ 100 Å).

In Figure 4-12, reflection 1 occurs at $q \sim 0.4$ Å^{-1}, which is similar to to reflection **b** in Figure 4-5. Reflection 2 is observed at $q \sim 1.0$ Å^{-1}, similar to to reflection **c**. However, not all of the spacings observed in Figure 4-12 are the same as those observed in x-ray diffraction experiments (Figure 4-5). Reflections 2 and 3 occur at $q \sim 2.1$ Å^{-1} and $q \sim 4.2$ Å^{-1}. These spacings do not correspond to reflections observed with x-ray diffraction as part of this work, but do correspond to spacings observed by others via electron diffraction [11,170]. Upon continued exposure to the electron beam, additional spacings corresponding to those observed in Figure 4-5 do develop, as will be discussed in the next section.

4.2.3 Beam Sensitivity

Geiss et al. make note of the sensitivity of neutral polypyrrole to electron beam damage, giving a critical dose (for complete loss of the diffraction pattern) of 20 A/m^2 at an accelerating voltage of 100 keV [11]. This is quite sensitive when compared to polyethylene, for example, which has a critical dose of 1000 A/m^2 under the same conditions [11]. In this study, polypyrrole was observed to be much more robust under the electron beam than Geiss predicts. It is likely that the high electrical conductivity of the material used in this work helped it be more resistant to beam damage. However, when the microscopy conditions are carefully controlled, one can observe the effect of exposure to the electron beam on the electron diffraction pattern. Three examples are shown in Figure 4-13.

The pink and black curves in Figure 4-13 are taken under carefully controlled exposures, with a small condenser aperture and spot size chosen to limit the number of electrons hitting the film. The diffraction pattern was focused by exposing polymer in one area of the film, then the beam was blanked and the sample was moved such that a new area of the film (not previously exposed) was in the beampath. The pink curve in Figure 4-13 is the result of the first three seconds of exposure of this new area of the film. After the pink curve was exposed, the same area was exposed to the beam for approximately thirty seconds, and then exposed for another three seconds while the black curve in Figure 4-13 was collected. After thirty seconds of exposure the general background scattering increased slightly, and the peak at $q \sim 0.4$ $Å^{-1}$ shifted to approximately $q \sim 0.34$ $Å^{-1}$. In order to see the effect of extensive exposure on the same region, the condenser aperture and spot size were increased to allow more electrons to interact with the film. The film was exposed to the electron beam for several minutes, and then the blue curve in Figure 4-13 was collected over the course of 5.6 seconds. Due to the increased electron flux, the intensity of the blue curve in Figure 4-13 is higher than the other two. It appears that the peaks at $q \sim 2.1$ $Å^{-1}$ and $q \sim 4.2$ $Å^{-1}$ have shifted to $q \sim 1.9$ $Å^{-1}$ and $q \sim 3.8$ $Å^{-1}$. This shift is likely not only a result of their being superimposed on a more significant background, as the

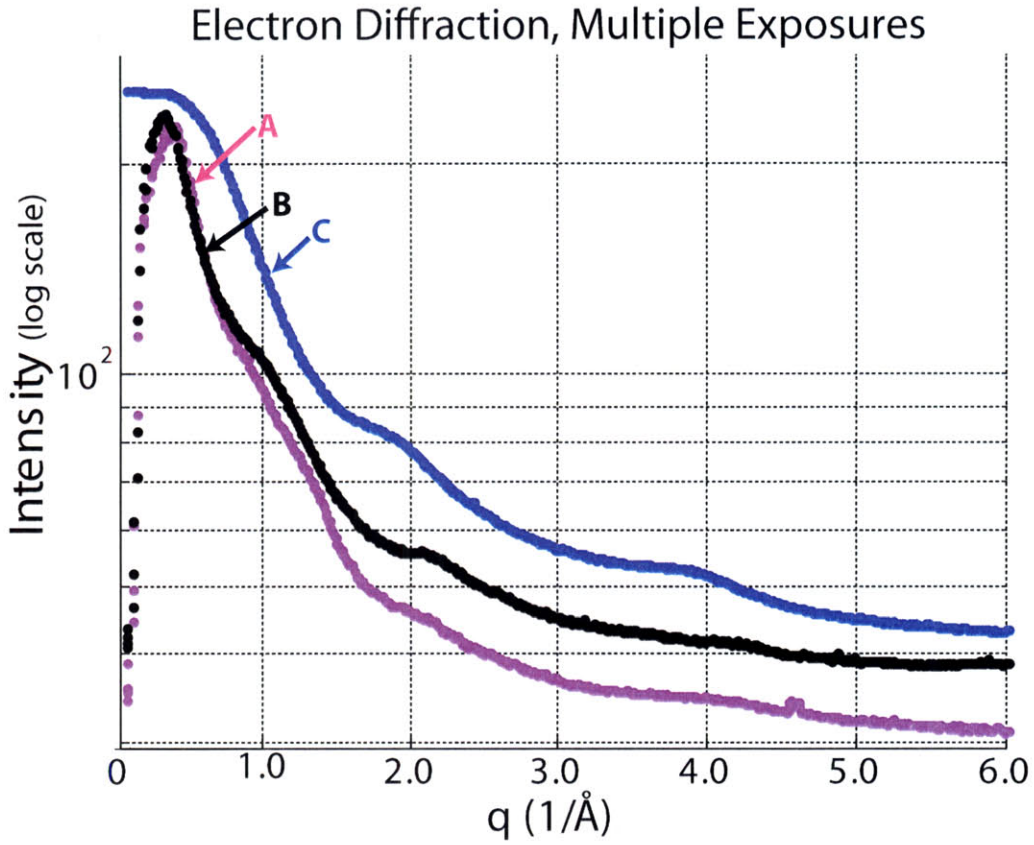

Figure 4-13: Electron diffraction patterns from thin polypyrrole film. Images were taken on JEOL 2011 with an accelerating voltage of 200 KeV and a working distance of 80 cm. A) (pink curve) Image was taken over 3 second exposure, film had never been previously exposed. Condenser aperture = 3. Small angle diffraction aperture = 2. Spot size = 4. B) (black curve) Image was taken over 3 second exposure, film had previously been exposed for 30 seconds. Condenser aperture = 3. Small angle diffraction aperture = 2. Spot size = 4. C) (blue curve) Image was taken over 5.6 second exposure. Film had been previously exposed for several minutes. Condenser aperture = 2. Small angle diffraction aperture = 2. Spot size = 2.

maximum of the peak at $q \sim 0.34$ Å^{-1} remains stationary even though it becomes more obscured by the increased background. The shoulder observable in the pink and black curves at approximately $q \sim 1.0$ Å^{-1} is either missing or totally obscured by the background in the blue curve.

The spacings observed in the highly irradiated sample's electron diffraction pattern ($q \sim 1.9$ Å^{-1} and $q \sim 3.8$ Å^{-1}) are spacings one would typically expect to find in polypyrrole samples. They could be the first and second orders of the face-to-face polypyrrole stack spacing of approximately 3.4 Å. It is not entirely clear why one would not observe this spacing until the film had been exposed for several minutes. One possibility is that for these very thin films, the polypyrrole chains lie face down on the electrode surface (so the pyrrole ring normal is parallel to the electrode normal). If this is the case, in pristine films one would not observe the 3.4 Å spacing and would instead observe rings that correspond to spacings perpendicular to the ring normal. This is in fact what we observe, as reflections 1 and 2 from Figure 4-12 correspond to reflections **b** and **c** from Figure 4-5, the two reflections perpendicular to the pyrrole ring normal. The development of the ($q \sim 1.9$ Å^{-1} and $q \sim 3.8$ Å^{-1}) peaks may be a result of disorder induced into the film upon continued electron beam exposure. The energy imparted to the film by exposure to the electron beam may cause some polypyrrole chains to stand up from the electrode, allowing us to observe the 3.4 Å face-to-face spacing.

While this initial highly preferential orientation has not been observed in x-ray of thick polypyrrole films doped with spherical anions such as PF_6^- (see [125] and Section 5.2.1) it has often been observed that very thin films have a different microstructure than thicker films. Our electron diffraction results corroborate Yang et al.'s scanning tunneling microscopy observations discussed previously, that polypyrrole film formation begins with a thin (130 - 500 Å) layer that is microstructurally different from the rest of the film [8]. The thicker layers that develop after the first few hundred Åwould be too thick to probe with electron diffraction, but x-ray diffraction shows them to be disordered and isotropic (Section 5.2.1).

It is also possible that polypyrrole assumes many different crystalline formations

even in the thinnest films, depending on the polymerization conditions. For example, Davidson et al. deposited polypyrrole from aqueous solution onto a gold surface [171], while Yang et al. produced their helices from acetonitrile solution onto highly ordered pyrolytic graphite [146]. Chu et al. used $FeCl_3$ to chemically oxidize polypyrrole and observed nm-sized crystals [12], while Fink et al. electropolymerized their films from organic solution onto ITO and observed electron diffraction patterns very similar to those observed here [170]. It was our goal to better elucidate the structure of polypyrrole actuators, to help increase our understanding of how structure accommodates actuation. For this reason, polymerization conditions that were as close as possible to those used to produce free-standing polypyrrole actuators were chosen. Subtle differences in the dopant, solvent, electrode material, polymerization rate and temperature of reaction may account for the differences between some patterns in the literature and those shown here.

4.3 Microstructural Response to Electrochemical Actuation

While scattering techniques are often used to determine the crystalline structure of polymers, in this case we are most interested in polypyrrole's properties as an actuator. We desire to understand how the microstructure of polypyrrole leads to and accommodates its unique electroactive properties. The mechanism of actuation is ion incorporation and expulsion, discussed in detail in Section 2.3. If the motion of ions entering and leaving the polymer film disrupts the characteristic reflections **a**,**b**,**c** or $\mathbf{\Gamma}$ (shown in Figure 4-5), one should be able to track this using scattering techniques in the same way the connection between nanoscale and macroscale actuation was first observed in muscle [173]. For example, when polypyrrole is oxidized in a solution of tetraethylammonium hexafluorophosphate in propylene carbonate (TEAPF6/PC), PF_6^- anions enter the polymer matrix and the film expands. If the PF_6^- penetrate the space between polypyrrole chains stacked face-to-face, we should observe a change

the d spacing and/or intensity of reflection **a**. Alternatively, the crystalline bundles responsible for the characteristic diffraction reflections are only a fraction of the total sample (as was depicted in Figure 4-5 and will be discussed in Section 4.4) so it is possible that actuation takes place without disrupting these bundles whatsoever. The following sections present our work to determine if this is the case.

4.3.1 Microstructural Change upon Mild Redox

In order to probe the effect of electrochemical oxidation and reduction on the structure of polypyrrole, a stack of polypyrrole films were held at an oxidative or reductive potential in an 0.05 M TEAPF6/PC solution for a certain amount of time. After the potential hold, the film stack was removed from the electrolyte solution and placed in the x-ray beam. The resulting patterns are shown in Figure 4-14.

The spacings in Figure 4-14 do not shift upon oxidation and reduction, even though actuation is observed at these potentials and timescales (as shown in the insert). This implies that the anions do not change the characteristic inter-chain spacings upon actuation. However, x-ray diffraction was conducted in transmission mode, which means the observed scattering was caused by the entire volume of sample penetrated by the x-ray beam. If the electrochemical treatment affected mostly the surfaces of the film, the changes may have been overwhelmed by the scattering from the unchanged bulk of the film.

4.3.2 Microstructural Change upon Severe Redox

Actuation in polypyrrole is a diffusion limited process, as it requires counterions to diffuse from the surface of the polymer film through its bulk. It is possible that over the timescale of the experiments shown in Figure 4-14 the majority of structural change occurs on the the surface of the film. It may take much longer to achieve structural change through the bulk of the film that can be observed with x-ray diffraction.

In an attempt to reduce the entire cross-section of the film, polypyrrole films were treated with severe electrochemical conditions. Two samples were reduced gal-

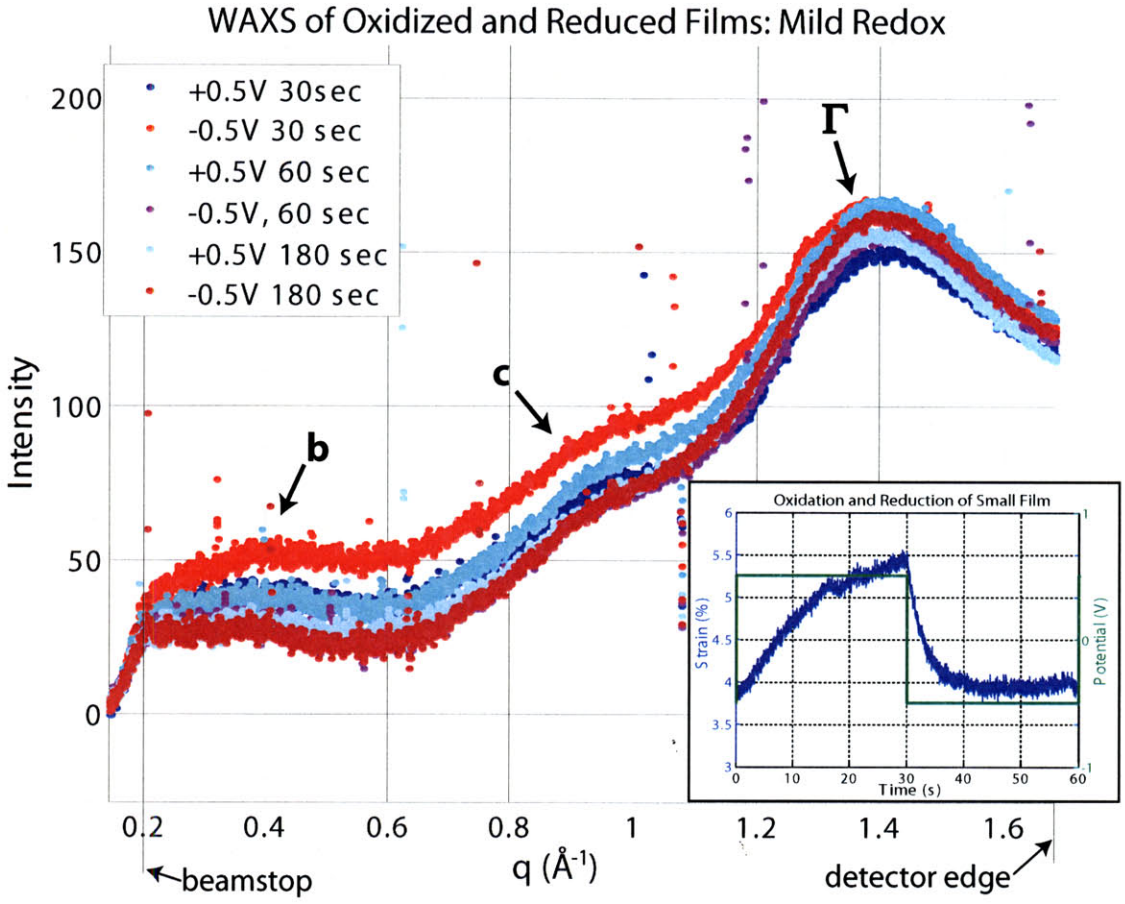

Figure 4-14: Diffraction of oxidized and reduced polypyrrole film. A stack of 10 films was suspended in an electrochemical cell with a 0.05 M solution of TEAPF6/PC. A potential of +0.5 V vs. Ag/Ag^+ was applied for 30 seconds, and the films were removed and exposed to the beam. The films were then re-introduced to the electrochemical cell, reduced at -0.5 V for 30 seconds, and then re-exposed. This procedure was continued for a 60 second oxidation and reduction, and a 180 second oxidation and reduction. Reflections **b**, **c**, and **Γ** correspond to the spacings illustrated in Figure 4-5. Reflection **a** from Figure 4-5 is out of the range of the detector in this case, but other experiments have shown it to remain constant as well. Diffraction patterns were taken at beamline G1 at Cornell High Energy Synchrotron Source. Wavelength = 1.42 Å. Air scattering background was subtracted from each curve. Inset: actuation of a small (2.3 mm × 4 mm) polypyrrole sample in TEAPF6/PC, in isotonic mode with an applied stress of 0.5 MPa. The waveform was the same as for the first two x-ray curves: +0.5 V and -0.5 V for 30 seconds. The sample exhibits approximately 1.5% strain under these conditions.

vanostatically in 0.05 M TEAPF6/PC at -1 A/m^2 for three hours. One sample was removed from the electrochemical bath while in the reduced state, while the other was re-oxidized at 1 A/m^2 for three hours. The two treated samples and one as-deposited sample were dried under vacuum for one hour. Their x-ray diffraction patterns are shown in Figure 4-15.

In the as-deposited film, the concentration of PF_6^- anions was 19%wt (by elemental analysis), and the conductivity of the film was 3.1×10^4 S/m. In the severely reduced film, the PF_6^- concentration was 3.8%wt, and the film was too resistive to be measured by four-point probe. In the re-oxidized film, the PF_6^- concentration was 12.2% while the conductivity was 1.45×10^4 S/m. This shows that the reduction was effective in removing PF_6^- anions, and the re-oxidation was effective in returning them to the film. However, the re-oxidation did not take the film back to its original state, as the PF_6^- concentration and conductivity are lower than in the as-deposited film. This may be because the severe electrochemistry caused some irreversible polymer degradation, which prevented the film from returning to its original high degree of doping.

The curves in Figure 4-15 can be separated into a series of gaussian peaks, in order to further examine the changes that occur upon reduction. This separation is shown in Figure 4-16. The as-deposited film has four peaks, corresponding to the characteristic polypyrrole spacings discussed in Section 4.1.4 and shown in Figure 4-5. The reduced film also has these four peaks, but the intensity of reflections **b** and $\mathbf{\Gamma}$ when compared to the other peaks are lower, and a new peak (labeled **b'** in Figure 4-16) has developed. In the re-oxidized film, the relative intensities of **b** and $\mathbf{\Gamma}$ increase again and reflection b' has disappeared.

In the bundles highlighted in Figure 4-5, reflection **b** corresponds to the space between stacks of polypyrrole chains and $\mathbf{\Gamma}$ corresponds to the counterion spacing. During the severe reduction, most of the PF_6^- anions left the film, causing the large decrease in the intensity of $\mathbf{\Gamma}$ shown in Figure 4-15. When the film was re-oxidized the anion concentration in the film increased but did not return to its original value, as did the intensity of $\mathbf{\Gamma}$ in the red curve of Figure 4-15.

The extreme decrease in anion concentration may also cause the spacing corre-

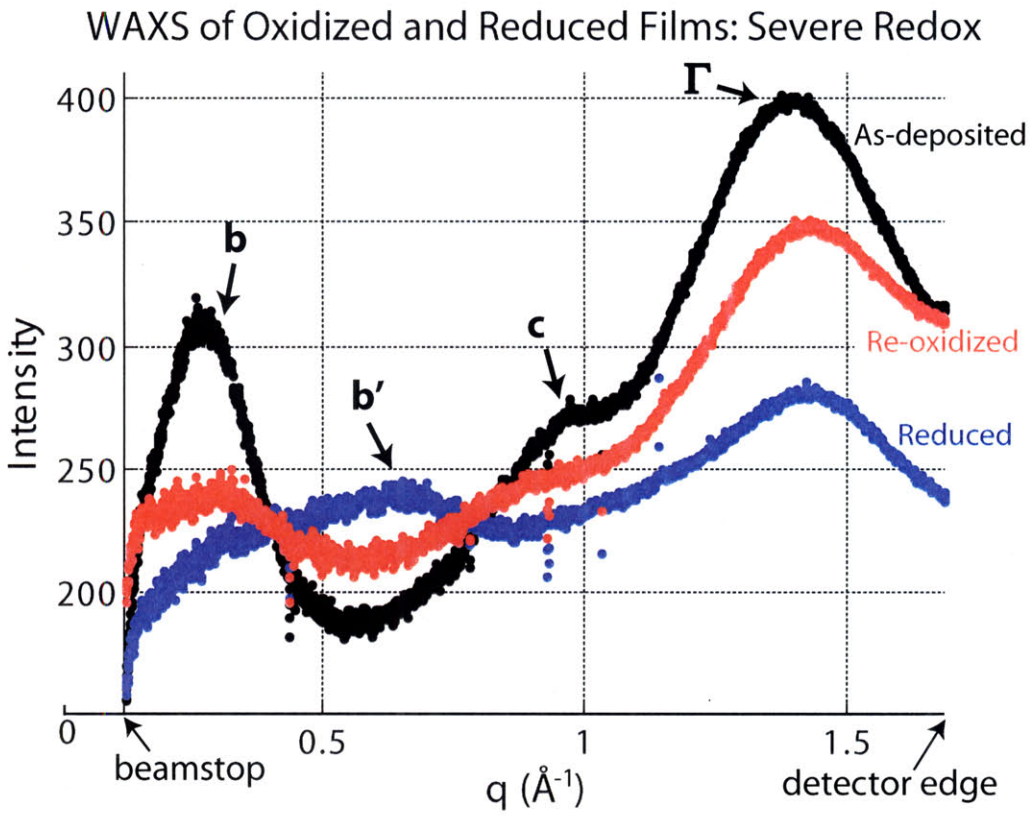

Figure 4-15: X-ray diffraction of films that underwent severe reduction and re-oxidation. Black curve: as-deposited polypyrrole film. Blue curve: polypyrrole galvanostatically reduced at -1 A/m^2 for three hours. The intensity of reflection **b** and **Γ** decrease, while a new reflection appears at $q \sim 0.63$ Å^{-1} appears, labeled **b'**. Red curve: polypyrrole galvanostatically reduced at -1 A/m^2 for three hours, then galvanostatically re-oxidized at +1 A/m^2 for three hours. Reflection **b'** disappears and the intensity of reflections **b** and **Γ** increase, but the diffraction pattern does not return all the way to the as-deposited state. Diffraction patterns taken on beamline G1 at Cornell High Energy Synchrotron Source. Wavelength = 1.42 Å. Air scattering background was subtracted from each curve.

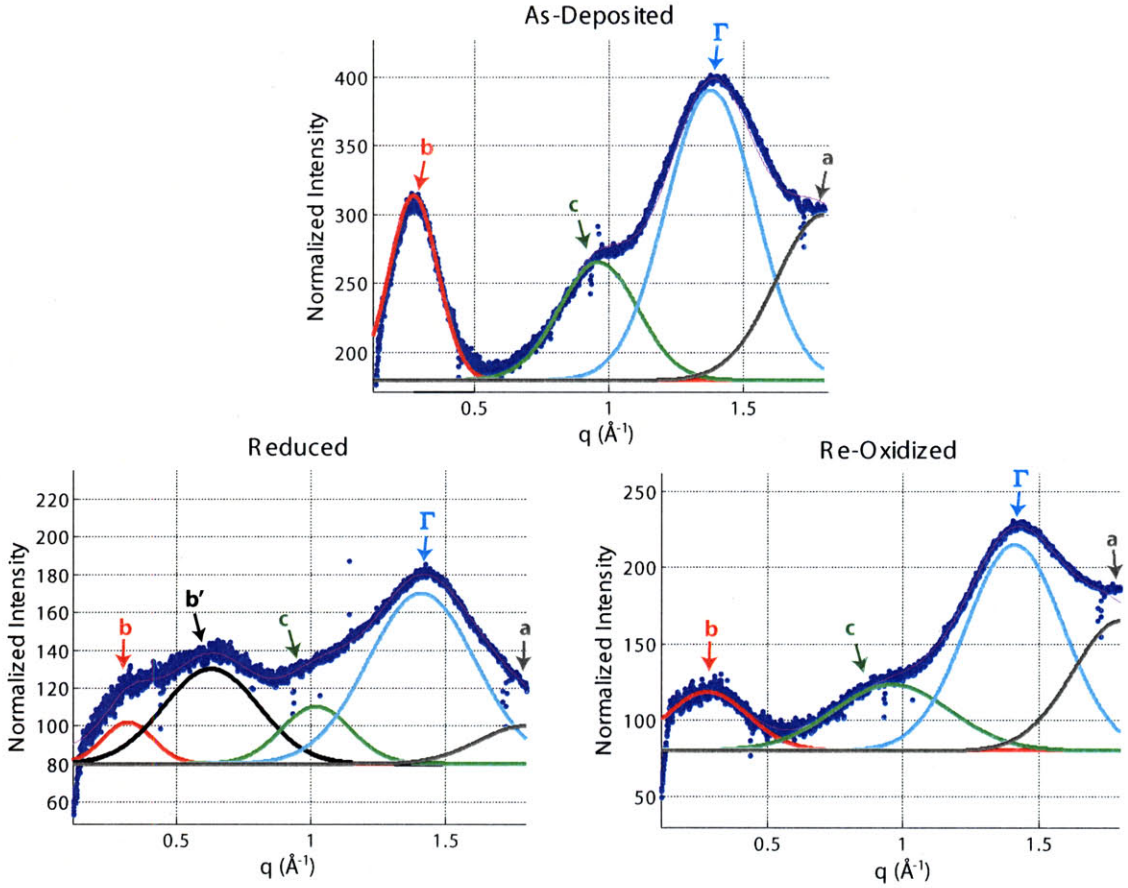

Figure 4-16: Separation of curves from Figure 4-15 into gaussian peaks. The blue curve is the data, while the pink line is the sum of the gaussian peaks. In the reduced curve, a new scattering peak (labeled b') arises at $q \sim 0.63$ Å^{-1}. The q spacing of the maxima of peaks **a**, **b**, **c** and **Γ** do not seem to change upon this severe electrochemical treatment.

sponding to reflection **b** to decrease. A smaller d spacing would be observed at a larger q, and could be responsible for the appearance reflection **b'** in Figures 4-15 and 4-16. In the as-deposited film, reflection **b** appears at $q \sim 0.27$ Å^{-1}, corresponding to d = 22.9 Å. Reflection **b'** appears at $q \sim 0.63$ Å^{-1}, corresponding to d = 9.97 Å. Each PF_6^- anion has a diameter of approximately 2.54 Å [69]. For this mechanism to cause the observed change in the diffraction pattern, several anions would have to vacate their locations between stacks of chains.

4.3.3 Microstructural Change in Very Thin Films

The structural change discussed in Section 4.3.2 requires several hours of severe electrochemistry to develop. We observe a macroscopic volume change during actuation on a timescale of seconds, so clearly the phenomenon observed in Section 4.3.2 is not the full story. It is still possible that the surfaces of the polypyrrole film undergo a structural change immediately, and the several hour galvanostatic reduction is only necessary to induce structural change throughout the relatively thick ($\sim$ 50 μm) films. To investigate this, reduction experiments were conducted on very thin ($\sim$ 50 nm thick) films, and the structure was probed by electron diffraction.

Thin polypyrrole films were electrodeposited for 30 seconds from a solution of 0.05 M TEAPF6/PC with 1%vol water at -40°C and a current density of 1 A/m^2. The film was patted dry, and samples were removed using the procedure described in Figure 4-11. The working electrode (still mostly covered with thin polypyrrole film) was then placed back into a clean electrolyte solution, and cycled between +1 V and -1 V at 0.1 V/s until the current response stabilized. It was then reduced at -1 V for 30 seconds, and immediately removed from the electrolyte bath. The as-deposited film was reddish in color, and the reduced film was greenish in color upon removal from the bath. Over the course of approximately one minute exposure to air, the reduced film turned reddish again. Samples were removed using the procedure described in Figure 4-11.

Electron diffraction patterns were taken of the as-deposited and reduced samples on a JEOL 2010F field emission TEM, with an accelerating voltage of 197 keV, and shown in Figure 4-17. The samples were exposed to the electron beam for several minutes, and the characteristic 3.4 Å spacing was observed (see discussion in section 4.2.3). In both the as-deposited and reduced films, the observed reflections were located at the same q. The reduction-induced reflection **b'** observed in Figure 4-16 at $q \sim 0.63$ Å^{-1} would be near the edge of our detection limit for Figure 4-17. However, other exposures at longer camera lengths confirm that this spacing does not appear in any exposures of the as-deposited or reduced film.

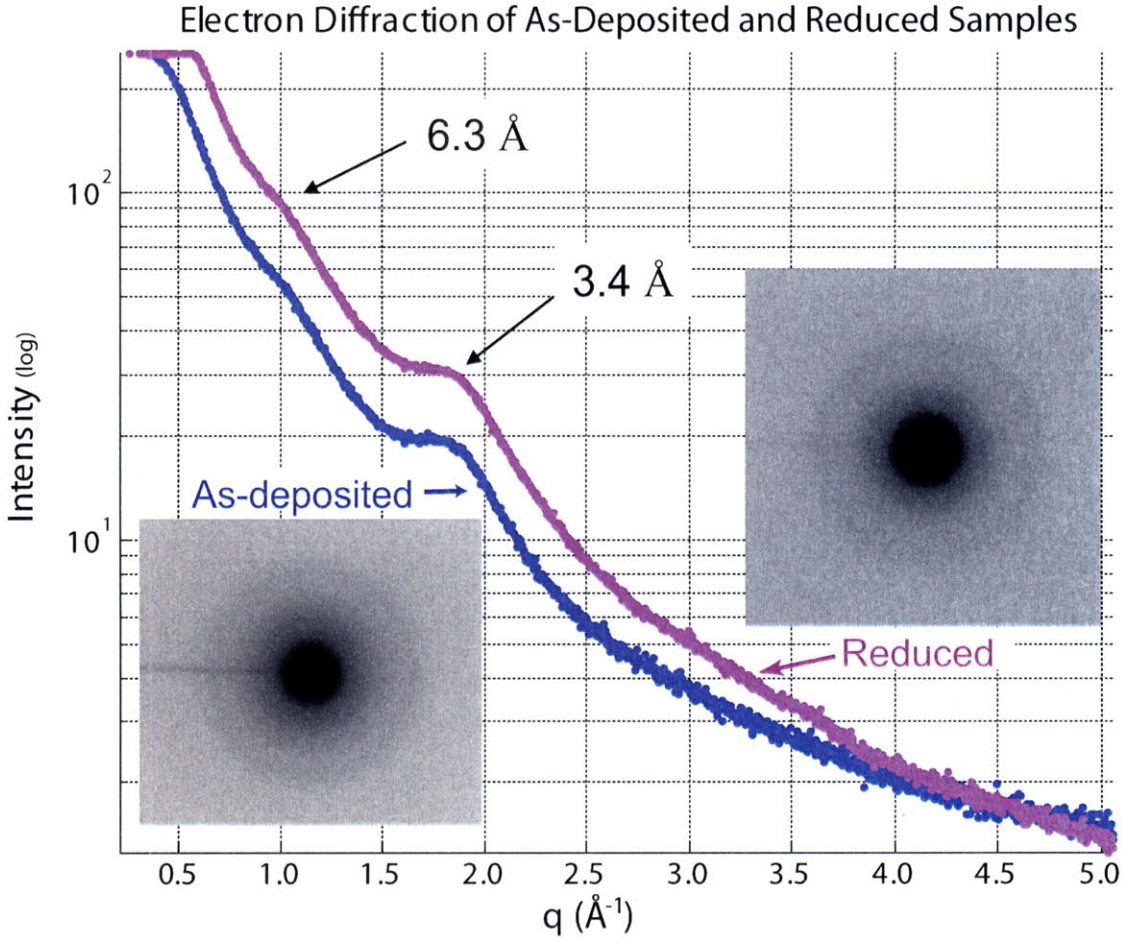

Figure 4-17: Electron diffraction of as-deposited and reduced polypyrrole samples. Blue curve: as-deposited polypyrrole film. Pink curve: polypyrrole film redcued at -1 V for 30 seconds. Diffraction patterns taken on JEOL 2010F, accelerating voltage = 197 keV. Spot size = 10nm. Camera length = 80 cm.

The JEOL 2010F used to take the patterns in Figure 4-17 is equipped with an Electron Energy Loss Spectroscopy (EELS) detector, which allows one to conduct elemental analysis of the TEM sample. As the electron beam travels through the samples, some electrons interact inelastically with the atoms in the sample. The amount of energy lost by these electrons is very sensitive to the type of atoms in the sample, and by comparing the energy of the transmitted electrons to those that did not interact with atoms in the sample (called "zero-loss" electrons) one can learn about the atomic number and chemical environment of the elements in the sample. EELS is an especially appropriate technique for analyzing polypyrrole samples, because it is most sensitive to light elements (as are found in polypyrrole samples). To learn more about EELS, the reader is directed to a text by Egerton [174] or Chapter 38 of Williams and Carter [175]. The results of EELS analysis of polypyrrole films are shown in Figure 4-18.

In Figure 4-18i, characteristic peaks are observed for carbon, nitrogen, oxygen and fluorine. The shape and magnitude of each peak is dependant on the effective scattering cross-section of the element, the amount of element present, and the chemical environment of that element. For example, fluorine present as part of a PF_6^- anion will give a peak of a different shape than fluorine that is part of a PF_5 atom. Without calibration for all of the exact species present in this sample, quantitative determination of the percentages of each element is impossible. However, the EELS signals are evidence that these elements are present.

The fluorine signal is missing in Figure 4-18ii, showing that fluorine is not present in detectable quantities in the reduced sample. This result is significant, as it means that even though the PF_6^- anions were removed by the electrochemical reduction, the characteristic spacings observed by electron diffraction did not change.

Because the thin polypyrrole films are exposed to air during the lift-off procedure, it is likely that oxygen from the ambient air oxidized both the as-deposited and reduced samples slightly. This explains the presence of the oxygen signal in the EELS spectrum, and the reddish color of the films after exposure to air. This chemical (as opposed to electrochemical) oxidation means that the reduced sample is no longer

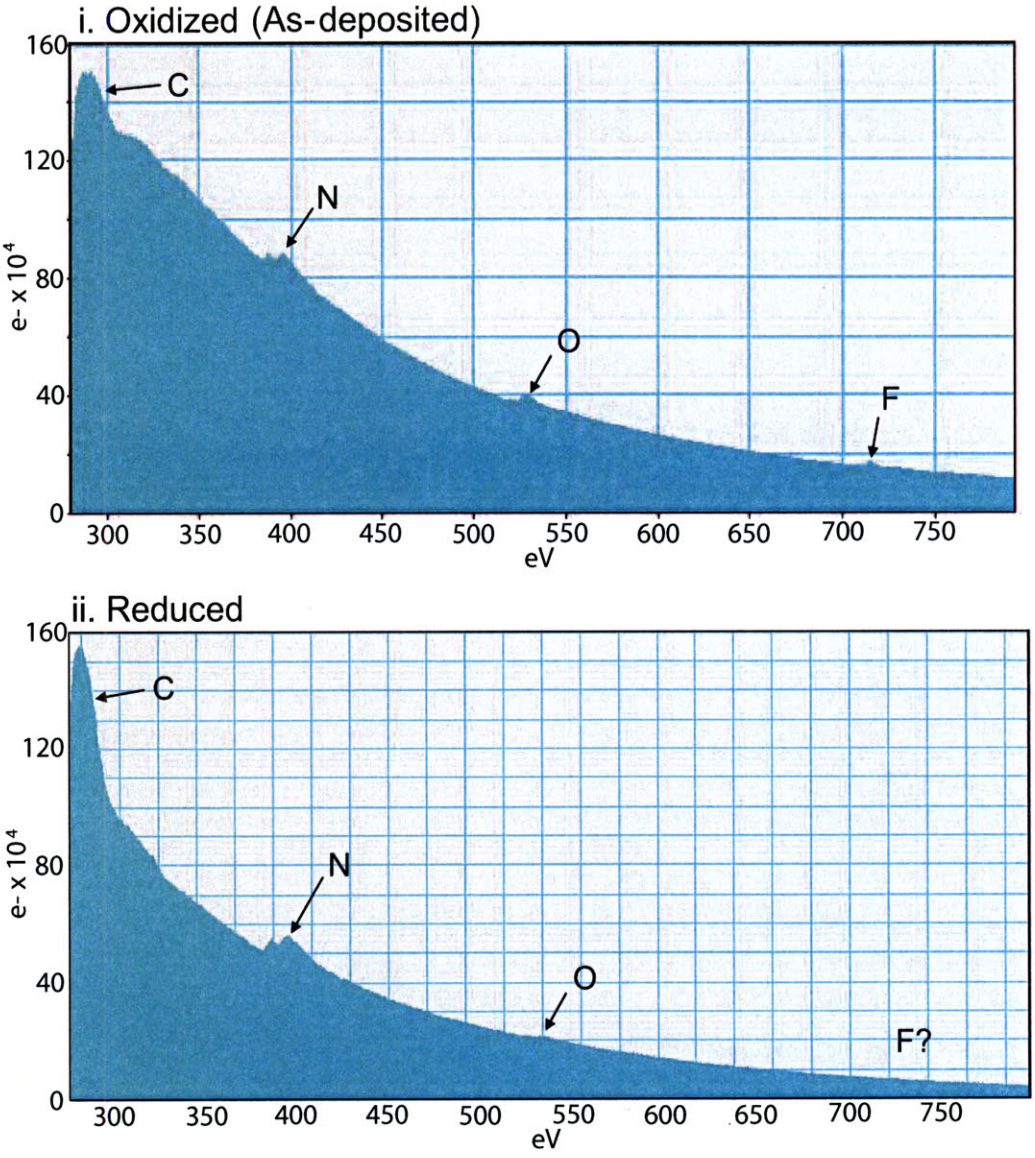

Figure 4-18: Energy electron loss spectroscopy of as-deposited and reduced polypyrrole samples. i) As-deposited sample. ii) Reduced sample. Characteristic energy losses for carbon, nitrogen, oxygen and fluorine are labeled.

completely reduced when it is observed in the microscope. However, while both samples show a signal for oxygen, only the as-deposited sample shows a signal for fluorine. Therefore, it is reasonable to conclude that the reduced sample is still in a significantly more reduced state than the as-deposited sample.

4.4 Chapter Conclusions

This chapter has presented and discussed our efforts towards elucidating the microstructure of polypyrrole via scattering techniques. While x-ray and electron diffraction are techniques extensively used to determine the microstructure of polymers, in this case the scattering results are somewhat difficult to interpret. It is clear from the diffraction data that there are not any large (μm-size) crystals in the film, and we did not observe even small crystals only nanometers in size. Estimates of polypyrrole crystal size using Equation 4.6 result in crystallites 10 - 20 Å in diameter, which contain only up to 5 repeat units for reflection **a** and 2 repeat units for reflection **c**. If the size of the ordered regions in polypyrrole are not larger a few stacked chains, the description of these regions as "crystals" is somewhat tenuous. The microstructure is best visualized as containing small "bundles" of polypyrrole chains stacked over a few repeat units (two bundles with 3 repeat units for reflection **a** and 1 repeat unit for reflection **c** were highlighted in Figure 4-5). These very small bundles of polypyrrole chains provide the characteristic reflections observed in the diffraction patterns, but their small size causes the peaks to be broad and overlapping, preventing a full crystallographic characterization of the material.

It should be noted that the bundled microstructure described here consists of linear chains, and does not include branching and covalent cross-linking. It is likely that some percentage of the chains are branched and/or cross-linked, as has been proposed for polypyrrole synthesized from other deposition recipes [176–179]. However, covalent cross-linking has not been directly observed (via spectroscopy or other methods) in polypyrrole deposited from our recipe. While we acknowledge it probably exists, we believe the extent of covalent cross-linking in our samples to be minimal due to the

very high electronic conductivities we achieve.

Instead of covalently cross-linked, we believe the chain bundles to be tightly bound due to π-orbital overlap [180]. The bundles act as pseudo-cross-links, connecting the chains within the polypyrrole matrix as shown in Figure 4-19i. As has been mentioned previously, elemental analysis studies of polypyrrole films deposited from our standard recipe have shown that they are only approximately 40%wt polymer. The remainder of the film consists of approximately equal parts PF_6^- and propylene carbonate. The bundles allow the polypyrrole chains to form a load-bearing network that dominates the films' mechanical properties, resulting in a robust film even though a majority of the material consists of small molecules that cannot support a tensile load. Polypyrrole bundles are illustrated with the other components in the film in Figure 4-19ii. The bundled network provides the high electronic conductivity (4×10^4 S/m) and high elastic modulus (0.3 GPa) of the as-deposited film, because the network consists of individually highly conductive and rigid chains.

It has been proposed that polypyrrole shows better electroactive properties than other conducting polymer systems due to covalent cross-linking [181]. However, electroactive strains comparable to polypyrrole's have recently been observed in electropolymerized poly(3,4-ethylenedioxythiophene) (PEDOT) [59, 63], which cannot form branches or cross-links because the necessary positions on the monomer are blocked. These results imply that a microstructural feature other than covalent-crosslinking is the key to successful conducting polymer actuation. Small chain bundles could provide the mechanical stability needed for continuous actuation, but their small size allows the majority of the material to be disordered and accommodate counterion swelling.

The chain bundles bundles become oriented with processing, as the polypyrrole chain axes align in the MD. The fact that the counterions (observed via reflection $\mathbf{\Gamma}$) do not become oriented with processing shows that the counterions are not part of these bundles, and are instead isotropically distributed throughout the film, around and in between the bundles. This is schematically illustrated in Figure 4-19 and will be further discussed in Section 5.4.2.

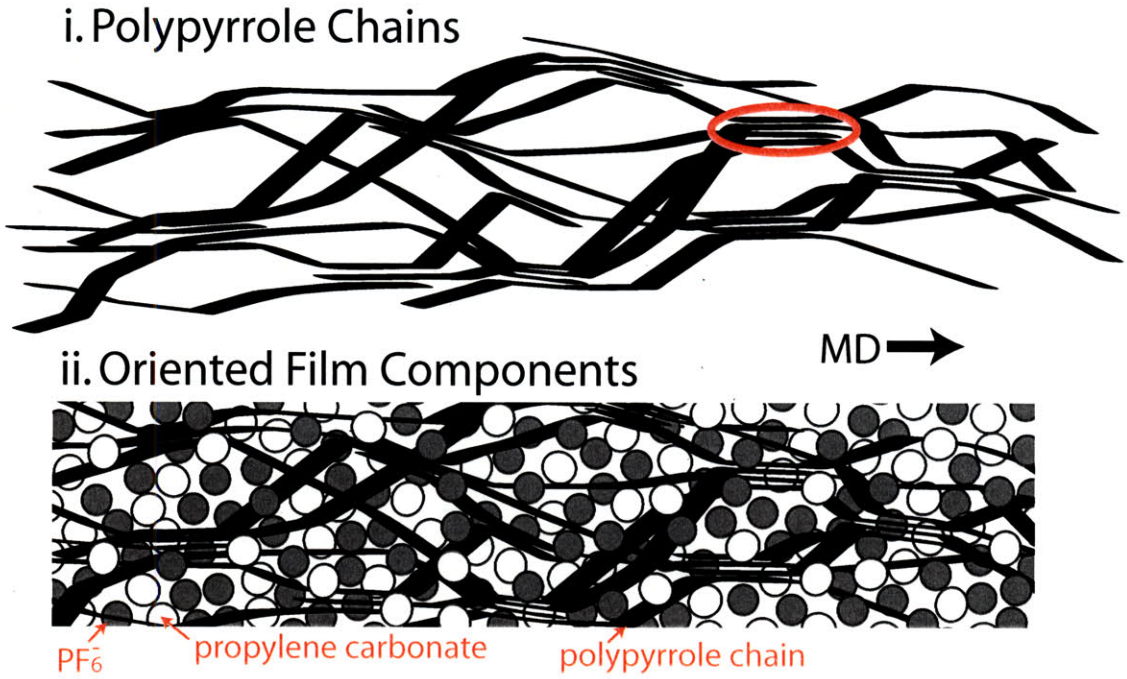

Figure 4-19: Illustration of bundled microstructure in oriented polypyrrole. The bundled microstructure also exists in unoriented (as-deposited) polypyrrole, but in as-deposited polypyrrole the bundles and chain axes are randomly distributed in all directions. In oriented films the chain axes and bundles are preferentially aligned in the MD, making it easier to illustrate the bundles and their relationship to the disordered components of the material. i) Polypyrrole chains only. Bundles act as pseudo-crosslinks, allowing a percolative path of polypyrrole chains through the sample. A single bundle is highlighted in orange. ii) Polypyrrole chains with other film components. The chains are highly swollen with solvent and counterions, but the film maintains its mechanical rigidity due to the connected path of individually rigid polypyrrole chains.

The results of Sections 4.3.1 and 4.3.3 show that the characteristic spacings of polypyrrole do not change upon application of the electrochemical conditions that cause a macroscale electroactive response. This means that the ion influx and expulsion observed during actuation takes place outside of the bundles. The bundles act as passive cross-links, holding together disordered material that swells and collapses during electrochemical cycling.

The bundle microstructure explains polypyrrole's seemingly conflicting properties well. Electropolymerized polypyrrole does not dissolve and does not melt, typical of a highly cross-linked polymer. However, a high degree of covalent cross-linking (and branching that is necessary to achieve it) is not typically found in highly conductive polymers because it requires defects in the orbital delocalization along the chain axes. The π-stacked bundles provide the mechanical and chemical robustness we observe, without disrupting the conjugation in the way that covalent cross-linking would. Furthermore, the regions of π-overlap will improve interchain charge transfer beyond what would be achievable in a polymer that was only physically entangled.

Chapter 5

Microstructure Manipulation I: Post-Deposition Processing

In this chapter, our efforts to manipulate polypyrrole microstructure by processing films post-deposition are discussed. We utilize two techniques to mechanically process polypyrrole: stretching and cold rolling. Stretched conducting polymer films have previously been shown to have anisotropic conductivity [93, 123, 130] and in polyaniline, anisotropic electroactive strain [21]. In this thesis we probe the uniaxial texture imparted by stretching polypyrrole and evaluate for the first time the anisotropic electroactive response it produces. Furthermore, we use cold rolling to impart a biaxial texture to polypyrrole films. We had hoped that the additional organization present in the biaxial microstructure would produce ordered channels in which ions could easily travel through the film, improving the electroactive properties even beyond what is achievable is uniaxially drawn films. Wide-angle x-ray diffraction was used to probe the microstructure of the stretched and rolled films, and showed significant polymer chain orientation without an appreciable change in the breadth of the diffraction peaks. This chain orientation led to anisotropy in conductivity, elastic modulus, and electroactive response for both the stretched and rolled films. The anisotropy of electroactive response was dependant on the rate of electrochemical actuation, and we discuss the deformation of interchain spaces during processing responsible for the anisotropy and the time dependence of the electroactive response.

5.1 Procedure

Polypyrrole films were synthesized using the standard deposition recipe presented in Section 2.1.1. They were processed as described in Section 5.1.1 within two days of deposition unless otherwise noted, and tested as described in Section 5.1.2.

5.1.1 Polypyrrole Film Processing

After synthesis, large area films (70 mm × 230 mm × 0.03 mm) were peeled off of the working electrode. Sections of these films (50 mm × 150 mm) were stretched on a Zwick/Roell Z010 Mechanical Tester under stress control, at a rate of 0.0167 MPa/min. The stretched sections will be referred to as "S". Different sections (20 mm × 60 mm) of the as-deposited films were rolled using a Durston C130 rolling mill. The rolled sections will be referred to as "R." The coordinate system used for oriented samples is defined as:

- ND (Normal Direction) = normal to the surface of the film
- MD (Machine Direction) = parallel to the stretch or roll direction
- TD (Transverse Direction) = parallel perpendicular to the MD and ND

Samples for electroactive testing (2 mm × 15 mm) were cut from the stretched and rolled films, some with their long axis parallel to the machine direction (labeled "S_{MD}" and "R_{MD}") and some with their long axis perpendicular to the machine direction (labeled "S_{TD}" and "R_{TD}"). For comparison, 2 mm × 15 mm samples were cut from the as-deposited polypyrrole film with no additional processing (labeled "A").

5.1.2 Processed Film Testing

The conductivity of each sample was measured using a standard four-point probe. Scanning electron micrographs of polypyrrole fracture surfaces were taken on a JEOL 5910 Scanning Electron Microscope, with an accelerating voltage of 20 kV and a spot size of 35. Prior to SEM analysis, the films were held in liquid nitrogen and fractured

by hand to expose the fracture surface. Wide-angle x-ray diffraction patterns were taken under vacuum, using Fuji BAS-MS imageplates. Single polypyrrole films were exposed with the incident x-ray beam (q_o) parallel to the ND. For q_o parallel to the MD or TD, small strips of polypyrrole (approximately 1 mm $\times$ 3 mm) were cut from larger samples in the MD or TD with care to maintain orientation, and stacked to a thickness of approximately 0.75 mm for exposure to the x-ray beam. The diffraction patterns were integrated using the Polar software package, developed at Brookhaven National Laboratories [182].

Mechanical properties and electroactive properties were measured on a custom-built dynamic mechanical analyzer, as described in Section 2.3 [183]. This apparatus allows one to clamp the polypyrrole film under tension in a three-electrode electrochemical cell, and measure the electroactive response that occurs upon application of a potential waveform. The electrolyte used for active testing was neat 1-butyl-3-methylimadazolium hexafluorophosphate (BMIMPF6). Each sample underwent the warm-up procedure discussed in Section 2.3.1. Before submersion in the electrolyte, the passive elastic modulus of each sample was measured by application of a 1% strain at a frequency of 1 Hz. After the initial modulus measurement, the film was slackened, submersed into electrolyte, and "warmed up" by application of a +2 V triangle wave at 0.1 V/s until the current response stabilized.

After warm-up, the films were measured in both isotonic and isometric modes (as described in detail in Sections 2.3.2 to 2.3.3). In isotonic mode, the films were held at a constant load (0.5 MPa) in the electrolyte. A potential waveform was applied, and the resulting length change was measured. The "active strain" is the contractile strain observed. In isometric mode, the film is held under tension at a constant length (approximately 1% strain). A potential waveform is applied, and the change in stress is measured. The "active stress" is the magnitude of the stress response.

5.2 Evaluation of Microstructure

5.2.1 Wide Angle X-ray Scattering

X-ray diffraction measurements were taken of as-deposited, stretched and rolled films with the x-ray beam incident to all three axes. The 2-d diffraction pattern for an as-deposited polypyrrole film is shown in Figure 5-1. For the as-deposited film, characteristic reflections **a**, **b**, **c** and **Γ** (as defined in Section 4.1.4) do not show anisotropy in any direction. This means that the polypyrrole chains and bundles are randomly oriented throughout the sample.

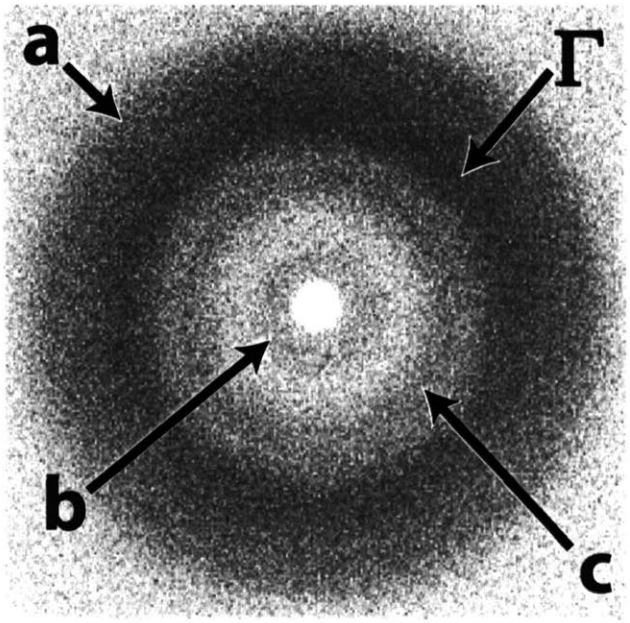

Figure 5-1: Wide-angle x-ray scattering of unprocessed polypyrrole, with q_o parallel to the ND. Reflections **a**, **b**, **c** and **Γ** all appear as isotropic rings, due to the lack of preferential orientation. The diffraction patterns when q_o is parallel to the TD and MD show the same features as the one shown, since the material is isotropic.

Wide angle x-ray patterns for stretched and rolled polypyrrole are shown in Figure 5-2 and Figure 5-3. For the stretched films, reflection **c** (which occurs along the chain axis) clearly aligns in the MD (Figure 5-4i). Reflections **a** and **b** occur transverse to the chain axis, so they are absent in the MD and instead they appear in the ND and TD as is expected for uniaxial alignment along the MD. As one increases

the elongation of the stretched films, the orientation improves and less scattering from reflection **c** is visible in the ND and TD. However, because these peaks are poorly defined and overlapping, we were not able to quantitatively calculate Herman's orientation parameters (Equation 4.4).

In the rolled films, reflection c again appears most strongly in the MD, confirming axial alignment with the MD (as shown in Figure 5-4ii). However, in this case reflection **a** appears in the ND and not in the TD (so it is visible in Figure 5-3ii but not Figure 5-3i), while reflection **b** appears in the TD and not in the ND (so it is visible in Figure 5-3i but not Figure 5-3ii). This shows that rolling aligns the chain axes in the MD, but the chains assume an additional degree of orientation with the polypyrrole rings parallel to the surface of the film. This is the first time that this biaxial texture has been shown in polypyrrole, where reflections **a** and **b** appear perpendicular to each other.

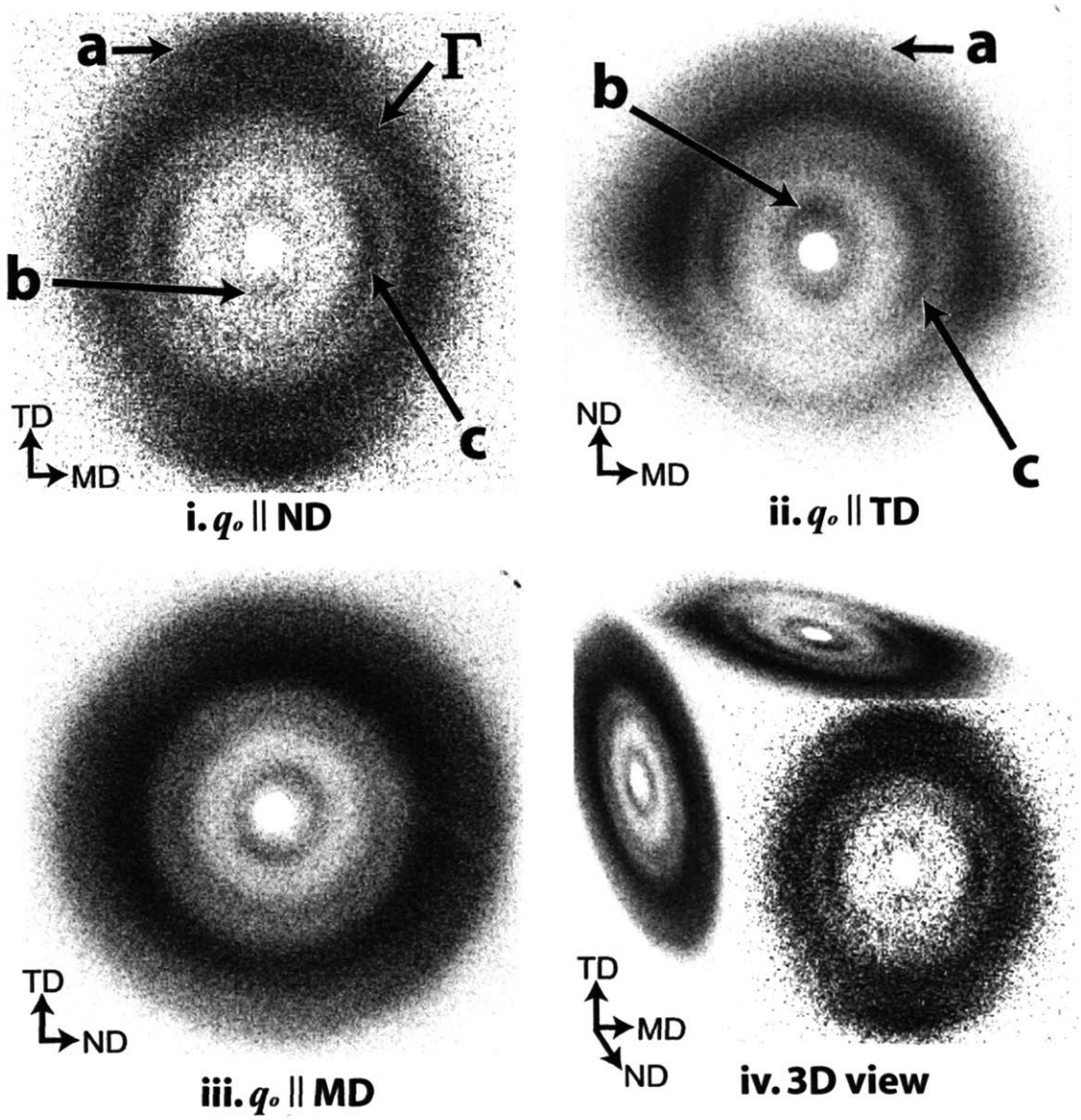

Figure 5-2: Wide-angle x-ray scattering of stretched polypyrrole. Reflections **a** and **b** orient in the ND and TD, while reflection **c** orients in the MD as seen in (i) and (ii). The diffraction pattern when q_o || MD is isotropic as seen in (iii), confirming uniaxial alignment in the MD. Reflection **Γ** does not orient, and remains an isotropic ring in all directions. Shadowing from the clamps holding the films in the x-ray beam is visible in (ii).

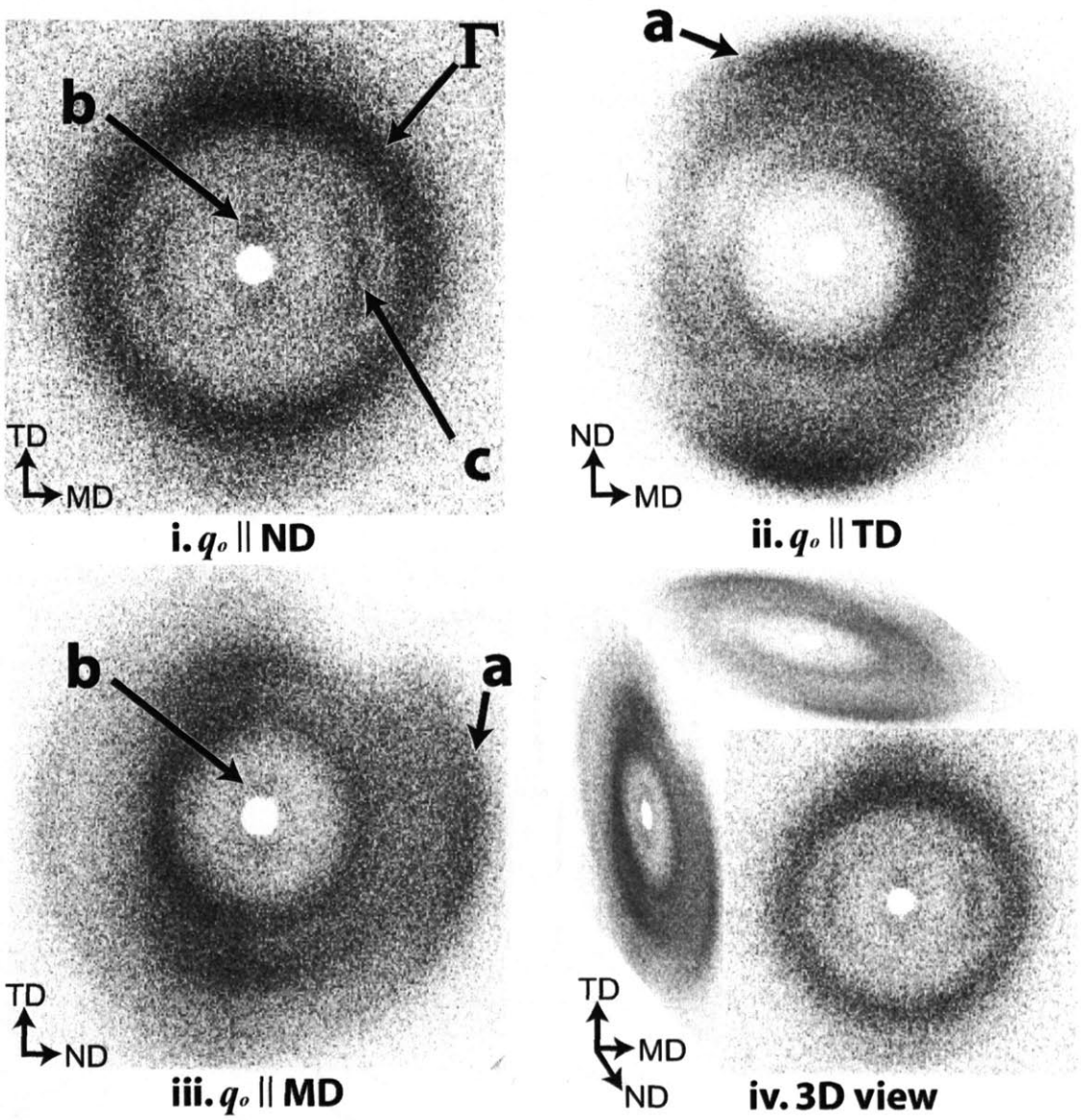

Figure 5-3: Wide-angle x-ray scattering of rolled polypyrrole. Reflection **a** orients in the ND, so it is barely visible in the q_o || ND pattern (i). Reflection **b** orients in the TD, so it is not observed in the q_o || ND pattern (ii). Reflection **c** primarily orients in the MD. Reflection **Γ** does not orient. Some clamp shadowing is visible on the q_o || TD and q_o || MD images (ii,iii).

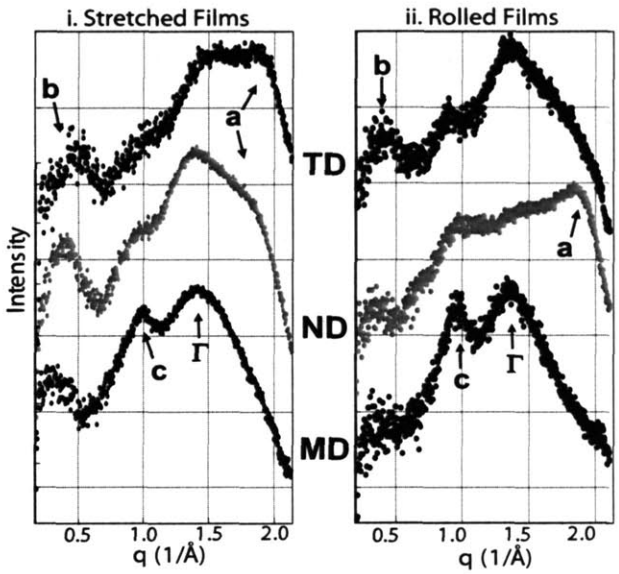

Figure 5-4: 1D WAXS patterns for stretched and rolled films. Curves are offset for clarity. i) Stretched films. Reflections **a** and **b** can be observed in the TD and ND. Reflection **c** is most clear in the machine direction, but some scattering from reflection **c** is evident in the other two directions. Reflection **Γ** does not clearly orient in any direction, as it is observed in all three curves. ii) Rolled films. Reflection **a** is most clear in the normal direction. Reflection **b** is most clear in the transverse direction. Reflection **c** is most clear in the machine direction, but some scattering from reflection **c** is evident in the other two directions. Reflection **Γ** does not clearly orient in any direction, but is more easily observed in the TD and MD than in the ND. This may be because it is overlapping with reflection **a** in the ND.

5.2.2 Scanning Electron Microscopy

Scanning electron microscopy was used to examine the fracture surface of processed films. When one observes the fractured stretched film looking down the TD, the surface appears smooth with striations along the MD (Figure 5-5i). Alternatively, when the surface is observed looking down the MD, the surface appears quite rough, with small fibrils poking out of the surface (Figure 5-5ii). In the rolled samples, the fracture surfaces along the MD and TD look similar, as both show a layered structure with layers perpendicular to the ND. As in the stretched films, the surface looking down the MD (Figure 5-5iii) is more rough than that looking down the TD (Figure 5-5iv).

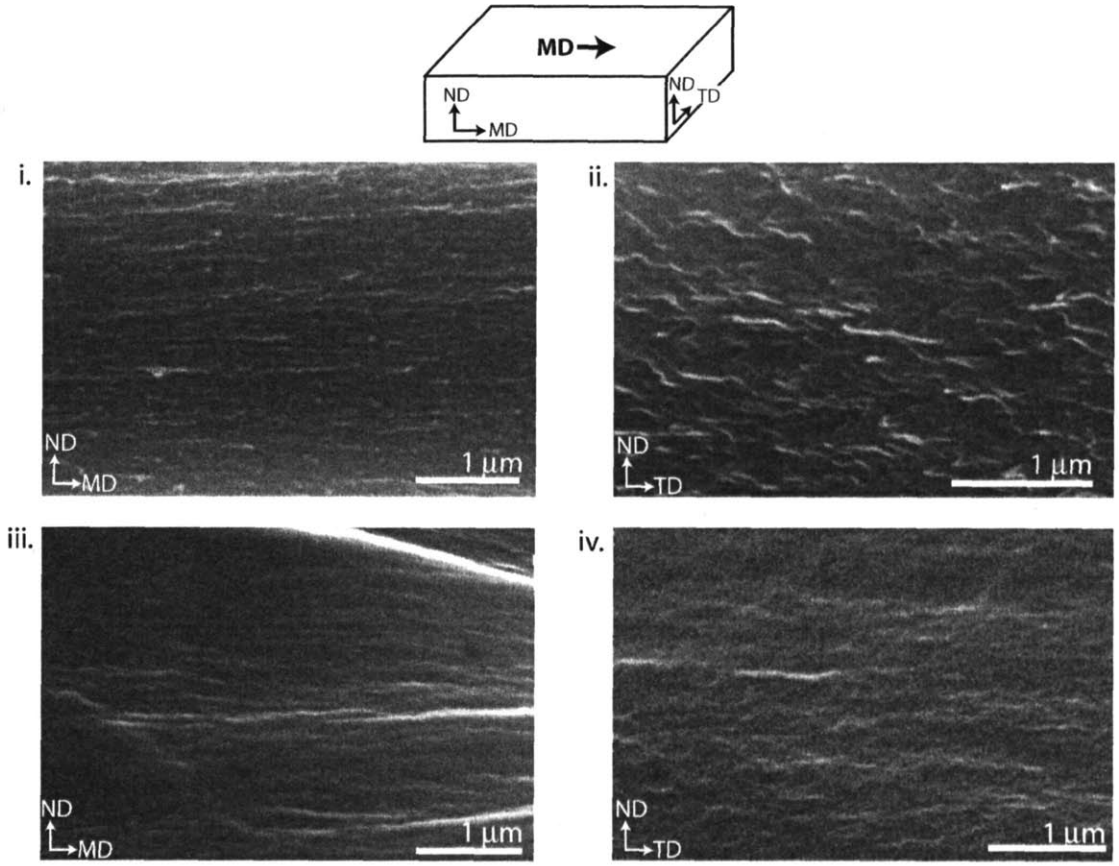

Figure 5-5: SEM images of processed film fracture surfaces. Films are processed so the chain axes are oriented in the MD, and fractured to expose the surface parallel (i and ii) or perpendicular (iii and iv) to the MD. Micrographs were taken on a JEOL JSM-5910 SEM. i) Stretched film, looking down the TD. Striations are visible along the MD. ii) Stretched film, looking down the MD. Fracture surface is rough and fibrillar. iii) Rolled film, looking down the TD. Striations are visible in the MD. iv) Rolled film, looking down the MD. The surface is more rough than in (iii), and shows some of the fibrillar morphology observed in (ii). Additional striations are also visible in the TD.

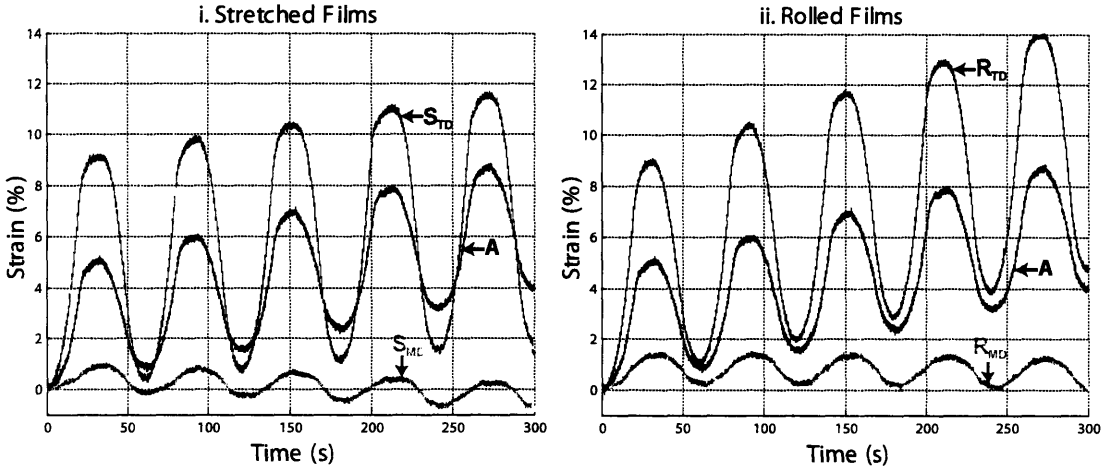

Figure 5-6: Isotonic response for stretched and rolled films tested immediately after deposition and processing. Films were held under a static force of 0.5 MPa in neat BMIMPF6, and a ±1.5 V triangle wave in potential was applied at a rate of 0.1 V/s. Strains are normalized by subtracting the initial strain that occurs upon application of the testing load. i) Films stretched to 55% elongation. Under these conditions, $(\epsilon_{TD}/\epsilon_{MD})_S = 7.02$. ii) Films rolled to 55% elongation. Under these conditions, $(\epsilon_{TD}/\epsilon_{MD})_R = 5.86$.

5.3 Electroactive Properties

Figure 5-6 compares the electroactive strain response for stretched and for rolled films to that of an unprocessed film. For the conditions shown in Figure 5-6, the as-deposited film shows an active strain of $\epsilon_A = 4.7\%$. The rolled film shows an active strain of $\epsilon_{MD} = 1.5\%$ in the MD, and $\epsilon_{TD} = 8.9\%$ in the TD. The stretched film shows an active strain of $\epsilon_{MD} = 1.4\%$ in the MD, and $\epsilon_{TD} = 9.5\%$ in the TD. The as-deposited and TD films (for both stretched and rolled samples) show an overall greater extension than contraction, as will be discussed in Section 5.4.2.

Both the stretched and rolled samples tested for Figure 5-6 were cut from films processed to approximately 55% linear elongation. However, not every point in the processed film has the same degree of polymer chain orientation due to localized plastic deformation. We use the local conductivity and local elastic modulus to compare the degree of orientation in small samples. In a perfectly oriented conducting polymer film, the polymer chains will be axially aligned with the MD. For such a sample, one would observe a very high conductivity and elastic modulus in the MD

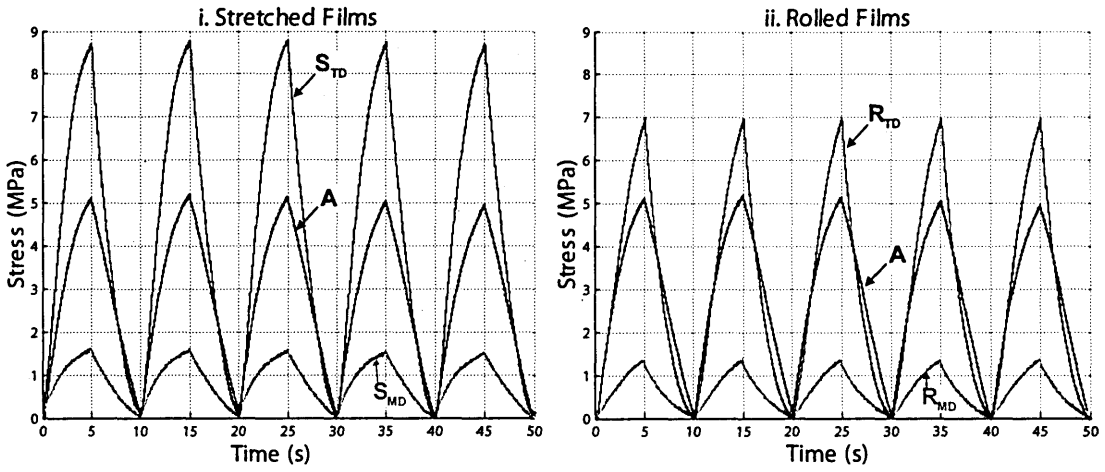

Figure 5-7: Isometric response for stretched and rolled films tested immediately after deposition and processing. Films were held under a constant stress of 0.5 MPa in neat BMIMPF6, and a ±1.5 V square wave in potential was applied at a frequency of 0.1 Hz. Strains are normalized by subtracting the stress at time = 0 seconds. i) Films stretched to 55% elongation. Under these conditions, $(\text{stress}_{TD}/\text{stress}_{MD})_S = 5.44$. ii) Films rolled to 55% elongation. Under these conditions, $(\text{stress}_{TD}/\text{stress}_{MD})_R = 4.92$.

Treatment	Direction	σ (10^4 S/m)	σ_{MD}/σ_{TD}	E (GPa)	E_{MD}/E_{TD}	Active Strain (%)*	$\varepsilon_{TD}/\varepsilon_{MD}$*	Active Stress (MPa)†	$\text{stress}_{TD}/\text{stress}_{MD}$†
none		2.37		0.38		4.73		5.15	
Roll ~ 55%	MD	5.28	4.73	0.46	1.48	1.52		1.43	
	TD	1.12		0.31		8.91	5.86	7.03	4.92
Stretch ~ 55%	MD	4.96	3.77	0.43	1.39	1.36		1.61	
	TD	1.31		0.31		9.55	7.02	8.76	5.44

Table 5.1: Electroactive results for stretched and rolled films, tested in neat BMIMPF6. Conductivity (σ) and Elastic modulus (E) are measured as described Section 5.1.2. *Isotonic testing, under conditions shown in Figure 5-6. †Isometric testing, under conditions shown in Figure 5-7.

because the measurement captures the high conductivity and modulus of the polymer backbone, and a very low conductivity and elastic modulus in the TD because the measurement captures the lower interchain conductivity and relatively weak interchain bonding. Therefore, a larger anisotropy in conductivity (σ_{MD}/σ_{TD}) and elastic modulus (E_{MD}/E_{TD}) is indicative of a larger degree of axial orientation in the MD. As shown in Table 5.1, on this basis the rolled samples show slightly better orientation than the stretched samples. However, the stretched samples show a larger electroac-

tive effect for isotonic testing. A comparable phenomenon is observed for isometric testing, an example of which is shown in Figure 5-7.

5.3.1 Rate of Actuation

Changing the voltage ramp, we observe a difference in the amount of active strain observed and the anisotropy of this active strain. Under the conditions shown in Figure 5-8, an active strain of 11.3% is observed in the TD when stretched films are cycled at 0.1 V/s. As the voltage ramp is increased, the time for each cycle decreases, as does the magnitude and anisotropy of active strain. When the films in Figure 5-8 are cycled at 0.1 V/s, $(\epsilon_{TD}/\epsilon_{MD})_S = 6.2$. When the voltage ramp is increased to 1 V/s, the anisotropy of active strain decreases, with $(\epsilon_{TD}/\epsilon_{MD})_S = 3.8$.

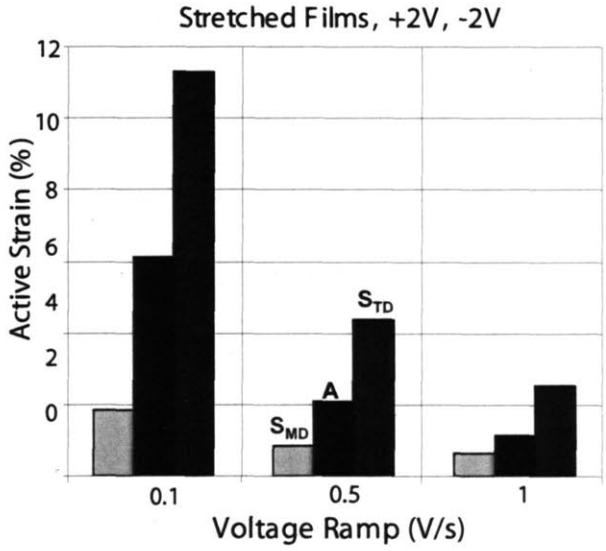

Figure 5-8: Isotonic testing of stretched samples in neat BMIMPF6 with a static force of 0.5 MPa. A ±2 V potential triangle wave was applied with the voltage ramp indicated. Strains are normalized by subtracting the initial strain that occurs upon application of the static force. Light grey bars: S_{MD}. Black bars: A. Dark grey bars: S_{TD}. At 0.1 V/s, $(\epsilon_{TD}/\epsilon_{MD})_S = 6.2$. At 0.5 V/s, $(\epsilon_{TD}/\epsilon_{MD})_S = 5.3$. At 1 V/s, $(\epsilon_{TD}/\epsilon_{MD})_S = 3.8$.

5.4 Discussion

5.4.1 Polymer Microstructure

While both the stretched and rolled films show polymer chain axial orientation in the MD, the x-ray diffraction patterns and micrographs of fracture surfaces show that the 3D distributions of the polypyrrole chains (and bundles) are different. The polypyrrole chain orientations for as-deposited, stretched, and rolled films are schematically illustrated in Figure 5-9. Note that Figure 5-9 is intended to clearly show the preferential orientation of the small polypyrrole bundles, not accurately describe the level of disorder of all components in this system. The stretched films show alignment in only one direction, with the chain axes parallel to the MD. This uniaxial chain alignment is responsible for the difference in fracture surface morphology shown in Figure 5-5i and Figure 5-5ii. When one examines the fracture surface looking down the TD (Figure 5-5i), a striated surface is observed due to the chain axial alignment in the MD. The fracture surface observed down the MD is rough and fibrillar (Figure 5-5ii) because the polymer chains are resistant to breakage along the backbone and pull apart from each other as the film fractures along the ND/TD plane.

The rolled films show a double texture, with the chain axes parallel to the MD and the ring normals parallel to the ND. Chain axial alignment in the MD causes the fracture surface observed down the MD (Figure 5-5iv) to be more rough than that observed down the TD (Figure 5-5iii), while ring normal alignment in the ND is reflected in the layered structure observed in both fracture surfaces. However, the degree of orientation in the MD and ND is not necessarily the same. In the rolled films (Figure 5-4ii) reflection **a** is highly anisotropic, observed only in the ND. This means that the pyrrole ring normals are very well oriented in the ND. Conversely, while reflection **c** is most intense in the MD, some scattering from reflection **c** is observed in all directions. This means that while the chain axes are preferentially oriented in the MD, they are not as well oriented as the pyrrole ring normals (as shown in Figure 5-9iii). While we do not measure the forces applied during our rolling process, these results suggest that the compressive forces exerted by the rollers are enough to force

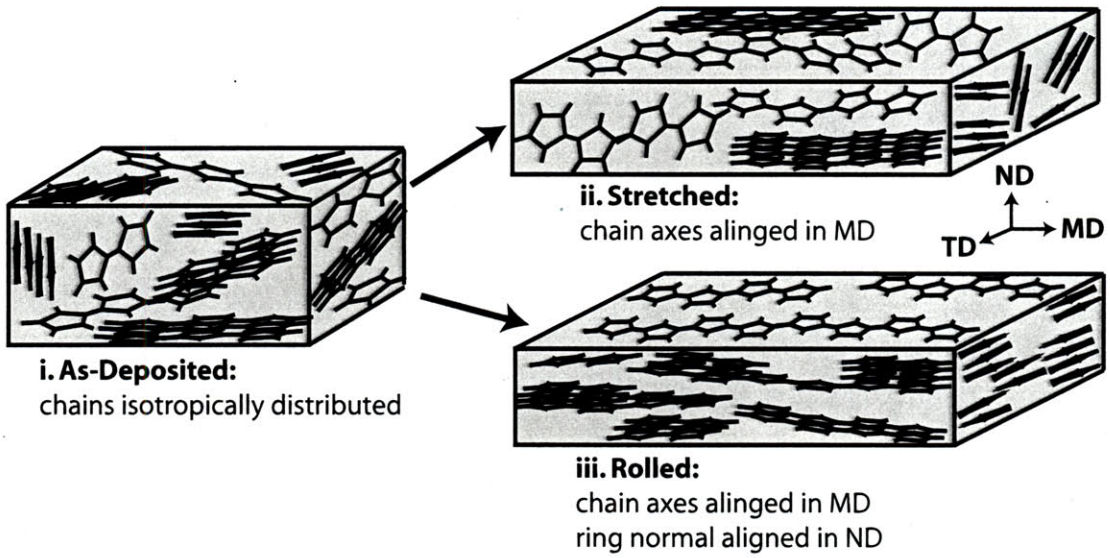

Figure 5-9: Microstructure of polypyrrole chains in as-deposited and processed films. i) Unprocessed film. The polypyrrole chains and bundles are isotropically distributed. ii) Stretched film. The polypyrrole chains and bundles are axially oriented in the MD, and randomly distributed and tilted around the MD (uniaxial orientation). iii) Rolled film. The chains and bundles are axially oriented in the MD, and the pyrrole ring normals are oriented in the ND (biaxial orientation).

the flat rings to lie parallel to the film surface, while the tensile stress is not enough to perfectly align the chain axes in the MD. Furthermore, tilting of the chains such that the ring normal is in the ND may be considerably easier than organizing the chains such that they are axial to the MD, as it would not require the same extent of disentanglement. A given chain segment could tilt to line up its pyrrole ring normals to the ND without requiring many other chain segments to move.

The stretched films show a larger electroactive response than do the rolled films, even when the rolled samples show a more anisotropic conductivity and elastic modulus (as for the films in Table 5.1). This may be because of the additional degree of orientation present in the rolled films when compared to the stretched films. In the rolled films the pyrrole ring normals align quite well in the ND, but the chains still have a large distribution of orientation about the MD. This distribution of flat chains with their faces parallel to the film surface may impede ion diffusion from the surface of the film.

5.4.2 Anisotropy of Actuation

Reduction of polypyrrole in neat BMIMPF6 leads to expansion as cations swell the film. These cations must find space between polymer chains, so the active strain occurs perpendicular to the chain axis. In unprocessed films, the chain axes are randomly distributed, so swelling and deswelling is observed equally in all directions. In oriented films (both stretched and rolled) the chain axis direction is preferentially aligned with the MD, so the observed active strain is concentrated perpendicular to the MD. The small amount of active strain observed in the MD is due to the misoriented chain component. Molecular modeling has suggested that there may be an intrinsic actuation mechanism in polypyrrole that would produce significant strains along the chain axis, as the polypyrrole chain straightens and curls upon oxidation and reduction [184]. Our results show that this is not the dominant mechanism in polypyrrole films.

With our testing methodology (as described in Section 2.3), we are limited to measuring the electroactive response in the MD and TD. Therefore, it is yet unclear whether the response in the ND is larger for stretched or rolled films. Stretched films should show an equal electroactive response in the ND and TD due to their uniaxial orientation, while the rolled films may show a very different response because the polypyrrole chain orientations in the ND and TD are different. In order to investigate this matter, instrumentation is currently being developed to measure the electroactive response in the ND for a free-standing processed film.

For the data shown in Figure 5-6, 30 to 36 mC of charge was passed during expansion of each cycle for the MD and TD samples for each set of films. The passage of a comparable amount of charge implies incorporation of a comparable number of cations, and should result in comparable volumetric expansion. With our testing methodology expansion and contraction is only measured in one direction at a time. When an MD film is actuated, it is likely that the film is expanding and contracting significantly perpendicular to the measured direction. This will be the case for both uniaxially and biaxially oriented films. Future work could include instrumentation

to systematically examine actuation in several dimensions at once, as this is where additional differences between actuation in uniaxially and biaxially oriented films will arise. However, if the goal is to produce an efficient linear actuator, expansion and contraction in directions not harnessed by the device are irrelevant. For these applications, an actuator that effectively actuates in only one direction is ideal.

The electroactive tests presented here were intended to expose the influence of molecular orientation on actuation. Thusly, the isotonic tests were limited to 5 to 10 cycles and a load of of 0.5 MPa, in an attempt to minimize molecular re-organization due to the load applied during testing. These conditions are sufficient to capture the anisotropy of active strain, but of insufficient duration to obtain a full picture of the maximum number of cycles achievable in oriented films. Polypyrrole actuated in neat BMIMPF6 has been previously shown to be very stable (a decrease of only 0.2% in active strain was observed over 6000 cycles [72, 73]) but thus far only unoriented polypyrrole has been tested. We expect oriented polypyrrole to be equally electrochemically robust when actuated in neat BMIMPF6, but it may not be as physically robust. In oriented films, the polymer chains are captured in a non-equilibrium, ordered configuration. As the polymer films are electrochemically cycled, the movement of small counterion molecules plasticizes the film and increases the mobility of the chains. The ion movement from electrochemical cycling may allow the polymer chains the mobility needed to revert to a more random chain orientation. For example, an unrecovered contraction is observed in the S_{MD} and R_{MD} samples in Figure 5-6. The small applied load (only 0.5 MPa) is not enough to prevent the re-orientation of polymer chains away from alignment in the MD, resulting in an irrecoverable contraction in the MD. The relaxation of polymer chains from axial alignment in the MD causes a deformation of aspect ration of the sample, as is schematically illustrated in two dimensions in Figure 5-10. This deformation of aspect ratio is observed as a irrecoverable contraction in the S_{MD} and R_{MD} samples, and an irrecoverable expansion in the S_{TD} and R_{TD} samples, as is shown in Figure 5-6.

Unrecovered expansion or contraction upon cycling may be avoided by increasing the loading or otherwise constraining the film. In the isometric test in Figure 5-7,

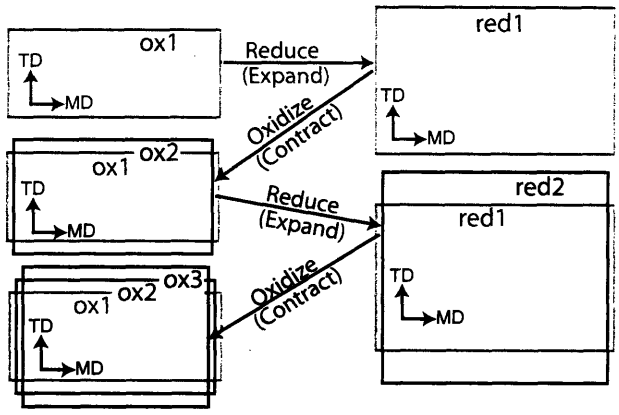

Figure 5-10: Schematic (2-D) diagram of expansion and contraction for oriented films under conditions shown in Figure 5-6. The percentage change in length and width upon oxidation and reduction are exaggerated for clarity. The area of the sample while oxidized is labeled ox1, ox2 and ox3. The area of the sample while reduced is labeled red1 and red 2. During each reduction, the area of the sample increases. During each oxidation, the area of the sample decreases, but finishes the cycle slightly larger than it began. Additionally, it is deformed from its original aspect ratio as described in the text.

for example, the film is geometrically constrained to maintain a constant length and irreversible increase or decrease of the active stress is not observed. Furthermore, it should be noted that we did not put significant efforts towards altering the electrochemical conditions to avoid irrecoverable expansion and contraction. It may be possible to adjust the electrochemical conditions to find a balance between allowing enough ion movement to cause a large electroactive response but not so much ion movement that the polymer chain mobility is so high that the sample irreversibly deforms. Future work will address the actuation of oriented films over very long times, to determine if re-orientation is a factor that must be prevented by the design of the loading mechanics or applied electrochemistry in electroactive devices.

Alternatively, we have observed (and discussed in Section 2.3.9) that the age of the polymer film affects the amount of deformation induced by a particular set of electrochemical conditions. As shown in Figure 5-11, the amount of irrecoverable expansion for the A, S_{TD} and R_{TD} samples is virtually eliminated when tested 12 weeks after processing. Unfortunately, the total active strain achievable is also reduced (e.g. $\epsilon_{S_{TD}} = 5.7\%$ in Figure 5-11, compared to $\epsilon_{S_{TD}} = 9.6\%$ under the same conditions in

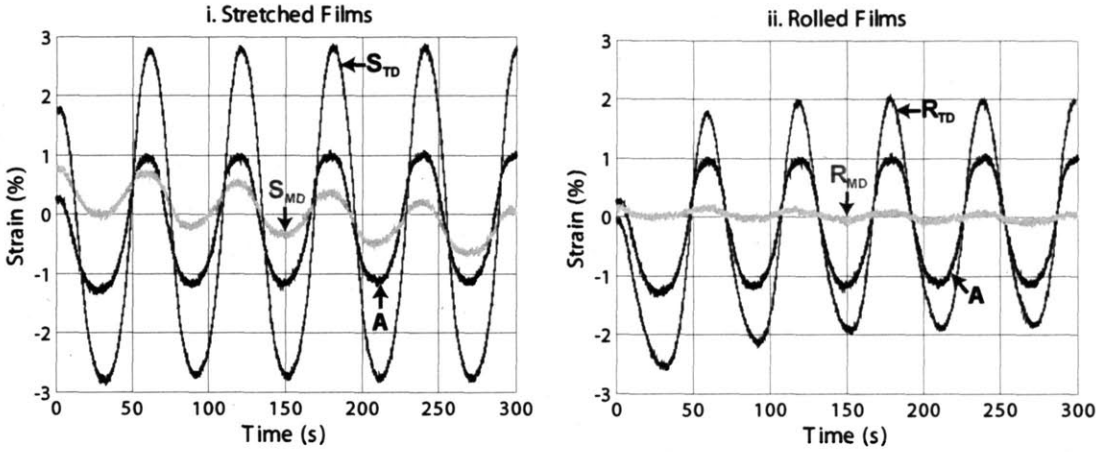

Figure 5-11: Isotonic response for stretched and rolled films tested 12 weeks after deposition and processing. Films were held under a static force of 0.5 MPa in neat BMIMPF6, and a ±1.5 V triangle wave in potential was applied at a rate of 0.1 V/s. Strains are normalized by subtracting the initial strain that occurs upon application of the testing load. i) Films stretched to 70% elongation. ii) Films rolled to 70% elongation.

Figure 5-6). We have not conducted a thorough study of polypyrrole ageing, as was discussed in Section 2.3.9, but these results suggest that the degradation of electroactive response with age is related to a decrease in mobility of the polypyrrole chains. In oriented films, this could be advantageous as it allows a more stable electroactive response over time. Ageing studies have not been conducted on polypyrrole deposited from our standard conditions, but a recent long-term study of polypyrrole doped with arylsulfonates reported that the conductivity decreases quickly at first (2 to 5 × over 5 years, depending on the synthesis conditions) but then remains relatively stable over the next 15 years [101]. The electroactive properties of the arylsulfonate films were not investigated, and whether a comparable ageing phenomena could be induced in a much shorter time period by exposure to increased temperature, for example, has not yet been probed. It may be the case that very stable polypyrrole films can be produced by artificially ageing, even if these films do not have quite as high electroactive strains as the new (but somewhat transitory) films. Perhaps if films with very high degrees of orientation (stretched or rolled to at least 100% elongation) were produced and aged, a very large (>10%) electroactive response could be achieved with minimal

irrecoverable expansion. In this scenario, the ageing provides the stability needed to make oriented polypyrrole an engineering material, while the orientation allows one to overcome the small strains typically found in aged films.

5.4.3 Anisotropic Diffusivity

When the voltage ramp is increased, the active strain in the TD decreases more than the active strain in the MD, showing that actuation in the TD is more time-limited than in the MD. It has been previously observed that diffusion of small molecules is much higher in the MD than the TD for oriented polycarbonate [185] and other glassy polymers [186]. This has been attributed to a deformation of the free volume in the sample upon polymer orientation, resulting in effective ellipsoids of free volume with their long axis parallel to the MD [185]. In the case of polypyrrole, there are solvent molecules and counterions in the spaces between polymer chains so this volume is not entirely "free," but the interchain spaces will be elongated with processing as shown in Figure 5-12. This means that there are effective pathways of easy diffusion between the polymer chains along the MD. In fact, the diffusivity of PF_6^- anions in stretched films produced as part of this work has been measured by pulse field gradient NMR, with the following results [82, 187, 188]:

- $D_{MD} = 1.69 \times 10^{-12}$ m^2/s
- $D_{TD} = 0.94 \times 10^{-12}$ m^2/s
- $D_{ND} = 0.97 \times 10^{-12}$ m^2/s

D_{TD} and D_{ND} are very similar, as is expected for uniaxial orientation. They are both significantly lower than D_{MD}, causing the actuation in the TD to be more time-limited than that in the MD (as was shown in Figure 5-8). Both uniaxially and biaxially films will show higher diffusivities in the MD than the other directions, but in biaxially oriented films the diffusivity in TD and ND should be different due to the different chain orientations in these directions. Measurements of as-deposited and rolled films produced as part of this work are currently underway.

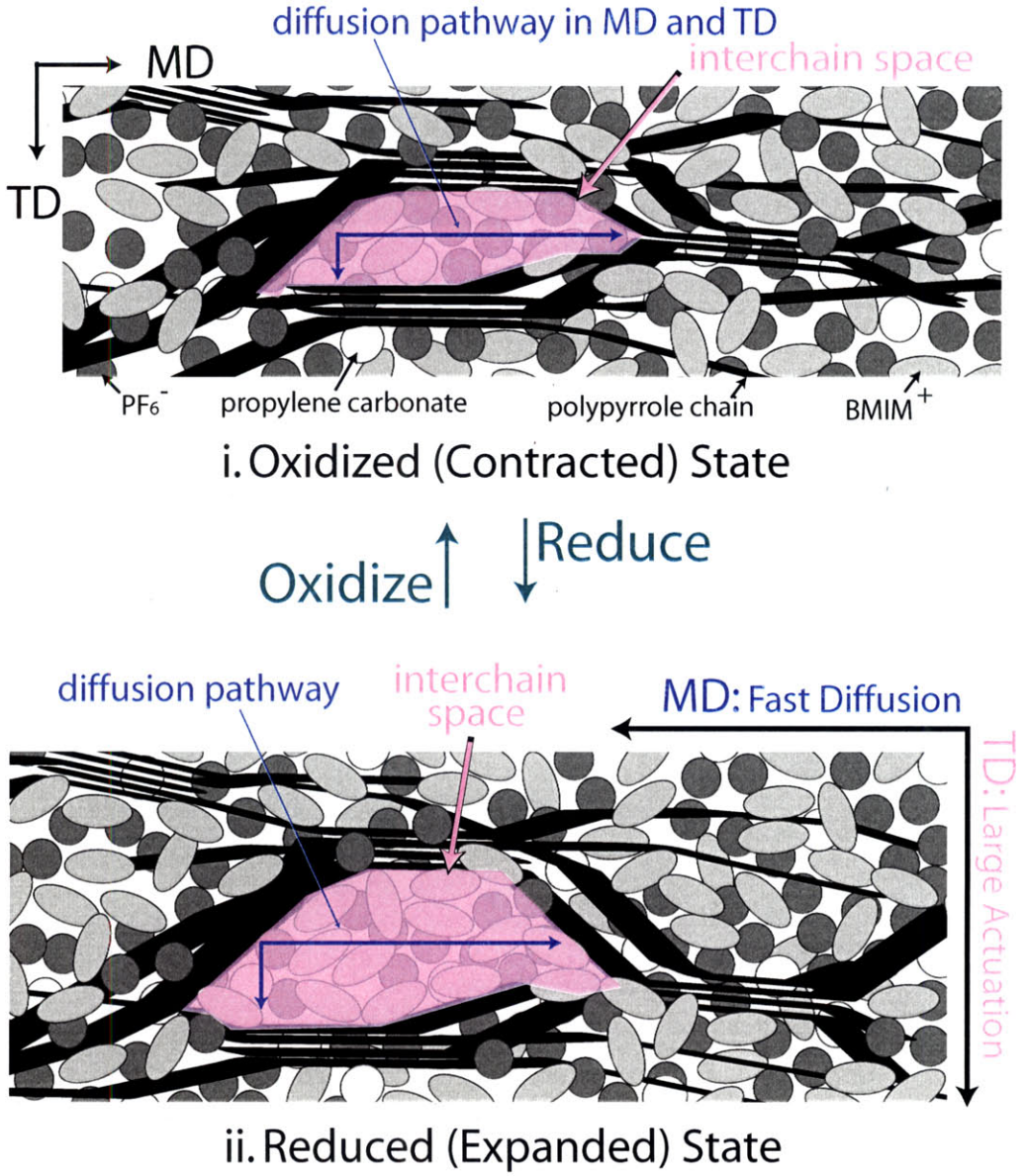

Figure 5-12: Change in interchain spaces upon oriented polymer actuation in BMIMPF6. After warm-up, the interchain spaces are swollen with PF_6^-, propylene carbonate, and BMIM+ cations. i) Oxidized state. In oriented polypyrrole films, the chain axes and bundles preferentially align in the MD. This causes the spaces between chains to become elongated in the MD, providing a longer path of easy diffusion for small molecules in the MD than in the TD. A single interchian space is highlighted in pink, while the anisotropy of diffusion pathways is shown with blue arrows. ii) Reduced state. Upon reduction in neat BMIMPF6, $BMIM^+$ cations swell the interchain spaces, pushing non-bundled chain segments apart. This causes a large actuation perpendicular to the chain axis. In processed films, the chain axes are oriented in the MD, so this large actuation is observed in the TD. One swollen interchain space is highlighted in pink. Even though the interchain spaces are swollen with $BMIM^+$, they are still longer in the MD than the TD, allowing for easier diffusion of small molecules in the MD than the TD, as is highlighted with the blue arrows.

The interchain spaces may provide an additional distinction between stretched and rolled films, as the forces applied to the films during the rolling process may cause interchain spaces to collapse, impeding the movement of counterions. Xie et al. showed that plastic deformation imparted by stretching or compressing a polycarbonate sample caused a decrease in free volume, but compression caused a larger decrease in free volume than stretching [189]. Rolling has been shown to decrease oxygen and antioxidant permeability in poly(methyl methacrylate) [186]. We also observe an increase in density when polypyrrole films are stretched or rolled, with a 2.3% increase for films stretched to ($\sigma_{MD}/\sigma_{TD} = 3$), and a 2.7% increase for films rolled to ($\sigma_{MD}/\sigma_{TD} = 2.8$). The decreased electroactive performance of the rolled films when compared to the stretched films may be due to a more tightly-packed microstructure resulting in smaller interchain spaces and a correspondingly lower counterion mobility. However, as is evident from the diffraction patterns in Figure 5-4, if a more tightly packed structure exists in the rolled films it does not increase the crystallinity or crystallite size enough to change the shape of the diffraction peaks. In other words, we do not observe a significant increase in number or size of bundles, but we believe after processing the bundles are closer together.

5.5 Chapter Conclusions

In this chapter, our efforts towards processing polypyrrole post-deposition have been presented. We have utilized different processing techniques to achieve uniaxial and biaxial textures in polypyrrole films. By processing the films such that the chain axes are preferentially oriented parallel to the MD, a much larger electroactive response is concentrated in the TD. This has resulted in an actuator that shows a 100% increase in active strain when compared to as-deposited films actuated under the same electrochemical conditions, and electroactive strains of up to 11.3% have been achieved. Stretched films (with uniaxial orientation) exhibit superior electroactive properties to rolled films (with biaxial orientation), probably due to superior ion transport through the film.

Orientation of polypyrrole films provides a simple way to improve the performance of this electroactive material without altering the chemistry of deposition or actuation. The electrochemical properties of polypyrrole films remain unchanged after processing, but the stress or strain that results from that electrochemistry is improved because it is concentrated in the direction of testing. By the addition of a processing (and perhaps an ageing) step between deposition and actuation engineers can double the performance of their polypyrrole-powered devices. Furthermore, these films provide anisotropic linear actuation not previously achievable in conducting polymers. This can be utilized for biomimetic applications such as active bandages or artificial fish fins [190–192] where the direction of actuation must be carefully controlled. By designing devices specifically for the unique properties these films offer, engineers can produce polypyrrole-driven devices not previously viable.

Chapter 6

Microstructure Manipulation II: Synthetic Approaches

In our attempts to make the best polypyrrole actuator possible, we seek to manipulate the microstructure of polypyrrole by whatever means we can. As was presented in Chapter 5, the microstructure can be altered post-synthesis via physical processing. This results in an anisotropic material, and has allowed us to achieve higher active stresses and strains than previously feasible.

It is also possible to alter the microstructure of by changing the parameters of the deposition recipe. It has previously been shown (and discussed at length in Chapter 3) that the choice of counterion [27, 94], solvent [27, 94, 95], electrode metal [6, 27], temperature [6, 93] and applied current or potential [6, 93–95] all affect the final microstructure of the polypyrrole film. By altering the "standard" deposition recipe (described in Section 2.1.1) to probe some of this parameter space, we seek to better understand how different morphologies affect actuation.

In our experiments, polypyrrole is polymerized electrochemically, resulting in black films that can be peeled off the electrode to be free-standing. They are doped with the anion used in the deposition electrolyte, and often swollen with residual solvent from deposition. The films are insoluble, unmeltable, conductive, and 10 to 40 μm thick. We utilize Scanning Electron Microscopy (SEM) and Wide-angle X-ray Diffraction (WAXS) to investigate the microstructure and morphology of these films. and

Film	Pyrrole Conc. (M)	Counterion Salt	Salt Conc. (M)	Solvent	Electrode Material	Temp. (°C)	Current Density (A/m^2)
A	0.05	TBAPF6	0.05	PC	Glassy Carbon	-40	1
B	0.25	TBAPF6	0.2	MB	Glassy Carbon	-10	1
C	0.25	TBAPF6	0.2	MB	Nickel Foil	-10	1
D	0.25	TBABF4	0.5	MB	Nickel Foil	25	2
E	0.25	TBATFSI	0.2	MB	Glassy Carbon	-10	1
F	0.25	TBATFSI	0.2	MB	Nickel Foil	-10	1
G	0.25	LiTFSI	0.2	MB	Glassy Carbon	-10	1.25

Table 6.1: Conditions for different polypyrrole electrodeposition recipes. Abbreviations for counterion salts are: tetrabutylammonium hexafluorophosphate (TBAPF6), tetrabutylammonium tetrafluoroborate (TBABF4), tetrabutylammonium bis(trifluoromethanesulfonly)imide (TBATFSI), lithium bis(trifluoromethanesulfonly)imide (LiTFSI). Abbreviations for solvents are: propylene carbonate (PC), methyl benzoate (MB). Films are deposited from the listed solutions at constant current density, at the temperature listed. For recipe A only, 1% vol water was added to the deposition solution.

subject the films to electroactive testing to elucidate the link between structure and electroactive properties.

6.1 Procedure

Polypyrrole films were deposited at constant current density and temperature, via the method described in Section 2.1.1 but using the specific conditions listed in Table 6.1. For Film A only, 1%vol water was added to the deposition solution. Pyrrole (Aldrich 99%) was vacuum distilled before use. All other materials were used as received. The molecular sizes of the various components are shown in Figure 6-1.

The counter electrode was a glassy carbon plate, and the working electrode was either a glassy carbon plate or nickel foil. After deposition, the polypyrrole film-covered working electrode was rinsed in a monomer-free solution of the salt and solvent used for deposition and allowed to dry in the fume hood. Free-standing films were peeled off of the electrode, and small samples (2 mm × 10 mm) were cut for testing. Average properties for the films from Table 6.1 are shown in Table 6.2.

The recipes shown in Table 6.1 were chosen in part to mimic a series of previous

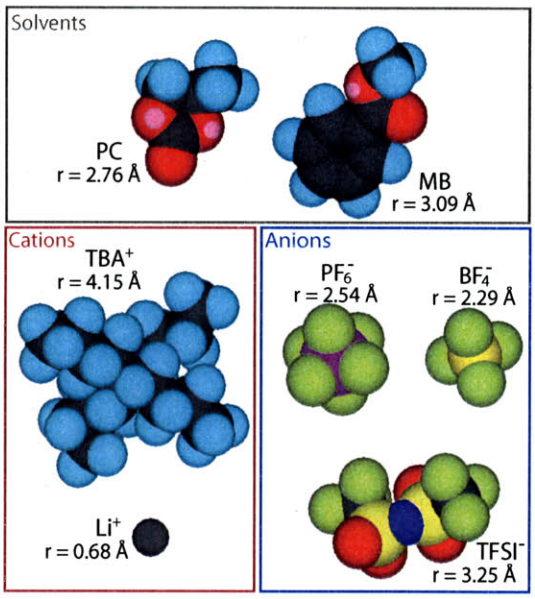

Figure 6-1: Sizes of species varied in polypyrrole depositions [69, 75]. Abbreviations are as described for Figure 6.1.

works, in which exceptionally large active stresses (up to 22 MPa [30]), strains (up to 36.7% [3]), and strain rates (up to 13.8%/s [94]) were reported. Active metrics of this magnitude have only been reported by one group, and as part of this study we seek to discover how they achieve such large metrics and why no one else can do so.

6.2 Surface Morphology

Scanning Electron Microscopy (SEM) images of the surfaces of the two working electrodes used for the films in Table 6.1 are shown in Figure 6-2. The glassy carbon surface is extremely smooth, so one must find a defect such as the one shown in Figure 6-2 in order to focus the microscope. These defects are rare, and the majority of the surface is smooth with occasional shallow grooves from polishing. The nickel foil surface is much rougher, and has a heavily grooved texture from the manufacturing process.

The solution and electrode-facing surfaces of the films from Table 6.1 as observed via SEM are shown in Figure 6-3 and Figure 6-4, respectively. Film A is the "standard" deposition recipe used throughout this work, and is quite smooth on both

Film	σ (S/m)	ρ (kg/m^3)	E (GPa)
A	3.6×10^4	1500	0.38
B	1.9×10^4	1400	
C	2.0×10^4	1300	
D	4.6×10^3	700	0.53
E	2.5×10^4	1300	1.29
F	3.6×10^3	400	0.04
G	4.9×10^3	1750	0.17

Table 6.2: Measured properties of films from Table 6.1. Conductivity (σ) is measured with a four point probe. For Films A and G, density (ρ) is measured using a Micromeretics AccuPyc 1340 Helium Pycnometer, and is repeatable to $\sim$ 10 kg/m^3. For all other films, insufficient sample was produced to measure true density using gas pycnometry, so apparent density (ρ) is estimated by measuring the volume by hand (only repeatable to $\sim$100 kg/m^3). One should note that films listed with a higher apparent density are not necessarily less porous, as they may be doped with a heavier counterion. Elastic modulus (E) is the "dry" elastic modulus, measured as described in Section 2.3.1. For Films B and C, insufficient film was produced for electroactive testing so the modulus was not measured.

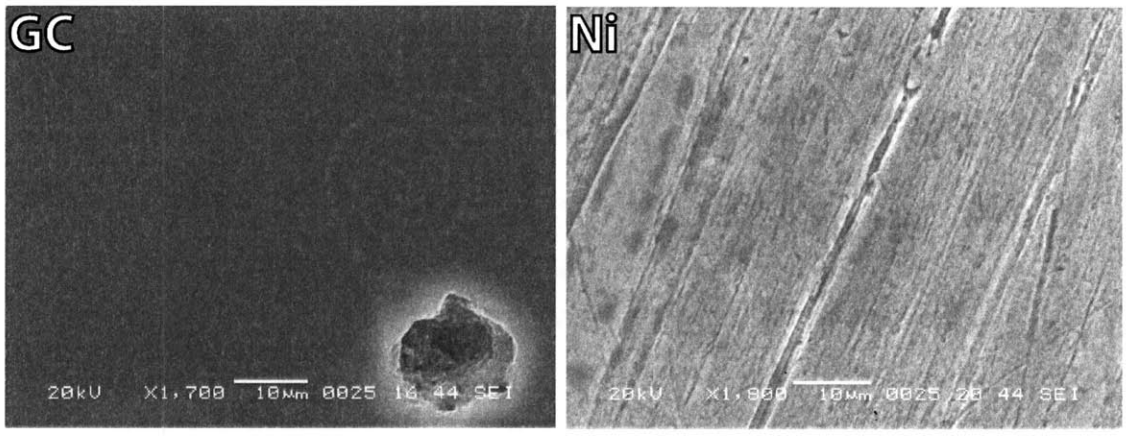

Figure 6-2: Glassy carbon (labeled "GC") and nickel foil (labeled "Ni") working electrode surfaces. The GC surface was very smooth. Defects are rare, but one is shown here for focusing. The Ni surface was much rougher than the GC surface, and had a consistent surface texture over the entire sample.

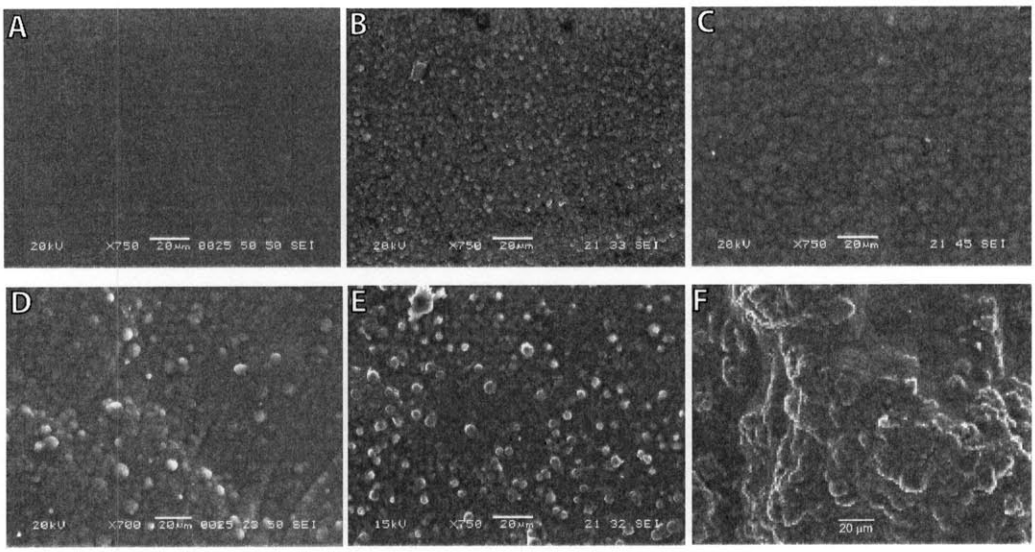

Figure 6-3: Solution-facing surfaces of polypyrrole films synthesized from the different recipes listed in Table 6.1. Images were taken on a JEOL JSM-5910 SEM. The information listed across the bottom of the micrographs is as follows: accelerating voltage, magnification, scalebar, image number (only visible in A and D), working distance (in mm), spot size, detector (SEI = secondary electron imaging).

sides. When the solvent is changed from PC to MB, the solution surface of the film becomes nodular (Figure 6-3 B,C). The size of the nodules is increased when the deposition is conducted at room temperature (Figure 6-3 D), consistent with previous studies [6]. Additional roughness occurs when a larger anion is used, even if the deposition is conducted at low temperature (Figure 6-3 E). The surface is the most nodular and wrinkled when the large anion and rough nickel foil electrode are used together (Figure 6-3 F).

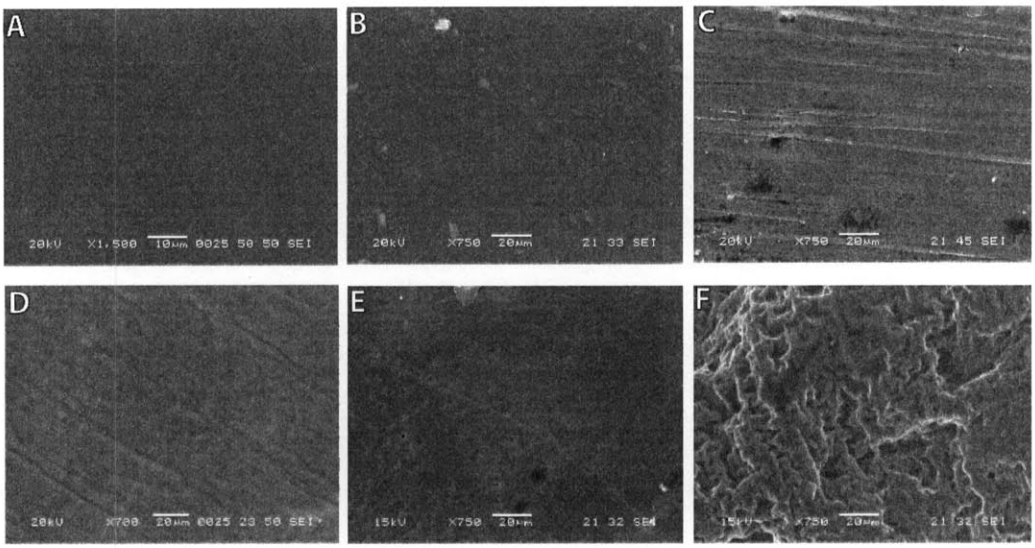

Figure 6-4: Electrode-facing surfaces of polypyrrole films synthesized from the different recipes listed in Table 6.1. Images were taken on a JEOL JSM-5910 SEM. The information listed across the bottom of the micrographs is as follows: accelerating voltage, magnification, scalebar, image number (only visible in A and D), working distance (in mm), spot size, detector (SEI = secondary electron imaging).

The electrode side of the films from Table 6.1 also show additional features as the recipe is altered from the "standard" deposition. When the nickel foil electrode is used, the electrode side of the film shows striations from the foil surface (Figure 6-4 C,D and F). When the deposition solution includes the large $TFSI^-$ anion, the electrode side of the film becomes more porous (Figure 6-4 E,F). Comparison of films A and F provides perhaps the most striking evidence that very different polypyrrole actuator materials can be produced by altering the deposition conditions.

6.3 Wide Angle X-ray Scattering

As was discussed at length in Chapter 4, most of the information we have about the crystal structure in polypyrrole comes from the interpretation of somewhat ambiguous diffraction patterns. The previously published percent crystallinity and the crystalline unit cell are guesses based on liberal interpretations of these patterns [10, 11, 165]. Because the peaks in the diffraction patterns are overlapping and ambiguous exact crystalline dimensions should be viewed with skepticism. By manipulating the struc-

ture of polypyrrole we have not achieved a highly crystalline state that will allow us to conclusively determine the crystal structure via scattering experiments, but we have been able to clearly demonstrate the microstructural origin of a particular feature of the diffraction pattern.

While polypyrrole does not have sufficiently large crystals to produce single-crystal x-ray diffraction patterns, there are several characteristic features to its wide angle x-ray scattering pattern (labeled **a**, **b**, **c**, and **Γ** in Figure 6-5), that were discussed extensively in Section 4.1 and are briefly reviewed here. Reflection **a** is attributed to the face-to-face distance between pyrrole rings on adjacent stacked chains [10, 123, 130, 131], while reflection **b** has been attributed to the distance between stacks of polypyrrole chains [123, 132]. Reflection **c** is attributed to a dipyrrole spacing along the polymer chain [10, 123]. Several different physical features have previously been assigned to reflection **Γ**, including scattering from the edge-to-edge distance between two polypyrrole chains with no counterion [164], pyrrole-counterion scattering [131], solvent-solvent scattering [158], and counterion-counterion scattering [123, 131, 158]. Because its associated diffraction ring does not become anisotropic upon stretching up to 150%, reflection **Γ** has also been assigned to inter-chain scattering between amorphous polypyrrole chains [6, 10, 158, 163–165].

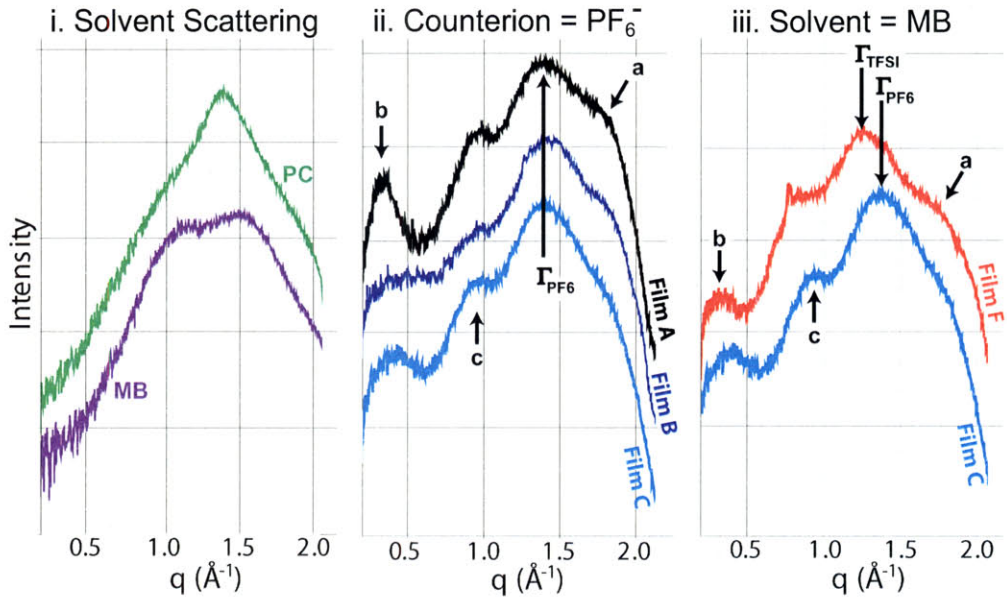

Figure 6-5: 1D x-ray diffraction patterns of solvents and films from Table 6.1. Curves are offset for clarity. i) Scattering from neat solvents: propylene carbonate (PC) and methyl benzoate (MB). Solvents were sealed in glass capillaries and exposed to the x-ray beam. Capillary scattering was then subtracted. ii) Films doped with PF_6^-: A, B, and C. Reflection $\mathbf{\Gamma}$ does not shift, even when the solvent is changed from PC to MB (Film A compared to Films B and C), or when the electrode is changed from glassy carbon to nickel foil (Films A and B compared to Film C). iii) Films deposited from MB solution. Even though the solvent and electrode material remain the same, the spacing of reflection $\mathbf{\Gamma}$ shifts from $q = 1.4$ Å^{-1} to $q = 1.26$ Å^{-1} when the $TFSI^-$ anion is used instead of the PF_6^- anion. This reflects the larger size of the $TFSI^-$ anion (r = 3.25 Å) [69] when compared to the PF_6^- anion (r = 2.54 Å) [69]. The sharp peak in the curve for film F at $q = 0.77$ Å^{-1} is due to contamination.

By examining the diffraction patterns of the films from Table 6.1, we can observe how the d spacing of reflection **Γ** is affected by the species used in the deposition. The two solvents used in Table 6.1 show significantly different x-ray scattering patterns, as is shown in Figure 6-5i. However, a change in solvent does not cause a change in reflection **Γ** as long as PF_6^- is used as the anion (Figure 6-5ii). Alternatively, by changing only the deposition counterion and keeping the solvent and electrode material constant, we can clearly show that the d spacing of reflection **Γ** is dependent on the counterion used during deposition (Figure 6-5iii). Interestingly, other studies that show a change in reflection **b** with counterion make no mention of reflection **Γ** [123]. We also observe a change in reflection **b** with counterion, but it is less clear than the change in reflection **Γ**, as reflection **b** also seems to be altered by the choice of solvent and electrode material. The fact that reflection **Γ** does not become anisotropic upon orientation (as was discussed in Chapter 5.2.1) means that the counterions do not assume any anisotropy even when the polymer chains become oriented.

6.4 Electroactive Characterization

The electroactive response to a potential square wave for Films E and F (which have very different surface morphologies and mechanical properties) is shown in Figure 6-6i. Film F shows a higher initial strain rate than Film E, and during shorter potential holds Film F shows a larger magnitude of active strain than Film E (Figure 6-6ii). However, Film F cannot sustain its high initial strain rate for an entire 60 second cycle, and at longer potential holds Film E shows a larger strain. Film F has a much higher surface area than Film E (Figures 6-3 and 6-4) but its conductivity and elastic modulus are almost an order of magnitude lower than Film E (Table 6.2). The very low elastic modulus combined with an increased surface area is likely responsible for the faster initial strain rate exhibited by Film F. The rough surface provides more surface area for counterions to diffuse into the polymer matrix, while the low elastic modulus allows the film to easily expand to accommodate the ion influx. However, the low conductivity prevents Film F from drawing enough charge

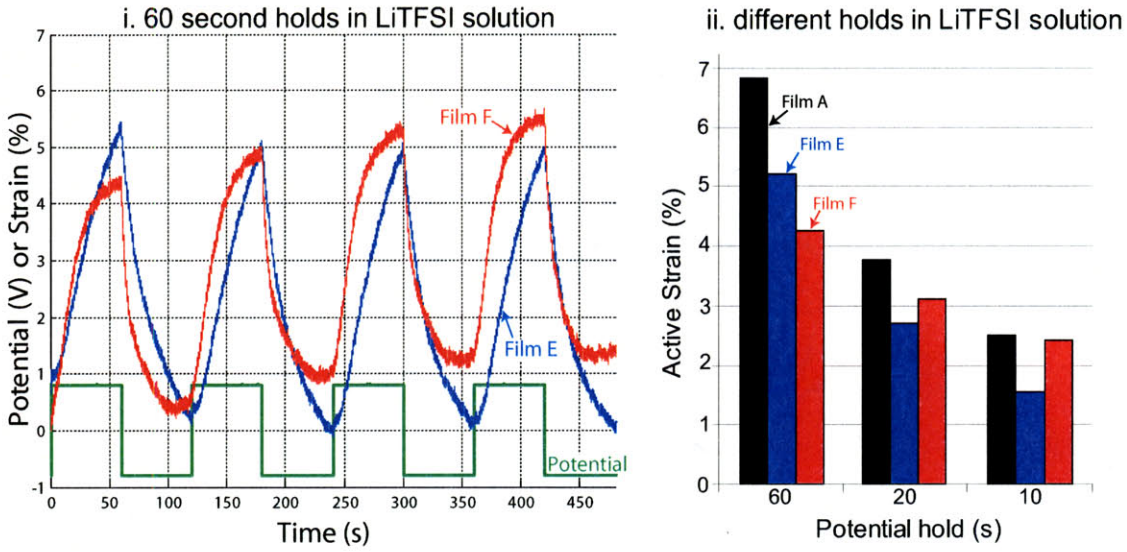

Figure 6-6: Actuation of films with different surface morphologies. Each film was warmed up as described in Section 2.3.1, and then actuated in isotonic mode as described in Section 2.3.2. The applied static force is 0.5 MPa, the electrolyte is 0.1 M LiTFSI in a 60:40 mix of water and propylene carbonate. A potential square wave of ± 0.8 V vs. Ag/Ag^+ is applied. The change in sample length is measured, and divided by the initial length to determine the strain. The strain is normalized by subtraction of the initial strain that occurs from passive application of force. i) Strain and potential vs. time data for 60 second holds. ii) Comparison of active strain for holds of different lengths.

to match the magnitude of actuation of Film E at longer timescales. Films E and F are compared because they are synthesized from the same recipe, the difference between the two is imparted by the different electrode materials. It should be noted that under these conditions, the "standard" Film A outperforms them both. Film A draws a larger charge over each potential cycle, resulting in increased ion movement and active strain. However, its smooth surface and high modulus may prevent it from matching the high initial strain rate of Film A if even shorter potential holds were tested.

6.4.1 Actuation Without Warm-up

Polypyrrole films deposited from the same recipe as Film G (LiTFSI/MB solution) have been previously reported to show strains of 16.7% when actuated at 2 mV/s in

aqueous 1 M LiTFSI [27]. When we prepare films from LiTFSI/MB solutions and acutate them under the aforementioned conditions, we get the results shown in Figure 6-7. In an effort to achieve the large published strains, these films were not subjected to the warm-up procedure described in Section 2.3.1 and were instead submerged into the electrolyte a maximum of one second before electroactive testing began. The lack of a warm-up treatment means that films are not at a known electrochemical state before testing, but larger strains may initially occur as the film acclimates to the electrochemical environment.

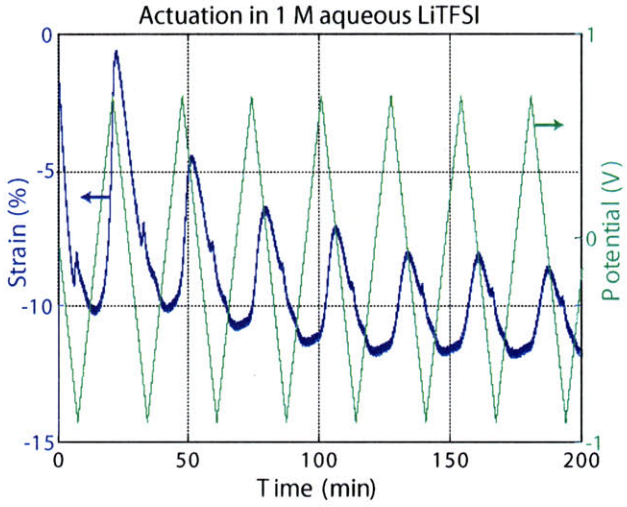

Figure 6-7: Isotonic actuation of Film G in aqueous LiTFSI with no warm-up. A -0.9 V, +0.7 V triangle wave was applied at 2 mV/s, following the procedure of Hara et al. [27]. The sample was submerged into the electrolyte approximately one second before the first cycle was started. The first cycle shows a contraction of 10.2%, but the response decreases as the cycles continue, reaching $\sim$ 3% by the seventh cycle.

During the first reduction in Figure 6-7, the polymer film contracts approximately 10.2%. This is significantly lower than the 16.7% reported by Hara et al., but larger than the strains shown for a warmed-up sample of Film G in Figure 6-6. It is clear that the response shown in Figure 6-7 is transitory, and the response decreases to approximately 3% by the seventh cycle. Hara et al. only show the first two cycles in their work, but even there the second cycle clearly shows less active strain than the first ($\sim$19% for the first cycle, $\sim$16% for the second) [27].

When a different sample of the same film was actuated without warm-up in a

solution of 1 M LiTFSI in a 60/40 mix of water/PC (in an attempt to repeat the results presented here [29]), the response shown in Figure 6-8 was observed. During the first expansion, the polypyrrole film swells with $TFSI^-$ anions and neutral propylene carbonate, resulting in the very large expansion of 19.8%. Propylene carbonate is a better solvent for polypyrrole than water, so a much larger swelling occurs upon exposure to propylene carbonate solution (Figure 6-8) than upon exposure to aqueous solution (Figure 6-7). After the initial swelling, the polymer film remains swollen with propylene carbonate and the active response is dominated by movement of the $TFSI^-$ anions. This results in a repeatable strain of 5.1% by the 15^{th} cycle. Hara et al. show a repeatable strain of approximately 15% for a similarly prepared film, actuated under the same electrochemical conditions [29]. However, it appears that one side of the sample that produced 15% linear strain was coated with gold to increase its conductivity [193].

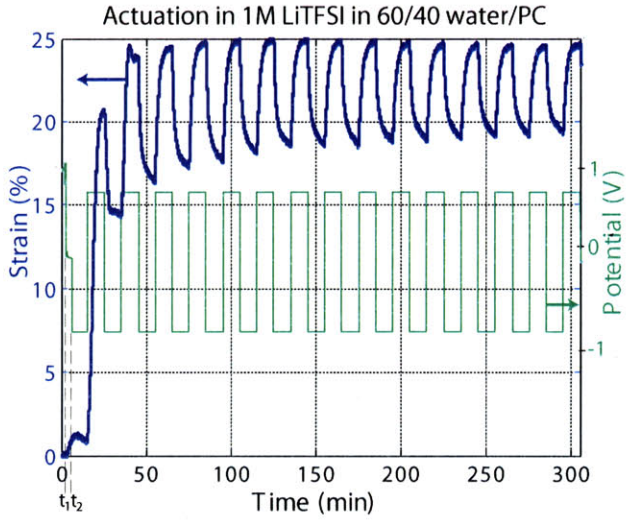

Figure 6-8: Isotonic actuation of Film G in 1M LiTFSI in 60/40 water/PC with no warm-up. At time t_1, the polypyrrole film was submerged in the electrolyte. At time t_2, the first potential cycle was started. A -0.1 V, +0.7 V square wave was applied with a frequency of 0.05 Hz, following the procedure of Hara et al. [29]. The first cycle shows and expansion of 19.8%, but the active strain decreases to 5.1% by the 15^{th} cycle.

6.5 Further Manipulation of Microstructure

As was discussed extensively in Chapter 5, stretching our standard (Film A) polypyrrole films increases the achievable active stress and strain by allowing one to harness more of the electroactive response in a particular direction. We seek to improve some of the other recipes shown in Table 6.1 by a similar treatment. Polypyrrole films deposited from MB solution have been shown to swell significantly when placed in an appropriate solvent or electrolyte system, as was discussed above [27]. Here, we attempt to take advantage of this expansion to stretch these films to large elongations. In Figure 6-9, one sample cut from Film E was stretched in air to an elongation of 210% (blue curve), resulting in a final machine direction (MD) conductivity of $\sigma_{MD} = 5.7 \times 10^4$ S/m. A different sample cut from Film E was stretched in air to an elongation of 10%, then submerged in 0.1 M LiTFSI/PC for the duration of the test. It was stretched to a final elongation of 280% (orange curve), with a final conductivity of $\sigma_{MD} = 3.7 \times 10^4$ S/m. One should note that the samples used for the curves shown in Figure 6-9 were very small (2 mm $\times$ 10 mm), so only axial (MD) conductivity could be measured.

The final conductivity for the wet film in Figure 6-9 was significantly lower than that of the dry film, even though the wet film was stretched to a higher linear elongation. During the first 10% elongation, both samples show approximately the same elastic modulus (slope of the stress vs. strain curve). However, after the wet film is submerged in the LiTFSI/PC solution, it expands an additional 60% without any appreciable increase in stress. This expansion is due to swelling of the film with propylene carbonate solution, which does not increase the orientation of the sample. While the wet film was stretched further than the dry film, its final conductivity is lower because some of that elongation was a result of swelling, not plastic deformation. This example shows that submersion in propylene carbonate solution while stretching does not help one produce more anisotropic samples, even though it allowed the sample to be stretched to a higher elongation.

Unfortunately, the components of Film E are too expensive for polypyrrole film

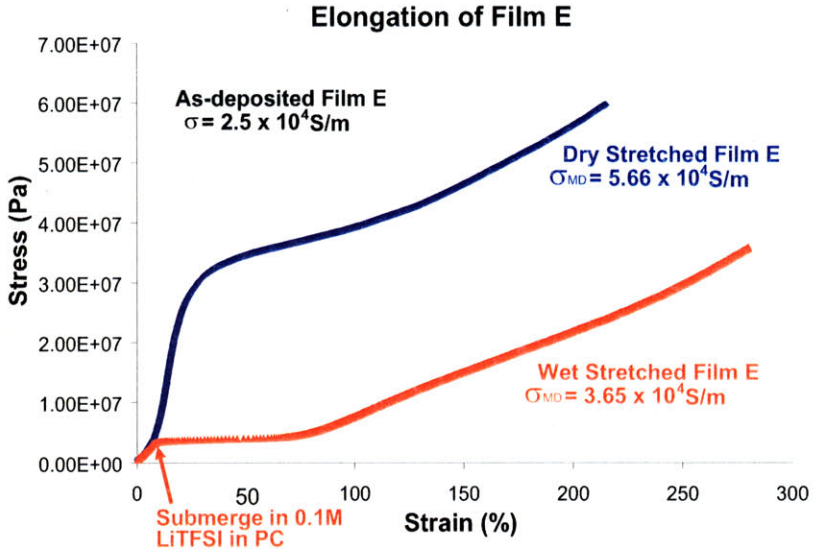

Figure 6-9: Tensile testing of films from deposition E. Each film was stretched at room temperature on a Perkin Elmer DMA 7e Dynamic Mechanical Analyzer, under stress ramp control (1000 kPa/min). The "dry film" (blue curve) was stretched in air. The "wet film" (orange curve) was stretched in air for the first 10 seconds, then submerged in 0.1 M LiTFSI in propylene carbonate for the rest of the test. Both films were stretched to failure, the dry film to 210% and the wet film to 280%.

production on a large (50 mm × 150 mm) scale, which prevented the experiment shown in Figure 6-9 from being repeated at a larger scale. Instead, large samples of Film G were synthesized. Film G also provides a film doped with the $TFSI^-$ anion that has a more nodular and porous morphology than the "standard" Film A (Figure 6-10), and has been reported to show only slightly lower strains than Film E [27].

Film G was and stretched in air on a Zwick/Roell Z010 Mechanical Tester under stress control, at a rate of 0.0167 MPa/min, to an elongation of approximately 50%. Samples were then cut with their axis along the MD and TD (referred to as G_{MD} and G_{TD}), and compared to a sample cut from as-deposited film G (referred to as G_A). These samples showed a conductivity ratio of $\sigma_{MD}/\sigma_{TD} = 4.04$, which is comparable to the stretched samples of Film A discussed in Section 5.3. However, as shown in Figure 6-11, this anisotropy of conductivity is not reflected in the active strain. The aforementioned films from Section 5.3 showed an anisotropy of active strain of $\epsilon_{TD}/\epsilon_{MD} = 7.0$, while in Figure 6-11 the anisotropy is almost nonexistent: $\epsilon_{TD}/\epsilon_{MD} = 0.9$. It is possible that the propylene carbonate solution swells film G so well that

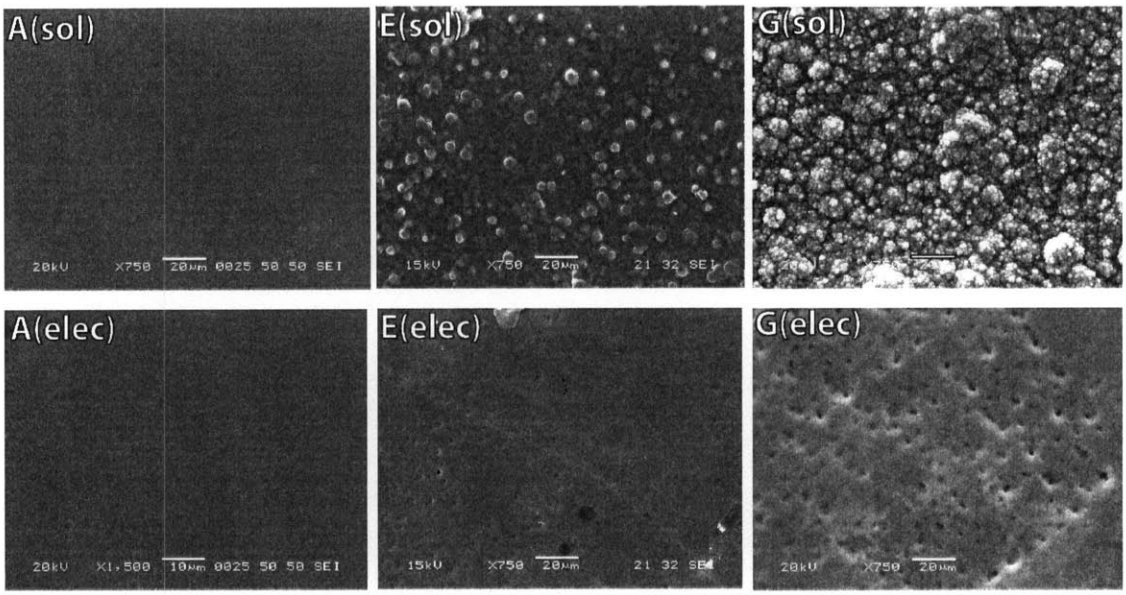

Figure 6-10: SEM micrographs of solution (top row) and electrode (bottom row) sides of films A, E and G. Film E and Film G are both doped with the $TFSI^-$ anion, and deposited on a glassy carbon electrode. They both show a nodular solution surface and a slightly porous electrode surface.

the orientation is effectively lost during warm-up. The anisotropy of elastic moduli (shown in Figure 6-12) is also effectively lost during warm-up, as would be expected if the polymer chains were no longer oriented in the MD. Future work should include WAXS of samples before and after testing, to verify that a loss of orientation occurred.

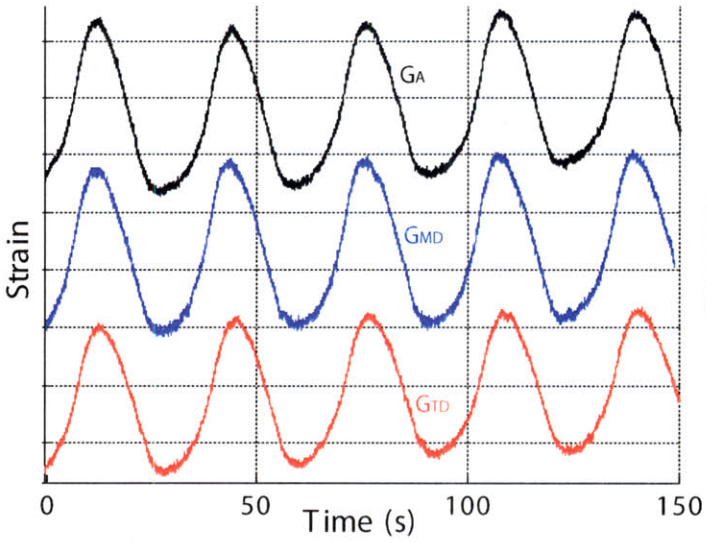

Film	σ (S/m)	σ_{MD}/σ_{TD}	ε (%)	$\varepsilon_{TD}/\varepsilon_{MD}$
G_A	5.23×10^3		2.8	
G_{MD}	1.33×10^4	4.04	2.9	
G_{TD}	3.30×10^3		2.6	0.9

Figure 6-11: Isotonic actuation of samples from stretched Film G in 0.1 M LiTFSI in propylene carbonate. Curves are offset for clarity, and the magnitude of active strain is listed in the table. Films were held at a constant stress of 0.5 MPa and actuated with a ±0.8 V triangle wave at 0.1 V/s.

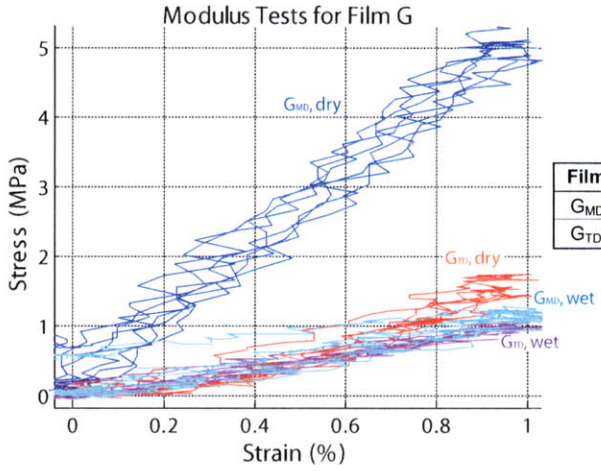

Film	E_{dry} (GPa)	E_{wet} (GPa)
G_{MD}	0.46	0.10
G_{TD}	0.15	0.09

Figure 6-12: Dry and wet modulus tests for stretched samples of film G. The modulus is the slope of the stress vs. strain curve. The dry moduli are measured before submersion in the electrolyte, and the wet film moduli are measured after electrochemical warm-up, as described in Section 2.3.1. Before warm-up, $E_{MD}/E_{TD} = 3$. After warm-up, $E_{MD}/E_{TD} = 1.1$

6.6 Chapter Conclusions

In the literature there have been several examples where films produced from aromatic esters and large anions reportedly produce exceptionally large strains [3,27–29, 94, 128]. However, when we have attempted to repeat those experiments, we do not achieve the same strains. We find a large transitory response in the first few cycles (e.g. 19.8% strain in Figure 6-8), but after the first few cycles the electroactive response dwindles. Furthermore, our attempts to improve the electroactive response in these films have thus far been unsuccessful, as we typically lose the effect of orientation as the film warms up.

Regardless of our ability to match the impressive metrics cited in the literature, alteration of the deposition recipe does produce a very different material from the standard propylene carbonate-based recipe. Changing the solvent and electrode material allows one to greatly increase the surface area, thereby increasing the kinetics of counterion incorporation and expulsion and therefore increasing the rate of electroactive response as was shown in Figure 6-6. As we search for the optimum morphology for polypyrrole actuation, it is useful to probe the effects of increasing film surface area, even at the expense of conductivity. As illustrated in the case of Films E and F (Figure 6-6), sometimes one must strike a balance between initial strain rate and total active strain. A high surface area, low modulus material such as Film F shows a very high initial strain rate, but cannot sustain that rate beyond the first 20 seconds of a potential step . A more conductive, dense film such as Film E does not actuate as quickly at first, but is able to achieve higher strains over a longer period of time.

As is shown in Figure 6-6, the standard Film A still seems to provide the best actuation. However, the different morphologies produced in this experiment may inspire future improvements for Film A. Perhaps one could increase the initial strain rate by physically increasing the surface roughness of Film A by post-deposition processing (to mimic the surface morphology of Film F). Because this physical manipulation of the surface morphology would not change the chemistry (or the conductivity) of Film A, it is possible that it would not reduce the maximum strain achievable over long

periods of time, allowing one to effectively harness the best of both worlds. This will be discussed further in Section 7.3.

Chapter 7

Conclusions and Future Outlook

7.1 Description of Polypyrrole Microstructure

Because polypyrrole is insoluble and unmeltable, most of the structural information available has been collected via scattering techniques. As was discussed extensively in Chapter 4, scattering data from polypyrrole is ambiguous. The polypyrrole x-ray diffraction pattern contains several characteristic reflections, which have previously been attributed to dimensions in a crystalline unit cell. While we agree with some of the physical origins of these assignments (as was discussed in Section 4.1.4), we find that a crystalline unit cell does not adequately describe polypyrrole's microstructure. We propose instead that polypyrrole consists of composite type arrangement of disordered chains held together by very small ordered regions, which we label bundles and described in depth in Section 4.4. This microstructure was first described in Figures 4-5 and 4-19, and we show a similar illustration (but for unoriented films) here in Figure 7-1.

During electrochemical cycling, counterions enter and leave the disordered regions between bundles, causing the film to expand and contract. The influx of counterions plasticizes the film, causing a large decrease in elastic modulus as was described in Section 2.3.8. The bundles act as passive physical cross-links in this process. Using synchrotron x-ray (Section 4.3.1) and electron (Section 4.3.3) diffraction, we have shown that the bundles themselves do not change when subjected to electrochemical

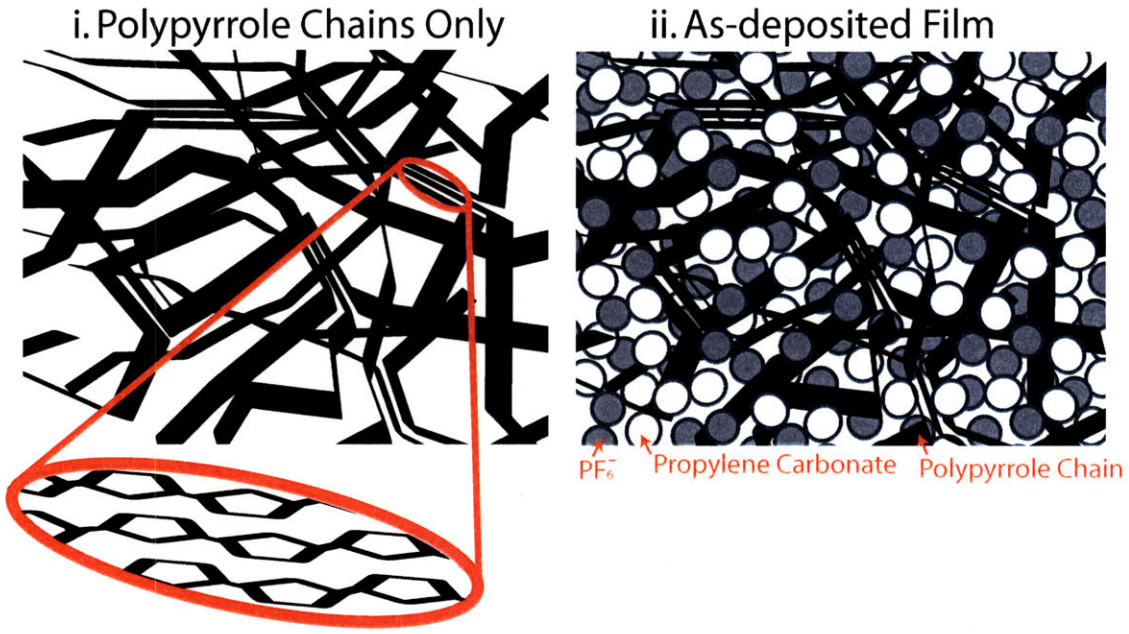

Figure 7-1: Illustration of bundled microstructure in as-deposited polypyrrole films. i) Polypyrrole chains only. Bundles act as physical-crosslinks, allowing a set of percolative paths of polypyrrole chains through the sample. A single bundle is highlighted in orange, and the polypyrrole chains that make up that bundle are illustrated. In the bundle, each chain is offset from the one below, as was discussed in Section 4.1.4. ii) Polypyrrole chains with other film components (from standard deposition recipe). The chains (~40%vol) are highly swollen with counterions (~25%vol) and solvent (up to ~35%vol in fresh film), but the film maintains its mechanical rigidity due to the connected path of individually rigid polypyrrole chains.

oxidation and reduction at the levels and timescales at which we observe macroscale actuation. This description of polypyrrole actuation has no "intrinsic mechanism," i.e. a redox-driven conformational change along the chain axis that some have proposed occurs in polypyrrole [184, 194]. The actuation of oriented films (as presented in Chapter 5) shows that a conformational change along the chain axis does not contribute in any significant way to actuation in bulk films. In the bulk, polypyrrole actuation is driven by a redox-induced swelling and de-swelling as was previously thought. Counterions move into the disordered regions between bundles, pushing non-bundled chain segments apart.

When a polypyrrole sample is electrochemically cycled, the components that make up the bulk of the polypyrrole film may change, but the bundled microstructure does not. For example, when the film is cycled in an electrolyte not used for deposition, the ions from that electrolyte are incorporated into the matrix (Figure 7-2ii as compared to Figure 7-2i). When polypyrrole is deposited from a different solution (for example Film F from Table 6.1, deposited from a solution of TBATFSI in methyl benzoate), the chains will be swollen with the counterions used (in this case, $TFSI^-$ anions as illustrated in Figure 7-2iv). The shapes of the diffraction peaks observable in WAXS (Figure 6-5) remain essentially unchanged when the deposition solvent or counterion is changed, suggesting a comparable average size and percentage of highly ordered regions.

Film A is our standard polypyrrole film, doped with PF_6^-, deposited from propylene carbonate onto a glassy carbon electrode. When Film A is subjected to room temperature vacuum treatment much of the propylene carbonate is lost, leading to a decrease in film volume (accompanied by an increase in film stiffness as was discussed in Section 2.3.1). This compact, dried film is illustrated in Figure 7-2iii. A similar phenomenon happens when the polypyrrole is deposited from methyl benzoate solution (such as in the case of Film F, doped with $TFSI^-$, deposited from methyl benzoate onto glassy carbon), since the methyl benzoate evaporates on its own. In both cases the film consists of mostly polymer chains and counterions, as is illustrated in Figure 7-2iii and Figure 7-2iv.

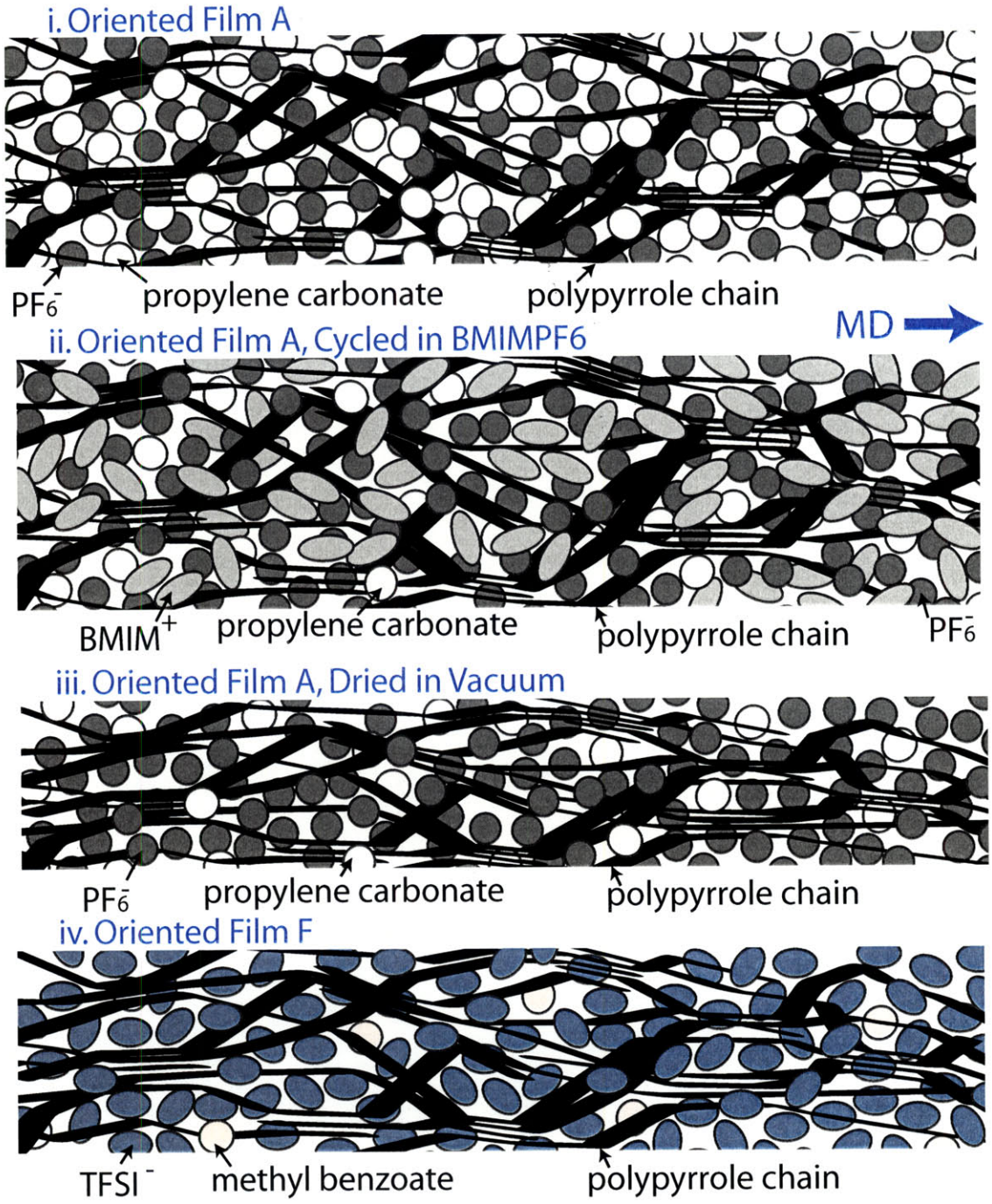

Figure 7-2: Illustration of bundled microstructure in oriented polypyrrole. i) Components of oriented Film A (percentages are approximate): 40% polymer, 30% PF_6^-, 30% propylene carbonate. ii) Components of oriented Film A after cycling in neat BMIMPF6: 40% polymer, 30% PF_6^-, 20% $BMIM^+$, 10% propylene carbonate. The electrochemical cycling introduces $BMIM^+$ cations to the film matrix, while some propylene carbonate is lost. iii) Components of oriented Film A after drying under vacuum: 55% polymer, 35% PF_6^-, 10% propylene carbonate. Much of the propylene carbonate evaporates due to the vacuum, but the PF_6^- anions remain. iv) Components of oriented Film F: 40% polymer, 50% $TFSI^-$, 10% methyl benzoate. Much of the methyl benzoate from the deposition has evaporated, but the chains are still swollen and doped with $TFSI^-$ anions.

In all of these cases the network of bundled polypyrrole chains provides the mechanical robustness and electrical conductivity of the film, and the effect of deposition or treatment conditions manifests itself mostly in the population of non-polymer components. It should be noted, however, that in this thesis we purposely chose from a relatively narrow range of deposition conditions that gave highly conductive polypyrrole films. It is possible that by choosing very different polymerization conditions (e.g. chemical oxidation in aqueous $FeCl_3$ solution), a completely amorphous, non-bundled microstructure could be achieved.

7.2 Manipulations of Polypyrrole to Improve Properties

In addition to gaining a deeper understanding the microstructure of polypyrrole, we sought to manipulate this structure to improve polypyrrole's electroactive properties. We produced films with different surface morphologies and mechanical properties by altering the deposition conditions, as has been discussed many times in the literature (and we reviewed in Chapter 3). The results of our work to this end are presented in Chapter 6. The surface morphology and mechanical properties influenced the rate and magnitude of the electroactive response, improving our understanding of what characteristics a successful polypyrrole actuator will have. By utilizing different electrolyte solutions in the deposition, we were also able to clearly identify the contribution of counterion scattering to the diffraction pattern (discussed in Section 6.3). The diffraction ring corresponding to counterion scattering does not become anisotropic upon processing, confirming our description of polypyrrole microstructure in which counterions remain randomly distributed even when the polymer chains are oriented.

We also manipulated the microstructure post deposition by physical processing. Free-standing polypyrrole films were stretched or cold rolled to produce uniaxially and biaxially textured films, as was presented in Chapter 5. This post-deposition processing allowed us to control polymer chain configuration, and provided insights

to the nanoscale mechanisms of actuation. Furthermore, the oriented films showed an increase in conductivity up to 3 × when compared to unprocessed films due to polymer chain alignment. Highly anisotropic active stresses and strains were observed, with up to 7 × larger active strains transverse to the orientation direction. This anisotropy resulted in an a 100% increase in active stress and 70% increase in active strain when compared to unprocessed films, and we achieved active strains over 10% (when cycled at 0.1 V/s) with this method. We find that larger active stresses and strains are achievable in stretched films than rolled films, and attribute this to improved ion transport through the film.

Both stretched and rolled polypyrrole films provide anisotropic actuation that has not previously been achieved in polypyrrole. This has exciting implications for electroactive device design, especially in applications such as biomimetic robotics, where complex bending motions are necessary to emulate fish or insect movement. An anisotropic polymer actuator could control the direction of actuation via its material properties, reducing the complexity of the mechanical transmission system needed.

7.3 Suggestions for Future Work

While the work presented in this thesis has enhanced our understanding of polypyrrole microstructure and actuation, it has also opened the door to new questions about polypyrrole and about conducting polymers in general.

The *in-situ* measurements of elastic modulus presented in Section 2.3.8 are only the beginning of our understanding of the dynamics of this complex system. Under the limited conditions we probed, we saw a clear decrease in modulus as counterions entered the film. However, we limited the applied electrochemical conditions to minimize neutral solvent transfer and dual ion movement. It would be interesting to open the electrochemical window in order to observe the elastic modulus under more complex swelling and de-swelling conditions.

In polypyrrole actuation, we have observed that the rate of expansion (as counterions enter the film) and contraction (as counterions leave the film) are not necessarily

the same. The change in elastic modulus shown in Section 2.3.8 could contribute to this inequality, if the contracted film has a higher modulus (so it is more resistant to expansion) than the expanded film (which would be less resistant to contraction). Even under a limited set of electrochemical conditions where neutral solvent transfer and dual ion movement are minimized, there is much to be learned about the electrochemical-dependent polymer compliance. The modulus must be probed at different frequencies while the polymer film is actuated at different potentials and frequencies in order to understand the time dependance of the system. Additionally polypyrrole films of different ages, densities, conductivities, and surface roughnesses should be investigated to identify the limiting elements for actuation. The *in-situ* modulus of oriented polypyrrole films should also be studied, to help understand the time-dependence of actuation in different directions.

As was discussed in Section 2.3.9, we observed a decrease in electroactive performance with age of the film. This is an area that demands further investigation, both so we can improve our storage conditions to prevent degradation with time, and so we can better understand the implications of ageing towards the lifetime of an actuator. Our previous attempts to monitor the effects of ageing have been to collect and compare samples and data from different depositions. Instead, samples from the same deposition should be compared after long-term storage in different conditions. Large (100 mm $\times$ 50 mm) films will be synthesized especially for this purpose, and should be measured periodically via gas pycnometry to check for densification over time. Additionally, their conductivity should be monitored to observe any degradation in electronic properties. The likely mechanism for conductivity degradation during ageing in ambient conditions is oxygen attack of the polypyrrole backbone [100], so some films will be stored in oxygen-free conditions for comparison. While an oxygen-free environment may help extend the lifetime of our standard polypyrrole films, it is not a practical solution if polypyrrole is to be used in devices. Instead, synthetic avenues may be pursued where the β-position of the pyrrole ring is blocked to prevent attack, and/or antioxidants are incorporated into the film (although antioxidant leakage from the film during electrochemical cycling must be prevented).

On the other hand, as was discussed in Section 5.4.2, in oriented films some ageing may be advantageous. In highly oriented films, repeated electrochemical cycling may increase polypyrrole chain mobility and allow the polymer chains to revert away from their oriented configuration. If the films can be aged in such a way that their mobility is decreased enough that they do not re-orient (but not so much that the films do not actuate) a more stable oriented product may be produced. Accelerated ageing treatments should be investigated, to find the point at which oriented polypyrrole films actuate repeatably, with no further decrease in performance with time. It may be necessary to combine processing techniques, orienting the films to increase the active strain achievable, then ageing the films to stabilize the response.

In this thesis we barely scratched the surface of the parameter space of polypyrrole deposition. The extremely large strains reported by Hara et al. [3,27–30,94,128] have been a source of frustration for the polypyrrole community, as they are generally transient and have not been reproduced. However, the strategy that Hara et al. employ - changing the material properties of polypyrrole via deposition variables - does have potential and should be pursued in a more rigorous manner. Our initial attempts to follow the path of Hara et al. have allowed us to increase the surface area and porosity of polypyrrole with a significant, but not insurmountable decrease in conductivity and mechanical robustness. Future research must be conducted both to understand what is so different about Hara et al.'s material that they achieve (or at least report) such large metrics, and how the lifetimes of these novel polypyrrole films can be improved so one could use these large active strains in a practical device.

We manipulated the structure of polypyrrole in two ways: by mechanically deforming the film post-deposition and by altering the conditions of polypyrrole deposition. Initial attempts to mesh the best of both worlds, where films were deposited from a novel deposition recipe and then stretched, were presented in Section 6.5. Unfortunately, these preliminary experiments were not entirely successful, as the orientation was lost upon electrochemical cycling. However, it may be possible to synthesize a flexible, high surface area polypyrrole film that can be oriented and retain its orientation upon actuation. Different deposition conditions could be attempted, or

processing could be done in such a way that the orientation becomes "locked-in." For example, after processing the film could be further polymerized, possibly by holding it in tension while soaking in monomer solution and then electrochemically polymerizing the unreacted species. If this methodology allows polypyrrole to polymerize within the film matrix (as opposed to only on the surface) it may provide the mechanical entanglements necessary to preserve orientation once the load is released.

Alternatively, perhaps we can learn from the morphologies achieved with these novel recipes and apply these morphologies to films produced under standard deposition conditions. For example, the results presented in Section 6.4 suggest that a higher surface area improves the rate of electroactive response. We are already able to impart high degrees of orientation to our standard films, resulting in large magnitudes of active strain (over 10% in Chapter 5). It would be interesting to increase the surface area of an oriented film by mechanical roughening. Theoretically, this should increase the surface area in contact with the electrolyte without altering the conductivity or molecular orientation of the bulk of the film, and could lead to a very large and very fast electroactive response.

7.4 Concluding Remarks

The subject area of this thesis (structure/property relationships in polypyrrole) is not new, as several groups have previously investigated the microstructure of this material. However, this work represents the first time that this structure has been investigated specifically as it relates to actuation, as well as the first time that polypyrrole actuation has been improved by deliberately controlling the microstructure. By focusing on the connection between nanoscale structural features and macroscale actuation, we have been able to develop a more accurate description of polypyrrole microstructure. By organizing these nanoscale features via materials processing, we have significantly improved the macroscale electroactive response achievable in PF_6^- doped polypyrrole. The success of this thesis was not in the science of uncovering the structure or the engineering of making a better actuator, but in the intersection of

the two. One could not have happened without the other.

The methods used to alter microstructure in this thesis can be applied individually or in novel combinations, in traditional or novel conducting polymer systems. It is our hope that the ideas and results presented herein will help remind conducting polymer researchers of the value that can be added by materials processing. The difference between the actuation metrics currently available and those needed for a given device may only be a matter of clever microstructure manipulation.

Bibliography

[1] K. Naoi, Y. Oura, M. Maeda, and S. Nakamura. Electrochemistry of surfactant-doped polypyrrole film, I. Formation of columnar structure by electropolymerization. *Journal of the Electrochemical Society*, 142(2):417–422, 1995.

[2] S. S. Pandey, W. Takashima, and K. Kaneto. Structure property correlation: Electrochemomechanical deformation in polypyrrole films. *Thin Solid Films*, 438:206–211, 2003.

[3] S. Hara, T. Zama, W. Takashima, and K. Kaneto. Tris(trifluoromethylsulfonyl)methide-doped polypyrrole as a conducting polymer actuator with large electrochemical strain. *Synthetic Metals*, 156(2-4):351–355, 2006.

[4] G. R. Mitchell and A. Geri. Molecular organization of electrochemically prepared conducting polypyrrole films. *J. Phys. D: Appl. Phys*, 20:1346–1353, 1987.

[5] J. M. Ko, H. W. Rhee, S. M. Park, and C. Y. Kim. Morphology and electrochemical properties of polypyrrole films prepared in aqueous and nonaqueous solvents. *Journal of the Electrochemical Society*, 137(3):905–909, 1990.

[6] C. O. Yoon, H. K. Sung, J. H. Kim, E. Barsoukov, J. H. Kim, and H. Lee. The effect of low-temperature conditions on the electrochemical polymerization of polypyrrole films with high density, high electrical conductivity and high stability. *Synthetic Metals*, 99:201–212, 1999.

[7] A. C. Cascalheira, A. S. Viana, and L. M. Abrantes. Effect of substrate preparation conditions on the morphology of polypyrrole coatings on copper - an AFM study. *Advanced Materials Forum II*, 455-456:661–664, 2004.

[8] R. Yang, D. F. Evans, L. Christensen, and W. A. Hendrickson. Scanning tunneling microscopy evidence of semicrystalline and helical conducting polymer structures. *Journal of Physical Chemistry*, 94(15):6117–6122, 1990.

[9] W. Adams. *An Electron Microscopy and X-Ray Scattering Investigation of the Deformation Morphology of Solid State Extruded Fibers and Melt Drawn Films of Polyethylene.* PhD Thesis, University of Massachusetts, 1984.

[10] Y. Nogami, J. P. Pouget, and T. Ishiguro. Structure of highly conducting PF6-doped polypyrrole. *Synthetic Metals*, 62:257–263, 1994.

[11] R. H. Geiss, G. B. Street, W. Volksen, and J. Economy. Polymer structure determination using electron diffraction techniques. *IBM Journal of Reserach and Development*, 27(4):321–329, 1983.

[12] X. Chu, V. Chan, L. D. Schmidt, and W. H. Smyrl. Crystalline fibers in chemically polymerized ultrathin polypyrrole films. *Journal of Applied Physics*, 77(12):6658–6663, 1995.

[13] J. D. W. Madden, N. A. Vandesteeg, P. A. Anquetil, P. G. A. Madden, A. Takshi, R. Z. Pytel, S. R. Lafontaine, P. A. Wieringa, and I. W. Hunter. Artificial muscle technology: Physical principles and naval prospects. *IEEE Journal of Oceanic Engineering*, 29(3):706–728, 2004.

[14] C. O. Chiang, C. R. Fincher, Y. W. Park, A. J. Heeger, H. Shirakawa, E. J. Louis, S. C. Gau, and A. G. MacDiarmid. Electrical conductivity in doped polyacetylene. *Physical Review Letters*, 39(17):1098–1101, 1977.

[15] A. Heeger. Semiconducting and metallic polymers: The fourth generation of polymeric materials. *Synthetic Metals*, 125:23–42, 2002.

[16] R. H. Baughman. Conducting polymers in redox devices and intelligent materials systems. *Makromolekulare Chemie - Macromolecular Symposia*, 51:193–215, 1991.

[17] A. MacDiarmid. Synthetic metals: A novel role for organic polymers. *Synthetic Metals*, 125:11–22, 2002.

[18] T. F. Otero, H. Grande, T. A. Skotheirm, R. L. Elsenbaumer, J. R. Reynolds, and M. Dekker. In *Electrochemomechanical Devices: Artificial Muscles Based on Conducting Polymers*, volume 2, pages 1015–1017. Marcel Dekker, New York, 1998.

[19] T. F. Otero, Y. Osada, and D. E. Derossi. In *Electrochemomechanical Device Based on Conducting Polymers*, pages 302–305. Springer, Germany, 2000.

[20] M. R. Gandhi, P. Murray, G. M. Spinks, and G. G. Wallace. Mechanism of electromechanical actuation in polypyrrole. *Synthetic Metals*, 73(3):247–256, 1995.

[21] T. Herod and J. Schlenoff. Doping-induced strain in polyaniline: Stretchoelectrochemistry. *Chem. Mater*, 5:951–955, 1993.

[22] B. Dufour, P. Rannou, D. Djurado, M. Zagorska, I. Kulszewicz-Bajer, and A. Pron. The role of chain and dopant engineering in the preparation of processable conducting polymers with desired properties. *Synthetic Metals*, 135-136:63–68, 2003.

[23] E. Smela, W. Lu, and B. Mattes. Polyaniline actuators part 1. PANI(AMPS) in HCl. *Synthetic Metals*, 151:25–42, 2005.

[24] E. Smela and B. Mattes. Polyaniline actuators part 2. PANI(AMPS) in methanesulfonic acid. *Synthetic Metals*, 151:43–48, 2005.

[25] E. Smela and N. Gadegaard. Volume change in polypyrrole studied by atomic force microscopy. *Journal of Physical Chemistry B*, 105(39):9395–9405, 2001.

[26] E. Smela and N. Gadegaard. Surprising volume change in PPy(DBS): An atomic force microscopy study. *Advanced Materials*, 11(11):953, 1999.

[27] S. Hara, T. Zama, W. Takashima, and K. Kaneto. TFSI-doped polypyrrole actuator with 26% strain. *Journal of Materials Chemistry*, 14:1516–1517, 2004.

[28] S. Hara, T. Zama, W. Takashima, and K. Kaneto. Gel-like polypyrrole based artificial muscles with extremely large strain. *Polymer Journal*, 36(11):933–936, 2004.

[29] S. Hara, T. Zama, W. Takashima, and K. Kaneto. Free-standing polypyrrole actuators with response rate of $10.8\%s^{-1}$. *Synthetic Metals*, 149(2-3):199–201, 2005.

[30] S. Hara, T. Zama, W. Takashima, and K. Kaneto. Artificial muscles based on polypyrrole actuators with large strain and stress induced electrically. *Polymer Journal*, 36(2):151–161, 2004.

[31] P. Anquetil, D. Rinderknecht, N. Vandesteeg, J. Madden, and I. Hunter. Large strain actuation in polypyrrole actuators. In *SPIE Smart Structures and Materials 2004: Electroactive Polymers Actuators and Devices*, volume 5385, pages 380–387, San Diego, CA, 2004.

[32] C. Biran, L. Toppare, T. Tincer, Y. Yagci, and V. Harabagiu. Mechanical properties of conducting H-type polysilozane-polypyrrole graft copolymers and polytetrahydrofuran-polypyrrole block copolymers. *Journal of Applied Polymer Science*, 86:1663–1666, 2002.

[33] A. Bozkurt, M. Parlak, C. Erecelebi, and L. Toppare. Conduction mechanism in H-type polysiloxane-polypyrrole block copolymers. *J. of Applied Science*, 85:52–56, 2002.

[34] D. Stanke, M. Hallensleben, and L. Toppare. Graft copolymers and composites of poly(methyl methacrylate) and polypyrrole, part 2. *Synthetic Metals*. 73:261–266. 1995.

[35] D. Stanke, M. L. Hallensleben, and L. Toppare. Electrically conductive poly(methyl methacrylate-g-pyrrole) via chemical oxidative polymerization. *Synthetic Metals*, 55-57:1108–1113, 1993.

[36] S. Jin, X. Liu, W. Zhang, Y. Lu, and G. Xue. Electrochemical copolymerization of pyrrole and styrene. *Macromolecules*, 33:4805–4808, 2000.

[37] E. Ruckenstein and Y. Sun. Polyaniline-containing electrical conductive composite prepared by two inverted emulsion pathways. *Synthetic Metals*, 74:107–113, 1995.

[38] E. Ruckenstien and L. Hong. Inverted emulsion pathway to polypyrrole and polypyrrole elastomer composites. *Synthetic Metals*, 66:249–256, 1994.

[39] W. Lee, Y. J. Kim, M. O. Jung, D. H. Kim, D. L. Cho, and S. Kaang. Preparation and properties of conducting polypyrrole-sulfonated polycarbonate composites. *Synthetic Metals*, 123:327–333, 2001.

[40] S. Sadki, P. Schottland, N. Brodie, and G. Sabouraund. The mechanisms of pyrrole electropolymerization. *Chem. Soc. Rev.*, 29:283–293, 2000.

[41] J. D. Madden. *Conducting Polymer Actuators*. PhD Thesis, Massachusetts Institute of Technology, 2000.

[42] J. Reynolds, C. Baker, C. Jolly, P. Poropatic, J. Ruiz, and J. Margolis. In *Electrically Conductive Polymers*. Chapman and Hall, New York, NY., 1989.

[43] A. Malinauskas. Chemical deposition of conducting polymers. *Polymer*, 42:39557–3972, 2001.

[44] G. Spinks, G. Wallace, J. Ding, D. Zhou, B. Xi, and J. Gillespie. Ionic liquids and polypyrrole helix tubes: Bringing the electronic braille screen closer to reality. In *SPIE Smart Structures and Materials 2003: Electroactive Polymer Actuators and Devices*, volume 5051, page 372, San Diego, CA, 2003.

[45] G. E. Collins and L. Buckley. Conductive polymer-coated fabrics for chemical sensing. *Synthetic Metals*, 78:93–101, 1996.

[46] K. Ishizu, K. Tsubaki, and S. Uchida. Encapsulation of polypyrrole by internal domain modification of double-cylinder-type copolymer brushes. *Macromolecules*, 35:10193–10197, 2002.

[47] B. L. He, Y. K. Zhou, W. J. Zhou, B. Dong, and H. L. Li. Preparation and characterization of ruthenium-doped polypyrrole composites for supercapacitor. *Materials Science and Engineering: A*, 374:322–326, 2004.

[48] C. C. B. Vollmer J. Bufon, T. Heinzel, P. Espindola, H. John, and J. Heinze. Relationship between chain length, disorder, and resistivity in polypyrrole films. *J. Phy. Chem. B*, 109:19191–19199, 2005.

[49] T. Ishiguro, H. Kaneko, Y. Nogami, H. Ishimoto, H. Nishiyama, J. Tsukamoto, A. Takahashi, M. Yamaura, T. Hagiwara, and K. Sato. Logarithmic temperature dependence of resistivity in heavily doped conducting polymers. *Physical Review Letters*, 69(4):660–663, 1992.

[50] A. J. Epstein. Electron Transport in Conducting Polymers. In G. Bidan, Patrick Bernier, and S. Lefrant, editors, *Advances in Synthetic Metals : Twenty Years of Progress in Science and Technology*, pages 349–366. Elsevier, Amsterdam ; New York, 1999.

[51] Siegmar Roth. *One-Dimensional Metals*. VCH, New York, 1995.

[52] R. H. Baughman and L. W. Shacklette. Conjugation length dependent transport in conducting polymers from a resistor network model. *J. Chem. Phys.*, 90(12):7492–7504', 1989.

[53] D. Schafersiebert, S. Roth, C. Budrowski, and H. Kuzmany. Influence of the conjugation length of polyacetylene chains on the DC conductivity. *Synthetic Metals*, 21(3):285–291, 1987.

[54] F. M. Smits. *Bell System Technical Journal*, 37:711–718, 1958.

[55] M. B. Samani, P. G. Whitten, and G. Spinks. Modelling of polypyrrole actuators. In *Materials Research Society Fall Meeting*, volume 889, Boston, MA, 2006.

[56] G. M. Spinks, L. Liu, G. G. Wallace, and D. Z. Zhou. Strain response from polypyrrole actuators under load. *Advanced Functional Materials*, 12(6-7):437–440, 2002.

[57] R. Pytel, E. Thomas, and I. Hunter. Anisotropy of electroactive strain in highly stretched polypyrrole actuators. *Chemistry of Materials*, 18(4):861–863, 2006.

[58] G. M. Spinks and V. T. Truong. Work-per-cycle analysis for electromechanical actuators. *Sensors and Actuators A*, 119(2):455–461, 2005.

[59] N. Vandesteeg. *Synthesis and Characterization of Conducting Polymer Actuators.* PhD Thesis, Massachusetts Institute of Technology, 2007.

[60] J. Madden, R. A. Cush, T. S. Kanigan, and I. W. Hunter. Fast contracting polypyrrole actuators. *Synthetic Metals*, 113:185–192, 2000.

[61] P. Anquetil. *Large Contraction Conducting Polymer Molecular Actuators.* PhD Thesis, Massachusetts Institute of Technology, 2004.

[62] A. R. Hillman, D. C. Loveday, M. J. Swann, S. Bruckenstein, and C. P. Wilde. Transport of neutral species in electroactive polymer-films. *Journal of the Chemical Society-Faraday Transactions*, 87(13):2047–2053, 1991.

[63] N. Vandesteeg, P. Anquetil, and I. Hunter. Poly(3,4-ethylenedioxythiophene) actuators: The role of cation and anion choice. In *SPIE Smart Structures and Materials 2004: Electroactive Polymers Actuators and Devices*, San Diego, CA, 2004.

[64] S. Skaarup, L. Bay, K. Vidanapathirana, S. Thybo, P. Tofte, and K. West. Simultaneous anion and cation mobility in polypyrrole. *Solid State Ionics*, 159(1-2):143–147, 2003.

[65] S. Bruckenstein, K. Brzezinska, and A. R. Hillman. EQCM studies of polypyrrole films, part 1. Exposure to aqueous sodium tosylate solutions under thermodynamically permselective conditions. *Electrochimica Acta*, 45(22-23):3801–3811, 2000.

[66] C. S. C. Bose, S. Basak, and K. Rajeshwar. Electrochemistry of poly(pyrrole chloride) films - a study of polymerization efficiency, ion-transport during redox and doping level assay by electrochemical quartz crystal microgravimetry, pH, and ion-selective electrode measurements. *Journal of Physical Chemistry*, 96(24):9899–9906, 1992.

[67] S. Bruckenstein, K. Brzezinska, and A. R. Hillman. EQCM studies of polypyrrole films, part 2. Exposure to aqueous sodium tosylate solutions under thermodynamically non-permselective conditions. *Physical Chemistry Chemical Physics*, 2(6):1221–1229, 2000.

[68] L. Bay, T. Jacobsen, S. Skaarup, and K. West. Mechanism of actuation in conducting polymers: Osmotic expansion. *Journal of Physical Chemistry B*, 105(36):8492–8497, 2001.

[69] M. Ue. Mobility and ionic association of lithium and quaternary ammonium-salts in propylene carbonate and gamma-butyrolactone. *Journal of the Electrochemical Society*, 141(12):3336–3342, 1994.

[70] L. Bay, N. Mogensen, S. Skaarup, P. Sommer-Larsen, M. Jorgensen, and K. West. Polypyrrole doped with alkyl benzenesulfonates. *Macromolecules*, 35(25):9345–9351, 2002.

[71] Y. Velmurugu and S. Skaarup. Ion and solvent transport in polypyrrole: Experimental test of osmotic model. *Ionics*, 11(5-6):370–374, 2005.

[72] W. Lu, A. G. Fadeev, B. H. Qi, E. Smela, B. R. Mattes, J. Ding, G. M. Spinks, J. Mazurkiewicz, D. Z. Zhou, G. G. Wallace, D. R. MacFarlane, S. A. Forsyth, and M. Forsyth. Use of ionic liquids for pi-conjugated polymer electrochemical devices. *Science*, 297(5583):983–987, 2002.

[73] J. Ding, D. Z. Zhou, G. Spinks, G. Wallace, S. Forsyth, M. Forsyth, and D. MacFarlane. Use of ionic liquids as electrolytes in electromechanical actuator systems based on inherently conducting polymers. *Chemistry of Materials*, 15(12):2392–2398, 2003.

[74] H. Tokuda, K. Hayamizu, K. Ishii, M. A. B. H. Susan, and M. Watanabe. Physicochemical properties and structures of room temperature ionic liquids. 2. Variation of alkyl chain length in imidazolium cation. *Journal of Physical Chemistry B*, 109(13):6103–6110, 2005.

[75] H. Tokuda, K. Hayamizu, K. Ishii, M. Abu Bin Hasan Susan, and M. Watanabe. Physicochemical properties and structures of room temperature ionic liquids. 1. Variation of anionic species. *Journal of Physical Chemistry B*, 108(42):16593–16600, 2004.

[76] S. Rivera-Rubero and S. Baldelli. Surface spectroscopy of room-temperature ionic liquids on a platinum electrode: A sum frequency generation study. *Journal of Physical Chemistry B*, 108(39):15133–15140, 2004.

[77] V. Halka, R. Tsekov, and W. Freyland. Peculiarity of the liquid/vapour interface of an ionic liquid: Study of surface tension and viscoelasticity of liquid BMIMPF(6) at various temperatures. *Physical Chemistry Chemical Physics*, 7(9):2038–2043, 2005.

[78] R. Pytel, E. Thomas, and I. Hunter. Charge-dependant elastic modulus in polypyrrole actuators. *In Preparation*, 2007.

[79] P. G. A. Madden, J. D. W. Madden, P. A. Anquetil, N. A. Vandesteeg, and I. W. Hunter. The relation of conducting polymer actuator material properties to performance. *IEEE Journal of Oceanic Engineering*, 29(3):696–705, 2004.

[80] J. Madden, P. Madden, and I. Hunter. Polypyrrole actuators: Modeling and performance. In *SPIE Smart Structures and Materials 2001: Electroactive Polymer Actuators and Devices*, volume 4329, pages 72–83, San Diego, CA, 2001.

[81] C. Deslouis, T. ElMoustafid, M. M. Musiani, and B. Tribollet. Mixed ionic-electronic conduction of a conducting polymer film. AC impedance study of polypyrrole. *Electrochimica Acta*, 41(7-8):1343–1349, 1996.

[82] C. Michal, J. Tso, and R. Pytel. Diffusion of hexafluorophosphate in polypyrrole as measured by pulse field gradient NMR. *To be published.*

[83] T. Otero and H. Grande. Reversible 2D to 3D electerode transitions in polypyrrole films. *Colloids and Surfaces*, 134:85–94, 1998.

[84] T. F. Otero and I. Boyano. Comparative study of conducting polymers by the ESCR model. *J. Phys. Chem. B.*, 107:6730–6738, 2003.

[85] G. Spinks, B. Xi, D. Zhou, V. T. Truong, and G. Wallace. Enhanced control and stability of polypyrrole electromechanical actuators. *Synthetic Metals*, 140:273–280, 2004.

[86] P. Murray, G. M. Spinks, G. G. Wallace, and R. P. Burford. In-situ mechanical properties of tosylate doped (pTS) polypyrrole. *Synthetic Metals*, 84(1-3):847–848, 1997.

[87] P. Murray, G. M. Spinks, G. G. Wallace, and R. P. Burford. Electrochemical induced ductile-brittle transition in tosylate-doped (pTS) polypyrrole. *Synthetic Metals*, 97(2):117–121, 1998.

[88] T. F. Otero, J. J. Lopez Cascales, and G. Vazquez Arenas. Mechanical characterization of free-standing polypyrrole film. *Materials Science and Engineering: C*, 27(1):18–22, 2007.

[89] B. B. Xi, V. T. Truong, P. Whitten, J. Ding, G. M. Spinks, and G. G. Wallace. Poly(3-methylthiophene) electrochemical actuators showing increased strain and work per cycle at higher operating stresses. *Polymer*, 47(22):7720–7725, 2006.

[90] W. Lu and B. R. Mattes. Factors influencing electrochemical actuation of polyaniline fibers in ionic liquids. *Synthetic Metals*, 152(1-3):53–56, 2005.

[91] Silvio Koehler, Andreas Bund, and Igor Efimov. Shear moduli of anion and cation exchanging polypyrrole films. *Journal of Electroanalytical Chemistry*, 589(1):82–86, 2006.

[92] M. B. Samani, D. C. Cook, J. D. Madden, G. Spinks, and P. Whitten. Quartz crystal microbalance study of volume changes and modulus shift in electrochemically switched polypyrrole. *Thin Solid Films*, Accepted for Publication, 2007.

[93] T. Hagiwara, M. Hirasaka, K. Sato, and M. Yamaura. Enhancement of the electrical conductivity of polypyrrole film by stretching: Influence of the polymerization conditions. *Synthetic Metals*, 36:241–252, 1990.

[94] S. Hara, T. Zama, W. Takashima, and K. Kaneto. Free-standing gel-like polypyrrole actuators doped with bis(perfluoroalkylsulfonyl)imide exhibiting extremely large strain. *Smart Materials and Structures*, 14:1501–1510, 2005.

[95] S. Maw, E. Smela, K. Yoshida, P. Sommer-Larsen, and R. Stein. The effects of varying deposition current density on bending behaviour in PPy(DBS)-actuated bending beams. *Sensors and Actuators A*, 89:175–184, 2001.

[96] T. Zama, S. Hara, W. Takashima, and K. Kaneto. The correlation between electrically induced stress and mechanical tensile strength of polypyrrole actuators. *Bulletin of the Chemical Society of Japan*, 77(7):1425–1426, 2004.

[97] M. Yamaura, K. Sato, T. Hagiwara, and K. Iwata. Memory effect of electrical conductivity upon the counter-anion exchange of polypyrrole films. *Synthetic Metals*, 48:337–354, 1992.

[98] R. H. Baughman. Conducting polymer artificial muscles. *Synthetic Metals*, 78(3):339–353, 1996.

[99] G. Spinks, D. Zhou, L. Liu, and G. Wallace. The amounts per cycle of polypyrrole electromechanical actuators. *Smart Materials and Structures*, 12:468–472, 2003.

[100] A. Kaynak, L. Rintoul, and A. Graeme. Change of mechanical and electrical properties of polypyrrole films with dopant concentration and oxidative aging. *Materials Research Bulletin*, 35(6):813–824, 2000.

[101] H. L. Ricks-Laskoski and L. J. Buckley. Twenty-year aging study of electrically conductive polypyrrole films. *Synthetic Metals*, 156(5-6):417–419, 2006.

[102] B. C. Ennis and V. T. Truong. Thermal and electrical stability of polypyrrole at elevated temperatures. *Synthetic Metals*, 59(3):387–399, 1993.

[103] V. T. Truong. Thermal degradation of polypyrrole: Effect of temperature and film thickness. *Synthetic Metals*, 52(1):33–44, 1992.

[104] T. L. Tansley and D. S. Maddison. Conductivity degradation in oxygen-aged polypyrrole. *Journal of Applied Physics*, 69(11):7711–7713, 1991.

[105] J. Joo, Z. Oblakowski, G. Du, J. P. Pouget, E. J. Oh, J. M. Wiesinger, Y. Min, A. G. MacDiarmid, and A. J. Epstein. Microwave dielectric response of mesoscopic metallic regions and the intrinsic metallic state of polyaniline. *Physical Review B*, 49(4):2977–2980, 1994.

[106] A. G. Macdiarmid and A. J. Epstein. The concept of secondary doping as applied to polyaniline. *Synthetic Metals*, 65(2-3):103–116, 1994.

[107] R. S. Kohlman, A. J. Epstein, T. Skotheim, R. Elsenbaumer, and J. Reynolds. In *Insulator-Metal Transition and Inhomogeneous Metallic State in Conducting Polymers*, volume 2, pages 85–121. Marcel Dekker, New York, NY, 1998.

[108] I. A. Bucklow and J. H. Potter. A simple electrical contact for resistivity ratio measurements. *Journal of Physics E - Scientific Instruments*, 4(10):781, 1971.

[109] J. H. Kim, J. H. Kim, H. K. Sung, H. J. Kim, C. O. Yoon, and H. Lee. Structural aspect of metal-insulator transition in doped conducting polymers. *Synthetic Metals*, 84:71–72, 1997.

[110] R. Menon, C. O. Yoon, D. Moses, and A. J. Heeger. In T. Skotheim, R. Elsenbaumer, and J. Reynolds, editors, *Metal-Insulator Transition in Doped Conducting Polymers*, volume 2. Marcel Dekker, inc., New York, NY, 1998.

[111] A. B. Kaiser. Systematic conductivity behavior in conducting polymers: Effects of heterogeneous disorder. *Advanced Materials*, 13(12-13):927–+, 2001.

[112] C. O. Yoon, M. Reghu, D. Moses, A. J. Heeger, Y. Cao, T. A. Chen, X. Wu, and R. D. Rieke. Hopping transport in doped conducting polymers in the insulating regime near the metal-insulator boundary: Polypyrrole, polyaniline and polyalkylthiophenes. *Synthetic Metals*, 75(3):229–239, 1995.

[113] C. Yoon, M. Reghu, D. Moses, and A. J. Heeger. Transport near the metal-insulator transition: Polypyrrole doped with PF6. *Physical Review B*, 49:10851–10863, 1994.

[114] M. Reghu, K. Vakiparta, C. O. Yoon, Y. Cao, D. Moses, and A. J. Heeger. Tuning through the critical regime of the metal-insulator transition in conducting polymers by pressure and magnetic field. *Synthetic Metals*, 65(2-3):167–171, 1994.

[115] K. Sato, M. Yamaura, T. Hagiwara, K. Murata, and M. Tokumoto. Sturdy on the electrical conduction mechanism of polypyrrole films. *Synthetic Metals*, 40(1):35–48, 1991.

[116] A. B. Kaiser. Thermoelectric-power and conductivity of heterogeneous conducting polymers. *Physical Review B*, 40(5):2806–2813, 1989.

[117] D. S. Maddison and T. L. Tansley. Variable range hopping in polypyrrole films of a range of conductivities and preparation methods. *Journal of Applied Physics*, 72(10):4677–4682, 1992.

[118] G. R. Mitchell, R. Cywinski, S. Mondal, and S. J. Sutton. The influence of molecular organization on charge transport in electrochemically prepared polypyrrole films. *J. Phys. D: Appl Phys.*, 22:1231–1234, 1989.

[119] M. Reghu, C. O. Yoon, C. Y. Yang, D. Moses, P. Smith, A. J. Heeger, and Y. Cao. Transport in polyaniline networks near the percolation-threshold. *Physical Review B*, 50(19):13931–13941, 1994.

[120] M. Pollak and C. J. Adkins. Conduction in granular metals. *Philosophical Magazine B-Physics of Condensed Matter Statistical Mechanics Electronic Optical and Magnetic Properties*, 65(4):855–860, 1992.

[121] J. Joo, V. N. Prigodin, Y. G. Min, A. G. MacDiarmid, and A. J. Epstein. Phonon-induced nonmetal-metal transition of a doped polyaniline. *Physical Review B*, 50(16):12 226 – 12 229, 1994.

[122] O. Chauvet, S. Paschen, L. Forro, L. Zuppiroli, P. Bujard, K. Kai, and W. Wernet. Magnetic and transport-properties of polypyrrole doped with polyanions. *Synthetic Metals*, 63(2):115–119, 1994.

[123] M. Yamaura, T. Hagiwara, and K. Iwata. Enhancement of electrical conductivity of polypyrrole film by stretching: Counter ion effect. *Synthetic Metals*, 20:209–224, 1988.

[124] G. R. Mitchell, F. J. Davis, R. Cywinski, and W. S. Howells. Neutron scattering study of electrically conducting films of polypyrrole. *J. Phys. C: Solid State Phys.*. 21:L411–L416, 1988.

[125] G. R. Mitchell, F. J. Davis, and C. H. Legge. The effect of dopant molecules on the molecular order of electrically-conducting films of polypyrrole. *Synthetic Metals*, 26:247–257, 1988.

[126] L. Bay, K. West, and S. Skaarup. Pentanol as co-surfactant in polypyrrole actuators. *Polymer*, 43:3527–3532, 2002.

[127] S. S. Pandey, W. Takashima, M. Fuchiwaki, and K. Kaneto. Effect of film morphology on the actuation behavior in polypyrrole films. *Synthetic Metals*, 135-136:59–60, 2003.

[128] S. Hara, T. Zama, S. Sewa, W. Takashima, and K. Kaneto. Highly stretchable and powerful polypyrrole linear actuators. *Chemistry Letters*, 32(7):576–577, 2003.

[129] Y. Wu, G. Alici, G. M. Spinks, and G. G. Wallace. Fast trilayer polypyrrole bending actuators for high speed applications. *Synthetic Metals*, 156(16-17):1017–1022, 2006.

[130] M. Yamaura, T. Hagiwara, M. Hirasaka, T. Demura, and K. Iwata. Structure and properties of biaxially stretched polypyrrole films. *Synthetic Metals*, 28(1-2):157–164, 1989.

[131] K. Wynne and B. Street. Poly(pyrrol-2-ylium tosylate): Electrochemical synthesis and physical and mechanical properties. *Macromolecules*, 18:2361–2368, 1985.

[132] W. Wernet, M. Monkenbusch, and G. Wegner. A new series of conducting polymers with layered structure: Polypyrrole N-alkylsulfates and N-alkylsulfonates. *Makromol. Chem. , Rapid Communications*, 6:157–164, 1984.

[133] T. Zama. S. Hara, W. Takashima, and K. Kaneto. Comparison of conducting polymer actuators based on polypyrrole doped with BF4(-). PF6(-). CF3SO3-. and ClO4. *Bulletin of the Chemical Society of Japan*. 78(3):506–511. 2005.

[134] M. Zhou and J. Heinze. Electropolymerization of pyrrole and electrochemical study of polypyrrole. 2. Influence of acidity on the formation of polypyrrole and the multipathway mechanism. *J. Phys. Chem B*, 103:8443–8450, 1999.

[135] R. Stankovic, O. Pavlovic, M. Vojnovic, and S. Jovanovic. The effects of preparation conditions on the properties of electrochemically synthesized thick-films of polypyrrole. *European Polymer Journal*, 30(3):385–393, 1994.

[136] Y. F. Li and J. Y. Ouyang. Effect of nonionic surfactant additives on the electropolymerization of pyrrole in aqueous solutions. *Synthetic Metals*, 113(1-2):23–28, 2000.

[137] P. Dyreklev, M. Granstrom, O. Inganas, L. M. W. K. Gunaratne, G. K. R. Senadeera, S. Skaarup, and K. West. The influence of polymerization rate on conductivity and crystallinity of electropolymerized polypyrrole. *Polymer*, 37(13):2609–2613, 1996.

[138] F. Anderson, R. Badlani, J. Mayer, and P. Mabrouk. Electrochemical synthesis and characterization of conducting polymers in supercritical carbon dioxide. *J. Am. Chem. Soc.*, 124:10284–10285, 2002.

[139] P. A. Mabrouk. Oxidative electropolymerization of pyrrole from neat monomer solution. *Synthetic Metals*, 150(1):101–105, 2005.

[140] Jianyong Ouyang and Yongfang Li. Effect of electrolyte solvent on the conductivity and structure of as-prepared polypyrrole films. *Polymer*, 38(8):1971–1976, 1997.

[141] S. Rapi, V. Bocchi, and G. P. Gardini. Conducting polypyrrole by chemical synthesis in water. *Synthetic Metals*, 24(3):217–221, 1988.

[142] S. J. Sutton and A. S. Vaughan. On the growth of polypyrrole from solutions of methanol and water. *Synthetic Metals*, 58(3):391–402, 1993.

[143] M. Ogasawara, K. Funahashi, T. Demura, T. Hagiwara, and K. Iwata. Enhancement of electrical conductivity of polypyrrole by stretching. *Synthetic Metals*, 14(1-2):61–69, 1986.

[144] S-I. Ohnishi, Y. Ikeda, S-I. Sugimoto, and I. Nitta. On the ESR singlet spectra frequently observed in irradiated polymers at a large dose. *Journal of Polymer Science*, 47(149):503–507, 1960.

[145] G. Vancso, T. T. Nagy, B. Turcsanyi, T. Kelen, and F. Tudos. Conjugation length of polyenyl radicals and polyenes in thermally degraded polyvinylchloride). *Makromolekulare Chemie-Rapid Communications*, 3(8):527–532, 1982.

[146] R. Yang, K. M. Dalsin, D. F. Evans, L. Christensen, and W. A. Hendrickson. Scanning tunneling microscopy imaging of electropolymerized, doped polypyrrole. Visual evidence of semicrystalline and helical nascent polymer growth. *Journal of Physical Chemistry*, 93:511–512, 1989.

[147] G. Garcia-Belmonte. Effect of electrode morphology on the diffusion length of the doping process of electronically conducting polypyrrole films. *Electrochemistry Communications*, 5(3):236–240, 2003.

[148] L. E. Alexander. *X-Ray Diffraction Methods in Polymer Science.* John Wiley & Sons, Inc., New York, NY, 1969.

[149] M. Kakudo and N. Kasai. *X-Ray Diffraction by Polymers.* Elsevier Publishing Company, New York, NY, 1972.

[150] B. F. Warren. *X-Ray Diffraction.* Addison-Wesley, Reading, Massachusetts, 1969.

[151] S. M. Allen and E. L. Thomas. *The Structure of Materials.* John Wiley & Sons, Inc., New York, NY, 1999.

[152] L. S. Tan, S. R. Simko, S. J. Bai, R. A. Vaia, B. E. Taylor, M. D. Houtz, D. M. Alexander, and R. J. Spry. Phase-separated, conducting composites from polyaniline and benzobisthiazole rigid-rod polymer. *Journal of Polymer Science part B: Polymer Physics*, 39:2539–2548, 2001.

[153] I. M. Ward. *Mechanical Properties of Solid Polymers.* Wiley-Interscience, London, 1971.

[154] D. Lesueur and N. D. Alberola. Dynamic mechanical behavior of electrochemically synthesized polypyrrole films. *Synthetic Metals*, 88(2):133–138, 1997.

[155] Masaharu Satoh, Harumasa Yamasaki, Shuzo Aoki, and Katsumi Yoshino. Temperature dependence of mechanical properties of electrochemically prepared polypyrole film. *Synthetic Metals*, 20(1):79–83, 1987.

[156] T. Kunugi and H. Okuzaki. Electrical and mechanical properties of the zone-drawn polypyrrole films. *Journal of Polymer Science part B: Polymer Physics*, 34:1269–1275. 1996.

[157] M. R. Warren and J. D. Madden. A structural investigation of polypyrrole as a function of oxidation state. *Mater. Res. Soc. Symp. Proc.*, 871E(I6.1), 2005.

[158] M. R. Warren and J. D. Madden. A structural, electronic and electrochemical study of polypyrrole as a function of oxidation state. *Synthetic Metals*, 156(9-10):724–730, 2006.

[159] D. A. Scherlis and N. Marzari. Pi-stacking in charged thiophene oligomers. *Journal of Physical Chemistry B*, 108(46):17791–17795, 2004.

[160] J. Blackwell and M. R. Nagarajan. Conformational-analysis of poly(mdi-butandiol) hard segment in polyurethane elastomers. *Polymer*, 22(2):202–208, 1981.

[161] R. J. Bonart, L. Morbitzer, and G. J. Hentze. X-ray investigations concerning the physical structure of cross-linking in urethane elastomers. II. Butanediol as chain extender. *J. Macromol. Sci. Phys. (B)*, 3:337. 1969.

[162] R. Briber. *Investigations of the Structure and Morphology of Random Block Copolymers.* PhD Thesis, University of Massachusetts, 1984.

[163] L. J. Buckley, D. K. Roylance, and G. E. Wnek. Influence of dopant ion and synthesis variables on mechanical properties of polypyrrole films. *Journal of Polymer Science*, 25:2179–2188, 1987.

[164] L. J. Buckley. *Structure/Property Studies of Electrochemically Synthesized Polypyrrole Films.* PhD Thesis, Massachusetts Institute of Technology, 1986.

[165] J. P. Pouget, Z. Oblakowski, Y. Nogami, P. A. Albouy, M. Laridjani, E. J. Oh, Y. Min, A. G. MacDiarmid, J. Tsukamoto, T. Ishiguro, and A. J. Epstein. Recent structural investigations of metallic polymers. *Synthetic Metals*, 65:131–140, 1994.

[166] T. Otero. In H. S. Nalwa, editor, *Conductive Polymers: Transport, Photophysics and Applications*, volume 4. John Wiley & Sons, New York, 1997.

[167] S. Rabiej. Determination of the crystallinity of polymer blends by an x-ray-diffraction method. *European Polymer Journal*, 29(4):625–633, 1993.

[168] D. B. Williams and C. B. Carter. *Transmission Electron Microscopy 1) Basics*, volume 1. Plenum Press, New York, NY, 1996.

[169] D. B. Williams and C. B. Carter. *Transmission Electron Microscopy 2) Diffraction*, volume 2. Plenum Press, New York, NY, 1996.

[170] J. Fink, B. Scheerer, W. Wernet, M. Monkenbusch, G. Wegner. H. J. Freund, and H. Gonska. Electronic structure of pyrrole-based conducting polymers: An electron-energy-loss-spectroscopy study. *Physical Review B.* 34(2):1101, 1986.

[171] R. G. Davidson, L. C. Hammond. T. G. Turner, and A. R. Wilson. An electron and x-ray diffraction study of conducting pyrrole/dodecyl sulfate. *Synthetic metals*, 81:1–4, 1996.

[172] F. Garnier, G. Tourillon, Y. Barraud, and Dexpert. First evidence of crystalline structure in conducting polythiophene. *Journal of Materials Science*, 20:2687–2694, 1985.

[173] J. Squire. *The Structural Basis of Muscular Contraction.* Plenum Press, New York, NY, 1981.

[174] R. F. Egerton. *Electron Energy-Loss Spectroscopy in the Electron Microscope.* Plenum Press, New York, NY, second edition, 1996.

[175] D. B. Williams and C. B. Carter. *Transmission Electron Microscopy 4) Spectrometry*, volume 4. Plenum Press, New York, NY, 1996.

[176] S. Lamprakopoulos, D. Yfantis, A. Yfantis, D. Schmeisser, J. Anastassopoulou, and T. Theophanides. An FTIR study of the role of H2O and D2O in the aging mechanism of conducting polypyrroles. *Synthetic Metals*, 144:229–234, 2004.

[177] D. Schmeisser, A. Bartl, L. Dunsch, H. Naarmann, and W. Gopel. Electronic and magnetic properties of polypyrrole films depending on their one-dimensional and two-dimensional microstructures. *Synthetic Metals*, 93(1):43–58, 1998.

[178] F. P. Bradner. J. S. Shapiro, H. J. Bowley, D. L. Gerrard, and W. F. Maddams. Some insights into the microstructure of polypyrrole. *Polymer*, 30(5):914–917, 1989.

[179] P. Pfluger and G. B. Street. Chemical, electronic, and structural-properties of conducting heterocyclic polymers - a view by XPS. *Journal of Chemical Physics*, 80(1):544–553, 1984.

[180] L. L. Miller and K. R. Mann. Pi-dimers and pi-stacks in solution and in conducting polymers. *Accounts of Chemical Research*, 29(9):417–423, 1996.

[181] C. Bohn, S. Sadki, A. Brennan, and J. Reynolds. In situ electrochemical strain gage monitoring of actuation in conducting polymers. *Journal of the Electrochemical Society*, 149(8):E281–E285, 2002.

[182] ftp://dell.chem.sunysb.edu/pub/polar/.

[183] P. C. H. Li and M. Thompson. Water-instigated changes in elastic modulus of polypyrrole studied by thin rod acoustic wave sensor. *Analytica Chimica Acta*, 353(2-3):255–262, 1997.

[184] X. Lin, J. Li, E. Smela, and S. Yip. Polaron-induced conformation change in single polypyrrole chain: An intrinsic actuation mechanism. *International Journal of Quantum Chemistry*, 102:980–985, 2005.

[185] J. L. Xia and C. H. Wang. Diffusion of camphorquinone in uniaxially drawn polycarbonate films. *Journal of Polymer Science part B-Polymer Physics*, 30(13):1437–1442, 1992.

[186] Arjen Boersma, Daniele Cangialosi, and Stephen J. Picken. Mobility and solubility of antioxidants and oxygen in glassy polymers III. Influence of deformation and orientation on oxygen permeability. *Polymer*, 44(8):2463–2471, 2003.

[187] W. S. Price. Pulsed-field gradient nuclear magnetic resonance as a tool for studying translational diffusion: Part I. Basic theory. *Concepts in Magnetic Resonance*, 9(5):299–336, 1997.

[188] W. S. Price. Pulsed-field gradient nuclear magnetic resonance as a tool for studying translational diffusion: Part II. Experimental aspects. *Concepts in Magnetic Resonance*, 10(4):197–237, 1998.

[189] L. Xie, D. W. Gidley, H. A. Hristov, and A. F. Yee. Evolution of nanometer voids in polycarbonate under mechanical-stress and thermal-expansion using positron spectroscopy. *Journal of Polymer Science part B: Polymer Physics.* 33(1):77–84, 1995.

[190] G. V. Lauder, P. Madden, R. Mittal, H. Dong, M. Bozkurtas, N. Davidson, J. Tangorra, and I. Hunter. Pectoral fin function in sunfish: Experimental hydrodynamics, computational fluid dynamics, and construction of a robotic model. *Integrative and Comparative Biology*, 45(6):1030–1030, 2005.

[191] J. Tangorra, P. Anquetil, T. Fofonoff, A. Chen, M. Del Zio, and I. Hunter. The application of conducting polymers to a biorobotic fin propulsor. *Bioinspiration & Biomimetics*, Accepted, 2007.

[192] J. L. Tangorra, S. N. Davidson, P. G. Madden, G. V. Lauder, and I. W. Hunter. The development of a biorobotic pectoral fin. In *Proceedings of the Engineering in Medicine and Biology Society*, New York, NY, 2006.

[193] http://www.eamex.co.jp/denshi_hp/movies/TFSI_60mm.wmv.

[194] X. Lin, J. Li, and S. Yip. Controlling bending and twisting of conjugated polymers via solitons. *Physical Review Letters*, 95:198303–1–198303–4, 2005.